

4 The Stellar and Sub-Stellar Initial Mass Function of Simple and Composite Populations

Pavel Kroupa¹ · Carsten Weidner^{2,3} · Jan Pflamm-Altenburg¹ · Ingo Thies¹ · Jörg Dabringhausen¹ · Michael Marks¹ · Thomas Maschberger^{4,5}

¹Argelander-Institut für Astronomie, Universität Bonn, Bonn, Germany

²Scottish Universities Physics Alliance (SUPA), School of Physics and Astronomy, University of St. Andrews, North Haugh, St. Andrews, UK

³Instituto de Astrofísica de Canarias, La Laguna (Tenerife), Spain

⁴Institute of Astronomy, Cambridge, UK

⁵Institut de Planétologie et d'Astrophysique de Grenoble, Grenoble Cédex 9, France

1	<i>Introduction and Historical Overview</i>	118
1.1	Solar Neighborhood	119
1.2	Star Clusters	120
1.3	Intermediate-Mass and Massive Stars	121
1.4	The Invariant IMF and Its Conflict with Theory	122
1.5	Philosophical Note	124
1.6	Hypothesis Testing	125
1.7	About This Text	126
1.8	Other IMF Reviews	127
2	<i>Some Essentials</i>	127
2.1	Unavoidable Biases Affecting IMF Studies	130
2.2	Discretizing an IMF: Optimal Sampling and the $m_{\max} - M_{\text{ecl}}$ Relation	131
2.3	Discretizing an IMF: Random Sampling and the Mass-Generating Function	135
2.4	A Practical Numerical Formulation of the IMF	136
2.5	Statistical Treatment of the Data	139
2.6	Binary Systems	141
3	<i>The Maximum Stellar Mass</i>	144
3.1	On the Existence of a Maximum Stellar Mass	144
3.2	The Upper Physical Stellar Mass Limit	145

3.3	The Maximal Stellar Mass in a Cluster, Optimal Sampling and Saturated Populations	147
3.3.1	Theory	147
3.3.2	Observational data	149
3.3.3	Interpretation	150
3.3.4	Stochastic or Regulated Star Formation?	151
3.3.5	A Historical Note	152
3.4	Caveats	153
4	<i>The Isolated Formation of Massive Stars</i>	153
5	<i>The IMF of Massive Stars</i>	157
6	<i>The IMF of Intermediate-Mass Stars</i>	159
7	<i>The IMF of Low-Mass Stars (LMSs)</i>	160
7.1	Galactic-Field Stars and the Stellar Luminosity Function	160
7.2	The Stellar Mass–Luminosity Relation	162
7.3	Unresolved Binary Stars and the Solar-Neighborhood IMF	166
7.4	Star Clusters	169
8	<i>The IMF of Very Low-Mass Stars (VLMSs) and of Brown Dwarfs (BDs)</i>	177
8.1	BD and VLMS Binaries	178
8.2	The Number of BDs per Star and BD Universality	181
8.3	BD Flavors	182
8.4	The Origin of BDs and Their IMF	184
9	<i>The Shape of the IMF from Resolved Stellar Populations</i>	186
9.1	The Canonical, Standard or Average IMF	187
9.2	The IMF of Systems and of Primaries	190
9.3	The Galactic-Field IMF	191
9.4	The Alpha Plot	191
9.5	The Distribution of Data Points in the Alpha-Plot	194
10	<i>Comparisons and Some Numbers</i>	197
10.1	The Solar-Neighborhood Mass Density and Some Other Numbers	197
10.2	Other IMF Forms and Cumulative Functions	198
11	<i>The Origin of the IMF</i>	199
11.1	Theoretical Notions	201
11.2	The IMF from the Cloud-Core Mass Function?	206
12	<i>Variation of the IMF</i>	209
12.1	Trivial IMF Variation Through the $m_{\max} - M_{\text{ecl}}$ Relation	209
12.2	Variation with Metallicity	210
12.3	Cosmological Evidence for IMF Variation	211
12.4	Top-Heavy IMF in Starbursting Gas	212

12.5	Top-Heavy IMF in the Galactic Center	213
12.6	Top-Heavy IMF in Some Star-Burst Clusters	214
12.7	Top-Heavy IMF in Some Globular Clusters (GCs)	215
12.8	Top-Heavy IMF in UCDs	218
12.9	The Current State of Affairs Concerning IMF Variation with Density and Metallicity and Concerning Theory	221
13	<i>Composite Stellar Populations: The IGIMF</i>	224
13.1	IGIMF Basics	225
13.2	IGIMF Applications, Predictions and Observational Verification	227
14	<i>The Universal Mass Function</i>	232
15	<i>Concluding Comments</i>	233
	<i>Acknowledgments</i>	235
	<i>References</i>	235

Abstract: The current knowledge on the stellar IMF is documented. It is usually described as being invariant, but evidence to the contrary has emerged: it appears to become top-heavy when the star-formation rate density surpasses about $0.1 M_{\odot}/(\text{year pc}^3)$ on a pc scale and it may become increasingly bottom-heavy with increasing metallicity and in increasingly massive elliptical galaxies. It declines quite steeply below about $0.07 M_{\odot}$ with brown dwarfs (BDs) and very low mass stars having their own IMF. The most massive star of mass m_{max} formed in an embedded cluster with stellar mass M_{ecl} correlates strongly with M_{ecl} being a result of gravitation-driven but resource-limited growth and fragmentation-induced starvation. There is no convincing evidence whatsoever that massive stars do form in isolation. Massive stars form above a density threshold in embedded clusters which become *saturated* when $m_{\text{max}} = m_{\text{max}*} \approx 150 M_{\odot}$ which appears to be the canonical physical upper mass limit of stars. Super-canonical massive stars arise naturally due to stellar mergers induced by stellar-dynamical encounters in binary-rich very young dense clusters.

Various methods of discretising a stellar population are introduced: *optimal sampling* leads to a mass distribution that perfectly represents the exact form of the desired IMF and the $m_{\text{max}} - M_{\text{ecl}}$ relation, while *random sampling* results in statistical variations of the shape of the IMF. The observed $m_{\text{max}} - M_{\text{ecl}}$ correlation and the small spread of IMF power-law indices together suggest that optimally sampling the IMF may be the more realistic description of star formation than random sampling from a universal IMF with a constant upper mass limit.

Composite populations on galaxy scales, which are formed from many pc scale star formation events, need to be described by the integrated galactic IMF. This IGIMF varies systematically from top-light to top-heavy in dependence of galaxy type and star formation rate, with dramatic implications for theories of galaxy formation and evolution.

1 Introduction and Historical Overview

The distribution of stellar masses that form together, the stellar initial mass function (IMF), is one of the most important astrophysical distribution functions. The determination of the IMF is a very difficult problem because stellar masses cannot be measured directly and because observations usually cannot assess all stars in a population requiring elaborate bias corrections. Indeed, the stellar IMF is not measurable (the IMF Unmeasurability Theorem on p. 129). Nevertheless, impressive advances have been achieved such that the shape of the IMF is reasonably well understood from low-mass brown dwarfs (BDs) to very massive stars.

The IMF is of fundamental importance because it is a mathematical expression for describing the mass spectrum of stars born collectively in “one event.” Here, *one event* means a *gravitationally driven collective process of transformation of the interstellar gaseous matter into stars on a spatial scale of about 1 pc and within about 1 Myr*. Throughout this chapter, such events are referred to as *embedded star clusters*, but they need not lead to gravitationally bound long-lived open or globular clusters. Another astrophysical function of fundamental importance is the star-formation history (SFH) of a stellar system.

The IMF and the SFH are connected through complex self-regulating physical processes on galactic scales, whereby it can be summarized that for late-type galaxies, the star-formation rate (SFR) increases with increasing galaxy mass and the deeper gravitational potential. For early-type galaxies, the same is true except that the SFH was of short duration (\lesssim few Gyr). Together, the IMF and SFH contain the essential information on the transformation of dark gas to shining

stars and the spectral energy distribution thereof. They also contain the essential information on the cycle of matter, which fraction of it is locked up in feeble stars and substellar objects and how much of it is returned enriched with higher chemical elements to the interstellar medium or atmosphere of a galaxy. Knowing the rate with which matter is converted to stars in galaxies is essential for understanding the matter cycle and the matter content in the universe at a fundamental level.

This chapter is meant to outline essentials in IMF work, to document its form which appears to be invariant for the vast majority of resolved star-formation events, and to describe modern evidence for IMF variation and how whole galaxies are to be described as composite or complex populations. The literature on the IMF is vast, and it is unfortunately not possible to cover every research paper on this topic, although some attempt has been made to be as inclusive as possible. [Section 1](#) gives a brief historical review and a short overview of the topic, and pointers to other reviews are provided in [Sect. 1.8](#).

1.1 Solar Neighborhood

Given the importance of the IMF, a major research effort has been invested to distill its shape and variability. It began by first considering the best-known stellar sample, namely, that in the neighborhood of the Sun.

The seminal contribution by Salpeter (1955) while staying in Canberra first described the IMF as a power law, $dN = \xi(m) dm = k m^{-\alpha}$, where dN is the number of stars in the mass interval $m, m + dm$ and k is the normalization constant. By modeling the spatial distribution of the then observed stars with assumptions on the star-formation rate, Galactic-disk structure and stellar evolution timescales, Salpeter arrived at the power-law index (or “slope”) $\alpha = 2.35$ for $0.4 \lesssim m/M_{\odot} \lesssim 10$, which today is known as the “Salpeter IMF”.¹

This IMF form implies a diverging mass density for $m \rightarrow 0$, which was interesting since dark matter was speculated, until the early 1990s, to possibly be made up of faint stars or substellar objects. Studies of the stellar velocities in the solar neighborhood also implied a large amount of missing, or dark, mass in the disk of the Milky Way (MW) (Bahcall 1984). Careful compilation in Heidelberg of the *Gliese Catalogue of Nearby Stars* beginning in the 1960s (Jahreiß and Wielen 1997)² and the application at the beginning of the 1980s of an innovative photographic pencil-beam survey technique reaching deep into the Galactic field in Edinburgh by Reid and Gilmore (1982) significantly improved knowledge of the space density of low-mass stars (LMSs, $m/M_{\odot} \lesssim 0.5$).

Major studies extending Salpeter’s work to lower and larger masses followed, showing that the mass function (MF) of Galactic-field stars turns over below one solar mass thus avoiding the divergence. Since stars with masses $m \lesssim 0.8 M_{\odot}$ do not evolve significantly over the age of the Galactic disk, the MF equals the IMF for these. While the work of Miller and Scalo (1979) relied on using the then-known nearby stellar sample to define the IMF for $m < 1 M_{\odot}$, Scalo (1986) relied mostly on a more recent deep pencil-beam star-count survey using photographic

¹As noted by Zinnecker (2011), Salpeter used an age of 6 Gyr for the MW disk; had he used the now adopted age of 12 Gyr, he would have arrived at a “Salpeter index” $\alpha \approx 2.05$ instead of 2.35.

²The latest version of the catalogue can be found at <http://www.ari.uni-heidelberg.de/datenbanken/aricns/>, while <http://www.nstars.nau.edu/> contains the Nearby Stars (NStars) data base.

plates. Scalo (1986) stands out as the most thorough and comprehensive analysis of the IMF in existence, laying down notation and ideas in use today.

The form of the IMF for low-mass stars was revised in the early 1990s in Cambridge, especially through the quantification of significant nonlinearities in the stellar mass–luminosity relation and evaluation of the bias due to unresolved binary systems (Kroupa et al. 1990, 1991, 1993). This work led to a detailed understanding of the shape of the stellar luminosity function (LF) in terms of stellar physics. It also resolved the difference between the results obtained by Miller and Scalo (1979) and Scalo (1986) through rigorous modeling of all biases affecting local trigonometric-based and distant photometric-parallax-based surveys, such as come from an intrinsic metallicity scatter, evolution along the main sequence, and contraction to the main sequence. In doing so, this work also included an updated local stellar sample and the then best-available deep pencil-beam survey. As such, it stands unique today as being the only rigorous analysis of the late-type-star MF using simultaneously both the *nearby trigonometric parallax* and the *far, pencil-beam* star-count data to constrain the one underlying MF of stars. This study was further extended to an analysis of other ground-based pencil-beam surveys being in excellent agreement with measurements with the HST of the LF through the entire thickness of the MW (• Fig. 4-9 below).

These results ($\alpha \approx 1.3$, $0.1\text{--}0.5 M_{\odot}$) were confirmed by Reid et al. (2002) using updated local star counts that included Hipparcos parallax data. Indeed, the continued, long-term observational effort on nearby stars by Neill Reid, John Gizis and collaborators forms one of the very major pillars of modern IMF work; continued discussion of controversial interpretations has much improved and sharpened our general understanding of the issues. A reanalysis of the nearby mass function of stars in terms of a log-normal form in the mass range $0.07\text{--}1 M_{\odot}$ was provided by Gilles Chabrier, finding agreement to the deep HST star-count data once unresolved multiple stars and a metal-deficient color-magnitude relation for thick-disk M dwarfs are accounted for (Chabrier 2003b). The log-normal form with a power-law extension to high masses is indistinguishable from the older canonical two-part power-law form (see • Fig. 4-24 below). The immense analysis by Bochanski et al. (2010) of the LF and MF of 15×10^6 field low-mass dwarfs ($0.1 \lesssim m/M_{\odot} \lesssim 0.8$) derived from Sloan Digital Sky Survey Data Release 6 photometry using the photometric parallax method again finds good consistency with the previous work on the stellar LF and MF.

The Galactic-field stellar IMF for $0.08 \lesssim m/M_{\odot} \lesssim 1$ can thus be regarded as being reasonably well constrained. It converges to a finite mass density such that low-mass stars cannot be a dynamically significant contributor to the MW disk. The dynamical evidence for significant amounts of dark matter in the disk was finally eroded by Kuijken and Gilmore (1991) and Flynn and Fuchs (1994).

1.2 Star Clusters

In contrast to the Galactic-field sample, where stars of many ages and metallicities are mixed, clusters offer the advantage that the stars have the same age and metallicity and distance. And so a very large effort has been invested to try to extract the IMF from open and embedded clusters as well as from associations.

On the theoretical side, the ever-improving modeling of stellar and BD atmospheres being pushed forward with excellent results notably by the Lyon group (Isabelle Baraffe and Gilles Chabrier) has allowed consistently better constraints on the faint-star MF by a wide variety of

observational surveys.³ Furthermore, the development of high-precision N -body codes that rely on complex mathematical and algorithmic regularization of the equations of motions through the work of Sverre Aarseth and Seppo Mikkola (Aarseth 1999) and others has led to important progress on understanding the variation of the dynamical properties⁴ of stellar populations in individual clusters and the Galactic field.

In general, the MF found for clusters is consistent with the Galactic-field IMF for $m < 1 M_{\odot}$, but it is still unclear as to why open clusters have a significant deficit of white dwarfs (Fellhauer et al. 2003). Important issues are the rapid and violent early dynamical evolution of clusters due to the expulsion of residual gas and the associated loss of a large fraction of the cluster population and the density-dependent disruption of primordial binary systems (Kroupa et al. 2001).

Young clusters have thus undergone a highly complex dynamical evolution which continues into old age (Baumgardt and Makino 2003) and are therefore subject to biases that can only be studied effectively with full-scale N -body methods, thus imposing a complexity of analysis that surpasses that for the Galactic-field sample. The pronounced deficit of BDs and low-mass stars in the 600-Myr-old Hyades are excellent observational proof on how dynamical evolution affects the MF (Bouvier et al. 2008; Röser et al. 2011). While estimating masses of stars younger than a few Myr is subject to major uncertainty,³ differential reddening is also a complicated problem to handle when studying the IMF (► Sect. 2.1).

Important Note

In order to constrain the shape and variation of the IMF from star-count data in clusters, high-precision N -body modeling must be mastered in addition to stellar-evolution theory and knowledge of the properties of multiple stars.

1.3 Intermediate-Mass and Massive Stars

Intermediate-mass and particularly massive stars are rare, and so larger spatial volumes need to be surveyed to assess their distribution by mass.

For intermediate-mass and massive stars, the Scalo (1986) IMF is based on a combination of Galactic-field star counts and OB association data and has a slope $\alpha \approx 2.7$ for $m \gtrsim 2 M_{\odot}$ with much uncertainty for $m \gtrsim 10 M_{\odot}$. The previous determination by Miller and Scalo (1979) also implied a relatively steep field-IMF with $\alpha \approx 2.5$, $1 \leq m/M_{\odot} \leq 10$ and $\alpha \approx 3.3$, $m > 10 M_{\odot}$. Elmegreen and Scalo (2006) point out that structure in the MF is generated at a mass if the SFR of the population under study varies on a timescale comparable to the stellar evolution

³Here, it should be emphasized and acknowledged that the intensive and highly fruitful discourse between Guenther Wuchterl and the Lyon group has led to the important understanding that the classical evolution tracks computed in Lyon and by others are unreliable for ages less than a few Myr (Tout et al. 1999; Wuchterl and Tscharnutter 2003). This comes about because the emerging star's structure retains a memory of its accretion history. In particular, Wuchterl and Klessen (2001) present a SPH computation of the gravitational collapse and early evolution of a solar-type star documenting the significant difference to a pre-main sequence track if the star is instead classically assumed to form in isolation.

⁴The *dynamical properties* of a stellar system are its *mass* and, if it is a multiple star, its orbital parameters (*semimajor axis*, *mass ratio*, *eccentricity*, both inner and outer if it is a higher-order multiple system). See also ► Sect. 2.6.

timescale of its stars near that mass. Artificial structure in the stellar IMF may be deduced in this case, and this effect is particularly relevant for the field IMF. Perhaps the peculiar structure detected by Gouliermis et al. (2005) in the field MF of stars in the Large Magellanic Cloud may be due to this effect.

An interesting finding in this context reported by Massey (1998, 2003) is that the OB stellar population found in the field of the LMC has a very steep MF, $\alpha \approx 4.5$, which can be interpreted to be due to the preferred formation of small groups or even isolated O- and B-type stars (e.g., Selier et al. 2011). Another or an additional effect influencing the deduced shape of the IMF via a changing SFR (Elmegreen and Scalo 2006) is the dynamical ejection of OB stars from dynamically unstable cores of young clusters. This may lead to such a steep IMF because, as dynamical work suggests, preferentially, the less-massive members of a core of massive stars are ejected (Clarke and Pringle 1992; Pflamm-Altenburg and Kroupa 2006). This process would require further study using fully consistent and high-precision N -body modeling of young clusters to see if the observed distribution of field-OB stars can be accounted for with this process alone or if indeed an exotic star-formation mode needs to be invoked to explain some of the observations.

The IMF for intermediate-mass and massive stars deduced from star counts in the field of a galaxy may therefore yield false information on the true shape of the stellar IMF, and stellar samples with well-defined formation histories such as OB associations and star clusters are more useful to constrain the IMF. Photometric surveys of such regions, while essential for reaching faint stars, do not allow a reliable assessment of the mass distribution of massive stars since their spectral energy distribution is largely output at short wavelengths beyond the optical. Spectroscopic classification is therefore an essential tool for this purpose.

Phil Massey's work at Tucson, based on extensive spectroscopic classification of stars in OB associations and in star clusters, demonstrated that for massive stars $\alpha = 2.35 \pm 0.1$, $m \gtrsim 10 M_{\odot}$ (Massey 1998), for a large variety of physical environments as found in the MW and the Magellanic Clouds, namely, OB associations and dense clusters and for populations with metallicity ranging from near-solar abundance to about one tenth metal abundance (► Fig. 4-8 below). The significant differences in the metallicity between the outer and the inner edge of the Galactic disk seem not to influence star-formation, as Yasui et al. (2008) find no apparent difference in the stellar MFs of clusters in the extreme outer Galaxy compared to the rest of the disk down to $0.1 M_{\odot}$.

1.4 The Invariant IMF and Its Conflict with Theory

The thus empirically constrained stellar IMF can be described well by a two-part power-law form with $\alpha_1 = 1.3$ for $m \lesssim 0.5 M_{\odot}$ and with the *Salpeter/Massey index*, $\alpha_2 = 2.35$ for $m \gtrsim 0.5 M_{\odot}$, being remarkably invariant.⁵ This IMF is referred to as the *canonical IMF* and is given in ► Sect. 9.1 as the simpler two-part power-law form by (► 4.55) and as the log-normal plus power-law form by (► 4.56). The empirical result leads to the statement of the following hypothesis:

⁵Note that Scalo (1998) emphasizes that the IMF remains poorly constrained owing to the small number of massive stars in any one sample. This is a true albeit conservative standpoint, and the present authors prefer to accept Massey's result as a working IMF Universality Hypothesis.

Invariant IMF Hypothesis

There exists a universal parent distribution function which describes the distribution of stellar masses in individual star-forming events.

The *Invariant IMF Hypothesis* needs to be tested with star-count data in galactic fields and in individual clusters and OB associations for possible significant deviations. But it is mandatory to take into account the biases listed in [Sect. 2.1](#) when doing so.

The *Invariant IMF Hypothesis* is not consistent with theory (see also [Sects. 11.1](#) and [12](#)). There are two broad theoretical ansatzes for the origin of stellar masses:

The Jeans-Mass Ansatz: According to the Jeans-mass argument (e.g., Jeans 1902; Larson 1998; Bate and Bonnell 2005; Bonnell et al. 2006, ([4.50](#)) below), star formation at lower metallicity ought to produce stars of, on average, heavier mass and thus an effectively top-heavy IMF (i.e., the ratio between the number of massive stars and low mass stars ought to increase). At lower metallicity, the cooling is less efficient causing larger Jeans masses as a requirement for gravitational collapse to a protostar and thus larger stellar masses. That warmer gas produces an IMF shifted to larger masses has been demonstrated with state-of-the art SPH simulations (e.g., Klessen et al. 2007).

The Self-Regulatory Ansatz: Another approach is formulated by Adams and Fatuzzo (1996) who argue that the Jeans-Mass Ansatz is invalid since there is no preferred Jeans mass in a turbulent molecular cloud. Instead, they invoke the central-limit theorem⁶ together with self-regulated assembly, and they suggest that the final stellar masses are given by the balance between feedback energy from the forming star (accretion luminosity, outflows) and the rate of accretion from the proto-stellar envelope and circum-stellar disk. As the protostar builds up its luminosity increases until the accretion is shut off. When shutoff occurs depends on the accretion rate. Indeed, Basu and Jones (2004) explain the observed power-law extension of the IMF at large stellar masses as being due to a distribution of different accretion rates. The self-regulating character of star formation has been studied profusely by the group around Christopher McKee (e.g., Tan et al. 2006) and has been shown to lead to decreasing star-formation efficiencies with increasing metallicity (Dib et al. 2010, 2011; Dib 2011). In low-metallicity gas, the coupling of the photons to the gas is less efficient, causing a less effective opposition against the accreting material. And, at lower metallicity, the cooling is reduced, causing a higher temperature of the gas and thus a higher speed of sound with a larger accretion rate. The final stellar IMF is expected to be populated by more massive stars in metal-poor environments.

Both approaches can be refined by studying a distribution of physical conditions in a given star-forming cloud, but both lead to the same conclusion, namely, that low metallicity and

⁶Citing from Basu and Jones (2004), “According to the central limit theorem of statistics, if the mass of a protostellar condensation $M_c = f_1 \times f_2 \times \dots \times f_N$, then the distribution of M_c tends to a lognormal regardless of the distributions of the individual physical parameters f_i ($i = 1, \dots, N$), if N is large. Depending on the specific distributions of the f_i , a convergence to a lognormal may even occur for moderate N .” The central limit theorem was invoked for the first time by Zinnecker (1984) to study the form of the IMF from hierarchical fragmentation of collapsing cloud cores.

high temperature ought to produce top-heavy stellar IMFs. This leads to the following robust theoretical IMF result:

The Variable IMF Prediction

Both the Jeans-mass and the self-regulation arguments invoke very different physical principles, and yet they lead to the same result: The IMF ought to become top-heavy under low-metallicity and high-temperature star-forming conditions.

Star formation in the very early universe must have therefore produced top-heavy IMFs (Bromm et al. 2001; Clark et al. 2011). But the samples of simple-stellar populations spanning all cosmological epochs (globular clusters to current star-formation in embedded clusters) available in the Local Group of galaxies have until recently not shown convincing evidence supporting The Variable-IMF Prediction. This issue is addressed in more detail in [Sect. 12.9](#).

1.5 Philosophical Note

Much of the current discussion on star formation, from the smallest to the largest (galaxy-wide) scales, can be categorized into two broad conceptual approaches which are related to the Jeans-Mass Ansatz versus the Self-Regulatory Ansatz of [Sect. 1.4](#):

Approach A is related to the notion that star formation is inherently stochastic such that the IMF is a probabilistic distribution function only. This is a natural notion under the argument that the processes governing star-formation are so many and complex that the outcome is essentially stochastic in nature. Followers of this line of reasoning argue for example that massive stars can form in isolation and that the mass of the most massive star cluster forming in a galaxy depends on the time-scale over which an ensemble of star clusters is considered (the *size-of-sample effect*, even at very low SFRs a galaxy would produce a very massive star cluster if one waits long enough, i.e., if the sample of clusters is large enough). Approach A can be formulated concisely as *nature plays dice when stars form*.

Approach B is related to the notion that nature is inherently self-regulated and deterministic. This is a natural notion given that physical processes must always depend on the boundary conditions which are a result of the physical processes at hand. An example of such would be gravitationally-driven growth processes with feedback in media with limited resources. The emerging phenomena such as the distribution of stellar masses, of star-cluster masses and/or of how phase-space is populated to make binary stellar systems are, at least in principle, computable. They are computable in the sense that statistical mathematics provides the required tools such that the distribution functions used to describe the outcomes are subject to constraints. For example, a young stellar population of mass M_{ecl} is excellently described by $\xi(m)$ with the condition $m \leq m_{\text{max}}(M_{\text{ecl}})$. However, purely random sampling from $\xi(m)$ even under this constraint will not reproduce a realistic population if nature follows Optimal Sampling (p. 132). This is because Optimal Sampling will never allow a cluster to be made up of $M_{\text{ecl}}/m_{\text{max}}$ stars of mass m_{max} , while constrained random sampling would. Approach B can be formulated concisely as *nature does not play dice when stars form*.

Depending on which of the two notions is applied, the resulting astrophysical description of galaxies leads to very diverging results. Either a galaxy can be described as an object in which stars form purely stochastically such that the galaxy-wide IMF is equal to the stellar IMF (Approach A). In this case, a thousand small groups of 20 pre-main sequence stars will have the same stellar IMF as one very young star cluster containing 20,000 stars, or an embedded cluster or a galaxy is understood to be a highly self-regulated system such that the galaxy-wide IMF differs from the stellar IMF (Approach B, [Sect. 13.1](#)). According to this notion, a thousand small groups of 20 pre-main sequence stars would not contain a single star with $m > 5 M_{\odot}$, while a very young star cluster of 20,000 stars would contain many such stars. The different approaches have very different implications for understanding the matter cycle in the universe.

1.6 Hypothesis Testing

The studies aimed at constraining the stellar IMF observationally typically have the goal of testing the Invariant IMF Hypothesis (p. 123) either in individual star-forming events such as in a star clusters or on galaxy-wide scales. Here, it is important to be reminded of the following:

Elementary Logics of Hypothesis Testing

Negation of a hypothesis I does not imply that the alternative hypothesis II is correct.

By showing that hypothesis I is consistent with some data does *not* imply that an alternative hypothesis II is therewith ruled out. A case in point is the discussion about dark matter and dark energy: Ruling out the standard cosmological (LCDM) model does not imply that any particular alternative is correct (Kroupa et al. 2010; Kroupa 2012). Conversely, ruling out a particular alternative does not imply that the LCDM model is correct (Wojtak et al. 2011).

Concerning the IMF, if a purely stochastic model (approach A, [Sect. 1.5](#)) is consistent with some observational data, then this does not imply that the alternative (optimal sampling, which is related to approach B) is falsified.

A case in point is provided by the following example relevant for the tests of the IGIMF theory on p. 231: The masses of an ensemble of observed dwarf galaxies are calculated from spectral energy distribution modeling using the universal canonical IMF. These masses are then applied in testing a possible variation of the galaxy-wide IMF in terms of the UV and H α flux ratios. If the universal IMF calculations allow for fluctuating SFRs whereas the variable IMF calculations do not, then the (wrong) conclusion of such an approach would plausibly be that nature appears to play dice because observational data naturally contain measurement uncertainties which act as randomization agents.

The consistent approach would instead be to compute the galaxy masses assuming a variable galaxy-wide IMF to test whether the hypothesis that the IMF varies systematically with galaxy mass can be discarded. The logically consistent procedure would be to calculate all fluxes within both scenarios independently of each other and assuming in both that the SFR can fluctuate and to test these calculations against the observed fluxes. The result of this consistent procedure is opposite to those of the above inconsistent procedure in that the data are in better agreement with the systematically variable IMF, that is, that nature does not play dice.

A final point to consider is when a hypothesis ought to be finally discarded. Two examples illustrate this: Consider the Taurus-Auriga and Orion star-forming clouds. Here, the number of stars with $m \gtrsim 1 M_{\odot}$ is significantly below the expectation from the purely stochastic model (see box IGIMF predictions/tests on p. 231). This unambiguously falsifies the stochastic model. But the data are in excellent agreement with the expectation from the IGIMF theory. Is it then meaningful to nevertheless keep adopting the stochastic model on cluster and galaxy problems? Another example, being perhaps more relevant to [Sect. 1.5](#), is the issue with the current standard cosmological model. It is ruled out by Peebles and Nusser (2010) and Kroupa (2012). Should it nevertheless be adopted in further cosmological and related research?

1.7 About This Text

As is evident from the above introduction, the IMF may be well defined and is quite universal in each star-forming event out of which comes a spatially and temporally well-correlated set of stars. But many such events will produce a summed IMF which may be different because the individual IMFs need to be added whereby the distribution of the star-formation events in mass, space, and time becomes an issue. It thus emerges that it is necessary to distinguish between simple stellar populations and composite populations. Some definitions are useful:

Definitions

- A *simple population* obtains from a spatially (\lesssim few pc) and temporarily (\lesssim Myr) correlated star-formation event (CSFE, also referred to as a *collective star formation event*, being essentially an embedded star cluster). The mass of a CSFE may range from a few solar masses (a few binary stars) upwards.
- A *composite* or *complex population* consists of more than one simple population.
- The *stellar IMF* refers to the IMF of stars in a simple population.
- A *composite* or *integrated IMF* is the IMF of a composite or complex population, that is, a population composed of many CSFEs, most of which may be gravitationally unbound. The galaxy-wide version is the IGIMF ([Sect. 13.1](#)).
- The PDMF is the present-day MF of a stellar population not corrected for stellar evolution nor for losses through stellar deaths. Note that a *canonical PDMF* is a PDMF derived from a canonical IMF.
- A *stellar system* can be a multiple star or a single star. It has *dynamical properties* (footnote 4 on p. 121).
- The *system luminosity* or *mass function* is the LF or MF obtained by counting all stellar systems. The *stellar LF* or *stellar MF* is the true distribution of all stars in the sample, thereby counting all individual companions in multiple systems. This is also referred to as the *individual-star LF/MF*.
- Note $1 \text{ km/s} = 1.0227 \text{ pc/Myr}$, $1 \text{ g cm}^{-3} = 1.478 \times 10^{22} M_{\odot} \text{ pc}^{-3}$, and $1 \text{ g cm}^{-2} = 4788.4 M_{\odot} \text{ pc}^{-2}$ for a solar-metallicity gas.
- The following additional abbreviations are used: SFR = star formation rate in units of $M_{\odot} \text{ year}^{-1}$; SFH = star formation history = SFR as a function of time; SFRD = star formation rate density in units of $M_{\odot} \text{ year}^{-1} \text{ pc}^{-3}$.

This treatise provides an overview of the general methods used to derive the IMF with special attention on the pitfalls that are typically encountered. The binary properties of stars and of brown dwarfs are discussed as well because they are essential to understand the true shape of the stellar IMF. While the stellar IMF appears to have emerged as being universal in star-formation events as currently found in the Local Group of galaxies, the recent realization that star clusters limit the mass spectrum of their stars is one form of IMF variation and has interesting implications for the formation of stars in a cluster and leads to the insight that composite populations must show IMFs that differ from the stellar IMF in each cluster. With this finale, this treatise reaches the cosmological arena.

1.8 Other IMF Reviews

The seminal contribution by Scalo (1986) on the IMF remains a necessary source for consultation on the fundamentals of the IMF problem. The landmark review by Massey (2003) on massive stars in the Local Group of galaxies is an essential read, as is the review by Zinnecker and Yorke (2007) on massive-star formation. Other reviews of the IMF are by Scalo (1998), Kroupa (2002), Chabrier (2003a), Bonnell et al. (2007), Elmegreen (2009), and Bastian et al. (2010). The proceedings of the “38th Herstmonceux Conference on the Stellar Initial Mass Function” (Gilmore and Howell 1998) and the proceedings of the “IMF50” meeting in celebration of Ed Salpeter’s 80th birthday (Corbelli et al. 2005) contain a wealth of important contributions to the field. A recent major but also somewhat exclusive conference on the IMF was held from June 20–25, 2010, in Sedona, Arizona, for researchers to discuss the recently accumulating evidence for IMF variations: “UP2010: Have Observations Revealed a Variable Upper End of the Initial Mass Function?” The published contributions are a unique source of information on this problem (Treyer et al. 2011). A comprehensive review of extreme star formation is available by Turner (2009).

2 Some Essentials

Assuming the relevant biases listed in Sect. 2.1 have been corrected for such that all binary and higher-order stellar systems can be resolved into individual stars in some complete population such as the solar neighborhood and that only main-sequence stars are selected for, then the number of single stars per pc^3 in the mass interval m to $m + dm$ is $dN = \Xi(m) dm$, where $\Xi(m)$ is the *present-day mass function* (PDMF). The number of single stars per pc^3 in the absolute P-band magnitude interval M_P to $M_P + dM_P$ is $dN = -\Psi(M_P) dM_P$, where $\Psi(M_P)$ is the stellar luminosity function (LF) which is constructed by counting the number of stars in the survey volume per magnitude interval and P signifies an observational photometric passband such as the V- or I-band. Thus,

$$\Xi(m) = -\Psi(M_P) \left(\frac{dm}{dM_P} \right)^{-1}. \quad (4.1)$$

Note that the minus sign comes in because increasing mass leads to decreasing magnitudes and that the LF constructed in one photometric passband P can be transformed into another band P' by

$$\Psi(M_P) = \frac{dN}{dM_{P'}} \frac{dM_{P'}}{dM_P} = \Psi(M_{P'}) \frac{dM_{P'}}{dM_P} \quad (4.2)$$

if the function $M_{p'} = \text{fn}(M_p)$ is known. Such functions are equivalent to color–magnitude relations.

Since the derivative of the stellar mass–luminosity relation (MLR), $m(M_p) = m(M_p, Z, \tau, \mathbf{s})$, enters the calculation of the MF, any uncertainties in stellar structure and evolution theory on the one hand (if a theoretical MLR is relied upon) or in observational ML-data on the other hand will be magnified accordingly. This problem cannot be avoided if the mass function is constructed by converting the observed stellar luminosities one by one to stellar masses using the MLR and then binning the masses because the derivative of the MLR nevertheless creeps in through the binning process because *equal luminosity intervals are not mapped into equal mass intervals*. The dependence of the MLR on the star’s chemical composition, Z , its age, τ , and spin vector \mathbf{s} is explicitly stated here since stars with fewer metals than the Sun are brighter (lower opacity), main-sequence stars brighten with time and loose mass, and rotating stars are dimmer because of the reduced internal pressure. Mass loss and rotation are significant factors for intermediate and especially high-mass stars (Penny et al. 2001).

The IMF, or synonymously here the IGIMF (Sect. 13.1), follows by correcting the observed number of main-sequence stars for the number of stars that have evolved off the main sequence. Defining $t = 0$ to be the time when the Galaxy that now has an age $t = \tau_G$ began forming, the number of stars per pc^3 in the mass interval $m, m + dm$ that form in the time interval $t, t + dt$ is $dN = \xi(m; t) dm b'(t) dt$, where the expected time dependence of the IMF is explicitly stated (Sect. 13.1) and where $b'(t) = b(t)/\tau_G$ is the normalized star-formation history, $(1/\tau_G) \int_0^{\tau_G} b(t) dt = 1$. Stars that have main-sequence lifetimes $\tau(m) < \tau_G$ leave the stellar population unless they were born during the most recent time interval $[\tau_G - \tau(m), \tau_G]$. The number density of such stars still on the main sequence with initial masses computed from their present-day masses and their ages in the range $m, m + dm$ and the total number density of stars with $\tau(m) \geq \tau_G$ are, respectively,

$$\Xi(m) = \xi(m) \frac{1}{\tau_G} \times \begin{cases} \int_{\tau_G - \tau(m)}^{\tau_G} b(t) dt & , \quad \tau(m) < \tau_G, \\ \int_0^{\tau_G} b(t) dt & , \quad \tau(m) \geq \tau_G, \end{cases} \quad (4.3)$$

where the time-averaged IMF, $\xi(m)$, has now been defined. Thus, for low-mass stars $\Xi = \xi$, while for a subpopulation of massive stars that has an age $\Delta t \ll \tau_G$, $\Xi = (\Delta t/\tau_G) \xi$ for those stars of mass m for which the main-sequence lifetime $\tau(m) > \Delta t$, indicating how an observed high-mass IMF in an OB association, for example, has to be scaled to the Galactic-field IMF for low-mass stars, assuming continuity of the IMF. In this case, the different spatial distribution via different disk-scale heights of old and young stars also needs to be taken into account, which is done globally by calculating the stellar surface density in the MW disk (Miller and Scalo 1979; Scalo 1986). Thus, we can see that joining the cumulative low-mass star counts to the snap-shot view of the massive-star IMF is nontrivial and affects the shape of the IMF in the notorious mass range $\approx 0.8\text{--}3 M_\odot$, where the main-sequence lifetimes are comparable to the age of the MW disk (Fig. 4-26, bottom panel). For a population in a star cluster or association with an age $\tau_{cl} \ll \tau_G$, τ_{cl} replaces τ_G in (4.3). Examples of the time modulation of the IMF are $b(t) = 1$ (constant star-formation rate) or a Dirac-delta function, $b(t) = \delta(t - t_0)$ (all stars formed at the same time t_0).

The stellar IMF can conveniently be written as an arbitrary number of power-law segments,

$$\xi_{BD} = k k_{BD} \left(\frac{m}{m_1} \right)^{-\alpha_0}, \quad (4.4)$$

$$\xi_{\text{star}}(m) = k \begin{cases} \left(\frac{m}{m_1}\right)^{-\alpha_1} & , \quad m_1 < m \leq m_2 \quad , \quad n = 1, \\ \left[\prod_{i=2}^{n \geq 2} \left(\frac{m_i}{m_{i-1}}\right)^{-\alpha_{i-1}}\right] \left(\frac{m}{m_n}\right)^{-\alpha_n} & , \quad m_n < m \leq m_{n+1} \quad , \quad n \geq 2, \end{cases} \quad (4.5)$$

where k_{BD} and k contain the desired scaling, $0.01 M_{\odot}$ is about the minimum mass of a BD (see footnote 15 on p. 187), and the mass ratios ensure continuity. Here, the separation into the IMF of BDs and of stars has already been explicitly stated (see [Sect. 8](#)).

Often used is the “logarithmic mass function” ([Table 4-3](#) below),

$$\xi_L(m) = (m \ln 10) \xi(m), \quad (4.6)$$

where $dN = \xi_L(m) d\ln m$ is the number of stars with mass in the interval $\ln m, \ln m + d\ln m$ ($\ln m \equiv \log_{10} m$).⁷

The stellar mass of a an embedded cluster, M_{ecl} , can be used to investigate the expected number of stars above a certain mass m ,

$$N(> m) = \int_m^{m_{\text{max}^*}} \xi(m') dm', \quad (4.7)$$

with the mass in stars of the whole (originally embedded) cluster, M_{ecl} , being calculated from

$$M_{1,2} = \int_{m_1}^{m_2} m' \xi(m') dm', \quad (4.8)$$

with $M_{\text{ecl}} = M_{1,2}$ for $m_1 = m_{\text{low}} \approx 0.07 M_{\odot}$ (about the hydrogen burning mass limit) and $m_2 = m_{\text{max}^*} = \infty$ (the *Massey assertion*, p. 145, but see [Sect. 3.3](#)). There are two unknowns ($N(> m)$ and k) that can be solved for by using the two equations above.

It should be noted that the IMF is not a measurable quantity: Given that we are never likely to learn the exact dynamical history of a particular cluster or population, it follows that we can *never* ascertain the IMF for any individual cluster or population. This can be summarized concisely with the following theorem:

The IMF Unmeasurability Theorem

The IMF cannot be extracted directly for any individual stellar population.

Proof: For clusters younger than about 1 Myr, star formation has not ceased, and the IMF is therefore not assembled yet, and the cluster cores consisting of massive stars have already dynamically ejected members (Pflamm-Altenburg and Kroupa 2006). Massive stars ($m \gtrsim 30 M_{\odot}$) leave the main sequence before they are fully assembled (Maeder and Behrend 2002). For clusters with an age between 0.5 and a few Myr, the expulsion of residual gas has lead to a loss of stars (Kroupa et al. 2001). Older clusters are either still loosing stars due to residual gas expulsion or are evolving secularly through evaporation driven by energy equipartition (Vesperini and Heggie 1997; Baumgardt and Makino 2003). There exists thus no time when all stars are assembled in an observationally accessible volume (i.e., a star cluster). An observer is never able to access all phase-space variables of all potential members of an OB association. The field population is a mixture of many star-formation events whereby it can practically not be proven that a complete population has been documented. \square

⁷Note that Scalo (1986) calls $\xi_L(m)$ the *mass function* and $\xi(m)$ the *mass spectrum*.

Note that the IMF Unmeasurability Theorem implies that individual clusters cannot be used to make deductions on the similarity or not of their IMFs, unless a complete dynamical history of each cluster is available.

Notwithstanding this pessimistic theorem, it is nevertheless necessary to observe and study star clusters of any age. Combined with thorough and realistic N -body modeling, the data do lead to essential *statistical* constraints on the IMF Universality Hypothesis (p. 189, see also p. 123).

2.1 Unavoidable Biases Affecting IMF Studies

Past research has uncovered a long list of biases that affect the conversion of the observed distribution of stellar brightnesses to the underlying stellar IMF. These are just as valid today, and in particular, analysis of the GAIA-space-mission data will need to take the relevant ones into account before the stellar IMF can be constrained anew. The list of all unavoidable biases affecting stellar IMF studies is provided here with key references addressing these:

Malmquist bias (affects MW-field star counts): Stars of the same mass but with different ages, metallicities, and spin vectors have different colors and luminosities which lead to errors in distance measurements in flux-limited field star counts using photometric parallax (Stobie et al. 1989).

Color-magnitude relation (affects MW-field star counts): Distance measurements through photometric parallax are systematically affected if the true color-magnitude relation of stars deviates from the assumed relation (Reid and Gizis 1997) (but see footnote 14 on p. 162).

Lutz–Kelker bias (affects MW-field star counts): A distance-limited survey is affected by parallax measurement uncertainties such that the spatial stellar densities are estimated wrongly (Lutz and Kelker 1973). Correcting for this bias will be required when analyzing GAIA-space mission star-count data.

Unresolved multiple stars (affects all star counts): Companions to stars can be missed because their separation is below the resolution limit or because the companion's luminosity is below the flux limit (Kroupa et al. 1991). When using photometric parallax to determine distances and space densities, unresolved multiple systems appear nearer and redder. This affects the measured disk scale height as a function of stellar spectral type (Kroupa et al. 1993). Missed companions have a significant effect on the deduced shape of the IMF for $m \lesssim 1 M_{\odot}$ (Kroupa et al. 1991, 1993; Malkov and Zinnecker 2001) but do not significantly affect the shape of the stellar IMF for more massive stars (Maíz Apellániz and Úbeda 2005; Weidner et al. 2009).

Stellar mass–luminosity relation (MLR, affects all star counts): Main sequence stars of precisely the same chemical composition, age, and spins follow one perfect mass–luminosity relation. Its nonlinearities map a featureless stellar IMF to a structured LF, but theoretical MLRs are not reliable (Kroupa et al. 1990). An ensemble of field stars do not follow one stellar mass–luminosity relation such that the nonlinearities in it that map to structure in the stellar LF are smeared out (Kroupa et al. 1993). Correcting for this bias will be required when analyzing GAIA-space mission star-count data. Pre-main sequence stars have a complicated and time-varying mass–luminosity relation (Piskunov et al. 2004).

Varying SFH (affects all star counts): Variations of the SFH of a population under study over a characteristic time scale leads to structure in the deduced IMF at a mass scale at

which stars evolve on that time scale, if the observer wrongly assumes a constant SFH (Elmegreen and Scalo 2006).

Stellar evolution (affects all star counts): Present-day stellar luminosities must be transformed to initial stellar masses. This relies on stellar-evolution theory (Scalo 1986).

Binary-stellar evolution (affects all star counts): Present-day stellar luminosities must be transformed to initial stellar masses, but this may be wrong if the star is derived from an interacting binary. If important, then this only affects the massive-star IMF (F. Schneider and R. Izzard, private communication).

Pre-main sequence evolution (affects all populations with stars younger than a few 10^8 year): In young star clusters, the late-type stellar luminosities need to be corrected for the stars not yet being on the main sequence (e.g., Hillenbrand and Carpenter 2000). Pre-main sequence evolution tracks are highly uncertain for ages $\lesssim 1$ Myr (Tout et al. 1999; Wuchterl and Tscharnuter 2003). Field star-count data contain an admixture of young stars which bias the star counts (Kroupa et al. 1993).

Differential reddening (affects embedded star clusters): Patchily distributed gas and dust affects mass estimation. Variable extinction necessitates the introduction of an extinction limit which increases the lower mass limit to which the survey is complete (Andersen et al. 2009).

Binning: Deriving the IMF power-law index from a binned set of data is prone to significant bias caused by the correlation between the assigned weights and the number of stars per bin. Two solutions have been proposed: variable-sized binning (Maíz Apellániz and Úbeda 2005) and newly developed (effectively) bias-free estimators for the exponent and the upper stellar mass limit (Maschberger and Kroupa 2009).

Crowding (affects star counts in star clusters): A compact faraway star cluster can lead to crowding and superpositions of stars which affects the determination of the IMF systematically (Maíz Apellániz 2008).

Early and late star cluster evolution (affects star-counts in star clusters): A large fraction of massive stars are ejected from the cluster core skewing the MF in the cluster downward at the high-mass end (Pflamm-Altenburg and Kroupa 2006; Banerjee et al. 2012). When the residual gas is blown out of initially mass-segregated young clusters, they preferentially lose low-mass stars within a few Myr (Marks et al. 2008). Old star clusters evolve through energy equipartition driven evaporation of low-mass stars (Vesperini and Heggie 1997; Baumgardt and Makino 2003).

2.2 Discretizing an IMF: Optimal Sampling and the $m_{\max} - M_{\text{ecl}}$ Relation

In view of [Sects. 1.4](#) and [1.5](#), it is clearly necessary to be able to set up and to test various hypothesis as to how a stellar population emanates from a star-formation event. Two extreme hypotheses are (1) the stars born together are always perfectly distributed according to the stellar IMF and (2) the stars born together represent a random draw of masses from the IMF. Here, one method of perfectly distributing the stellar masses according to the form of the IMF is discussed. [Section 2.3](#) describes how to generate a random population of stars highly efficiently.

Note that throughout this chapter, the relevant physical quantity of a population is taken to be its mass and *never* the number of stars, N , which is not a physical quantity.

It is useful to consider the concept of optimally sampling a distribution function. The problem to be addressed is that there is a mass reservoir, M_{ecl} , which is to be distributed according to the IMF such that no gaps arise.

Ansatz: Optimal Sampling

Given a predefined form of a continuous distribution function, $\xi(m)$, of the variable $m \in [m_L, m_U]$ (Note: $m_U = m_{\text{max}*}$ is adopted here for brevity of notation) such that $m_2 > m_1 \implies \xi(m_1) > \xi(m_2) > 0$, then the physical reservoir M_{ecl} is *optimally distributed* over $\xi(m)$ if the maximum available range accessible to m is covered with the condition that a m occurs once above a certain limit $m_{\text{max}} \in [m_L, m_U]$, $\int_{m_{\text{max}}}^{m_U} \xi(m) dm = 1$.

We define $\xi(m) = k p(m)$, where $p(m)$ is the density distribution function of stellar masses. The last statement in the above ansatz implies $k = 1/(\int_{m_{\text{max}}}^{m_U} p(m) dm)$. Since the total mass in stars, $M_* = k \int_{m_L}^{m_{\text{max}}} m p(m) dm$, one obtains

$$M_* = \frac{\int_{m_L}^{m_{\text{max}}} m p(m) dm}{\int_{m_{\text{max}}}^{m_U} p(m) dm}.$$

It thus follows immediately that $m'_{\text{max}} > m_{\text{max}} \implies M_* > M_{\text{ecl}}$ and also $m'_{\text{max}} < m_{\text{max}} \implies M_* < M_{\text{ecl}}$. Thus, only $m'_{\text{max}} = m_{\text{max}} \implies M_* = M_{\text{ecl}}$. The concept of optimal sampling appears to be naturally related to how M_{ecl} is divided up among the stars: The largest chunk goes to m_{max} , and the rest is divided up hierarchically among the lesser stars (see Open Question II on p. 150).

The above ansatz can be extended to a discretized optimal distribution of stellar masses: Given the mass, M_{ecl} , of the population, the following sequence of individual stellar masses yields a distribution function which exactly follows $\xi(m)$,

$$m_{i+1} = \int_{m_{i+1}}^{m_i} m \xi(m) dm, \quad m_L \leq m_{i+1} < m_i, \quad m_1 \equiv m_{\text{max}}. \quad (4.9)$$

The normalization and the most massive star in the sequence are set by the following two equations:

$$1 = \int_{m_{\text{max}}}^{m_{\text{max}*}} \xi(m) dm, \quad (4.10)$$

with

$$M_{\text{ecl}}(m_{\text{max}}) - m_{\text{max}} = \int_{m_L}^{m_{\text{max}}} m \xi(m) dm \quad (4.11)$$

as the closing condition. These two equations need to be solved iteratively. An excellent approximation is given by the following formula (equation 10 in Pflamm-Altenburg et al. 2007, assuming $m_{\text{max}*} = 150 M_{\odot}$):

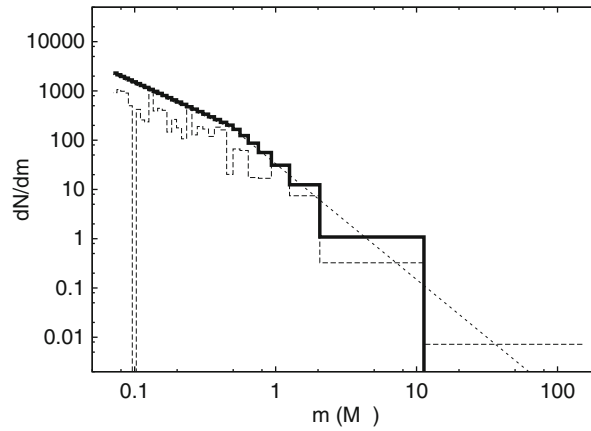
$$\log_{10} \left(\frac{m_{\text{max}}}{M_{\odot}} \right) = 2.56 \log_{10} \left(\frac{M_{\text{ecl}}}{M_{\odot}} \right) \left(3.82^{9.17} + \left[\log_{10} \left(\frac{M_{\text{ecl}}}{M_{\odot}} \right) \right]^{9.17} \right)^{-\frac{1}{9.17}} - 0.38. \quad (4.12)$$

Note that (4.11) contains a correction term m_{max} : The mass, M_{ecl} , between m_L and m_{max} does not include the star with m_{max} as this star lies between m_{max} and $m_{\text{max}*}$. The semi-analytical calculation of the $m_{\text{max}} - M_{\text{ecl}}$ relation by Kroupa and Weidner (2003) and

Weidner et al. (2010) is less accurate by not including the correction term m_{\max} . The correction turns out to be insignificant as both semi-analytical relations are next to identical (► Fig. 4-2) and are a surprisingly good description of the observational data (► Fig. 4-5).

► Equation 4.9 defines, here for the first time, how to sample the IMF perfectly in the sense that the stellar masses are spaced ideally such that no gaps arise and the whole accessible range m_L to m_{\max} is fully filled with stars. This is referred to as optimal sampling (see also equation 8.2 in Aarseth 2003 for a related concept). The disadvantage of this method is that the target mass M_{ecl} cannot be achieved exactly because it needs to be distributed into a discrete number of stars. The mass of the generated stellar population is M_{ecl} to within $\pm m_L$ ($\equiv m_{\text{low}} \approx 0.07 M_{\odot}$ for most applications) because the integral (► 4.9) is integrated from m_{\max} downward.⁸

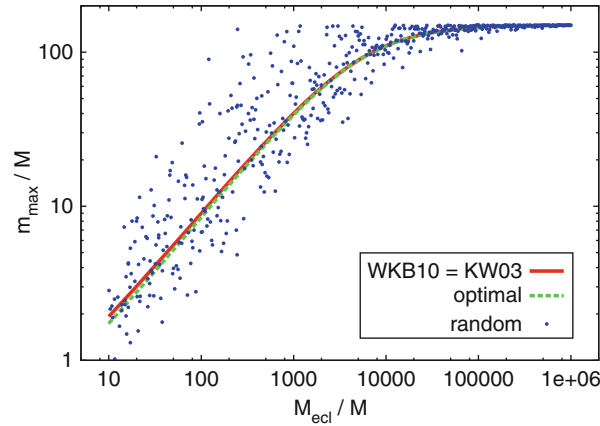
► Figure 4-1 demonstrates how an IMF constructed using optimal sampling compares to one generated with random sampling from the IMF for a population with $M_{\text{ecl}} = 150 M_{\odot}$. ► Figures 4-2 and ► 4-3, respectively, show $m_{\max} - M_{\text{ecl}}$ and average stellar mass model data using both sampling techniques.



■ Fig. 4-1

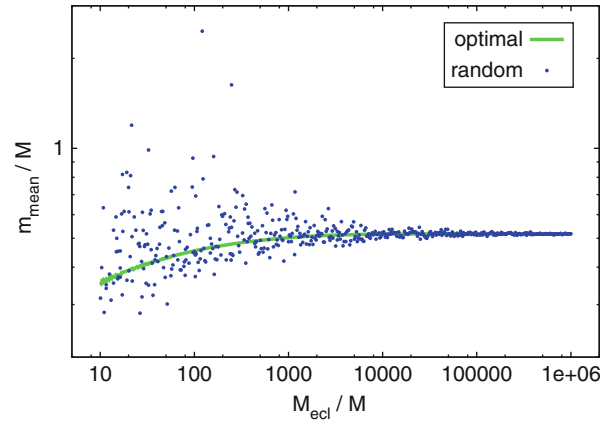
Stellar IMF (dN/dm) versus stellar mass (m) for a $M_{\text{ecl}} = 149.97 M_{\odot}$ cluster. The *thin dashed line* is the analytical canonical IMF (► 4.55). The *thick histogram* is a population of individual stars generated according to optimal sampling (► 4.9), starting with $m_{\max} = 12 M_{\odot}$ (► 4.12). The optimally sampled population contains 322 stars. The mass-dependent bin width is chosen to ensure that ten stars are in each bin. The *thin dashed histogram* is a population of stars chosen randomly from the IMF using the mass-generating function (► Sect. 2.3) with $M_{\text{ecl}} = 150.22 M_{\odot}$ being reached without an upper limit ($m_{\max} = \infty$). This population contains 140 stars. The same bins are used as in the *thick solid histogram*. Note how optimal sampling perfectly reproduces the IMF while random sampling shows deviations in the form of gaps. Which is closer to reality (remembering that observational data contain uncertainties that act as randomization agents)?

⁸The publicly available C program Optimf allowing the generation of a stellar population of mass M_{ecl} is available at <http://www.astro.uni-bonn.de/en/download/software/>



■ Fig. 4-2

The maximum stellar mass, m_{\max} , is plotted against the stellar mass of the population, M_{ecl} , for optimal sampling (short-dashed green line) and for randomly drawing a population of stars from the IMF (filled blue circles). For each sampling method, 100 populations are generated per dex in M_{ecl} . The canonical physical maximum stellar mass, $m_{\max*} = 150 M_{\odot}$, is assumed. The semi-analytical $m_{\max} - M_{\text{ecl}}$ relation from Kroupa and Weidner (2003) and Weidner et al. (2010) (red solid curve) and the corrected version from (4.12) (green dashed curve) are nearly identical. Which is closer to reality, random or optimal sampling from the IMF? The small scatter in the observational $m_{\max} - M_{\text{ecl}}$ relation (Fig. 4-5) and the small scatter in observationally derived IMF power-law indices around the Salpeter value (Fig. 4-27, Open Question III on p. 195) suggest that optimal sampling may be a more realistic approach to nature than purely random sampling



■ Fig. 4-3

The average stellar mass of stellar populations of mass M_{ecl} generated with optimal sampling and random sampling from the IMF; otherwise as Fig. 4-2. Note the extreme random deviations from the canonical IMF if it is interpreted to be a probabilistic distribution function

Important Hint

Nature may be preferring optimal sampling. This is evident from the quite tight observational $m_{\max} - M_{\text{ecl}}$ data (► Fig. 4-5), from Open Question III (p. 195) and from the Sociological Hypothesis (p. 196). Theoretical support that nature may not be playing dice comes from the emergence of the $m_{\max} - M_{\text{ecl}}$ relation in SPH and FLASH computations of star formation in turbulent molecular clouds (see the BVB conjecture on p. 148).

2.3 Discretizing an IMF: Random Sampling and the Mass-Generating Function

In order to randomly discretize a stellar population, we need to be able to generate stellar masses independently of each other. This can be done with constraints (e.g., ensuring that the $m_{\max} - M_{\text{ecl}}$ relation is fulfilled by applying $m \leq m_{\max}(M_{\text{ecl}})$ or that stellar masses $m \leq m_{\max*} \approx 150 M_{\odot}$) or without constraints ($m_{\max} = \infty$). This is achieved via the mass-generating function. A *mass-generating function* is a mapping from a uniformly distributed random variable X to the stellar mass which is distributed according to the IMF. Generating functions allow efficient random discretization of continuous distributions (see Kroupa 2008 for more details).

A generating function can be written in the following way. Assume the probability distribution function depends on the variable $\zeta_{\min} \leq \zeta \leq \zeta_{\max}$ (in this case the stellar mass, m). Consider the probability, $X(\zeta)$, of encountering a value for the variable in the range ζ_{\min} to ζ ,

$$X(\zeta) = \int_{\zeta_{\min}}^{\zeta} p(\zeta') d\zeta', \quad (4.13)$$

with $X(\zeta_{\min}) = 0 \leq X(\zeta) \leq X(\zeta_{\max}) = 1$ and $p(\zeta)$ is the probability distribution function, or probability density, normalized such that the latter equal sign holds ($X = 1$). For the two-part power-law IMF, the corresponding probability density is

$$\begin{aligned} p_1(m) &= k_{p,1} m^{-\alpha_1}, \quad 0.07 \leq m \leq 0.5 M_{\odot} \\ p_2(m) &= k_{p,2} m^{-\alpha_2}, \quad 0.5 \leq m \leq m_{\max}, \end{aligned} \quad (4.14)$$

where $k_{p,i}$ are normalization constants ensuring continuity at $0.5 M_{\odot}$ and

$$\int_{0.07 M_{\odot}}^{0.5 M_{\odot}} p_1 dm' + \int_{0.5 M_{\odot}}^{m_{\max}} p_2 dm' = 1, \quad (4.15)$$

whereby m_{\max} may follow from the mass of the population, M_{ecl} . Defining

$$X'_1 = \int_{0.07 M_{\odot}}^{0.5 M_{\odot}} p_1(m') dm', \quad (4.16)$$

it follows that

$$X_1(m) = \int_{0.07 M_{\odot}}^m p_1(m') dm', \quad \text{if } m \leq 0.5 M_{\odot}, \quad (4.17)$$

or

$$X_2(m) = X'_1 + \int_{0.5 M_{\odot}}^m p_2(m') dm', \quad \text{if } m > 0.5 M_{\odot}. \quad (4.18)$$

The generating function for stellar masses follows by inverting the above two equations $X_i(m)$.

The procedure is then to choose a uniformly distributed random variate $X \in [0, 1]$ and to select the generating function $m(X_1 = X)$ if $0 \leq X \leq X'_1$, or $m(X_2 = X)$ if $X'_1 \leq X \leq 1$. Stellar masses are generated until M_{ecl} is reached to within some preset tolerance. This algorithm is readily generalized to any number of power-law segments (([Sect. 4.5](#)), ([Sect. 9.1](#)), such as including a third segment for brown dwarfs and allowing the IMF to be discontinuous near $0.07 M_{\odot}$ ([Sect. 8.4](#)). Such a form has been incorporated into Aarseth's N -body4/6/7 programs.

For a general $\xi(m)$ and if $X(m)$ cannot be inverted, stellar masses may be generated by constructing a table of $X(m)$, m values,

$$M(m) = \int_{0.07 M_{\odot}}^m m' \xi(m') dm', \quad X(m) = \frac{M(m)}{M_{\text{ecl}}}, \quad (4.19)$$

such that $X(m_{\text{max}}) = 1$. For a random variate X , the corresponding m is obtained by interpolating the table, whereby the X is distributed uniformly and the procedure is repeated until M_{ecl} is reached to some preset tolerance.

Another highly efficient method for generating stellar masses randomly from arbitrary distribution functions is discussed in ([Sect. 2.4](#)).

2.4 A Practical Numerical Formulation of the IMF

Assuming the stellar IMF to be a probability density distribution such that stellar masses can be generated randomly ([Sect. 2.3](#)) from the IMF with ($m \leq m_{\text{max}}$) or without ($m_{\text{max}} = \infty$) constraints remains a popular approach. The two-part description can be straightforwardly expanded to a multipart power law. However, the direct implementation of this description requires multiple IF statements. In the following, a handy numerical formulation is presented for randomly generating stellar masses which replaces complicated IF constructions by two straightforward loops (Pflamm-Altenburg and Kroupa 2006).

Historically, multi-power-law IMFs start indexing intervals and slopes at zero instead of one. For simplicity, we here index n intervals from 1 up to n . We now consider an arbitrary IMF with n intervals fixed by the mass array $[m_0, \dots, m_n]$ and the array of functions f_1, \dots, f_n . On the i -th interval $[m_{i-1}, m_i]$, the IMF is described by the function f_i . The segment functions refer to the “linear” IMF, $\xi(m) = dN/dm$, and not to the logarithmic IMF, $\xi_L(m) = dN/d\log_{10} m$. At this point, it is not required that the segment functions f_i are scaled by a constant such that continuity is ensured on the interval boundaries. They only need to describe the functional form.

For the case of a multi-power law, these functions are

$$f_i(m) = m^{-\alpha_i}. \quad (4.20)$$

The segment functions may also be log-normal distributions, as, for example, in the IMFs of Miller and Scalo (1979) or Chabrier (2003a), but in general, they can be arbitrary.

We first define the two Θ -mappings (Θ -closed and Θ -open)

$$\Theta_{[]}(x) = \begin{cases} 1 & x \geq 0 \\ 0 & x < 0 \end{cases}, \quad (4.21)$$

$$\Theta_{] [}(x) = \begin{cases} 1 & x > 0 \\ 0 & x \leq 0 \end{cases}, \quad (4.22)$$

and the function

$$\Gamma_{[i]}(m) = \Theta_{[]}(m - m_{i-1}) \Theta_{[]}(m_i - m) . \quad (4.23)$$

The $\Gamma_{[i]}(m)$ function is unity on the interval $[m_{i-1}, m_i]$ and zero otherwise.

The complete IMF can now be conveniently formulated by

$$\xi(m) = k \prod_{j=1}^{n-1} \Delta(m - m_j) \sum_{i=1}^n \Gamma_{[i]}(m) C_i f_i(m) , \quad (4.24)$$

where k is a normalization constant and the array (C_1, \dots, C_n) is to ensure continuity at the interval boundaries. They are defined recursively by

$$C_1 = 1 \quad , \quad C_i = C_{i-1} \frac{f_{i-1}(m_{i-1})}{f_i(m_{i-1})} . \quad (4.25)$$

For a given mass m , the $\Gamma_{[i]}$ makes all summands zero except the one in which m lies. Only on the inner interval boundaries do both adjoined intervals give the same contribution to the total value. The product over

$$\Delta(x) = \begin{cases} 0.5 & x = 0 \\ 1 & x \neq 0 \end{cases} \quad (4.26)$$

halves the value due to this double counting at the interval boundaries. In the case of n equals one (one single power law), the empty product has, by convention, the value of unity.

An arbitrary integral over the IMF is evaluated by

$$\int_a^b \xi(m) dm = \int_{m_0}^b \xi(m) dm - \int_{m_0}^a \xi(m) dm, \quad (4.27)$$

where the primitive of the IMF is given by

$$\begin{aligned} \int_{m_0}^a \xi(m) dm &= k \sum_{i=1}^n \Theta_{[]}(a - m_i) C_i \int_{m_{i-1}}^{m_i} f_i(m) dm \\ &+ k \sum_{i=1}^n \Gamma_{[i]}(a) C_i \int_{m_{i-1}}^a f_i(m) dm. \end{aligned} \quad (4.28)$$

The expressions for the mass content, that is, $m \xi(m)$, and its primitive are obtained by multiplying the above expressions in the integrals by m and one has to find the primitives of $m f_i(m)$.

Stars can now be dived from an IMF, $\xi(m)$, based on the above formulation and the concept of the generating function (● Sect. 2.3) in the following way: A random number X is drawn from a uniform distribution and then transformed into a mass m . The mass segments transformed into the X -space are fixed by the array $\lambda_0, \dots, \lambda_n$ defined by

$$\lambda_i = \int_{m_0}^{m_i} \xi(m) dm. \quad (4.29)$$

If $P(X)$ denotes the uniform distribution with $P(X) = 1$ between 0 and λ_n , both functions are related by

$$\int_{m_0}^{m(X)} \xi(m') dm' = \int_0^X P(X') dX' = X. \quad (4.30)$$

If a given X lies between λ_{i-1} and λ_i , the corresponding mass m lies in the i -th interval $[m_{i-1}, m_i]$ and it follows

$$X(m) = \lambda_{i-1} + k C_i (F_i(m) - F_i(m_{i-1})) , \quad (4.31)$$

or

$$m(X) = F_i^{-1} \left(\frac{X - \lambda_{i-1}}{k C_i} + F_i(m_{i-1}) \right), \quad (4.32)$$

where F_i is a primitive of f_i and F_i^{-1} is the primitive's inverse mapping. The complete expression for the solution for m is given by

$$m(X) = \sum_{i=1}^n \lambda \Gamma_{[i]} F_i^{-1} \left(\frac{X - \lambda_{i-1}}{k C_i} + F_i(m_{i-1}) \right) \cdot \prod_{j=1}^{n-1} \Delta(X - \lambda_j), \quad (4.33)$$

where $\lambda \Gamma_i$ are mappings which are unity between λ_{i-1} and λ_i and zero otherwise. Note that the primitives are determined except for an additive constant, but it is canceled out in the relevant expressions in (4.28) and (4.33).

The most used segment function for the IMF is a power law,

$$f(m) = m^{-\alpha}. \quad (4.34)$$

The corresponding primitive and its inverse mapping is

$$F(m) = \begin{cases} \frac{m^{1-\alpha}}{1-\alpha} & \alpha \neq 1 \\ \ln(m) & \alpha = 1 \end{cases}, \quad (4.35)$$

and

$$F^{-1}(X) = \begin{cases} ((1-\alpha)X)^{\frac{1}{1-\alpha}} & \alpha \neq 1 \\ \exp(X) & \alpha = 1 \end{cases}. \quad (4.36)$$

The other segment function used is a log-normal distribution, that is, a Gaussian distribution of the logarithmic mass,

$$\xi(lm) \propto \exp \left(-\frac{(lm - lm_c)^2}{2\sigma^2} \right), \quad (4.37)$$

where $lm \equiv \log_{10} m$. The corresponding segment function is

$$f(m) = \frac{1}{m} \exp \left(-\frac{(lm - lm_c)^2}{2\sigma^2} \right), \quad (4.38)$$

with the primitive

$$F(m) = \sqrt{\frac{\pi}{2}} \sigma \ln 10 \operatorname{erf} \left(\frac{lm - lm_c}{\sqrt{2}\sigma} \right), \quad (4.39)$$

and the inverse of the primitive

$$F^{-1}(X) = 10^{\sqrt{2}\sigma \operatorname{erf}^{-1} \left(\sqrt{\frac{2}{\pi}} \frac{X}{\sigma \ln 10} \right) + lm_c}, \quad (4.40)$$

where erf and erf^{-1} are the Gaussian error function,

$$\text{erf}(Y) = \frac{2}{\sqrt{\pi}} \int_0^Y e^{-y^2} dy, \quad (4.41)$$

and its inverse, respectively.

Several accurate numerical approximations of the Gaussian error function exist, but approximations of its inverse are quite rare. One such handy numerical approximation of the Gaussian error function which allows an approximation of its inverse, too, has been presented by Sergei Winitzki⁹ based on a method explained in Winitzki (2003):

The approximation of the error function for $Y \geq 0$ is

$$\text{erf}(Y) \approx \left(1 - \exp \left(-Y^2 \frac{\frac{4}{\pi} + a Y^2}{1 + a Y^2} \right) \right)^{\frac{1}{2}}, \quad (4.42)$$

with

$$a = \frac{8}{3\pi} \frac{\pi - 3}{4 - \pi}. \quad (4.43)$$

Values for negative Y can be calculated with

$$\text{erf}(Y) = -\text{erf}(-Y). \quad (4.44)$$

The approximation for the inverse of the error function follows directly,

$$\text{erf}^{-1}(Y) \approx \left(-\frac{2}{\pi a} - \frac{\ln(1 - Y^2)}{2} + \sqrt{\left(\frac{2}{\pi a} + \frac{\ln(1 - Y^2)}{2} \right)^2 - \frac{1}{a} \ln(1 - Y^2)} \right)^{\frac{1}{2}}. \quad (4.45)$$

Important Result

The above algorithm for dicing stars from an IMF supporting power-law and log-normal segment functions has been coded in the publicly available software package libimf available at <http://www.astro.uni-bonn.de/download/software/>

2.5 Statistical Treatment of the Data

Whichever is a better description of nature, optimal or random sampling from the IMF, a set of observationally derived stellar masses will appear randomized because of uncorrelated measurement uncertainties. Statistical tools are therefore required to help analyze the observed set of masses in the context of their possible parent distribution function and upper limit.

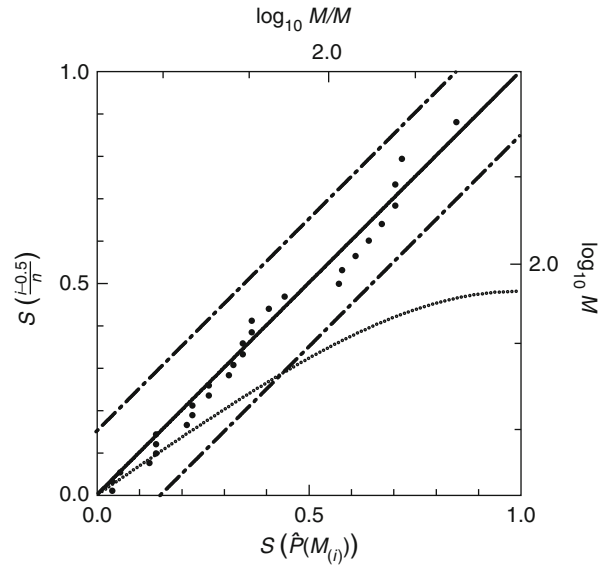
We concentrate here in particular on analyzing the high-mass end of the IMF, which follows a power-law probability density. Estimating the exponent via binning (using constant-size bins in logarithmic space) can introduce significant bias (Maíz Apellániz and Úbeda 2005; Maschberger and Kroupa 2009), especially for meager data sets. This can be remedied by using bins containing approximately the same number of data points (Maíz Apellániz and Úbeda 2005).

⁹homepages.physik.uni-muenchen.de/~Winitzki/erf-approx.pdf

However, binning does not allow one to estimate the upper limit of the mass function. A more suitable approach to estimate both exponent and upper limit simultaneously is to use the maximum likelihood method. The estimate there is given just by the largest data point and is consequently also naturally biased to too small values. Maschberger and Kroupa (2009) give a correction factor which leads to unbiased results for the upper limit.

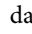
Besides biases due to the statistical method, observational limitations can also introduce biases in the exponent. The influence of unresolved binaries for the high-mass IMF slope is less than ± 0.1 dex (Maíz Apellániz 2008; Weidner et al. 2009). Random superpositions, in contrast, can cause significant biases, as found by Maíz Apellániz (2008). Differential reddening can affect the deduced shape of the IMF significantly (Andersen et al. 2009). A further point in data analysis besides the estimation of the parameters is to validate the assumed power-law form for the IMF and in particular to decide whether, for example, a universal upper limit ($m_{\max*} = 150M_{\odot}$) is in agreement with the data.

For this purpose, standard statistical tests, for example, the Kolmogorov–Smirnov test, can be utilized, but their deciding powers are not very high. They can be significantly improved by making a stabilizing transformation, S (Maschberger and Kroupa 2009). A graphical goodness-of-fit assessment can then be made using the stabilized probability-probability (SPP) plot, for example, ► Fig. 4-4. This plot has been constructed using a truncated power law ($m_{\max*} = 143M_{\odot}$) and is aimed to help to decide whether a truncated or an infinite power law fits the stellar masses of the 29 most massive stars in R136 (masses taken from Massey and Hunter



■ Fig. 4-4

SPP plot of the massive stars in R136 using a power law truncated at $143 M_{\odot}$ (From Maschberger and Kroupa 2009). The data are following this hypothesis and lie along the diagonal within the 95% acceptance region of the stabilized Kolmogorov–Smirnov test (limited by *dashed lines*). An infinite power law as the parent distribution function, the *dotted line* bending away from the diagonal, can be ruled out. The stellar MF in R136 is thus a power law with index $\alpha = 2.2$ truncated at $143 M_{\odot}$


1998, using the isochrones of Chlebowski and Garmany 1991). The points are constructed from the ordered sample of the masses, with the value of the stabilized cumulative probability, $S(\hat{P}(m_{(i)}))$ as x-coordinate (using the estimated parameters) and the stabilized empirical cumulative probability, $S(\frac{i-0.5}{n})$, as the y-coordinate. The data follow the null hypothesis of a truncated power law and lie therefore along the diagonal. The null hypothesis would be challenged significantly if the data would leave the region enclosed by the dashed parallels to the diagonal, which is the 95% acceptance region of the stabilized Kolmogorov–Smirnov test. An alternative hypothesis of an infinite power law (with the same exponent) is shown as the dotted line which strongly bends away from the diagonal and is in significant disagreement with the data. Plots like  Fig. 4-4 can be constructed for any combination of null hypothesis and alternative hypothesis and have great potential to improve the statistical analysis of the upper mass end of the IMF.

Important Result

A program to estimate the parameter of power-law distributed data and to calculate goodness-of-fit tests for them is available in the publicly available software package statpl available at <http://www.astro.uni-bonn.de/download/software/>

2.6 Binary Systems

In order to infer the stellar IMF, it is necessary to account for all stars in the population, including the companions of multiple systems. Indeed, the vast majority of stars are observed to form in multiple systems. However, since dynamically not evolved star-forming regions of an age around about 1 Myr such as the Taurus-Auriga subclusters have a high multiplicity fraction of nearly 100%, this immediately implies that most stars by far must form as binaries. This is because if they were to form as triple or higher-order systems, then they would decay on their system crossing time scale which is far shorter than 1 Myr leading, by 0.5–1 Myr, to a substantial population of single stars which is not observed (Goodwin and Kroupa 2005; Goodwin et al. 2007).

The IMF appearing largely invariant to star-formation conditions (but see  Sect. 12.9) constitutes a statistical statement on one of the birth dynamical properties of stars (namely, their distribution of masses). So, since both the IMF and the birth binary population (BBP) are the result of the same (star formation) process and since the IMF is a result of this process “one level deeper down” than the BBP, it is quite natural to suggest that the formal mathematical distribution function of all of the birth dynamical properties (see footnote 4 on p. 121) of stars are also quite invariant. It follows that the star-formation outcome in terms of stellar masses (the IMF) and multiple systems (the birth binary population – BBP) can be formulated by the Star Formation Universality Hypothesis:

The Star-Formation Universality Hypothesis

IMF universality \iff BBP universality.

For stars with $m \lesssim 5 M_\odot$, the birth binary population is deduced from an elaborate analysis.

The birth binary population (BBP)

- Random pairing from the canonical IMF (☛ 4.55) for $0.1 \lesssim m/M_\odot \lesssim 5$.
- Thermal eccentricity distribution of eccentricities, $f_e(e) = 2e$.
- The period distribution function

$$f_{p,\text{birth}} = \eta \frac{IP - IP_{\min}}{\delta + (IP - IP_{\min})^2}, \quad (4.46)$$

where $\eta = 2.5$, $\delta = 45$, $IP_{\min} = 1$, and $\int_{IP_{\min}}^{IP_{\max}} f_{p,\text{birth}} dIP = 1$ such that the birth binary fraction is unity ($IP_{\max} = 8.43$; $IP \equiv \log_{10} P$ and P is in days). Here, $f_e de$ and $f_p dIP$ are the fraction of all orbits with eccentricity in the range $e, e + de$ and log period in the range $IP, IP + dIP$, respectively. Note that conversion between P and the semimajor axis is convenient through Kepler's third law: $a^3/P_{\text{year}}^2 = m_1 + m_2$, where a is in AU, $P_{\text{year}} = P/365.25$ is the period in years, and m_1, m_2 are the primary- and secondary-star masses in M_\odot .

The following are to be noted:

1. The BBP was derived by using observations of pre-main sequence and main-sequence binary populations as initial and final boundary conditions, respectively. Kroupa (1995a) postulated that there exist two stellar-dynamical operators, Ω_P and Ω_q , which independently transform the period- and mass-ratio distribution functions (that are independent products of the star-formation process for the majority of binaries) between the initial and final states. It is possible to demonstrate that both Ω_P and Ω_q exist. Furthermore, they are equal and are given by a characteristic star cluster consisting of 200 binary systems with a characteristic radius of about 0.8 pc (Kroupa 1995c; Marks et al. 2011),

$$\Omega_P = \Omega_q \equiv \Omega = (200 \text{ binaries}, R_{\text{ch}} \approx 0.8 \text{ pc}). \quad (4.47)$$

Important Result

The interpretation of this result is that the BBP is, like the IMF, a fundamental outcome of star formation and that most stars in the MW disk stem from star-formation events that are dynamically equivalent to the characteristic, or dominant-mode, cluster.

2. The deduced maximum binary period in the BBP of $10^{8.43}$ d corresponds to a spatial scale of $\approx 10^4$ AU which is the typical dimension of a pre-stellar cloud core (Kirk et al. 2005).
3. The evolved BBP, which matches the Galactic field stellar and binary population, also accounts simultaneously for the individual-star and the system LFs (☛ Fig. 4-15).

The BBP is the deduced (Kroupa 1995a, c) outcome of star formation in low to intermediate density ($\rho \lesssim 10^5 M_\odot/\text{pc}^3$) cloud regions (e.g., embedded clusters), but the rules layed out in (☛ 4.46) may well be formally applicable to higher density regions as well, whereby wide binaries are naturally truncated due to close-packing.

Important Note

In this sense, the BBP is a formal mathematical description of the outcome of star formation. Just like the formal stellar IMF (◆ 4.55), it may never be accessible to observations (the IMF Unmeasurability Theorem, p. 129). But, just like the stellar IMF, it is extractable from the observations.

The binary fraction

$$f = \frac{N_{\text{bin}}}{N_{\text{bin}} + N_{\text{sing}}}, \quad (4.48)$$

where $N_{\text{bin}}, N_{\text{sing}}$ are the number of binary- and single-stellar systems in the survey, respectively, is high ($f_{\text{bin}} > 0.8$) in dynamically unevolved populations, whereas $f_{\text{bin}} \approx 0.5$ for typically open clusters and the Galactic field as follows from applying Ω on the BBP (i.e., by performing N -body integrations of dissolving star clusters, Kroupa 1995b; Marks et al. 2011).

Note that the BBP needs to be transformed to the *initial binary population* by the process of pre-main sequence eigenevolution (Kroupa 1995d), which introduces the observed correlations between mass ratio, eccentricity, and period for short-period binaries, while the dynamically evolved initial binary population yields the observed mass-ratio and period distribution functions with $f \approx 0.5$ (Marks and Kroupa 2011).

For $m \gtrsim 5 M_{\odot}$ stars, the pairing rules change perhaps, reflecting the outcome of star formation in dense regions such as in the cores of embedded clusters ($\rho \gtrsim 10^5 M_{\odot}/\text{pc}^3$). Using a large sample of young clusters (for a review, see Sana and Evans 2010 and also Sana et al. 2011a), it is found that at least 45–55% of O stars are spectroscopic binaries: The mass ratios for these are larger in comparison with the late-type stars above: Massive binaries have a flat mass-ratio distribution and $0.2 \leq q \leq 1$. These systems have short periods, typically less than about 10 d, but extend from 0.3 to $10^{3.5}$ d. The measured distribution function is provided by equation (5.2) in Sana and Evans (2010). The overall binary fraction among O stars is at least 85% (García and Mermilliod 2001) as the spectroscopic fraction is augmented by wider visual binaries with separations between 40 and 200 AU (Sana et al. 2011b). The vast spectroscopic survey by Chini et al. (2012) of about 800 O and B-type stars affirms such results and establishes, even for runaway stars, the very high binary fraction and q about 1 pairing.

This leads to the following question.

Open Question I

Why do the differing BBP properties between $0.1 M_{\odot}$ and a few M_{\odot} on the one hand side and above a few M_{\odot} on the other hand side not correspond to the structure evident in the IMF, which is a featureless power law above about $0.5 M_{\odot}$ with a flattening below this mass? (◆ Sect. 9.1).

Below about $0.1 M_{\odot}$ very low mass stars and brown dwarfs, with $f_{\text{bin,BD}} \approx 0.15 - 0.2$, follow entirely separate rules (◆ Sect. 8.1) being an accompanying but distinct population to stars.

It has so far not been possible to predict nor to fully understand the distribution of binary-star birth properties from theory. The currently most advanced self-consistent gravohydrodynamical simulation without feedback of star formation using the SPH technique (Moeckel and Bate 2010) leads to too compact clusters of about a 1,000 stars and brown dwarfs from which a binary population emerges which does not quite have the observed distribution

of periods and mass ratios. However, this may be due to the currently unavoidable omission of feedback which would limit the depth of the gravitational collapse perhaps alleviating the binary-star problem (Kroupa 2011).

3 The Maximum Stellar Mass

While the stellar IMF appears to have a universal two-part power-law form (([4.55](#)) below), the existence of a physical truncation mass as a function of embedded star cluster mass would suggest a form of IMF variation ([Sect. 12.1](#)). Here, the evidence for such a truncation is presented.

3.1 On the Existence of a Maximum Stellar Mass

The empirically determined range of stellar masses poses important constraints on the physics of stellar formation, structure and stellar evolution, as well as on the feedback energy injected into a galaxy's atmosphere by a population of brand-new stars. The physical limit at low masses is now well established ([Sect. 8](#)), and an upper mass limit appears to have been found recently.

A theoretical physical limitation to stellar masses has been known since many decades. Eddington (1926) calculated the limit which is required to balance radiation pressure and gravity, the *Eddington limit*: $L_{\text{Edd}}/L_{\odot} \approx 3.5 \times 10^4 m/M_{\odot}$. Hydrostatic equilibrium will fail if a star of a certain mass m has a luminosity that exceeds this limit, which is the case for $m \gtrsim 60 M_{\odot}$. It is not clear if stars above this limit cannot exist, as massive stars are not fully radiative but have convective cores. But more massive stars will lose material rapidly due to strong stellar winds. Schwarzschild and Härm (1959) inferred a limit of $\approx 60 M_{\odot}$ beyond which stars should be destroyed due to pulsations. But later studies suggested that these may be damped (Beech and Mitalas 1994). Stothers (1992) showed that the limit increases to $m_{\text{max}*} \approx 120\text{--}150 M_{\odot}$ for more recent Rogers–Iglesia opacities and for metallicities $[\text{Fe}/\text{H}] \approx 0$. For $[\text{Fe}/\text{H}] \approx -1$, $m_{\text{max}*} \approx 90 M_{\odot}$. A larger physical mass limit at higher metallicity comes about because the stellar core is more compact, the pulsations driven by the core having a smaller amplitude, and because the opacities near the stellar boundary can change by larger factors than for more metal-poor stars during the heating and cooling phases of the pulsations thus damping the oscillations. Larger physical mass limits are thus allowed to reach pulsational instability.

Related to the pulsational instability limit is the problem that radiation pressure also opposes accretion for protostars that are shining above the Eddington luminosity. Therefore, the question remains how stars more massive than $60 M_{\odot}$ may be formed. Stellar formation models lead to a mass limit near $40\text{--}100 M_{\odot}$ imposed by feedback on a spherical accretion envelope (Kahn 1974; Wolfire and Cassinelli 1987). Some observations suggest that stars may be accreting material in disks and not in spheres (e.g., Chini et al. 2004). The higher density of the disk material may be able to overcome the radiation at the equator of the protostar. But it is unclear if the accretion rate can be boosted above the mass-loss rate from stellar winds by this mechanism. Theoretical work on the formation of massive stars through disk accretion with high accretion rates thereby allowing thermal radiation to escape polewards (e.g., Iijima and Adams 1996) indeed lessen the problem and allow stars with larger masses to form.

Another solution proposed is the merging scenario. In this case, massive stars form through the merging of intermediate-mass protostars in the cores of dense stellar clusters driven by core contraction due to very rapid accretion of gas with low specific angular momentum, thus again avoiding the theoretical feedback-induced mass limit (Bonnell et al. 1998; Stahler et al. 2000, and the review by Zinnecker and Yorke 2007). It is unclear though if the very large central densities required for this process to act are achieved in reality, but it should be kept in mind that an observable young cluster is, by necessity, exposed from its natal cloud and is therefore likely to be always observed in an expanding phase such that the true maximally reached central density may be very high for massive clusters, $\sim 10^8 M_\odot/\text{pc}^3$ (Dabringhausen et al. 2010; Marks and Kroupa 2010; Conroy 2011).

The search for a possible maximal stellar mass can only be performed in massive, star-burst clusters that contain sufficiently many stars to sample the stellar IMF beyond $100 M_\odot$. Observationally, the existence of a finite physical stellar mass limit was not evident until very recently. Indeed, observations in the 1980s of R136 in the Large Magellanic Cloud (LMC) suggested this object to be one single star with a mass of about $2,000\text{--}3,000 M_\odot$. Weigelt and Baier (1985) for the first time resolved the object into eight components using digital speckle interferometry, therewith proving that R136 is a massive star cluster rather than one single supermassive star. The evidence for any physical upper mass limit was very uncertain, and Elmegreen (1997) stated that “observational data on an upper mass cutoff are scarce, and it is not included in our models (of the IMF from random sampling in a turbulent fractal cloud).” Although Massey and Hunter (1998) found stars in R136 with masses ranging up to $140\text{--}155 M_\odot$, Massey (2003) explained that the observed limitation is statistical rather than physical. We refer to this as the *Massey assertion*, that is, that $m_{\text{max}*} = \infty$. Meanwhile, Selman et al. (1999) found, from their observations, a probable upper mass limit in the LMC near about $130 M_\odot$, but they did not evaluate the statistical significance of this suggestion. Figer (2003) discussed the apparent cutoff of the stellar mass spectrum near $150 M_\odot$ in the Arches cluster near the Galactic center, but again did not attach a statistical analysis of the significance of this observation. Elmegreen (2000) also noted that random sampling from an unlimited IMF for all star-forming regions in the Milky Way (MW) would lead to the prediction of stars with masses $\gtrsim 1,000 M_\odot$, unless there is a rapid turn-down in the IMF beyond several hundred M_\odot . However, he also stated that no upper mass limit to star formation has ever been observed, a view also emphasized by Larson (2003).

Thus, while theory clearly expected a physical stellar upper mass limit, the observational evidence in support of this was very unclear. This, however, changed in 2004.

3.2 The Upper Physical Stellar Mass Limit

Given the observed sharp drop-off of the IMF in R136 near $150 M_\odot$, that is, that the R136 stellar population is observed to be saturated (p. 148), Weidner and Kroupa (2004) studied the above *Massey assertion* in some detail. R136 has an age ≤ 2.5 Myr (Massey and Hunter 1998) which is young enough such that stellar evolution will not have removed stars through supernova explosions. It has a metallicity of $[\text{Fe}/\text{H}] \approx -0.5$ dex (de Boer et al. 1985). From the radial surface density profile, Selman et al. (1999) estimated there to be 1,350 stars with masses between 10 and $40 M_\odot$ within 20 pc of the 30 Doradus region, within the center of which lies R136. Massey and Hunter (1998) and Selman et al. (1999) found that the IMF can be well approximated by a Salpeter power law with exponent $\alpha = 2.35$ for stars in the mass range $3\text{--}120 M_\odot$.

(see also [Fig. 4-4](#)). This corresponds to 8,000 stars with a total mass of $0.68 \times 10^5 M_\odot$. Extrapolating down to $0.1 M_\odot$, the cluster would contain 8×10^5 stars with a total mass of $2.8 \times 10^5 M_\odot$. Using a canonical IMF with a slope of $\alpha = 1.3$ (instead of the Salpeter value of 2.35) between 0.1 and $0.5 M_\odot$, this would change to 3.4×10^5 stars with a combined mass of $2 \times 10^5 M_\odot$ for an average mass of $0.61 M_\odot$ over the mass range 0.1 – $120 M_\odot$. Based on the observations by Selman et al. (1999), Weidner and Kroupa (2004) assumed that R136 has a mass in the range $5 \times 10^4 \leq M_{\text{R136}}/M_\odot \leq 2.5 \times 10^5$. Using the *canonical stellar IMF* ([Eq. 4.55](#) below), they found that $N(> 150 M_\odot) = 40$ stars are missing if $M_{\text{ecl}} = 2.5 \times 10^5 M_\odot$, while $N(> 150 M_\odot) = 10$ stars are missing if $M_{\text{ecl}} = 5 \times 10^4 M_\odot$. The probability that no stars are observed although 10 are expected, assuming $m_{\text{max}*} = \infty$, is $P = 4.5 \times 10^{-5}$. Thus, the observations of the massive stellar content of R136 suggest a physical stellar mass limit near $m_{\text{max}*} = 150 M_\odot$.

A reanalysis of the stellar spectra plus new stellar modeling suggests, however, $m_{\text{max}*} \approx 300 M_\odot$ for R136 (Crowther et al. 2010). But Banerjee et al. (2012) demonstrate that $m > 150 M_\odot$ stars form readily from merging binaries in star-burst clusters. Their high-precision Aarseth- N -body models of binary-rich initially mass-segregated R136-type clusters demonstrate that stars much more massive than the $m_{\text{max}*} = 150 M_\odot$ limit appear from massive binaries that merge after becoming eccentric and hard through a stellar-dynamical encounter near the cluster core. Such binaries may be ejected from the cluster before merging, thus appearing to an observer as free-floating single stars of mass up to $300 M_\odot$. The fundamental upper mass limit may thus nevertheless be $m_{\text{max}*} \approx 150 M_\odot$.

Results similar to those of Weidner and Kroupa (2004) were obtained by Figer (2005) for the Arches cluster. The Arches is a star-burst cluster within 25 pc in projected distance from the Galactic center. It has a mass $M \approx 1 \times 10^5 M_\odot$ (Bosch et al. 2001), age 2–2.5 Myr and $[\text{Fe}/\text{H}] \approx 0$ (Najarro et al. 2004). It is thus a counterpart to R136 in that the Arches is metal rich and was born in a very different tidal environment to R136. Using his HST observations of the Arches, Figer (2005) performed the same analysis as Weidner and Kroupa (2004) did for R136. The Arches appears to be dynamically evolved, with substantial stellar loss through the strong tidal forces (Portegies Zwart et al. 2002), and the stellar mass function with $\alpha = 1.9$ is thus flatter than the Salpeter IMF. Using his updated IMF measurement, Figer calculated the expected number of stars above $150 M_\odot$ to be 33, while a Salpeter IMF would predict there to be 18 stars. Observing no stars but expecting to see 18 has a probability of $P = 10^{-8}$, again strongly suggesting $m_{\text{max}*} \approx 150 M_\odot$. The Arches cluster is thus another example of a saturated stellar population.

Given the importance of knowing if a finite physical upper mass limit exists and how it varies with metallicity, Oey and Clarke (2005) studied the massive-star content in nine clusters and OB associations in the MW, the LMC and the SMC. They predicted the expected masses of the most massive stars in these clusters for different upper mass limits (120, 150, 200, 1,000, and $10,000 M_\odot$). For all populations, they found that the observed number of massive stars supports with high statistical significance the existence of a general upper mass cutoff in the range $m_{\text{max}*} \in (120, 200 M_\odot)$.¹⁰

The general indication thus is that a physical stellar mass limit near $150 M_\odot$ seems to exist. While biases due to unresolved multiples that may reduce the true maximal mass need to be studied further, the absence of variations of $m_{\text{max}*}$ with metallicity poses a problem.

¹⁰More recent work on the physical upper mass limit can be found in Koen (2006) and Maíz Apellániz et al. (2007, 2008).

A constant $m_{\max*}$ would only be apparent for a true variation as proposed by the theoretical models; *if metal-poor environments have a larger stellar multiplicity*, the effects of which would have to compensate the true increase of $m_{\max*}$ with metallicity. Interestingly, in a recent hydrodynamical calculation, Machida et al. (2009) find a higher binary fraction for low metallicities.

3.3 The Maximal Stellar Mass in a Cluster, Optimal Sampling and Saturated Populations

Above, we have seen that there seems to exist a universal physical stellar mass limit, $m_{\max*}$. However, an elementary argument suggests that star clusters must additionally limit the masses of their constituent stars: A pre-star-cluster gas core with a mass M_{core} can, obviously, not form stars with masses $m > \epsilon M_{\text{core}}$, where $\epsilon \approx 0.33$ is the star-formation efficiency (Lada and Lada 2003). Thus, given a freshly hatched cluster with stellar mass M_{ecl} , stars in that cluster cannot surpass masses $m_{\max} = M_{\text{ecl}}$, which is the identity relation corresponding to a “cluster” consisting of one massive star. Note that if we were to construct a (unphysical) model in which N stars are stochastically chosen from the IMF then such a constraint would not appear.

3.3.1 Theory

As discussed by Smith et al. (2009), there are two main theories of massive star formation: The first theory is essentially a scaled up version of low-mass star formation, where massive stars form from well-defined massive cores supported by turbulence. This model requires the existence of massive pre-stellar cores that manage to evade fragmentation during their formation stages. Perhaps radiative feedback can limit the fragmentation, but Smith et al. (2009) demonstrate that radiative feedback does not lead to the formation of massive pre-stellar cores in isolation.

The second theory is based on the *competitive accretion scenario* or on a refined version thereof, the *fragmentation limited starvation model*. Cores are the seeds of the formation of stars, and the most massive of these have a larger gravitational radius of influence and are therewith more successful at accreting additional mass. They can thus grow into massive stars. The massive seeds typically tend to form and stay at the center of the gravitational potential of the forming star cluster which they contribute to because the gas densities and thus the accretion rates are largest there. They accrete material via Bondi–Hoyle accretion, but when the velocity relative to the system is low, the accretion is mainly regulated by the tidal field. There is no requirement for stellar mergers, which, however can occur in dense regions (➤ 4.60) and contribute to the buildup of the IMF.

The first theory would imply that the formation of massive stars can occur in isolation, that is, without an accompanying star cluster. The existing data on the spatial distribution of massive stars do, however, not support this possibility (➤ Sect. 4). The second theory requires massive stars to be associated with star clusters. This is demonstrated by Smith et al. (2009) using SPH simulations of a gas cloud with a changing equation of state as a result of the cooling process shifting from line emission to dust emission with increasing density and with radiative heating as a model of the feedback process. Peters et al. (2010, 2011b) study this issue independently with three-dimensional, radiation-hydrodynamical simulations that include heating

by ionizing and non-ionizing radiation using the adaptive-mesh code FLASH and verify that massive star formation is associated with low-mass star formation as fragmentation cannot be suppressed, even including radiative feedback. Simpler isothermal SPH computations without feedback by Bonnell et al. (2004) and the FLASH simulations by Peters et al. (2010, 2011b) show that the most massive star in the forming cluster evolves with time, t , according to the following relation:

$$m_{\max}(t) = 0.39 M_{\text{ecl}}(t)^{2/3}. \quad (4.49)$$

The general form of the observed IMF (◆ 4.55) is also obtained. This is therefore a prediction of the second theory whereby it is important to note that (◆ 4.49) is a result of purely gravitationally driven star formation calculations with and without feedback. Interestingly, Peters et al. (2010, 2011b) conclude that computations with feedback lead to a closer agreement with the observed $m_{\max} - M_{\text{ecl}}$ data. The following result emerges.

The Bonnell-Vine-Bate (BVB) Conjecture

“Thus an individual cluster grows in numbers of stars as the most massive star increases in mass. This results in a direct correlation ..., and provides a physical alternative to a probabilistic sampling from an IMF” (Bonnell et al. 2004).

Main result: The self-consistent gravo-hydrodynamical simulations of star formation thus yield the result that the growth of the most massive star is intimately connected with the growth of its hosting cluster, thereby populating the stellar IMF.

How does nature arrange the mass of the star-forming material over the emerging stellar masses? That massive stars can form in isolation can be discarded statistically (◆ Sect. 4). But how regulated or rather deterministic is the formation of massive stars and their star clusters?

Here, it is useful to return to the concept of optimal sampling (◆ Sect. 2.2): IF nature distributes the available mass M_{ecl} optimally over the IMF, then the $m_{\max} - M_{\text{ecl}}$ relation emerges. It is plotted in ◆ Fig. 4-5 as the thick-solid curves for two values of $m_{\max*}$.

For a given M_{ecl} , the observationally derived m_{\max} values show a spread rather than one value: Can stars with masses larger than the optimal m_{\max} , or even with masses beyond the canonical upper mass limit of $m_{\max*}$, occur? In discussing these issues, it proves useful to define the concept of a *saturated population*.

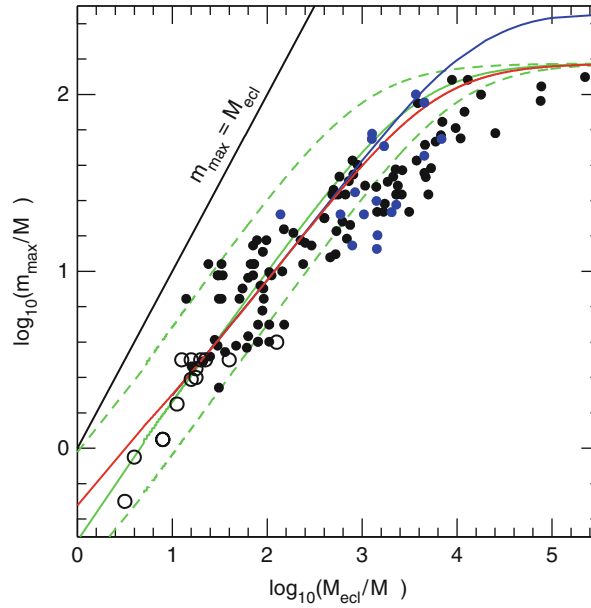
Definitions

Saturated population: A population for which $m_{\max} = m_{\max*}$ and $\int_{m_{\max}}^{\infty} \xi(m) dm \geq 1$. Only a simple population can be saturated.

Unsaturated population: A population for which $m_{\max} < m_{\max*}$.

Supersaturated population: A simple population containing super-canonical ($m > m_{\max*}$) stars.

Thus, a simple stellar population is saturated if its most-massive star has the physically allowed maximum mass (e.g., R136 and Arches). An unsaturated population is a simple population in which m_{\max} does not reach $m_{\max*}$ (e.g., ρ Oph and ONC). The star-burst cluster R136 is associated with super-canonical stars (Crowther et al. 2010) and is therefore a supersaturated population. This occurs naturally through merged massive binaries (Banerjee et al. 2012). Indeed, as an example that such stars are known to exist is discussed by Vanbeveren (2011).



■ Fig. 4-5

The $m_{\max} - M_{\text{ecl}}$ relation. The *black solid dots* are observed clusters (Weidner et al. 2010), with newly compiled data being shown as *blue solid dots*. The data are compiled subject to an age constraint (no cluster older than 4 Myr is accepted) and to the constraint that the cluster still be embedded. The *open circles* are the most-massive star versus cluster mass in 14 young stellar groups in Taurus, Lupus3, Chal, and IC348 (Kirk and Myers 2011). These are dynamically unevolved (Kroupa and Bouvier 2003b) and can be taken to represent pristine configurations. The *lower (red) thick solid line* is (4.12) with $m_{\max*} = 150 M_{\odot}$, and the *blue thick solid line* is the same but for $m_{\max*} = 300 M_{\odot}$. The *thin solid line* shows the identity relation, where a “cluster” consists only of one star. Assuming unconstrained random picking from the canonical IMF with $m_{\max*} = 150 M_{\odot}$, one sixth of all models would lie below the *lower (green) dashed curve*, while five sixth would lie below the *upper (green) dashed curve*, that is, two third of all data ought to lie between the *dashed curves*. The median, below which would lie 50% of all data for random sampling from the IMF, is plotted as the *thick (green) solid curve*. Significant deviations from random sampling from the stellar IMF are evident in that the scatter of the observational data is smaller and the median lies below the random-sampling median. The theoretical prediction (4.49) follows nearly precisely the *solid lines* for $M_{\text{ecl}} < 10^4 M_{\odot}$. Note also that the horizontal axis corresponds to a density. For example, if all clusters form with a half-mass radius of 0.5 pc, then the density scale becomes $\log_{10} \rho_* = \log_{10} M_{\text{ecl}}/M_{\odot} + 0.28$, where ρ_* is in units of M_{\odot}/pc^3 . Thus, stars more massive than $10 M_{\odot}$ appear only when $\rho_{\text{gas}} > 10^3 M_{\odot}/\text{pc}^3$ for a star-formation efficiency of 33%. Note that the clusters *saturate* (p. 148) for $M_{\text{ecl}} > 10^4 M_{\odot}$.

3.3.2 Observational data

A compilation of clusters only subject to a constraint in age and gas content (to ensure youth and dynamical virginity) for which the cluster mass and the initial mass of the heaviest star can be estimated observationally demonstrates that there exists a strong correlation between the

embedded-cluster mass and the most-massive stellar mass within it. The observational data are plotted in [Fig. 4-5](#).

By performing statistical tests, Weidner and Kroupa (2006) and Weidner et al. (2010) show with very high confidence that the observational data are not consistent with the most-massive star being randomly drawn from the IMF.¹¹ In addition, if the process of star formation was equivalent to pure random sampling of stars from the IMF, then this would predict the existence of star clusters dominated by O stars or even the formation of massive stars in isolation (e.g., Haas and Anders 2010). But this hypothesis is ruled out with high confidence because the theoretically *expected* fraction of massive stars that ought to appear to be isolated (1–4%) although they formed in clusters is already larger than the *observed* fraction of candidate isolated massive stars (see [Sect. 4](#)).

The newest additions of observational data enhance the empirical evidence for the existence of a physical $m_{\max} - M_{\text{ecl}}$ relation, even at masses $M_{\text{ecl}} \lesssim 15 M_{\odot}$: The low-mass data by Kirk and Myers (2011) show a remarkably small spread implying that even the lowest-mass “clusters” limit the mass of their most massive star in a nontrivial way. Indeed, the distribution of all data shows that random sampling from the IMF is ruled out since the spread is smaller than the expected spread given the 1/6th and 5/6th quantiles. The data in [Fig. 4-5](#) also show that for $M_{\text{ecl}} \lesssim 10^3 M_{\odot}$, the semi-analytical model ([4.12](#)) is an excellent description. At larger cluster masses, this model is a fairly good description as well although some systematic deviation is evident.

It thus appears that the process of star formation ends up close to optimally sampling the IMF and that it does not correspond to purely randomly generating stars from the IMF in support of the BVB conjecture (p. 148). But why?

Open Question II

Why is it that the star-formation process samples the IMF close to if not optimally?

3.3.3 Interpretation

The observational data suggest that the dominant physical process responsible for the $m_{\max} - M_{\text{ecl}}$ relation is a competitive resource-limited growth process. This would be natural since the protostars begin as a distribution of low-mass seed masses and accrete at various rates, thereby depleting the surrounding interstellar medium, as is in fact evident in self-consistent gravo-hydrodynamical simulations of star formation with and without feedback as discussed above.

For $M_{\text{ecl}} > 10^{2.2} M_{\odot}$, the small spread persists in the observational data, but the data fall below the semi-analytical model ([4.12](#)). This may hint at additional processes becoming important perhaps related to the ability for $m \gtrsim 10 M_{\odot}$ stars to continue to grow through

¹¹ A study by Maschberger and Clarke (2008) of the most-massive star data in young star clusters concluded that “the data are not indicating any striking deviation from the expectations of random drawing.” This statement has been frequently misinterpreted that other sampling mechanisms are ruled out. However, the Maschberger and Clarke analysis focuses on low-mass clusters where the data were insufficient to decide whether star clusters are populated purely randomly from an IMF with constant upper mass limit or, for example, in a sorted fashion. The differences appear clearly at higher cluster masses, not included in their analysis but in Weidner and Kroupa (2006) and Weidner et al. (2010). Maschberger & Clarke (2008) adapt their data set according to the requested result and so their study does not constitute an acceptable scientific standard.

accretion alone. Another physical process of possible relevance leading to a reduction of $dm_{\max}/dM_{\text{ecl}}$ for $m_{\max} \gtrsim 10 M_{\odot}$ may be due to an instability in the cold inter-stellar medium (ISM) developing at a mass around $M_{\text{ecl}} = 10^2 M_{\odot}$ similar to the ISM instabilities discussed in Pflamm-Altenburg and Kroupa (2009a). Such an accretion instability may lead to enhanced accretion of gas onto the pre-cluster cloud core from the surrounding molecular cloud. If $m_{\max} \gtrsim 10 M_{\odot}$ stars have a reduced accretion efficiency, then this may explain the flattening since a smaller fraction of the newly accreted gas adds to the growth of m_{\max} and is instead used up by the formation of less-massive cluster stars (*fragmentation-induced starvation* of Peters et al. 2010, 2011b). Furthermore, it may be possible that for $M_{\text{ecl}} > 10^2 M_{\odot}$, sub-cluster merging may be becoming an important physical process: Each sub-cluster with $M_{\text{ecl}} \lesssim 100 M_{\odot}$ follows the $m_{\max} - M_{\text{ecl}}$ relation such that upon amalgamation of the sub-clusters, m_{\max} changes less than M_{ecl} . The steepening of the $m_{\max} - M_{\text{ecl}}$ relation for $M_{\text{ecl}} \gtrsim 10^3 M_{\odot}$ may be affected by the coalescence of massive protostars in the dense centers of forming embedded clusters.

Peters et al. (2010, 2011b) discuss the physics driving the $m_{\max} - M_{\text{ecl}}$ relation (for $M_{\text{ecl}} \lesssim 10^2 M_{\odot}$) and find that m_{\max} -growth curves flatten with increasing M_{ecl} because infalling gas is accreted by the other stars in the emerging cluster. In particular, the appearance of close companions to the most-massive star reduces its growth, while the star cluster continues to form. Feedback allows the growth of the most-massive star to be sustained for longer essentially by heating the gas such that it is less susceptible to fall into the potentials of lower-mass companions and stars and is therewith forced to follow the main potential toward the center, thereby leading to better agreement with the observed $m_{\max} - M_{\text{ecl}}$ relation. If no cluster of low-mass stars were to form such that none of the gas is accreted by the other low-mass stars, then $m_{\max} \propto M_{\text{ecl}}$, which is a dependency which is too steep compared to the data.

3.3.4 Stochastic or Regulated Star Formation?

The existence of an observed $m_{\max} \propto M_{\text{ecl}}^{2/3}$ relation (● 4.49) different to the one expected from random sampling from the IMF thus implies that the formation of massive stars is associated with surrounding low-mass star formation. This suggests that the formation of stars within the cloud cores is mostly governed by gravitationally driven growth processes in a medium with limited resources.

If the outcome of star formation were to be inherently stochastic, as is often assumed to be the case, in the sense that stars are randomly selected from the full IMF, then this would imply that stellar feedback would have to be, by stringent logical implication, the randomization agent. In other words, the well-ordered process of stars arising from a molecular cloud core by pure gravitationally driven accretion as shown to be the case by self-consistent gravo-hydrodynamical simulations would have to be upset completely through feedback processes. As there is no physically acceptable way that this might arise, and since in fact the work of Peters et al. (2010, 2011b) has demonstrated that feedback actually helps establish the $m_{\max} - M_{\text{ecl}}$ relation, it is concluded that star formation cannot be a random process, and its outcome cannot be described by randomly choosing stars from an IMF.¹²

¹²Choosing stars randomly from the IMF is, however, a good first approximation for many purposes of study.

Returning to [Sect. 1.5](#), the following two alternative hypotheses can thus be stated:

IMF Random Sampling Hypothesis

A star formation event always produces a probabilistically sampled IMF.

IMF Optimal Sampling Hypothesis

A star formation event always produces an optimally sampled IMF such that the $m_{\max} - M_{\text{ecl}}$ relation holds true.

As stated above, the IMF random sampling hypothesis can already be discarded on the basis of the existing data and simulations. But can the current data discard the IMF optimal sampling hypothesis? The scatter evident in [Fig. 4-5](#) may suggest that optimal sampling is ruled out, since if it were true for every cluster, then a one-to-one relation between m_{\max} and M_{ecl} would exist. However, the following effects contribute to introducing a dispersion of m_{\max} values for a given M_{ecl} , even if an exact $m_{\max} - M_{\text{ecl}}$ relation exists:

- The measurement of M_{ecl} and m_{\max} are very difficult and prone to uncertainty.
- An ensemble of embedded clusters of a given stellar mass M_{ecl} is likely to end up with a range of m_{\max} because the pre-cluster cloud cores are likely to be subject to different boundary conditions (internal distribution of angular momentum, different thermodynamic state, different external radiation field, different metallicity, etc.). The details of self-regulation depend on such quantities, and this may be compared to the natural dispersion of stellar luminosities at a given stellar mass due to different metallicity, stellar spins, and orientations relative to the observer and different stellar ages.

At present, the IMF optimal sampling hypothesis can thus not be discarded, but its statement here may be conducive to further research to investigate how exactly valid it is.

3.3.5 A Historical Note

Larson (1982) had pointed out that more massive and dense clouds correlate with the mass of the most massive stars within them, and he estimated that $m_{\max} = 0.33 M_{\text{cloud}}^{0.43}$ (masses are in M_{\odot}). An updated relation was derived by Larson (2003) by comparing m_{\max} with the stellar mass in a few clusters, $m_{\max} \approx 1.2 M_{\text{cluster}}^{0.45}$. Both are flatter than the semi-analytical relation and therefore do not fit the data in [Fig. 4-5](#) as well (Weidner and Kroupa 2006). Elmegreen (1983) constructed a relation between cluster mass and its most massive star based on an assumed equivalence between the luminosity of the cluster population and its binding energy for a Miller–Scalo IMF (a self-regulation model). This function is even shallower than the one estimated by Larson (2003).

3.4 Caveats

Unanswered questions regarding the formation and evolution of massive stars remain. There may be stars forming with $m > m_{\text{max}*}$ which implode “invisibly” after 1 or 2 Myr. The explosion mechanism sensitively depends on the presently still rather uncertain mechanism for shock revival after core collapse (e.g., Janka 2001). Since such stars would not be apparent in massive clusters older than 2 Myr, they would not affect the empirical maximal stellar mass, and $m_{\text{max}*,\text{true}}$ would be unknown at present.

Furthermore, stars are often in multiple systems. Especially, massive stars seem to have a binary fraction of 80% or even larger and apparently tend to be in binary systems with a preferred mass ratio $q \gtrsim 0.2$ (Sect. 2.6). Thus, if all O stars would be in equal-mass binaries, then $m_{\text{max}*,\text{true}} \approx m_{\text{max}*}/2$.

Finally, it is noteworthy that $m_{\text{max}*} \approx 150 M_{\odot}$ appears to be the same for low-metallicity environments ($[\text{Fe}/\text{H}] = -0.5$, R136) and metal-rich environments ($[\text{Fe}/\text{H}] = 0$, Arches), in apparent contradiction to the theoretical values (Stothers 1992). Clearly, this issue needs further study.

Main Results

A fundamental upper mass limit for stars appears to exist, $m_{\text{max}*} \approx 150 M_{\odot}$. The mass of a cluster defines the most-massive star in it and leads to the existence of a $m_{\text{max}} - M_{\text{ecf}}$ relation, which results from competitive resource-limited growth and self-regulation processes. The outcome of a star formation event appears to be close to an optimally sampled IMF.

4 The Isolated Formation of Massive Stars

An interesting problem relevant for the discussion in Sect. 3.3 with major implications for star-formation theory and the IMF in whole galaxies is whether massive stars can form alone without a star cluster, that is, in isolation (e.g., Li et al. 2003; Krumholz and McKee 2008).

Related to this is one of the most important issues in star-formation theory, namely, the still incomplete understanding of how massive stars ($m \gtrsim 10 M_{\odot}$) form. From Fig. 4-5, a gas density of $\rho_{\text{gas}} \gtrsim 10^3 M_{\odot}/\text{pc}^3$ for the formation of $m > 10 M_{\odot}$ stars can be deduced. At least four competing theories have been developed: the competitive accretion scenario (Bonnell et al. 1998, 2004; Bonnell and Bate 2006), collisional merging (Bonnell and Bate 2002), the single core collapse model allowing isolated massive star formation (Krumholz et al. 2009), the fragmentation-induced starvation model (Peters et al. 2010, 2011b) and the outflow-regulated clump-collapse models (Wang et al. 2010) where massive stars result from the collapse of turbulent cluster-forming clumps, whose internal dynamics are regulated by protostellar outflows.

To help advance this topic, it is necessary to find conclusive constraints for the formation of massive stars from observations. One important piece of evidence can be deduced from the formation sites of massive stars. While competitive accretion, collisional merging, and fragmentation-induced starvation descriptions and outflow-regulated clump collapse predict

the formation of massive stars within star clusters, the core collapse model needs a sufficiently massive and dense cloud core and allows for an isolated origin of O stars.

This latter model appears to be inconsistent with the data (► Sect. 3.3). And, even the currently most advanced radiation-magnetohydrodynamical simulations including ionization feedback of a $1,000 M_{\odot}$ rotating cloud lead to suppression of fragmentation by merely a factor of about two (Peters et al. 2011a), so that massive star formation cannot be separated from the formation of embedded clusters.

Nevertheless, the isolated formation of massive stars remains a popular option in the research community. Discussing field O stars, Massey (1998) writes (his p. 34) “One is tempted to conclude that these O3 stars formed pretty much where we see them today, as part of very modest star-formation events, ones that perhaps produce “a single O star plus some change,” as Jay Gallagher aptly put it.” Selier et al. (2011) write “There is, however, a statistically small percentage of massive stars ($\approx 5\%$) that form in isolation (de Wit et al. 2005; Parker and Goodwin 2007)” while Camargo et al. (2010) confess “On the other hand, de Wit et al. (2005) estimate that nearly 95% of the Galactic O star population is located in clusters or OB associations, or can be kinematically linked with them.” Lamb et al. (2010) state “In a study of Galactic field O stars, de Wit et al. (2004, 2005) find that 4 ± 2 per cent of all Galactic O stars appear to have formed in isolation, without the presence of a nearby cluster or evidence of a large space velocity indicative of a runaway star,” while Krumholz et al. (2010) explain “de Wit et al. (2004, 2005) find that 4 ± 2 per cent of galactic O stars formed outside of a cluster of significant mass, which is consistent with the models presented here (for example, runs M and H form effectively isolated massive single stars or binaries), but not with the proposed cluster-stellar mass correlation.” Such events of isolated massive star formation are conceivable if the equation of state of the interstellar medium can become stiff (Li et al. 2003). Hence, the search for isolated O stars and the deduction whether or not these stars have formed in situ can be vital in narrowing down theories and advancing the research field. Generally, in order to propose that massive stars form in isolation rather contrived initial conditions in the cloud core are required such as a strong magnetic field, no turbulence and a highly peaked density profile (Girichidis et al. 2011).

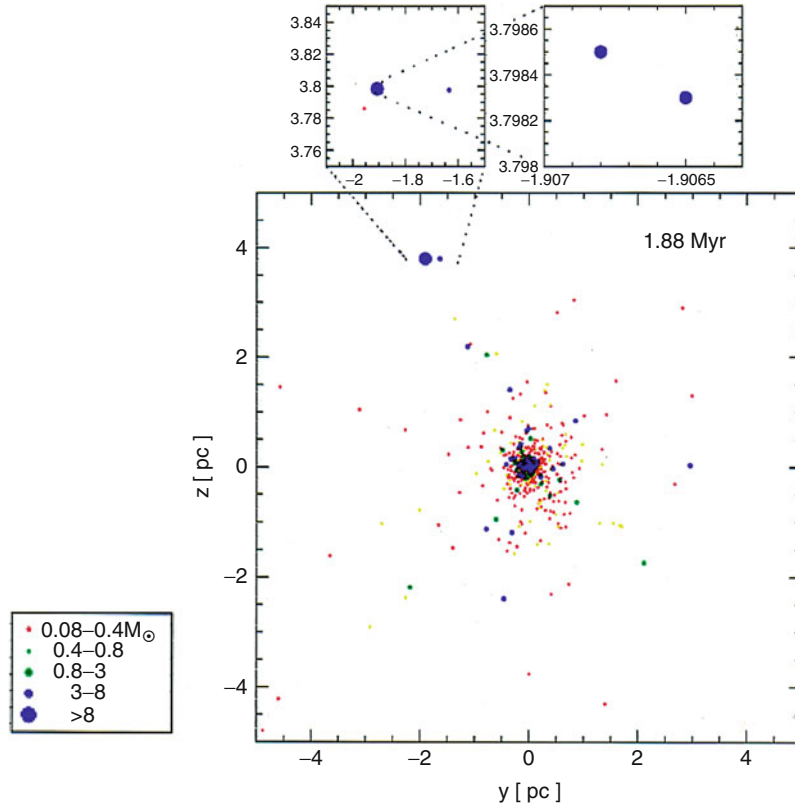
The existence of massive stars formed in isolation would be required if the stellar distribution within a galaxy was a result of a purely stochastic process in contradiction to the IGIMF theory (► Sect. 13.1), and would not be in agreement with the existence of the $m_{\max} - M_{\text{ccl}}$ relation (► 4.49).

This discussion does not have an easy observational solution because massive stars have been observed to be quite far away from sites where late-type stars or star clusters are forming and it can never be proven beyond any arbitrarily small doubt that a given star comes from a cluster.

One possible way to prove that a massive star formed in isolation, that is, with at most a few companions, would be to discover an isolated massive star with wide companions. This would invalidate the star having been ejected from a cluster. Unfortunately, even this possible criterion is not fool proof evidence for the occurrence of isolated massive star formation, as the example in ► Fig. 4-6 demonstrates.

Thus, a decision on whether star formation is random enough to allow the formation of massive stars by themselves in isolation can only be reached through statistical arguments since it can never be proven beyond doubt that some particular massive star did not form in isolation. It is thus essential to understand all possible physical mechanisms that contribute to massive stars being distributed widely throughout a galaxy.

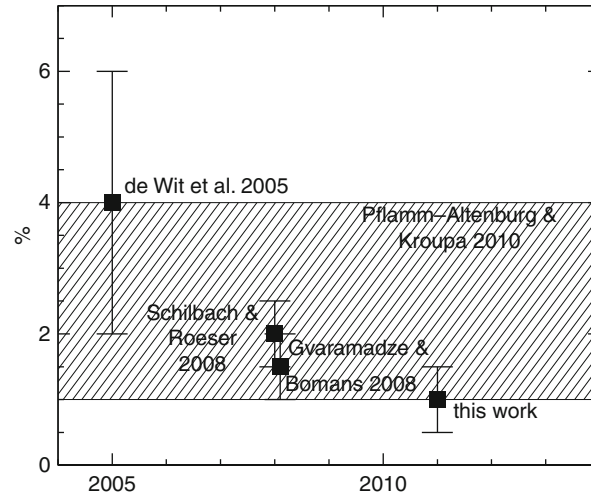
The “OB field star” MF has $\alpha \approx 4.5$, which has been interpreted to be the result of isolated high-mass star formation in small clouds (Massey 1998). Precise proper-motion measurements



■ Fig. 4-6

An N -body5 (Aarseth 1999) model of a star cluster initially not mass segregated, in virial equilibrium, with a randomly drawn IMF with stellar masses between 0.08 and $30 M_{\odot}$ and with a binary fraction of 100% (☉ 4.46). The cluster consists of 400 binaries distributed in a Plummer model with a half-mass radius of $r_{0.5} = 0.1$ pc. The stellar masses are denoted by different symbols as defined in the key. Mass segregation develops within the energy-equipartition time scale $t_{\text{eq}} < 0.4$ Myr (Kroupa 2008) such that the low-mass stars expand outward. The snapshot shows the system at a time of 1.88 Myr. By this time, a massive star system has been expelled from the cluster by a relatively gentle (about 2 km/s) cluster-potential–star recoil. The expelled massive star, which is an equal-mass binary formed after an exchange encounter within the cluster core, has a very wide intermediate-mass companion as well as a very wide M dwarf companion. It is easy to misinterpret such a hierarchical multiple system, located more than 4 pc away from a compact young cluster, to be an ideal candidate for isolated massive star formation

have, however, shown that a substantial number of even the best candidates for such an isolated population have high space motions (Ramspeck et al. 2001) which are best understood as the result of energetic stellar-dynamical ejections when massive binary systems interact in the cores of star clusters in star-forming regions. This interpretation poses important constraints on the initial properties of OB binary systems (Clarke and Pringle 1992; Kroupa 2001a; Pflamm-Altenburg and Kroupa 2006; Gvaramadze and Gualandris 2011). Still, de Wit et al. (2004, 2005) found that $4\% \pm 2\%$ of all O stars may have formed outside any cluster environment.



■ Fig. 4-7

Estimates of the percentage of massive stars formed in isolation as a function of publication year. The present-day (2011) estimate of the fraction of O stars which cannot be traced back to their birth clusters is at the lower limit of what is expected from the two-step mechanism (*shaded area*) (From Gvaramadze et al. 2012)

This percentage, however, had to be reduced twice (► Fig. 4-7) because Schilbach and Röser (2008) showed that 6 out of 11 stars that apparently formed in isolation can be back-traced to their parent clusters. Moreover, Gvaramadze and Bomans (2008) demonstrated that one of the best examples for isolated Galactic high-mass star formation (de Wit et al. 2005), the star HD 165319, has a bow shock and is thus a runaway star, most likely ejected from the young massive star cluster NGC 6611. This further reduces the percentage of massive stars possibly formed in isolation, bringing it to $1.5\% \pm 0.5\%$. And finally, using the WISE data, Gvaramadze et al. (2012) discovered a bow shock generated by one more star (HD 48279) from the sample of the best examples for isolated Galactic high-mass star formation. Correspondingly, the percentage of massive stars which may have formed in isolation is reduced to $1.0\% \pm 0.5\%$. Another example of a possible very massive star having formed in isolation is VFTS 682 which is an about $150 M_{\odot}$ heavy star located about 30 pc in projection from the star burst cluster R136 in the Large Magellanic Cloud (Bestenlehner et al. 2011). However, realistic binary-rich N -body models of initially mass-segregated R136-type clusters show that such massive stars are ejected with the observed velocities in all computations therewith readily allowing VFTS 682 to be interpreted as a slow runaway from R136 (Banerjee et al. 2012).

Massive stars may perfectly appear to have formed in isolation despite originating in clusters: The “two-step-ejection scenario,” which places massive stars outside their parent cluster such that they may fake isolated formation, has been presented by Pflamm-Altenburg and Kroupa (2010). This is based on massive binaries first being dynamically ejected from their parent star cluster. The subsequent type II supernova explosion then places the remaining massive star on a random trajectory such that it can nearly never be traced back to its parent star cluster. This is necessarily the case for 1–4% of all O stars assuming all massive stars to form in star clusters which obey the $m_{\text{max}} - M_{\text{ecl}}$ relation. Further, if the ejected O star system consists of a tight inner binary with an outer companion the Kozai mechanism is likely to force the

inner binary into coalescence leading to a rejuvenated massive star (a massive blue straggler). When the outer companion explodes the massive blue straggler would be released in a random direction such that neither its age nor its motion would allow it to be traced to its cluster of origin.

Thus, as shown above, after excluding all observed O stars that can be traced back to young star clusters as well as those with bow shocks, the current observational evidence for the possible existence of isolated O star formation amounts to 1% of all known O stars. This is at the lower limit of the expected two-step ejection fraction of O stars that cannot be traced back to their cluster of origin. There is therefore no meaningful evidence for the formation of massive stars in isolation. The hypothesis that the isolated formation of massive stars can be a significant contributor to the population of massive stars such that the IMF of a whole galaxy effectively becomes a purely probabilistic invariant distribution function can formally be negated by noting that the observed IMF is too invariant (◆ Fig. 4-27). That is, an isolated massive star would correspond to an IMF that significantly differs, by chance, from the theoretical parent distribution function. But for each such extreme case there would be many more cases of coeval stellar populations that by chance have “strange” IMFs. There is no observational evidence whatsoever for this: all known resolved stellar populations are canonical.

Main Result

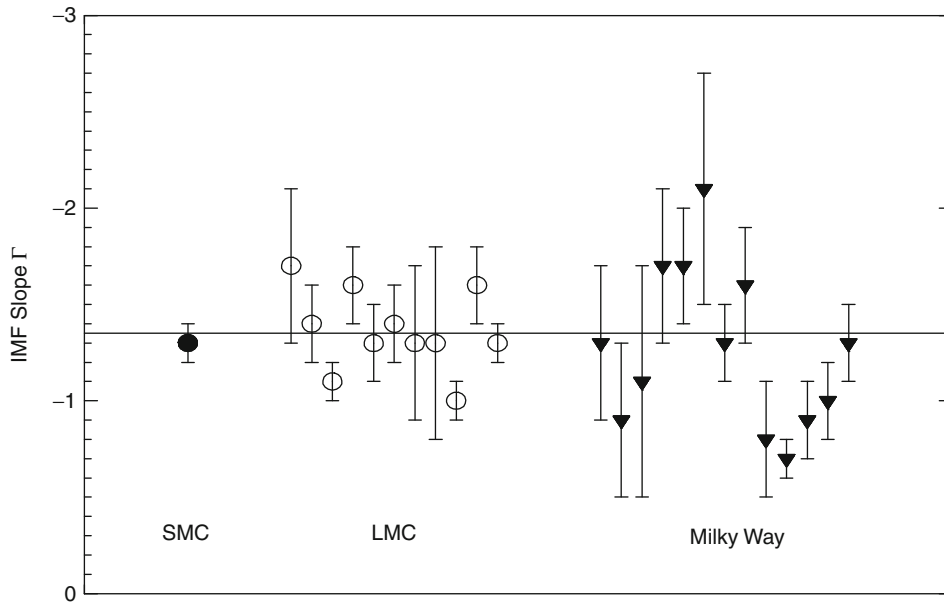
The observed field massive stars are the necessary outcome of the formation of massive stars as multiple systems in the cores of embedded clusters. There is no convincing evidence for the formation of isolated massive stars.

5 The IMF of Massive Stars

In what follows, the IMF power law indices are α_1 for $0.07 \leq m/M_\odot < 0.5$, α_2 for $0.5 \leq m/M_\odot \lesssim 1$, α_3 for $1 \lesssim m/M_\odot$.

Studying the distribution of massive stars ($\gtrsim 10 M_\odot$) is complicated because they radiate most of their energy at far-UV wavelengths that are not accessible from the Earth and through their short main-sequence lifetimes, τ , that remove them from star-count surveys. For example, a $85 M_\odot$ star cannot be distinguished from a $40 M_\odot$ star on the basis of M_V alone (Massey 2003). Constructing $\Psi(M_V)$ in order to arrive at $\Xi(m)$ for a mixed-age population does not lead to success if optical or even UV bands are used. Instead, spectral classification and broadband photometry for estimation of the reddening on a star-by-star basis has to be performed to measure the effective temperature, T_{eff} , and the bolometric magnitude, M_{bol} , from which m is obtained allowing the construction of $\Xi(m)$ directly (whereby $\Psi(M_{\text{bol}})$ and $\Xi(m)$ are related by (◆ 4.1)). Having obtained $\Xi(m)$ for a population under study, the IMF follows by applying (◆ 4.3) after evolving each measured stellar mass to its initial value using theoretical stellar evolution tracks.

Massey (2003) stresses that studies that only rely on broadband optical photometry consistently arrive at IMFs that are significantly steeper with $\alpha_3 \approx 3$, rather than $\alpha_3 = 2.2 \pm 0.1$ found for a wide range of stellar populations using spectroscopic classification. Indeed, the application of the same methodology by Massey on a number of young populations of different metallicity and density shows a remarkable uniformity of the IMF above about $10 M_\odot$ (◆ Fig. 4-8).



■ Fig. 4-8

The IMF slope $\Gamma = 1 - \alpha_3$ determined in a homogeneous manner for OB associations and clusters in the MW, LMC, and SMC. The Small Magellanic Cloud (SMC) has a metallicity $Z = 0.005$ ($[\text{Fe}/\text{H}] \approx -0.6$), the Large Magellanic Cloud (LMC) has $Z = 0.008$ ($[\text{Fe}/\text{H}] \approx -0.4$), and the Milky Way (MW) has $Z = 0.018$ ($[\text{Fe}/\text{H}] \approx -0.05$) within a distance of 3 kpc around the Sun (with kind permission from Massey (2003))

The available IMF measurements do not take into account the bias through unresolved systems which may, in principle, be substantial since the proportion of multiple stars is higher for massive stars than for low-mass Galactic-field stars (e.g., Duchêne et al. 2001). For example, in the Orion Nebula Cluster (ONC), each massive star has, on average, 1.5 companions (Preibisch et al. 1999), while in the cluster NGC 6231, García and Mermilliod (2001) find that 80% of all O stars are radial-velocity binaries.

However, Maíz Apellániz (2008) and Weidner et al. (2009) demonstrate that the observed IMF for massive stars is not affected significantly by unresolved multiple systems: The models, where initial masses are derived from the luminosity and color of unresolved multiple systems, show that even under extreme circumstances (100% binaries or higher order multiples), the difference between the power-law index of the mass function (MF) of all stars and the observed MF is small ($\Delta\alpha \lesssim 0.1$). Thus, if the observed IMF has the Salpeter index $\alpha_3 = 2.35$, then the true stellar IMF has an index not flatter than $\alpha_3 = 2.25$.

Massive main-sequence stars have substantial winds flowing outward with velocities of a few 100 to a few 1,000 km/s (Kudritzki and Puls 2000). For example, $10^{-6.5} < \dot{m} < 10^{-6} M_{\odot}/\text{year}$ for $m = 35 M_{\odot}$ with main-sequence lifetime $\tau = 4.5$ Myr (García-Segura et al. 1996a) and $10^{-5.6} < \dot{m} < 10^{-5.8} M_{\odot}/\text{year}$ for $m = 60 M_{\odot}$ with $\tau = 3.45$ Myr (García-Segura et al. 1996b). More problematical is that stars form rapidly rotating and are sub-luminous as a result of reduced internal pressure. But they decelerate significantly during their main-sequence lifetime owing to the angular-momentum loss through their winds and become more luminous more

rapidly than nonrotating stars (Maeder and Meynet 2000). For ages less than 2.5 Myr, the models deviate only by 5–13% from each other in mass, luminosity, or temperature (Weidner and Kroupa 2006). Large deviations are evident for advanced stages of evolution though because of the sensitivity to the different treatment of the stellar physics.

The mass–luminosity relation for a population of stars that have a range of ages is broadened, making mass estimates from M_{bol} uncertain by up to 50% (Penny et al. 2001), a bias that probably needs to be taken into account more thoroughly in the derivations of the IMF. Another problem is that $m \gtrsim 40 M_{\odot}$ stars may finish their assembly after burning a significant proportion of their central H so that a zero-age main sequence may not exist for massive stars (Maeder and Behrend 2002). However, the agreement between slowly rotating tidally locked massive O-type binaries with standard nonrotating theoretical stellar models is very good (Penny et al. 2001).

Main Results

The IMF of massive stars is well described by a *Salpeter/Massey* slope, $\alpha_3 = 2.3$, independent of environment as deduced from resolved stellar populations in the Local Group of galaxies. Unresolved multiple stars do not significantly affect the massive-star power-law index.

A note to the statement that $\alpha_3 = 2.3$ is independent of environment: This is strictly only valid for star formation with densities less than about $10^5 M_{\odot}/\text{pc}^3$ and for metallicities of $[\text{Fe}/\text{H}] \gtrsim -2$ as are observed in the Local Group of galaxies. Evidence has emerged that star formation at higher densities leads to top-heavy IMFs (see [Fig. 4-31](#) below).

6 The IMF of Intermediate-Mass Stars

Intermediate-mass ($\approx 1\text{--}8 M_{\odot}$) stars constitute a complicated sample to deal with in terms of inferring their mass function from star counts in the Galactic field as well as in star clusters. Their lifetimes are comparable to the age of the Galactic disk down to the lifetime of typical open clusters (a few 10^8 year, [Fig. 4-26](#) below). Also, the distribution function of multiple systems changes in this mass range ([Sect. 2.6](#)). Corrections of their luminosities for stellar evolution and binarity are thus more challenging than in the other mass ranges. Also, the diffusion of stellar orbits within the MW disk away from the birth orbits has a comparable time scale (the dynamical period of the Milky Way) such that an ensemble of intermediate-mass stars does not have an as well constrained Galactic-disk thickness as the massive (≈ 50 pc) or low-mass (≈ 500 pc) stars. This affects the combination of the essentially two-dimensional (in the Galactic disk plane) star counts of massive stars with the three-dimensional (solar neighborhood within a few hundred pc) star counts of late-type main sequence stars to a common density of stars in dependence of stellar luminosity. This issue is dealt with excellently by Scalo (1986). The resulting constraints on the IMF in this mass range are rather uncertain. Indeed, in [Fig. 4-26](#), it is evident that the scatter of deduced α -indices is very large in this mass range, and the analysis by Scalo (1986) may even suggest a discontinuity in the Galactic-disk IMF in this mass range.

The stellar IMF has $\alpha_2 \approx 2.3$ for stars with $0.5 < m/M_{\odot} < 1$ (main results on p. 177) and $\alpha_3 \approx 2.3$ for $m \gtrsim 8 M_{\odot}$ ([Sect. 5](#)) such that $\alpha_3 \approx 2.3$ for $1 \lesssim m/M_{\odot} \lesssim 8$ appears natural. However,

as noted in [Sect. 2.6](#), the initial binary properties appear to be different for $m < \text{few } M_\odot$ in comparison to those for $m > \text{few } M_\odot$ implying open question I on p. 143.

Here, it is assumed that the IMF is continuous across this mass range, and thus attention is given to the massive ([Sect. 5](#)) and low-mass stars ([Sect. 7](#)). But in view of the discontinuity issue uncovered on p. 178 for stars and brown dwarfs, the continuity assumption made here needs to be kept in mind.

7 The IMF of Low-Mass Stars (LMSs)

Here, stars with $0.1 \lesssim m/M_\odot \lesssim 1$ (the LMSs) are discussed. They are late-type main sequence stars which constitute the vast majority of all stars in any known stellar population ([Table 4-1](#) below). Also, their initial binary properties follow rather simple rules ([Sect. 2.6](#)). Very low-mass stars (VLMSs) with $m \lesssim 0.15 M_\odot$ are the subject of [Sect. 8](#).

There are three well-tried approaches to determine $\Psi(M_V)$ in ([4.1](#)). The first two are applied to Galactic-field stars (parallax- and flux-limited star-counts) and the third to star clusters (establishment of members). The sample of Galactic-field stars close to the Sun (typically within 5–20 pc distance depending on m) is especially important because it is the most complete and well-studied stellar sample at our disposal.

7.1 Galactic-Field Stars and the Stellar Luminosity Function

Galactic-field stars have an average age of about 5 Gyr and represent a mixture of many star-formation events. The IMF deduced for these is therefore a time-cumulated composite IMF (i.e., the IGIMF, [Sect. 13.1](#)). For $m \lesssim 1.3 M_\odot$, the composite IMF equals the stellar IMF according to the presently available analysis, and so it is an interesting quantity for at least two reasons: For the mass budget of the Milky Way disk and as a benchmark against which the IMFs measured in present- and past-occurring star-formation events can be compared to distill possible variations about the mean.

The *first and most straightforward method* consists of creating a local volume-limited catalogue of stars yielding the nearby LF, $\Psi_{\text{near}}(M_V)$. Completeness of the modern *Jahreiss–Gliese Catalogue of Nearby Stars* extends to about 25 pc for $m \gtrsim 0.6 M_\odot$, trigonometric distances having been measured using the Hipparcos satellite, and only to about 5 pc for less massive stars for which we still rely on ground-based trigonometric parallax measurements.¹³ The advantage of the LF, $\Psi_{\text{near}}(M_V)$, created using this catalogue, is that virtually all companion stars are known, that it is truly distance limited, and that the distance measurements are direct.

¹³Owing to the poor statistical definition of $\Psi_{\text{near}}(M_V)$ for $m \lesssim 0.5 M_\odot$, $M_V \gtrsim 10$, it is important to increase the sample of nearby stars, but controversy exists as to the maximum distance to which the LMS census is complete. Using spectroscopic parallax, it has been suggested that the local census of LMSs is complete to within about 15% to distances of 8 pc and beyond (Reid and Gizis 1997). However, Malmquist bias allows stars and unresolved binaries to enter such a flux-limited sample from much larger distances (Kroupa 2001c). The increase of the number of stars with distance using trigonometric distance measurements shows that the nearby sample becomes incomplete for distances larger than 5 pc and for $M_V > 12$ (Jahreiss 1994; Henry et al. 1997). The incompleteness in the northern stellar census beyond 5 pc and within 10 pc amounts to about 35% (Jao et al. 2003), and further discovered companions (e.g., Delfosse et al. 1999; Beuzit et al. 2004) to known primaries in the distance range $5 < d < 12$ pc indeed suggest that the extended sample may not yet be complete. Based on the work by Reid et al. (2003a, b), Luhman (2004), however, argues that the incompleteness is only about 15%.

■ Table 4-1

See ● Sect. 10.1. The number fraction $\eta_N = 100 \int_{m_1}^{m_2} \xi(m) dm / \int_{m_1}^{m_u} \xi(m) dm$; the mass fraction $\eta_M = 100 \int_{m_1}^{m_2} m \xi(m) dm / M_{cl}$, $M_{cl} = \int_{m_1}^{m_u} m \xi(m) dm$, in percent of main-sequence stars in the mass interval m_1 to m_2 ; and the stellar contribution, ρ^{st} , to the Oort limit and to the Galactic-disk surface mass density, $\Sigma^{st} = 2h\rho^{st}$, near to the Sun, taking $m_l = 0.07 M_\odot$, $m_u = 120 M_\odot$, and the Galactic-disk scale height $h = 250$ pc ($m < 1 M_\odot$ Kroupa et al. 1993) and $h = 90$ pc ($m > 1 M_\odot$, Scalo 1986). Results are shown for the canonical IMF (● 4.55) for the high-mass-star Galactic-field IMF ($\alpha_3 = 2.7$, $m > 1 M_\odot$) and for the PDMF ($\alpha_3 = 4.5$, Scalo 1986; Kroupa et al. 1993) which describes the distribution of stellar masses now populating the Galactic disk. For gas, $\Sigma^{gas} = 13 \pm 3 M_\odot/\text{pc}^2$ and remnants $\Sigma^{rem} \approx 3 M_\odot/\text{pc}^2$ (Weidemann 1990). The average stellar mass is $\bar{m} = \int_{m_l}^{m_u} m \xi(m) dm / \int_{m_l}^{m_u} \xi(m) dm$. m_{max} and M_{ecd} are calculated using equations ● 4.10 and ● 4.11, with $m_{max*} = 120 M_\odot$. N_{cl} is the number of stars that have to form in a star cluster such that the most massive star in the population has the mass m_{max} . The mass of this population is M_{cl} , and the condition is $\int_{m_{max}}^{120 M_\odot} \xi(m) dm = 1$ with $\int_{0.07}^{m_{max}} \xi(m) dm = N_{cl} - 1$. $\Delta M_{cl}/M_{cl}$ is the fraction of mass lost from the cluster due to stellar evolution, assuming that for $m \geq 8 M_\odot$, all neutron stars and black holes are kicked out due to an asymmetrical supernova explosion but that white dwarfs are retained (Weidemann et al. 1992). The masses of the white dwarfs are estimated as $m_{WD} = 0.109 m_{ini} + 0.394 [M_\odot]$, which is a linear fit to the masses of observed white dwarfs (Kalirai et al. 2008). The evolution time for a star of mass m_{to} to reach the turnoff age is available in ● Fig. 4-26. Note that brown dwarfs are not considered for any of the numbers listed in this table

Mass range (M_\odot)	η_N (%)			η_M (%)			ρ^{st} (M_\odot/pc^3)	Σ^{st} (M_\odot/pc^2)
	α_3	α_3	α_3	α_3	α_3	α_3	α_3	α_3
	2.3	2.7	4.5	2.3	2.7	4.5	4.5	4.5
0.07–0.5	77.71	79.39	82.38	28.42	37.96	52.90	2.17×10^{-2}	9.73
0.5–1	13.25	13.54	14.05	16.66	22.24	31.00	1.27×10^{-2}	5.70
1–8	8.45	6.87	3.57	33.44	31.62	16.01	6.56×10^{-3}	2.95
8–120	0.59	0.20	0.00	21.48	8.18	0.09	3.69×10^{-5}	1.66×10^{-2}
$\overline{m}/M_\odot =$	0.545	0.417	0.310				$\rho_{\text{tot}}^{\text{st}} = 0.041$	$\Sigma_{\text{tot}}^{\text{st}} = 18.4$

m_{max} (M_\odot)	$\alpha_3 = 2.3$		$\alpha_3 = 2.7$		m_{to} (M_\odot)	$\Delta M_{\text{d}}/M_{\text{d}}$ (%)	
	N_{cl}	M_{cl} (M_\odot)	N_{cl}	M_{cl} (M_\odot)		$\alpha_3 = 2.3$	$\alpha_3 = 2.7$
1	13	3.2	15	3.8	80	2.2	0.5
8	173	82	489	187	60	4.0	0.9
20	601	307	2415	970	40	6.7	1.7
40	1756	893	8839	3623	20	12.2	3.6
60	3803	1993	21509	8885	8	21.5	8.2
80	8023	4275	48750	20224	3	32.1	15.8
100	20820	11236	133129	55385	1	45.2	29.9
119	509319	277416	3.38×10^6	1.41×10^6	0.7	48.6	34.4

The *second method* is to make deep pencil-beam surveys using photographic plates or CCD cameras to extract a few hundred low-mass stars from a hundred-thousand stellar and galactic images. This approach, pioneered by Gerry Gilmore and Neill Reid, leads to larger stellar

samples especially so since many lines of sight into the Galactic field ranging to distances of a few hundred pc to a few kpc are possible. The disadvantage of the LF, $\Psi_{\text{phot}}(M_V)$, created using this technique is that the distance measurements are indirect relying on photometric parallax. Such surveys are flux-limited rather than volume-limited, and pencil-beam surveys which do not pass through virtually the entire stellar disk are prone to Malmquist bias (Stobie et al. 1989). This bias results from a spread of luminosities of stars that have the same color because of their dispersion of metallicities and ages, leading to intrinsically more luminous stars entering the flux-limited sample and thus biasing the inferred absolute luminosities and the inferred stellar space densities. Furthermore, binary systems are not resolved in the deep surveys, or if formally resolved, the secondary is likely to be below the flux limit.

The local, *nearby LF* and the Malmquist-corrected deep *photometric LF* are displayed in [Fig. 4-9](#). They differ significantly for stars fainter than $M_V \approx 11.5$ which caused some controversy in the past.¹⁴ That the local sample has a spurious but significant overabundance of low-mass stars can be ruled out by virtue of the large velocity dispersion in the disk, ≈ 30 pc/Myr. Any significant overabundance of stars within a sphere with a radius of 30 pc would disappear within 1 Myr and cannot be created by any physically plausible mechanism from a population of stars with stellar ages spanning the age of the Galactic disk. The shape of $\Psi_{\text{phot}}(M_V)$ for $M_V \gtrsim 12$ is confirmed by many independent photometric surveys. That all of these could be making similar mistakes, such as in color transformations, becomes unlikely on consideration of the LFs constructed for completely independent stellar samples, namely, star clusters ([Fig. 4-10](#)).

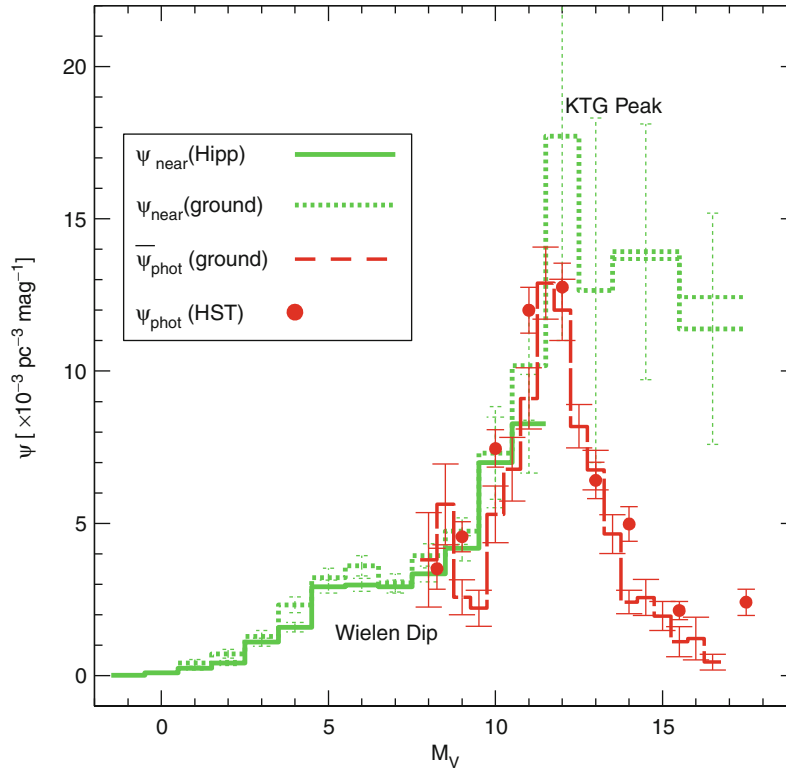
7.2 The Stellar Mass–Luminosity Relation

The MF is related to the LF via the derivative of the stellar mass–luminosity relation ([4.1](#)).

[Equation 4.1](#) shows that any nonlinear structure in the MLR is mapped into observable structure in the LF, provided the MF does not have a compensating structure. Such a conspiracy is implausible because the MF is defined through the star-formation process, but the MLR is a result of the internal constitution of stars. The MLR and its derivative are shown in [Fig. 4-11](#). It is apparent that the slope is very small at faint luminosities leading to large uncertainties in the MF near the hydrogen burning mass limit.

The physics underlying the nonlinearities of the MLR are due to an interplay of changing opacities, the internal stellar structure, and the equation of state of the matter deep inside the

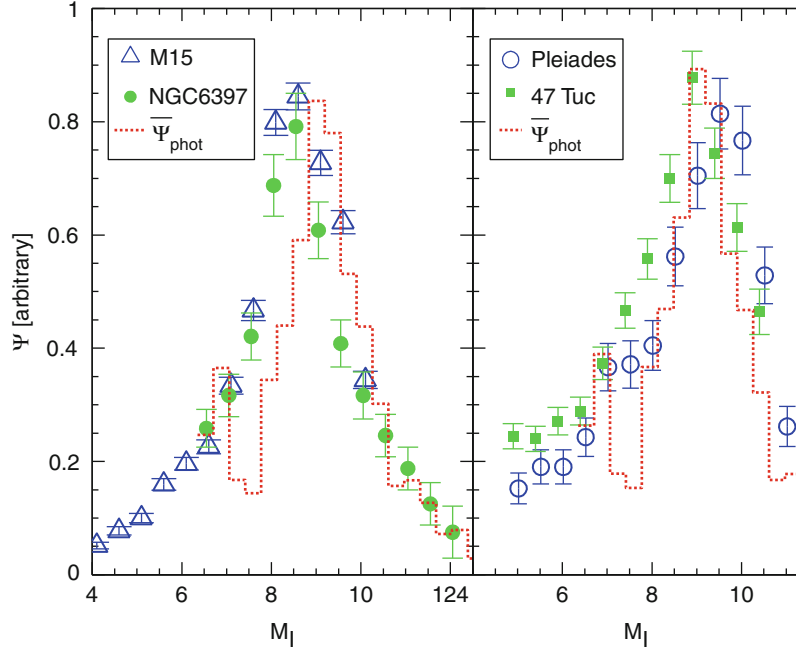
¹⁴This controversy achieved a maximum in 1995, as documented in Kroupa (1995a). The discrepancy evident in [Fig. 4-9](#) between the nearby LF, Ψ_{near} , and the photometric LF, Ψ_{phot} , invoked a significant dispute as to the nature of this discrepancy. On the one hand (Kroupa 1995a), the difference is thought to be due to unseen companions in the deep but low-resolution surveys used to construct Ψ_{phot} , with the possibility that photometric calibration for VLMSs may remain problematical so that the exact shape of Ψ_{phot} for $M_V \gtrsim 14$ is probably uncertain. On the other hand (Reid and Gizis 1997), the difference is thought to come from nonlinearities in the $V - I, M_V$ color–magnitude relation used for photometric parallax. Taking into account such structure, it can be shown that the photometric surveys underestimate stellar space densities so that Ψ_{phot} moves closer to the extended estimate of Ψ_{near} using a sample of stars within 8 pc or further. While this is an important point, the extended Ψ_{near} is incomplete (see footnote 13 on p. 160) and theoretical color–magnitude relations do not have the required degree of nonlinearity (e.g., Fig. 7 in Bochanski et al. 2010). The observational color–magnitude data also do not conclusively suggest a feature with the required strength (Baraffe et al. 1998). Furthermore, Ψ_{phot} agrees almost perfectly with the LFs measured for star clusters of solar and population II metallicity for which the color–magnitude relation is not required ([Fig. 4-10](#)) so that nonlinearities in the color–magnitude relation cannot be the dominant source of the discrepancy.



■ Fig. 4-9

Stellar luminosity functions (LFs) for solar-neighborhood stars. The photometric LF corrected for Malmquist bias and at the midplane of the Galactic disk (Ψ_{phot}) is compared with the nearby LF (Ψ_{near}). The average, ground-based Ψ_{phot} (dashed histogram, data predating 1995, is confirmed (Kroupa 1995a) by Hubble Space Telescope (HST) star-count data which pass through the entire Galactic disk and are thus less prone to Malmquist bias (solid dots). The ground-based volume-limited trigonometric-parallax sample (dotted histogram) systematically overestimates Ψ_{near} due to the Lutz–Kelker bias, thus lying above the improved estimate provided by the Hipparcos-satellite data (solid histogram, Jahreiß and Wielen 1997; Kroupa 2001c). The Lutz–Kelker bias (Lutz and Kelker 1973) arises in trigonometric-parallax-limited surveys because the uncertainties in parallax measurements combined with the nonlinear increase of the number of stars with reducing parallax (increasing distance) lead to a bias in the deduced number density of stars when using trigonometric-parallax-limited surveys. The depression/plateau near $M_V = 7$ is the *Wielen dip*. The maximum near $M_V \approx 12$, $M_I \approx 9$ is the *KTG peak*. The thin dotted histogram at the faint end indicates the level of refinement provided by additional stellar additions (Kroupa 2001c), demonstrating that even the immediate neighborhood within 5.2 pc of the Sun probably remains incomplete at the faintest stellar luminosities. Which LF is the relevant one for constraining the MF? Kroupa et al. (1993) uniquely used both LFs simultaneously to enhance the constraints. See text

stars. Starting at high masses ($m \gtrsim \text{few } M_\odot$), as the mass of a star is reduced, H^- opacity becomes increasingly important through the short-lived capture of electrons by H-atoms, resulting in reduced stellar luminosities for intermediate and low-mass stars. The $m(M_V)$ relation becomes less steep in the broad interval $3 < M_V < 8$ leading to the *Wielen dip* (● Fig. 4-9). The $m(M_V)$

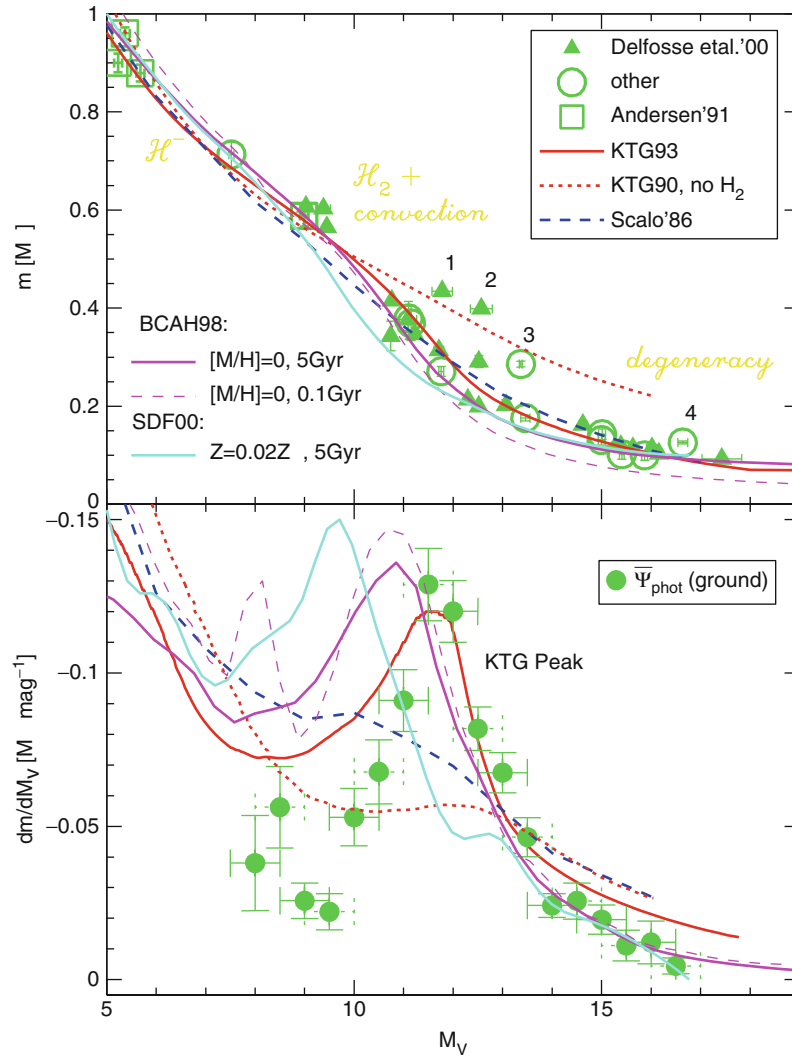


■ Fig. 4-10

I-band LFs of stellar systems in four star clusters: globular cluster (GC) *M15* (de Marchi and Paresce 1995a, distance modulus $\Delta m = m - M = 15.25$ mag), GC *NGC 6397* (Paresce et al. 1995, $\Delta m = 12.2$), young Galactic cluster *Pleiades* (Hambly et al. 1991, $\Delta m = 5.48$), and GC *47 Tuc* (de Marchi and Paresce 1995b, $\Delta m = 13.35$). The dotted histogram is $\bar{\Psi}_{\text{phot}}(M_I)$ from Fig. 4-9, transformed to the *I*-band using the linear color-magnitude relation $M_V = 2.9 + 3.4 (V - I)$ (Kroupa et al. 1993), and $\Psi_{\text{phot}}(M_I) = (dM_V/dM_I) \Psi_{\text{phot}}(M_V)$ (4.2). The KTG peak is very pronounced in all LFs. It is due to an extremum in the derivative of the MLR (Fig. 4-11)

relation steepens near $M_V = 10$ because the formation of H_2 in the very outermost layer of main-sequence stars causes the onset of convection up to and above the photo-sphere leading to a flattening of the temperature gradient and therefore to a larger effective temperature as opposed to an artificial case without convection but the same central temperature. This leads to brighter luminosities and full convection for $m \lesssim 0.35 M_\odot$. The modern Delfosse data beautifully confirm the steepening in the interval $10 < M_V < 13$ predicted in 1990. In Fig. 4-11, the dotted MLR demonstrates the effects of suppressing the formation of the H_2 molecule by lowering its dissociation energy from 4.48 to 1 eV (Kroupa et al. 1990, hereinafter KTG). The $m(M_V)$ relation flattens again for $M_V > 14$, $m < 0.2 M_\odot$ as degeneracy in the stellar core becomes increasingly important for smaller masses limiting further contraction (Hayashi and Nakano 1963; Chabrier and Baraffe 1997). Therefore, owing to the changing conditions within the stars with changing mass, a pronounced local maximum in $-dm/dM_V$ results at $M_V \approx 11.5$, postulated by KTG to be the origin of the maximum in Ψ_{phot} near $M_V = 12$.

The implication that the LFs of all stellar populations should show such a feature, although realistic metallicity-dependent stellar models were not available yet, was noted (Kroupa et al. 1993). The subsequent finding that all known stellar populations have the KTG peak



■ Fig. 4-11

The mass–luminosity relation (MLR, *upper panel*) and its derivative (*lower panel*) for late-type stars. *Upper panel*: The observational data (solid triangles and open circles, Delfosse et al. 2000; open squares, Andersen 1991) are compared with the empirical MLR of Scalo (1986) and the semiempirical KTG93-MLR tabulated in Kroupa et al. (1993). The under-luminous data points 1,2 are GJ2069Aa,b and 3,4 are Gl791.2A,B. All are probably metal-rich by ≈ 0.5 dex (Delfosse et al. 2000). Theoretical MLRs from Baraffe et al. (1998) (BCAH98) and Siess et al. (2000) (SDF00) are also shown. The observational data (Andersen 1991) show that $\log_{10}[m(M_V)]$ is approximately linear for $m > 2 M_\odot$. See also Malkov et al. (1997). *Lower panel*: The derivatives of the same relations plotted in the upper panel are compared with $\bar{\Psi}_{\text{phot}}$ from Fig. 4-9. Note the good agreement between the location, amplitude, and width of the KTG peak in the LF and the extremum in dm/dM_V .

(► Figs. 4-9 and ► 4-10) constitutes one of the *most impressive achievements of stellar-structure theory*. Different theoretical $m(M_V)$ relations have the maximum in $-dm/dM_V$ at different M_V , suggesting the possibility of testing stellar structure theory near the critical mass $m \approx 0.35 M_\odot$, where stars become fully convective (Kroupa and Tout 1997; Brocato et al. 1998). But since the MF also defines the LF, the shape and location cannot be unambiguously used for this purpose unless it is postulated that the IMF is invariant. Another approach to test stellar models is by studying the deviations of observed $m(M_V)$ data from the theoretical relations (► Fig. 4-12).

A study of the position of the maximum in the I -band LF has been undertaken by von Hippel et al. (1996) and Kroupa and Tout (1997) finding that the observed position of the maximum shifts to brighter magnitude with decreasing metallicity, as expected from theory (► Figs. 4-13 and ► 4-14).

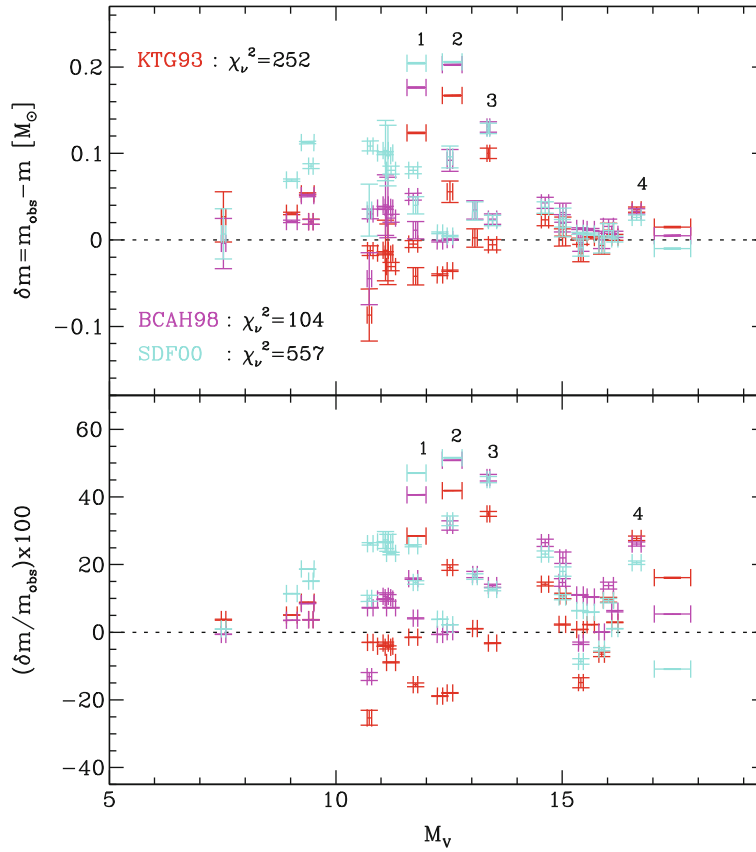
7.3 Unresolved Binary Stars and the Solar-Neighborhood IMF

In addition to the nonlinearities in the $m(M_p)$ relation, unresolved multiple systems affect the MF derived from the photometric LF, in particular since no stellar population is known to exist that has a binary proportion smaller than about 50%, apart possibly from dynamically highly evolved globular clusters and open clusters (Sollima et al. 2007, 2010; Marks et al. 2011).

Suppose an observer sees 100 systems. Of these 40, 15 and 5 are binary, triple, and quadruple, respectively, these being realistic proportions. There are thus 85 companion stars which the observer is not aware of if none of the multiple systems are resolved. Since the distribution of secondary masses is not uniform but typically increases with decreasing mass for F-, G- and K-type primaries (it decreases for M-type primaries, Malkov and Zinnecker 2001; Marks et al. 2011), the bias is such that low-mass stars are significantly underrepresented in any survey that does not detect companions (Kroupa et al. 1991; Malkov and Zinnecker 2001). Also, if the companion(s) are bright enough to affect the system luminosity noticeably then the estimated photometric distance will be too small, artificially enhancing inferred space densities which are, however, mostly compensated for by the larger distances sampled by binary systems in a flux-limited survey, together with an exponential density falloff perpendicular to the Galactic disk (Kroupa 2001c). A faint companion will also be missed if the system is formally resolved, but the companion lies below the flux limit of the survey.

Comprehensive star-count modeling of the solar neighborhood that incorporates unresolved binary systems, metallicity, and age spreads and the density falloff perpendicular to the Galactic disk with appropriate treatment of Malmquist and Lutz–Kelker bias show that the IMF, from which the solar neighborhood populations within a few pc and a few hundred pc stem, can be *unified with one MF* which is a two-part power law with $\alpha_1 = 1.3 \pm 0.5$, $0.07 < m/M_\odot \leq 0.5$, $\alpha_2 \approx 2.2$, $0.5 < m/M_\odot \leq 1$, a result obtained for two different MLRs (Kroupa et al. 1993; Kroupa 2001c). The index α_2 is constrained tightly owing to the well-constrained Ψ_{near} , the well-constrained empirical MLR in this mass range and because unresolved binary systems do not significantly affect the solar-neighborhood LF in this mass range because primaries with $m \gtrsim 1 M_\odot$ are rare and are not sampled. The stellar sample in the mass range $0.5\text{--}1 M_\odot$ is therefore complete.

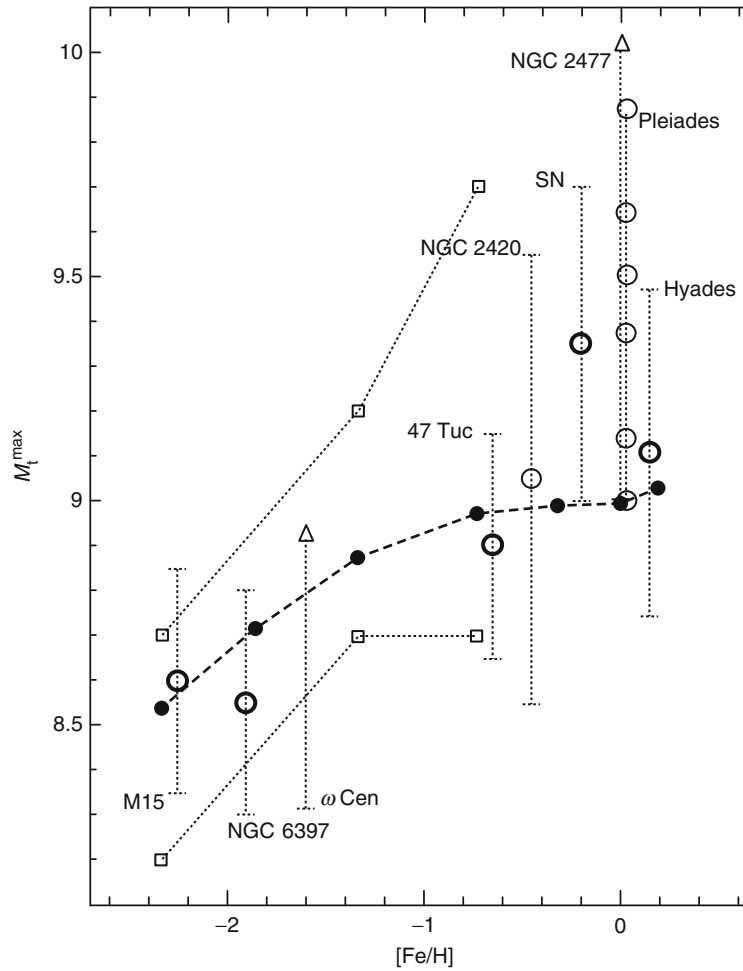
► Figure 4-15 demonstrates models of the individual-star and system LFs for the KTG93 MLR shown in ► Fig. 4-11. The significant difference between the individual-star and system LFs is evident, being most of the explanation of the disputed discrepancy between the observed



■ Fig. 4-12

Deviations of the MLRs ($\delta m = m_{\text{obs}} - m(M_V)$) from the empirical data, m_{obs} , with errors ϵ_m shown in [Fig. 4-11](#) in M_\odot (*upper panel*) and in percent (*lower panel* with uncertainties $-(m(M_V)/m_{\text{obs}}^2) \times \epsilon_m$). Colors refer to the models of [Fig. 4-11](#). Reduced χ_ν^2 ($\nu = 26$ for 31 data points, ignoring the four outliers) values indicate the formal goodness of fit. Formally, none of the MLRs available is an acceptable model for the data. This is not alarming though because the models are for a single-metallicity, single-age population while the data span a range of metallicities and ages typical for the solar neighborhood stellar population, as signified by $\delta m \gg \epsilon_m$ in most cases. The χ_ν^2 values confirm that the BCAH98 models (Baraffe et al. 1998) and the semiempirical KTG93 MLR (Kroupa et al. 1993) provide the best-matching MLRs. Note that the KTG93 MLR was derived from mass-luminosity data prior to 1980, but by using the shape of the peak in $\Psi_{\text{phot}}(M_V)$ as an additional constraint, the constructed MLR became robust. The *lower panel* demonstrates that the deviations of observational data from the model MLRs are typically much smaller than 30%, excluding the putatively metal-rich stars (1–4)

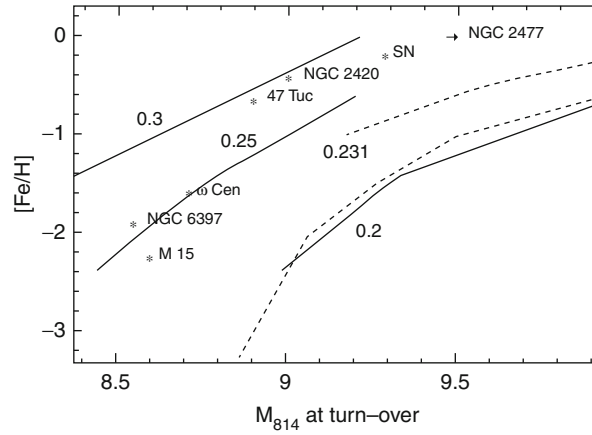
Ψ_{near} and Ψ_{phot} . Note though that the observed photometric LF contains triple and quadruple systems that are not accounted for by the model. Note also that the photometric LF has been corrected for Malmquist bias and so constitutes the system LF in which the broadening due to a metallicity and age spread and photometric errors has been largely removed. It is therefore directly comparable to the model system LF, and both indeed show a very similar



■ Fig. 4-13

The position of the maximum in $-dm/dM_i$ as a function of metallicity of the theoretical mass-luminosity data of Kroupa and Tout (1997) is shown as *solid dots*. The *open squares* represent bounds by the stellar-structure models of D'Antona and Mazzitelli (1996), and the *open circles* are observational constraints for different populations (e.g., SN for the composite solar-neighborhood population, Pleiades for the simple population of an intermediate-age cluster). *Thick circles* are more certain than the *thin circles*, and for the Pleiades, a sequence of positions of the LF-maximum is given, from *top to bottom*, with the following combinations of (distance modulus, age): (5.5, 70 Myr), (5.5, 120 Myr), (5.5, main sequence), (6, 70 Myr), (6, 120 Myr), and (6, main sequence). For more details, see Kroupa and Tout (1997)

KTG peak. The observed nearby LF, on the other hand, has not been corrected for the metallicity and age spread nor for trigonometric distance errors, and so it appears broadened. The model individual-star LF, in contrast, does not, by construction, incorporate these and thus appears with a more pronounced maximum. Such observational effects can be incorporated rather easily



■ Fig. 4-14

Similar to [Fig. 4-13](#) but from von Hippel et al. (1996), their Fig. 5: The absolute *I*-band-equivalent magnitude of the maximum in the LF as a function of metallicity for different populations. The solid and dashed lines are loci of constant mass (0.2, 0.231, 0.3 M_{\odot}) according to theoretical stellar structure calculations. See von Hippel et al. (1996) for more details

into full-scale star-count modeling (Kroupa et al. 1993). The deviation of the model system LF from the observed photometric LF for $M_V \gtrsim 14$ may indicate a change of the pairing properties of the VLMS or BD population ([Sect. 8](#)).

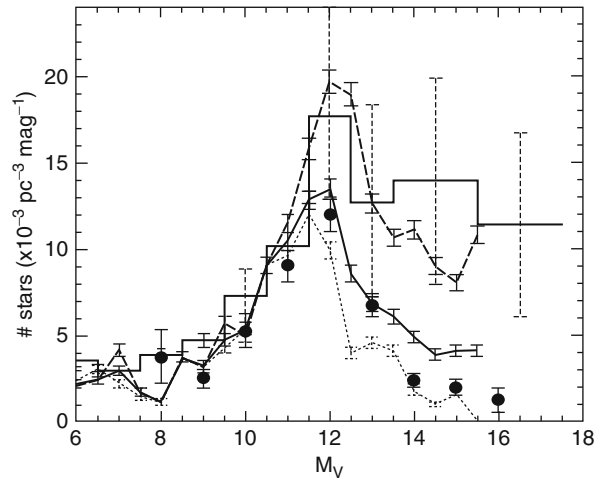
Since the nearby LF is badly defined statistically for $M_V \gtrsim 13$, the resulting model, such as shown in [Fig. 4-15](#), is a *prediction* of the true, individual-star LF that should become apparent once the immediate solar-neighborhood sample has been enlarged significantly through the planned space-based astrometric survey Gaia (Gilmore et al. 1998), followed by an intensive follow-up imaging and radial-velocity observing program scrutinizing every nearby candidate for unseen companions (Kroupa 2001c). Despite such a monumental effort, the structure in $\Psi_{\text{near}}^{\text{GAIA}}$ will be smeared out due to the metallicity and age spread of the local stellar sample, a factor to be considered in detail.

Main Results

The universal structure in the stellar LF of main sequence stars (the Wielen dip and the KTG peak) is well understood. It is due to nonlinearities in the stellar mass–luminosity relation. Binary systems have a highly significant effect on the LF of late-type stars. The solar-neighborhood IMF which unifies Ψ_{near} and Ψ_{phot} has $\alpha_1 = 1.3$ (0.07–0.5 M_{\odot}) and $\alpha_2 = 2.2$ (0.5–1 M_{\odot}).

7.4 Star Clusters

Star clusters less massive than about $M = 10^5 M_{\odot}$ and to a good degree of approximation also those with $M > 10^5 M_{\odot}$ offer populations that are co-eval, equidistant, and that have the same chemical composition. But, seemingly as a compensation of these advantages, the extraction



■ Fig. 4-15

Comparison of the model field luminosity function (curves) of a single-metallicity and single-age population that is without measurement errors, with observations in the photometric V-band (a comparison of the corresponding LFs in bolometric magnitudes can be found in Kroupa 1995e). The model assumes the standard or canonical stellar IMF, (4.55) below. The model single star luminosity function is normalized to the nearby luminosity function at $M_V \approx 10$, $M_{bol} \approx 9$, giving the normalization constant in the MF k (4.5), and the plot shows $k \Psi_{mod,sing}$ (long dashed curve), $k \Psi_{mod,sys}(t = 0)$ (dotted curve, 100% birth binary fraction in dynamically unevolved embedded clusters, see 4.16) without pre-main sequence brightening, and $k \Psi_{mod,sys}(t = 1 \text{ Gyr})$ (solid curve, 48% surviving binary fraction in dissolved clusters, see 4.16). Note that the solid curve is the luminosity function for a realistic model of the Galactic field population of systems consisting of 48% binaries (which result from disruption of the 100% binary birth population of Sect. 2.6 in the embedded clusters) which have a period distribution consistent with the observed G-, K-, and M-dwarf period distribution, the mass ratio distributions for G-dwarf systems as observed (Duquennoy and Mayor 1991), and the overall mass-ratio distribution given by Fig. 2 in Kroupa et al. (2003), where a concise description of the “standard star-formation model” can be found. The observed nearby stellar luminosity function, Ψ_{near} , which is not corrected for Lutz-Kelker bias (Lutz and Kelker 1973, Tables 2 and 8 in Kroupa 1995a) and which is smoothed by using larger bin widths at the faint end, as detailed in Sect. 4 of that paper, is plotted as the solid-line histogram. The filled circles represent the best-estimate Malmquist corrected photometric luminosity function, $\bar{\Psi}_{phot}$ (4.9). By correcting for Malmquist bias (Stobie et al. 1989), the LF becomes that of a single-age, single-metallicity population (Taken from Kroupa (1995e))

of faint cluster members is very arduous because of contamination by the background or foreground Galactic-field population. The first step is to obtain photometry of everything stellar in the vicinity of a cluster and to select only those stars that lie near one isochrone, taking into account that unresolved binaries are brighter than single stars. The next step is to measure proper motions and radial velocities of all candidates to select only those high-probability members that have coinciding space motion with a dispersion consistent with the a priori unknown but estimated internal kinematics of the cluster. Since nearby clusters for which proper-motion

measurements are possible appear large on the sky, the observational effort is overwhelming. An excellent example of such work is the 3D mapping of the Hyades cluster by Röser et al. (2011). For clusters such as globulars that are isolated, the second step can be omitted, but in dense clusters, stars missed due to crowding need to be corrected for.

The stellar LFs in clusters turn out to have the same general shape as Ψ_{phot} (Fig. 4-10), with the maximum being slightly offset depending on the metallicity of the population (Figs. 4-13 and 4-14). A 100 Myr isochrone (the age of the Pleiades) is also plotted in Fig. 4-11 to emphasize that for young clusters additional structure (in this case, another maximum near $M_V = 8$ in the LF is expected via (4.1)). This is verified for the Pleiades cluster (Belikov et al. 1998) and is due to stars with $m < 0.6 M_\odot$ not having reached the main sequence yet (Chabrier and Baraffe 2000).

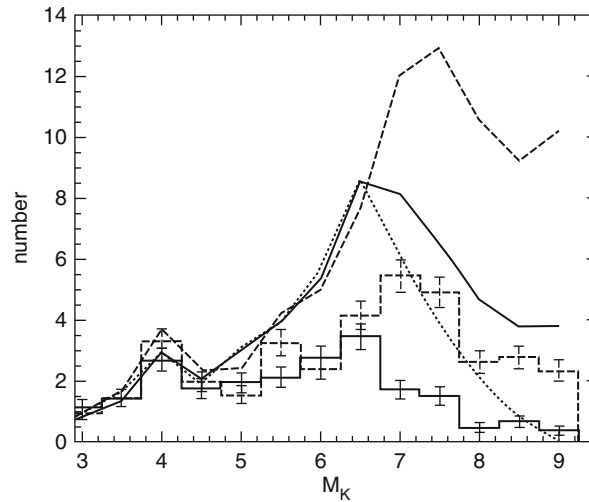
LFs for star clusters are, like Ψ_{phot} , system LFs because binary systems are not resolved in the typical star-count survey. The binary-star population evolves due to encounters, and after a few initial crossing times, only those binary systems survive that have a binding energy larger than the typical kinetic energy of stars in the cluster (Heggie 1975; Marks et al. 2011).

A further complication with cluster LFs is that star clusters preferentially lose single low-mass stars across the tidal boundary as a result of ever-continuing redistribution of energy during encounters while the retained population has an increasing binary proportion and increasing average stellar mass. The global PDMF thus flattens with time with a rate proportional to the fraction of the cluster lifetime, and for highly evolved initially rich open clusters, it evolves toward a delta function near the turnoff mass, the mass-loss rate being a function of galactocentric distance. This is a major issue for aged open clusters (initially $N < 10^4$ stars) with lifetimes of only a few 100 Myr.

These processes are now well quantified, and Fig. 4-16 shows that a dynamically very evolved cluster such as the Hyades has been depleted significantly in low-mass stars. Even so, the binary-star correction that needs to be applied to the LF in order to arrive at the individual-star present-day LF is significant.

A computationally challenging investigation of the systematic changes of the MF in evolving clusters of different masses has been published by Baumgardt and Makino (2003). Baumgardt and Makino quantify the depletion of the clusters of low-mass stars through energy-equipartition-driven evaporation and conclusively show that highly evolved clusters have a very substantially skewed PDMF (Fig. 4-17). If the cluster ages are expressed in fractions, τ_f , of the overall cluster lifetime, which depends on the initial cluster mass, its concentration, and orbit, then different clusters on different orbits lead to virtually the same PDMFs at the same τ_f . Their results were obtained for clusters that are initially in dynamical equilibrium and that do not contain binary stars (these are computationally highly demanding), so that future analysis, including initially non-virialized clusters and a high primordial binary fraction (Sect. 2.6), will be required to further refine these results.

For the massive and long-lived globular clusters ($N \gtrsim 10^5$ stars), theoretical stellar-dynamical work shows that the MF measured for stars near the cluster's half-mass radius is approximately similar to the global PDMF, while inward and outward of this radius the MF is flatter (smaller α_1) and steeper (larger α_1), respectively, owing to dynamical mass segregation (Vesperini and Heggie 1997). However, mass loss from the cluster flattens the global PDMF such that it no longer resembles the IMF anywhere (Fig. 4-17), for which evidence has been found in some cases (Piotto and Zoccali 1999, see also Sect. 12.7). The MFs measured for globular clusters must therefore generally be flatter than the IMF, which is indeed born-out by observations (Fig. 4-26 below). However, again the story is by no means straightforward because



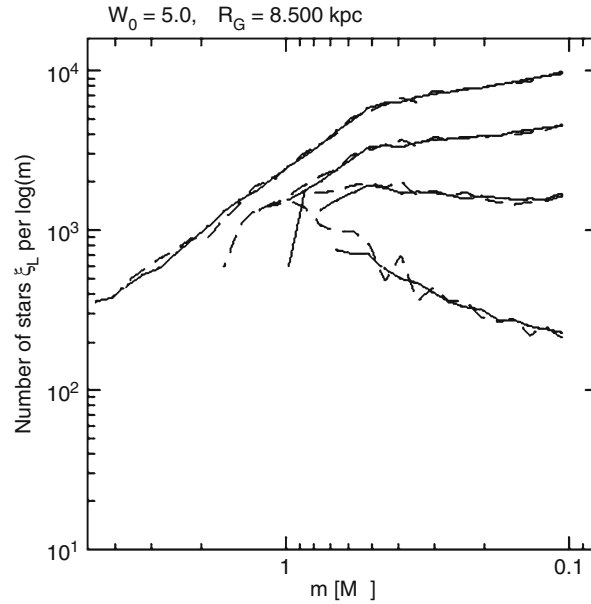
■ Fig. 4-16

Models of the K -band individual-star and system LFs in an ensemble of 20 dynamically highly evolved clusters (*thin* and *thick histograms*, respectively). An observer would deduce the *thick histogram*, which can only be transformed to the individual-star PDMF in the cluster if adequate correction for unresolved binaries is made. Such a correction leads to the *upper thin histogram* from which the PDMF can be inferred via (4.1). Each cluster model consists initially of 200 binaries with a half-mass radius of 0.85 pc, and the LFs are shown at an age of 480 Myr (44 initial crossing times) and count all stars and systems within the central sphere with a radius of 2 pc. The clusters are random renditions from the same parent distributions (binary-star orbital parameters, IMF, stellar positions, and velocities) and are initially in dynamical equilibrium. The *upper dashed curve* is the initial individual-star LF (KTG93 MLR, Fig. 4-11, and canonical IMF, (4.55) below), and the *solid curve* is the model Galactic-field LF of systems, also shown in Fig. 4-15. This is an accurate representation of the Galactic-field population in terms of the IMF and mixture of single and binary stars and is derived by stars forming in clusters such as shown here that dissolve with time. Both of these LFs are identical to the ones shown in Fig. 4-15. The *dotted curve* is the initial system LF (100% binaries) (From Kroupa (1995c))

globular clusters have significantly smaller binary fractions than population II clusters (Ivanova et al. 2005). The binary-star corrections are therefore smaller for globular cluster MFs implying a larger difference between α_1 for GCs and open clusters for which the binary correction is very significant.

Therefore, and as already pointed out by Kroupa (2001b), it appears quite realistically possible that population II IMFs were in fact flatter (smaller α_1) than population I IMFs, as would be qualitatively expected from simple fragmentation theory (Sect. 12.2). Clearly, this issue needs detailed investigation which, however, is computationally highly demanding, requiring the use of state-of-the-art N -body codes and special-purpose hardware.

The first realistic calculations of the formation of an open star cluster such as the Pleiades demonstrate that the binary properties of stars remaining in the cluster are comparable to those observed even if all stars initially form in binary systems according to the BBP ((4.46),

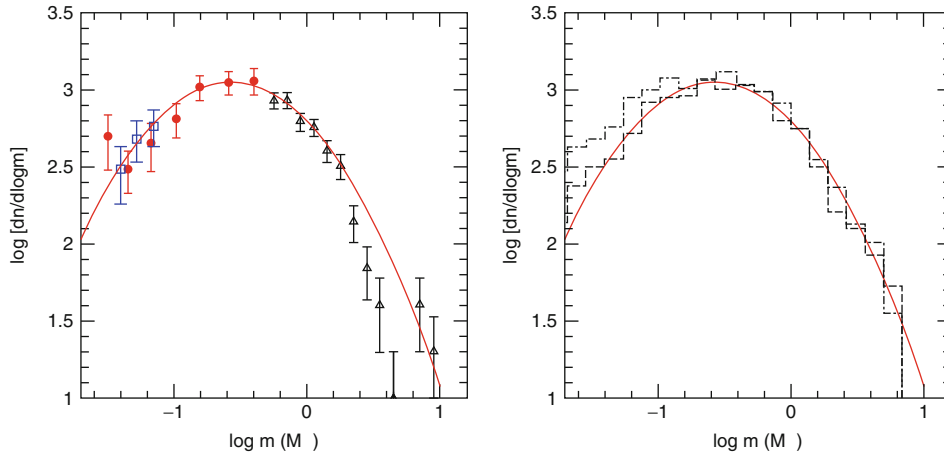


■ Fig. 4-17

PDMFs in a King-model cluster with concentration $W_0 = 5$ on a circular orbit about the MW center with radius 8.5 kpc. Shown are the MFs of all bound stars at ages corresponding to $\tau_f = 0\%$, 30%, 60%, and 90% of the cluster lifetime (from top to bottom). For each, age the solid line represents one computation with 1.28×10^5 stars, and the dashed lines show the sum of four clusters each with 8,000 stars (scaled to the same number of stars as the massive computation). Results for other circular and eccentric orbits and cluster concentrations are virtually indistinguishable (From Baumgardt and Makino (2003). Note the progressive depletion of low-mass stars as the cluster ages)

Kroupa et al. 2001, 2003). That work also demonstrates the complex and counterintuitive interplay between the initial concentration, mass segregation at the time of residual gas expulsion, and the final ratio of the number of BDs to stars (► Fig. 4-18). Thus, this modeling shows that an initially denser cluster evolves to significant mass segregation when the gas explosively leaves the system. Contrary to naive expectation, according to which a mass-segregated cluster should loose more of its least massive members during expansion after gas expulsion, the ensuing violent relaxation of the cluster retains more free-floating BDs than the less-dense model. This comes about because BDs are split from the stellar binaries more efficiently in the denser cluster. This, however, depends on the BDs and stars following the same pairing rules, which is now excluded (► Sect. 8). During the long-term evolution of the mass function, initially mass segregated star clusters loose more low-mass stars when they are close to dissolution as has been found by Baumgardt et al. (2008) after comparing star loss from clusters in N -body calculations with the observed star functions of globular clusters. But additionally, the gas expulsion from embedded clusters has to be carefully taken into account to explain the correlation between concentration of a globular cluster and the slope of its PDMF (► Sect. 12.7).

These issues remain an active area of research because at least two changes need to be made to the modeling: On the one hand, BDs need to be treated as a population separate from the



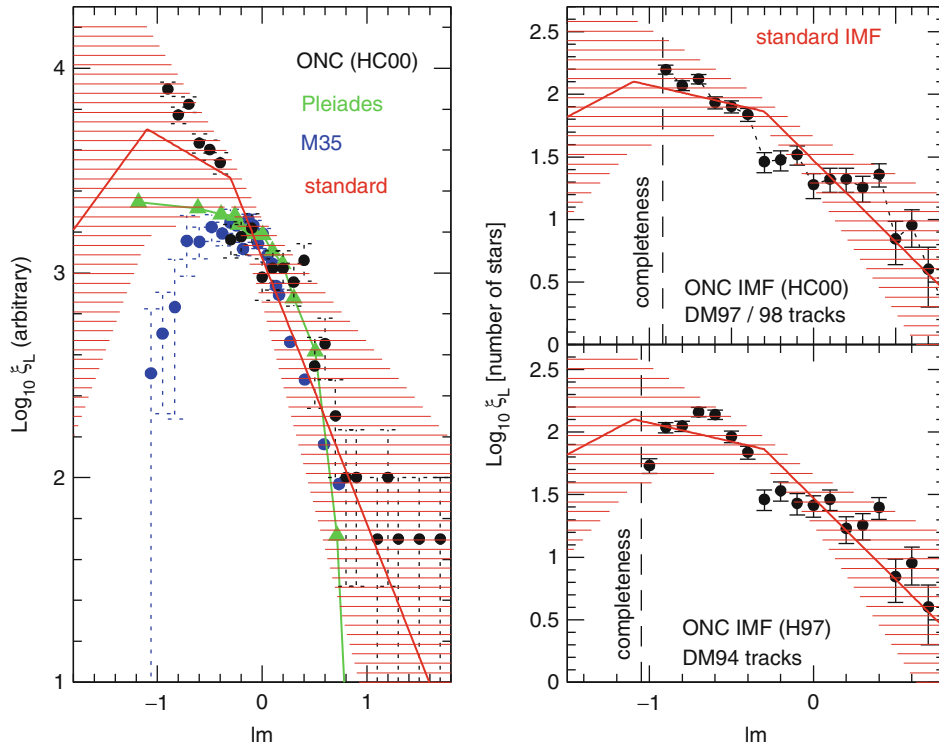
■ Fig. 4-18

The observationally deduced MF in the Pleiades cluster. *Left panel:* The symbols are observational data (for details, see Moraux et al. 2004) and the curve is a log-normal fit. *Right panel:* The curve is the same log-normal fit. Theoretical system MFs for two initial models of the Pleiades cluster according to Kroupa et al. (2001) are plotted at an age of 100 Myr. These models assume the young cluster to be deeply embedded in gas, with a star-formation efficiency of 33%, a gas-expulsion time scale shorter than the crossing time and to contain 10^4 stars and BDs, whereby all stars and BDs are paired randomly to binary systems (i.e., in these models, BDs are not treated as a separate population, see Sect. 8 for more realistic models). Model A (*dashed histogram*) has an initial central number density $\rho_C = 10^{4.8}$ stars/pc³, while model B (*dotted histogram*) has $\rho_C = 10^{5.8}$ stars/pc³. The embedded phase lasts 0.6 Myr, and during this time, mass segregation develops in the initially denser cluster model B. Note that these models are not a fit but a prediction of the Pleiades MF, assuming it had a canonical IMF (Sect. 4.55). Note that the initially denser cluster (*upper histogram*) retains more BDs as a result of these being ionized off their stellar primaries in the denser environment of model B. Also, note that the observational data suggest a deficit of early-type stars in the Pleiades (*left panel*) which is reminiscent of the deficit of massive stars noted for the ONC (Pflamm-Altenburg and Kroupa 2006)

stellar one (Sect. 8) so that the free-floating BDs that result, in the currently available models, from the disruption of star-BD binaries, will not be available in reality. On the other hand, some observations suggest that star clusters may form highly mass-segregated. The mass-dependent loss of stars thus definitely remains an issue to be studied.

The above work suggests that even clusters as young as the Pleiades are significantly evolved because clusters of all masses form from highly concentrated embedded morphologies (Kroupa 2005; Marks and Kroupa 2010, 2012; Conroy 2011). Also, the low-mass stars in clusters as young as the Pleiades or M35 (Fig. 4-19 below) have not yet reached the main sequence, so that pre-main sequence stellar-evolution calculations have to be resorted to when transforming measured luminosities to stellar masses via the MLR.

For ages younger than a few Myr, this becomes a serious problem: Classical pre-main sequence theory, which assumes hydrostatic contraction of spherical non-, sometimes

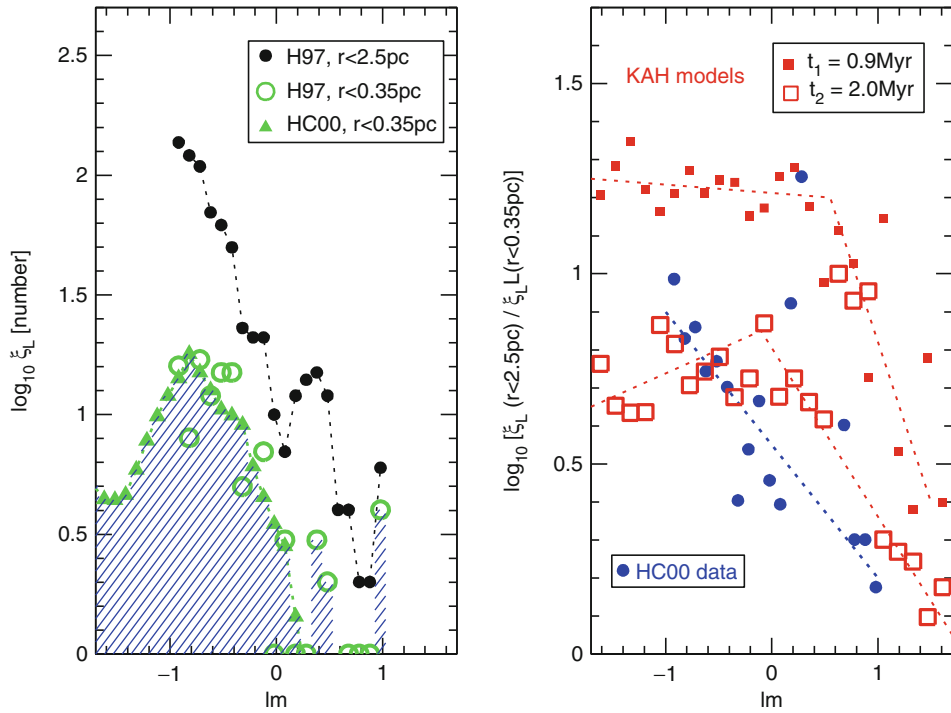


■ Fig. 4-19

Left panel: The observationally deduced system mass functions ($lm \equiv \log_{10}(m/M_{\odot})$) (a) in the ONC (Hillenbrand and Carpenter 2000): optical data within $r \leq 2.5$ pc, $\tau_{cl} < 2$ Myr, $[Fe/H] = -0.02$ (Esteban et al. 1998) (b) in the Pleiades (Hamby et al. 1999): $r \leq 6.7$ pc, $\tau_{cl} \approx 100$ Myr, $[Fe/H] = +0.01$, and (c) in M35 (Barrado y Navascués et al. 2001): $r \leq 4.1$ pc, $\tau_{cl} \approx 160$ Myr, $[Fe/H] = -0.21$, where r is the approximate projected radius of the survey around the cluster center and τ_{cl} the nuclear age. The strong decrease of the M35 MF below $m \approx 0.5 M_{\odot}$ remains present despite using different MLRs (e.g., DM97, as in the right panel). None of these MFs are corrected for unresolved binary systems. The canonical individual-star IMF (4.55) is plotted as the three *straight lines* assuming here continuity across the VLMS/BD mass range. **Right panel:** The shape of the ONC IMF differs significantly for $m < 0.22 M_{\odot}$ if different pre-main sequence evolution tracks, and thus essentially different theoretical MLRs, are employed (DM stands for tracks calculated by D’Antona and Mazzitelli, see Hillenbrand and Carpenter 2000 for details)

slowly-rotating stars from idealized initial states, breaks down because of the overlap with the star-formation processes that defies detailed treatment. Stars this young remember their accretion history, invalidating the application of classical pre-main sequence stellar evolution tracks, a point made explicitly clear by Tout et al. (1999), Wuchterl and Klessen (2001), and Wuchterl and Tscharnuter (2003), and are in any case rotating rapidly and are nonspherical. Such realistic pre-main sequence tracks are not available yet. The uncertainties due to such processes have been partially discussed though (Baraffe et al. 2002, 2009; Baraffe and Chabrier 2010).

Research on the IMF in very young clusters benefits from spectroscopic classification of individual stars to place them on a theoretical isochrone of existing classical pre-main-sequence



■ Fig. 4-20

Left panel: Mass segregation is very pronounced in the ONC, as is evident by comparing the observationally deduced MF for all stars within $r = 2.5$ pc with the MF for all stars with $r < 0.35$ pc (Hillenbrand and Carpenter 2000, HC00) ($lm \equiv \log_{10}(m/M_{\odot})$). For both samples, the reddening $A_V < 2.5$ mag (Hillenbrand 1997, H97, is for an optical and spectroscopic survey, whereas HC00 is a near-infrared survey). **Right panel:** The ratio, $\xi_L(r < 2.5 \text{ pc}) / \xi_L(r < 0.35 \text{ pc})$ (solid dots), of the MFs shown in the left panel increases significantly with decreasing mass, demonstrating the significant depletion of low-mass stars in the central region of the ONC. Stellar-dynamical models of the ONC (Kroupa et al. 2001) approximately reproduce this trend at an age of 2 Myr for the canonical IMF (► 4.55), whereby the system masses of surviving binary systems are counted instead of the individual stars many of which are in unresolved binaries even if no initial mass segregation is assumed (at $t = 0$, $\xi_L(r < 2.5 \text{ pc}) / \xi_L(r < 0.35 \text{ pc}) = \text{constant}$). The model snapshots shown are from model B in Kroupa et al. (2001) under the assumption that prior to gas-expulsion, the central stellar density was $\rho_c = 10^{5.8} \text{ stars/pc}^3$. The dotted lines are eye-ball fits to the plotted data (See also ► Fig. 4-18)

evolution theory to estimate masses (e.g., Meyer et al. 2000; Luhman 2004; Barrado y Navascués et al. 2004; Slesnick et al. 2004). In such cases, the deduced age spread becomes comparable to the age of the cluster (► 4.3). Binary systems are mostly not resolved but can feign an apparent age spread even if there is none in the underlying population as has been shown by Weidner et al. (2009). Differential reddening due to inhomogeneously distributed remnant gas and dust has a significant effect on estimating stellar masses (Andersen et al. 2009). But also episodic accretion onto the protostars can mimic such age spreads (Tout et al. 1999; Baraffe et al. 2009; Baraffe and Chabrier 2010). The reality of age spreads is an important issue as it defines whether

star clusters are almost coeval or host prolonged star formation. The finding of 10–30 Myr old dwarfs by the Lithium depletion method in the ≈ 1 Myr ONC by Palla et al. (2007) seems to indicate the latter. But careful numerical calculations have shown that a collapsing molecular cloud can trap a corresponding amount of stars from a surrounding older OB association into the forming cluster (Pflamm-Altenburg and Kroupa 2007). The ONC is embedded in the Orion OB1 association that has an age of 10–15 Myr which could explain the older dwarfs in the ONC.

A few results are shown in [Figs. 4-19](#) and [4-20](#). While the usual argument is for an invariant IMF, as is apparent for most population I stars (e.g., Fig. 5 in Chabrier 2003a; Fig. 3 in Bastian et al. 2010), [Fig. 4-19](#) shows that some appreciable differences in measured MFs are evident. The M35 MF appears to be highly deficient in low-mass stars. This clearly needs further study because M35 and the Pleiades appear to be otherwise fairly similar in terms of age, metallicity (M35 is somewhat less metal-rich than the Pleiades), and the size of the survey volume.

Taking the ONC as the best-studied example of a very young and nearby rich cluster (age ≈ 1 Myr, distance ≈ 450 pc; $N \approx 5,000$ –10,000 stars and BDs; Hillenbrand and Carpenter 2000; Luhman et al. 2000; Muench et al. 2000; Kroupa 2000; Slesnick et al. 2004), [Fig. 4-19](#) shows how the shape of the deduced IMF varies with improving (but still classical) pre-main sequence contraction tracks. This demonstrates that any substructure cannot, at present, be relied upon to reflect possible underlying physical mechanisms of star formation.

Main Results

Currently available evidence from resolved stellar populations largely points toward an IMF of late-type ($m \lesssim 1 M_{\odot}$) stars which is independent of the environment and which can be described well by a power law with an index of about $\alpha_2 = 2.3$ for $m \gtrsim 0.5 M_{\odot}$ and $\alpha_1 = 1.3$ for $m \lesssim 0.5 M_{\odot}$.

8 The IMF of Very Low-Mass Stars (VLMSs) and of Brown Dwarfs (BDs)

These are stars near to the hydrogen-burning mass limit (VLMS) or objects below it (BDs). BDs are not massive enough to achieve sufficiently high central pressures and temperatures to stabilize against continued contraction by burning H and thus indefinitely cool to unobservable luminosities and temperatures. The term “brown dwarf” was coined by Jill Tarter in her 1975 Ph.D. thesis and was later generally accepted as a name for substellar (i.e., non-hydrogen-burning) objects which presumably form like stars.

Observationally, it is very difficult to distinguish between VLMSs and BDs because a sufficiently young BD may have colors and spectral features corresponding to a VLMS. BDs were studied as theoretical objects in 1963 by Hayashi and Nakano (1963), who performed the first truly self-consistent estimate of the minimum hydrogen burning mass limit, m_H , by computing the luminosity at the surface and the energy release rate by nuclear burning. Modern theory of the evolution and internal constitution of BDs has advanced considerably owing to the inclusion of an improved equation of state and realistic model atmospheres that take into account absorption by many molecular species as well as dust allowing the identification of characteristic photometric signatures (Chabrier and Baraffe 2000). This work shows that the critical mass below which an object cannot be stabilized by nuclear fusion is $m_H = 0.075 M_{\odot}$ for solar metallicity. For lower metallicity, m_H is larger since a larger luminosity (due to the lower opacity)

requires more efficient nuclear burning to reach thermal equilibrium and thus a larger mass. The first BDs were detected in 1995, and since then, they have been found in the solar neighborhood and in young star clusters (Basri 2000), allowing increasingly sophisticated estimates of their mass distribution (Bouvier et al. 2003).

For the solar neighborhood, near-infrared large-scale surveys have now identified many dozens of BDs probably closer than 25 pc (e.g., Allen et al. 2005). Since these objects do not have reliable distance measurements, an ambiguity exists between their ages and distances, and only statistical analysis that relies on an assumed star-formation history for the solar neighborhood can presently constrain the IMF (Chabrier 2002), finding a 60% confidence interval $\alpha_0 = 0.3 \pm 0.6$ for $0.04\text{--}0.08 M_\odot$ approximately for the Galactic-field BD IMF (Allen et al. 2005).

Surveys of young star clusters have also discovered BDs by finding objects that extend the color–magnitude relation toward the faint locus while being kinematical members. Given the great difficulty of this endeavor, only a few clusters now possess constraints on the MF. The Pleiades star cluster has proven especially useful, given its proximity ($d \approx 127$ pc) and young age ($\tau_{\text{cl}} \approx 100$ Myr). Results indicate $\alpha_0 \approx 0.5\text{--}0.6$. Estimates for other clusters (ONC, σ Ori, IC 348, Cha I) also indicate $\alpha_0 \lesssim 0.8$. In their Table 1, Allen et al. (2005) summarize the available measurements for 11 populations finding that $\alpha_0 \approx 0\text{--}1$ and Andersen et al. (2008) find the low-mass IMF in seven young star-forming regions to be most consistent with being sampled from an underlying log-normal (Chabrier) IMF.

However, while the log-normal (Chabrier) IMF is indistinguishable in the stellar regime from the simpler canonical two-part power-law IMF (see [Fig. 4-24](#) below), it is to be noted that these and other constraints on the IMF of BDs rely on assuming the IMF to be continuous across the stellar/BD boundary. In the following, it will emerge that this assumption is not consistent with the binary properties of stars and BDs. The IMF can therefore not be a continuous log-normal across the VLMS/BD boundary.

8.1 BD and VLMS Binaries

The above estimates of the BD IMF suffer under the same bias affecting stars, namely, from unseen companions which need to be taken into account to infer the true BD IMF.

BD–BD binary systems are known to exist (Basri 2000) in the field (Bouy et al. 2003; Close et al. 2003) and in clusters (Martín et al. 2003). Their frequency is not yet fully constrained since detailed scrutiny of individual objects is time-intensive on large telescopes, but the data suggest a binary fraction of about 15% only. The results show conclusively that the semimajor axis distribution of VLMSs and BDs is much more compact than that of M dwarfs, K dwarfs, and G dwarfs. Bouy et al. (2003), Close et al. (2003), Martín et al. (2003), and Phan-Bao et al. (2005) all find that BD binaries with semimajor axis $a \gtrsim 15$ AU are very rare. Using Monte-Carlo experiments on published multiple-epoch radial-velocity data of VLMSs and BDs, Maxted and Jeffries (2005) deduce an overall binary fraction between 32% and 45% with a semimajor axis distribution that peaks near 4 AU and is truncated at about 20 AU. In the Pleiades cluster where their offset in the color–magnitude diagram from the single-BD locus makes them conspicuous, Pinfield et al. (2003) find the BD binary fraction may be as high as 60%. This, however, appears unlikely as a survey of more than 6 years UVES/VLT spectroscopy has shown the BD binary fraction to be 10–30% and that incompleteness in the few AU separation region is not significant (Joergens 2008). Using a very deep infrared survey of the Pleiades, Lodieu et al. (2007) suggest a BD binary fraction of 28 to 44 per cent, consistent with the Maxted and Jeffries (2005) result but only marginally so with the Pinfield et al. (2003) value.

It has already been shown that the disruption in embedded clusters of stellar binaries in a stellar population which initially consists of 100% binary stars with periods (i.e., binding energies) consistent with the observed pre-main sequence and proto-stellar binary data (● 4.46) leads to the observed main-sequence binary population in the Galactic field (Kroupa 1995d; Goodwin and Kroupa 2005; Marks and Kroupa 2011). Systems with BD companions have an even lower binding energy, and the truncated semimajor axis distribution of BDs may be a result of binary disruption in dense clusters of an initial stellar-like distribution.

This notion is tested by setting up the *star-like hypothesis* (Kroupa et al. 2003):

Star-like Hypothesis for BDs

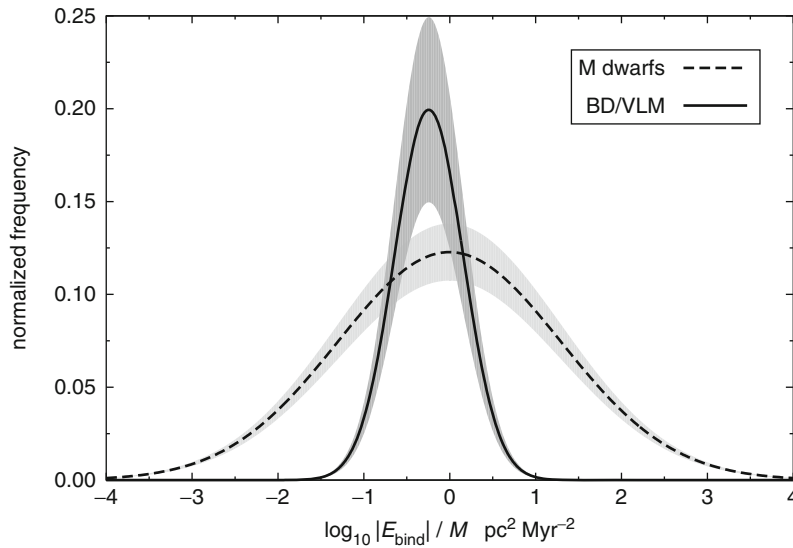
BDs form as stars do from molecular-cloud cores.

The star-like hypothesis implies that BDs form according to the same binary pairing rules (the BBP, ● 4.46) as stars do.

If BDs form as stars do then this hypothesis ought to be true since objects with masses $0.04\text{--}0.07 M_{\odot}$ should not have very different pairing rules than stars that span a much larger range of masses ($0.1\text{--}1 M_{\odot}$) but show virtually the same period-distribution function independently of primary mass (the M-, K-, and G-dwarf samples, Fischer and Marcy 1992; Mayor et al. 1992; Duquennoy and Mayor 1991, respectively). Thus, the hypothesis is motivated by observed orbital distribution functions of stellar binaries not being sensitive to the primary mass, which must come about if the overall physics of the formation problem is similar. Further arguments for a star-like origin of BDs comes from the detection of accretion onto and disks about very young BDs and that the BDs and stars in Taurus-Auriga have indistinguishable spatial and velocity distributions (White and Basri 2003).

Assuming the star-like hypothesis to hold, Kroupa et al. (2001, 2003) perform N -body calculations of ONC- and Taurus-Auriga-like stellar aggregates to predict the semimajor axis distribution functions of BD–BD, star–BD, and star–star binaries. These calculations demonstrate that the binary proportion among BDs becomes smaller than among low-mass stars after a few crossing times, owing to their weaker binding energies. The distribution of separations, however, extends to similar distances as for stellar systems (up to $a \approx 10^3$ AU), disagreeing completely with the observed BD–BD binary distribution. The star-like hypothesis thus predicts far too many wide BD–BD binaries. This can also be seen from the distribution of binding energies of real BD binaries. It is very different to that of stars by having a low-energy cutoff, ${}^{\text{BD}}E_{\text{bin,cut}} \approx -10^{-0.9} M_{\odot} (\text{pc/Myr})^2$, that is much higher than that of the M dwarfs, ${}^{\text{M}}E_{\text{bin,cut}} \approx -10^{-3} M_{\odot} (\text{pc/Myr})^2$ (● Fig. 4-21). This is a very strong indicator for some fundamental difference in the dynamical history of BDs.

Furthermore, the N -body distributions contain a substantial number of star–BD pairs, which also disagrees with the existence of very few BD companions to nearby stars (Basri 2000; Phan-Bao et al. 2005). Basically, if BDs form exactly like stars, then the number of star–BD binaries would be significantly larger than is observed, since, for example, G-dwarfs prefer to pair with M-dwarfs (why should BDs be any different from M dwarfs in their pairing to G dwarfs?). The observed general absence of BD companions is referred to as the *BD desert* (Zucker and Mazeh 2001) since stellar companions and planets are found at such separations (Halbwachs et al. 2000; Vogt et al. 2002). A few very wide star–BD systems can form during the final stages of dissolution of a small cluster (de La Fuente Marcos 1998), and three such common proper-motion pairs have perhaps been found (Gizis et al. 2001).



■ Fig. 4-21

The distribution of binding energies, $E_{\text{bin}} = -G m_1 m_2 / (2 a)$, of BDs (solid line) compared to those of M dwarfs (MDs, dashed line). The BD distribution is computed as a Gaussian distribution based on BD/VLMs data from the Very Low Mass Binary Archive (<http://vlmbinaries.org>). Specifically, the Gaussian distribution has a mean semimajor axis $\log_{10}(a_{\text{mean}}/\text{AU}) = 0.6$ with a half width of $\log_{10}(\sigma_a/\text{AU}) = 0.4$. The upper and lower envelopes correspond to BD binary fractions of $f_{\text{BD}} = 0.25$ and 0.15 , respectively (area under the curves). The MD energy distribution is computed by assuming the a -distribution from Fischer and Marcy (1992) (which is practically identical to that of G dwarfs) and choosing 10^7 masses, $m_i \in (0.1 - 0.5 M_{\odot})$, from the canonical stellar IMF (4.55) and random pairing. For the MDs, the Gaussian distribution has $\log_{10}(a_{\text{mean}}/\text{AU}) = 1.5$ and $\log_{10}(\sigma_a/\text{AU}) = 1.3$ such that $f_{\text{MD}} = 0.45$ and 0.35 for the upper and lower envelopes, respectively

Finally, the star-like hypothesis also predicts far too few star–star binaries in Taurus–Auriga, where binary disruption has not been active. This comes about because the large number of star–BD systems in this model limits the number of star–star binaries given the finite number of stellar primaries.

It is thus concluded that the observed BD population is incompatible with the star-like hypothesis. Therefore, BDs need to be treated as a separate, or extra, population (Kroupa et al. 2003). This is confirmed by Parker and Goodwin (2011), who constrain BD binary properties from the observed ones given that their dynamical evolution in the birth clusters needs to be corrected for.

BD/Star Population Synthesis Theorem

When setting up a population of BDs and stars, BDs need to be algorithmically treated separately from the stars.

Proof: The BD desert, see the rejection of the star-like hypothesis above and/or Kroupa et al. (2003). A practical formulation of this theorem is posed as a Gedanken Experiment on p. 184. \square

8.2 The Number of BDs per Star and BD Universality

Briceño et al. (2002) report that Taurus-Auriga appears to form significantly fewer BDs per star than the ONC. Both systems are very different physically but have similar ages of about 1 Myr. This finding was interpreted to be the first possible direct evidence of a variable IMF, being consistent qualitatively with the Jean-mass,

$$M_J \propto \rho^{-1/2} T^{3/2}, \quad (4.50)$$

being larger in Taurus-Auriga than in the ONC because its gas density, ρ , is smaller by one to two orders of magnitude, while the temperatures, T , are similar to within a factor of a few (Sect. 1.4).

Given this potentially important finding, Kroupa et al. (2003) computed N -body models of the stellar aggregates in Taurus-Auriga in order to investigate the hypothesis that BDs form star-like. They find that the same initial number of BDs per star in Taurus-Auriga and in the ONC leads to different observed ratios because BD–BD and star–BD binaries are disrupted more efficiently in the ONC; the observer thus sees many more BDs there than in the comparatively dynamically unevolved Taurus-Auriga groups. But, as already noted above, the star-like hypothesis must be discarded because it leads to too many wide BD–BD binaries, and also it predicts too many star–BD binaries. Given this problem, Kroupa and Bouvier (2003a) study the production rate of BDs per star assuming BDs are a separate population, such as ejected embryos (Reipurth and Clarke 2001), or as gravitational instabilities in extended circum-proto-stellar disks (Goodwin and Whitworth 2007; Thies et al. 2010). Again, they find that both, the physically very different environments of Taurus-Auriga and the ONC, can have produced the same ratios (about one BD per four stars) if BDs are ejected embryos with a dispersion of ejection velocities of about 2 km/s (this number is revised to 1.3 km/s below).

Based on some additional observations, Luhman (2004) revised the Briceño et al. (2002) results by finding that the number of BDs per star had been underestimated in Taurus-Auriga. Since the new spectroscopic study of Slesnick et al. (2004) also revised the number of BDs per star in the ONC downward, Luhman (2004) retracts the significance of the claimed difference of the ratio in Taurus-Auriga and the ONC. Is a universal, invariant, BD production scenario still consistent with the updated numbers?

Let the true ratio of the number of BDs per late-type star be

$$R \equiv \frac{N(0.02 - 0.08 M_\odot)}{N(0.15 - 1.0 M_\odot)} \equiv \frac{N_{\text{BD,tot}}}{N_{\text{st,tot}}}. \quad (4.51)$$

Note that here stars more massive than $1.0 M_\odot$ are not counted because Taurus-Auriga is mostly producing late-type stars given the limited gas mass available (see also Fig. 4-5). But the observed ratio is

$$R_{\text{obs}} = \frac{N_{\text{BD,obs}}}{N_{\text{st,obs}}} = N_{\text{BD,tot}} (\mathcal{B} + \mathcal{U}) \frac{(1 + f)}{N_{\text{st,tot}}} = R (\mathcal{B} + \mathcal{U}) (1 + f), \quad (4.52)$$

since the observed number of BDs, $N_{\text{BD,obs}}$, is the total number produced multiplied by the fraction of BDs that are gravitationally bound to the population (\mathcal{B}) plus the unbound fraction,

\mathcal{U} , which did not yet have enough time to leave the survey area. These fractions can be computed for dynamical models of the Taurus-Auriga and ONC and depend on the mass of the Taurus-Auriga subgroups and of the ONC and on the dispersion of velocity of the BDs. This velocity dispersion can either be the same as that of the stars if BDs form like stars or larger if they are ejected embryos (Reipurth and Clarke 2001). The observed number of “stars” is actually the number of systems such that the total number of individual stars is $N_{\text{st,tot}} = (1 + f) N_{\text{st,obs}}$, where f is the binary fraction of stars (► 4.48). Note that here, no distinction is made between single or binary BDs, which is reasonable given the low binary fraction (about 15%) of BDs. For Taurus-Auriga, Luhman (2004) observes $R_{\text{TA,obs}} = 0.25$ from which follows

$$R_{\text{TA}} = 0.18 \text{ since } f_{\text{TA}} = 1, \mathcal{B} + \mathcal{U} = 0.35 + 0.35 \quad (4.53)$$

(Kroupa et al. 2003). According to Slesnick et al. (2004), the revised ratio for the ONC is $R_{\text{ONC,obs}} = 0.28$ so that

$$R_{\text{ONC}} = 0.19 \text{ because } f_{\text{ONC}} = 0.5, \mathcal{B} + \mathcal{U} = 1 + 0 \quad (4.54)$$

(Kroupa et al. 2003). Note that the regions around the stellar groupings in Taurus-Auriga not yet surveyed should contain about 30% of all BDs, while all BDs are retained in the ONC. The ONC and TA thus appear to be producing quite comparable BD/star number ratios.

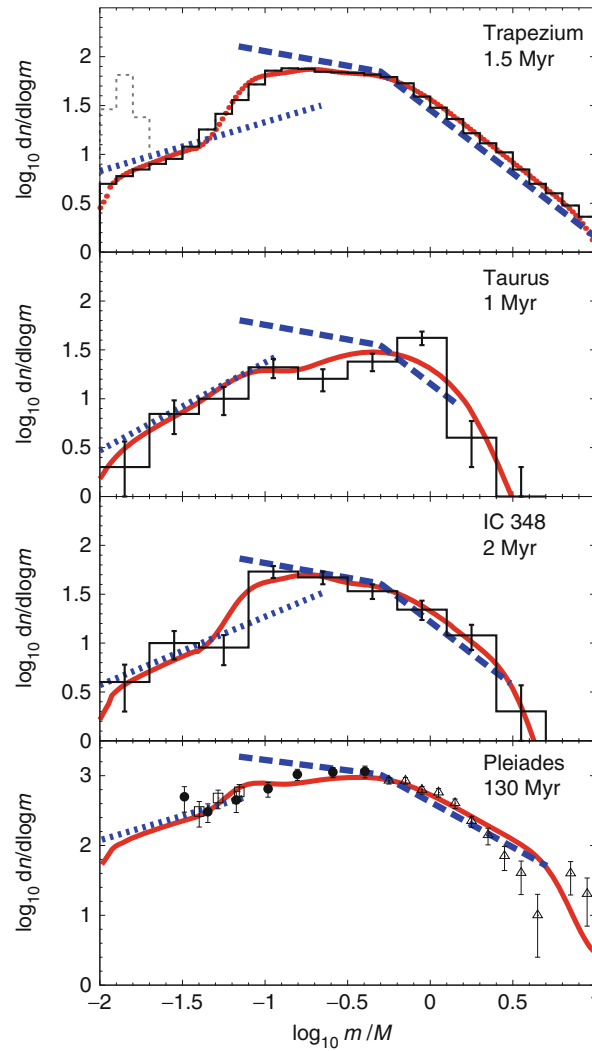
Therefore, the updated numbers imply that about *one BD is produced per five late-type stars* and that the dispersion of ejection velocities is $\sigma_{\text{ej}} \approx 1.3$ km/s. These numbers are an update of those given in Kroupa et al. (2003), but the results have not changed much. Note that a BD with a mass of $0.06 M_{\odot}$ and a velocity of 1.3 km/s has a kinetic energy of $10^{-1.29} M_{\odot} (\text{pc/Myr})^2$ which is rather comparable to the cutoff in BD–BD binding energies (► Fig. 4-21). *This supports the notion that most BDs may be mildly ejected embryos*, for example, from the Goodwin and Whitworth (2007) and Thies et al. (2010) circum-*proto-stellar* disks.

It appears thus that the different physical environments evident in Taurus-Auriga and the ONC produce about the same number of BDs per late-type star, so that there is no convincing evidence for differences in the IMF among current nearby star-forming regions across the hydrogen burning mass limit.

There is also no substantial evidence for a difference in the *stellar* IMF in these two star-forming regions, contrary to the assertion by, for example, Luhman (2004). ► Figure 4-22 shows the MF in four young clusters. The caveat that the classical pre-main sequence evolution tracks, upon which the observational mass determinations rely, are really applicable for such young ages (► Sect. 7.4) needs to be kept in mind though. Also, the observationally derived MFs are typically obtained by treating the luminous objects as single, while a majority are likely to be binary.

8.3 BD Flavors

BDs can come in different flavors depending on their formation (Kroupa and Bouvier 2003a): star-like BDs, ejected embryos, collisional BDs, and photo-evaporated BDs. As seen above, star-like BDs appear to be very rare because BDs do not mix with stars in terms of pairing properties. The rarity of the star-like BD flavour is supported theoretically because in order to have a cloud core produce only a BD or a BD-BD binary it needs to acquire an extreme density



■ Fig. 4-22

The observationally determined MFs in four young clusters, the names and approximate ages of which are indicated in the panels, are shown as the histograms or data with error bars. The *thick solid (red) curve* is the model of unresolved systems by Thies and Kroupa (2007). In this model, the stars have a binary fraction of 100% in Taurus and 50% in the other cases, with companion masses selected randomly from the canonical IMF (4.46). The two-part power-law canonical IMF (4.55) is shown as the *thick dashed line*. The BDs are described by the additional power-law IMF shown as the *dotted (blue) line*. In the model, they have a binary fraction of 15% and do not mix with the stars (the brown dwarf desert). It can be seen that the model is essentially invariant and leads to an excellent description of the data despite the BD and stellar IMFs being discontinuous (Fig. 4-23). Further details are found in Sect. 8.4

to become gravitationally unstable towards collapse. Such conditions are very rare in typical turbulent molecular clouds that have Mach numbers less than about 6 (Hennebelle and Chabrier 2008, 2009).

A more recently discussed possible channel of BD formation is via the fragmentation of massive circum-stellar disks (FMCSs) beyond about 100 AU and subsequent dynamical separation of the resulting weakly bound BD companion (Goodwin and Whitworth 2007; Stamatellos et al. 2007a; Stamatellos and Whitworth 2009; Thies et al. 2010; Basu and Vorobyov 2012). This mechanism for producing BDs can be considered a revised version of the ejected BD scenario. It appears to be the most promising physical mechanism for producing the dominant flavor of BDs.

An environmental dependency of the VLMS and BD IMF is expected for the FMCS channel as shown by Stamatellos et al. (2011). They point out that disk fragmentation is enhanced when the star plus disk accretes episodically as long as the accretion intervals are long enough to allow the disk to cool. In dense environments, episodic accretion would occur too frequently thereby inhibiting fragmentation as the accreting star's luminosity is kept as a high accretion luminosity thereby heating the disk.

The collisional removal of accretion envelopes for the production of unfinished stars needs to be discounted as a source for BDs because this process is far too rare (Kroupa and Bouvier 2003a). The removal of accretion envelopes through photo-evaporation can occur, but only within the immediate vicinity of an O star and never in Taurus-Auriga (Whitworth and Zinnecker 2004). Even in the presence of some ionising stars, as in the cluster NGC 6611 which ionises the Eagle nebula, Oliveira et al. (2009) find no measurable effect of photo-evaporation on the sub-stellar MF. However, Kroupa and Bouvier (2003a) show that the radius within which photo-evaporation may be able to remove substantial fractions of an accretion envelope within 10^5 year is comparable to the cluster size in star-burst clusters that contain thousands of O stars. In such clusters, photo-evaporated BDs may be very common. Globular clusters (GCs) may then be full of BDs.

GC-BD Hypothesis

In GCs, the number ratio of BDs to stars may be very large ($\gg 1/5$).

8.4 The Origin of BDs and Their IMF

It has thus emerged that in order to construct a realistic stellar and BD population, BDs and VLMSs need to be treated according to a different initialization algorithm to that of stars. They need to be separated when setting up the binary populations. This can be visualized with the following Gedanken Experiment which is a practical formulation of the BD/Star Population Theorem on p. 180.

Gedanken Experiment

Imagine a box contains BDs, M-, K-, and G-dwarf stars. In order to pair these to obtain the correct birth binary population (p. 28), a distinction between M-, K-, and G-dwarfs need not be made. But, nearly every time a BD is picked as a companion to a star, or a star is picked as a companion to a BD, the system needs to be discarded.

The physical interpretation of this mathematical result is that BDs form along with stars, just as planets do, but, just like planets, they do not result from the same formation mechanism. Rather, similarly as planets, BDs stem from gravitationally preprocessed material.

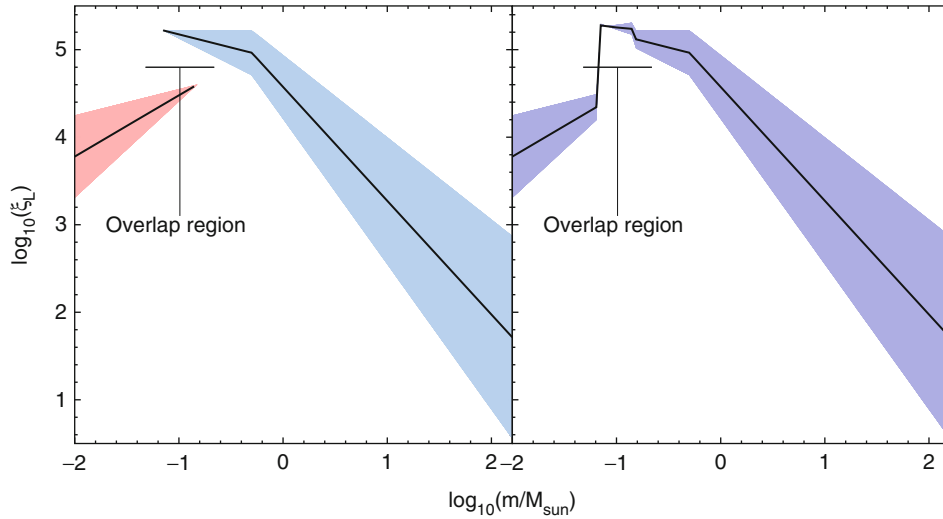
Indeed, the conditions in a molecular cloud core very rarely are such that a dense-enough core can collapse under self-gravity without accreting too much material for it to not transcend the BD/star mass boundary, which is why most BDs do not derive from a star-like origin (see also [Sect. 11.2](#)). But the outer regions of circum-proto-stellar disks accumulate material which has time to loose entropy ([Sect. 8.3](#)). These outer regions are sufficiently dense to locally collapse under self-gravity either because they become unstable or because they are perturbed. They are not too dense and thus remain optically thin for a sufficiently long time to allow the collapsing object to cool radiatively, and the region around the collapsing object has a limited supply of local disk material. Fragmentation may occur in marginally stable disks upon an external perturbation by the gravity of other stars (Thies et al. 2005, 2010) or by the gas-dynamical interaction of two disks (Shen et al. 2010). Both such processes thus enlarge the parameter space of circum-stellar disk conditions for BD formation since most stars form in a clustered mode.

A circum-proto-stellar disk therefore sets the boundary conditions in favor of BD formation. This is the same, but even more extreme, for planet formation, for which a highly processed molecular cloud core is required in the sense that gravo-hydrodynamical dynamics is augmented significantly by the dynamics between solid particles in a circum-stellar disk. Thus, while the formation of BDs is still a purely gravo-hydrodynamical process within an extended disk, planet formation is seeded by the coagulation of dust to larger solids which may then induce gas accretion from the circum-stellar disk.

The differences in the binary properties of BDs and stars therefore indicate that they are two different classes of objects with their own separate mass distributions. The MF of planets is also never considered a continuous extension of the stellar IMF (Dominik 2011).

The IMF of BDs needs to be derived from the observational star count data by taking the above into account. Thies and Kroupa (2007, 2008) have done so. The results for Taurus-Auriga, the ONC, IC 348, and Pleiades demonstrate that the IMF appears to be universal with $\alpha_0 \approx 0.3$ albeit with a significant discontinuity near $0.1 M_\odot$ ([Fig. 4-22](#)). The data imply that there is an overlap region: For the analysis to correctly account for the observed data, there must be VLMSs that form as BDs do, while there are massive BDs that form as stars do ([Fig. 4-23](#)). Without account of this overlap the IMF as well as the binary properties as a function of the mass may feign continuity (as suggested by Kaplan et al. 2012). Noteworthy is that this analysis re-derives the same BD-to-star fraction as deduced above: About one BD forms per five stars. The same result on the number ratio has been inferred by Andersen et al. (2008) who, however, need to describe the BD MF as a decreasing log-normal form as a result of insisting the IMF to be continuous across the BD/stellar mass range. As stated above, this approach cannot account for the BD desert, and the correct approach is to treat the BDs/VLMSs as a distinct population from the stars implying two separate IMFs for BDs and stars. This correct approach leads to a power-law solution for the BD MF with $\alpha \approx 0.3$, that is, a mildly rising MF toward small masses, and separate BD and stellar IMFs.

The universality of the BD–stellar IMF is interesting and may suggest that the formation of BDs is mostly dependent on the conditions prevalent in circum-proto-stellar disks. Indeed, in a large ensemble of SPH simulations of circum-stellar disks in young star clusters, Thies et al. (2010) find that a theoretical BD and VLMS MF emerges which is the same as the observationally deduced one.



■ Fig. 4-23

Left frame: The canonical IMF (solid line, (4.55)) with separate BD and stellar components. The upper and lower envelopes of the shaded regions are the minimum and maximum IMF when the uncertainties are taken into account. Both components overlap between 0.07 and $0.15 M_{\odot}$. **Right frame:** The sum of the BD and the stellar components as it would appear to an observer if perfect mass-measurements were available of all stars and BDs in all multiple systems. Note the “bump” that marks the overlap region. However, as demonstrated in Fig. 4-22, the real observational data wash out such features owing to the measurement uncertainties and the errors in transforming observed fluxes to masses. The model mass-histograms (thick red lines in Fig. 4-22) then fit the observed mass-histograms excellently for the young clusters for which such data are available

The observational and theoretical result that the BD branch becomes insignificant (i.e., the BD MF falls off steeply) above $0.1\text{--}0.2 M_{\odot}$ follows from a combination of two effects: the limited amount of material around late-type pre-main sequence stars that can be accreted onto a gravitational instability within the outer region of a circum-proto-stellar mass and the rare occurrence of massive protostars which are likely to have massive disks.

Main Results

Brown dwarfs are a separate population when compared to stars due to their distinct binary properties. The BD IMF has a power-law index $\alpha_0 \approx 0.3$, and the IMF is discontinuous but with a significant overlap of masses between the sub-stellar and stellar regime. This may hide the discontinuity unless a proper analysis is done. About one BD forms per five stars.

9 The Shape of the IMF from Resolved Stellar Populations

From the above discourse, it thus becomes apparent that we have good constraints on the stellar and BD IMF. These are valid only for the regime of present-day (“normal”) star formation, that is, star-formation densities $\rho \lesssim 10^5 M_{\odot} \text{pc}^{-3}$ and metallicities $[\text{Fe}/\text{H}] \gtrsim -2$. Since stars are formed

as binary systems (► Sect. 2.6), the system IMF is provided in ► Sect. 9.2 for binary fractions of 100% (the birth system IMF) and for a binary fraction of 50% (the typical Galactic-field or open star cluster system IMF). The Galactic-field IMF, which is the IGIMF valid for the Milky Way, is provided in ► Sect. 9.3. In ► Sect. 12, it is concluded that the IMF becomes top-heavy for star formation under denser conditions and that it may be bottom-light under metal-poor conditions.

The distribution of stars by mass in “normal” systems is a power law with exponent or index $\alpha_2 \approx 2.3$ for stellar masses $m \gtrsim 0.5 M_\odot$. There exists a physical stellar mass limit, $m_{\text{max}*} \approx 150 M_\odot$ such that $m \leq m_{\text{max}*}$ (► Sect. 3). The distribution of stars below the K/M dwarf transition mass, $0.5 M_\odot$, can also be described by a power law but with exponent $\alpha_1 \approx 1.3$ (► Sect. 7). Given the latest results described in ► Sect. 8, the mass distribution below the mass $m_1 \approx 0.1 M_\odot$ is uncertain, but measurements indicate a power law with exponent $0 < \alpha_0 < 1$. Because the binary properties of VLMSs and BDs differ substantially from those in the low-mass star regime, it emerges stringently that BDs and some VLMSs need to be considered as a separate population that is linked to, but different from stars. Fitting a functional description of the mass distribution with the continuity constraint across m_1 would therefore be wrong. It follows that one single function such as the log-normal form, which may be associated with the likelihood of occurrence of masses from the fragmentation limit,¹⁵ $m_0 \approx 0.01 M_\odot$, through to the physical stability limit, $m_{\text{max}*}$, is not the correct description of the stellar and BD IMF.

With these recent insights (power-law IMF over two orders of magnitude in mass and discontinuity near the sub-stellar mass limit), little of the argument for the advantages of a log-normal or any other mathematical form (► Table 4-3 below) remains. Indeed, any such other mathematical form has the disadvantage that the tails of the distribution react to changes in the parametrization in a way perhaps not wanted when testing models. To give an example, a single log-normal form would change the slope of the IMF at large masses even if only the LF for late-type stars is to be varied. The canonical (► 4.55) two-part power-law stellar IMF, on the other hand, would allow changes to the index at low masses without affecting the high-mass end, and the addition of further power-law segments is mathematically convenient. The canonical two-part power-law stellar IMF also captures the essence of the physics of star formation, namely, a featureless power-law form for the largest range of stellar masses and a turnover near some fraction of a solar mass. This turnover appears to be present already in the pre-stellar cloud-core MF and may be due to the decreasing likelihood that low-mass cloud clumps collapse under self-gravity (► Sect. 11.2).

9.1 The Canonical, Standard or Average IMF

The various constraints arrived at above are summarized by an IMF that is a single power law for BDs and a two-part power law for stars (► 4.55), using the notation from (► 4.4) to (► 4.5).

¹⁵When a cloud collapses, its density increases, but its temperature remains constant as long as the opacity remains low enough to enable the contraction work to be radiated away. The Jeans mass (► 4.50) consequently decreases and further fragments with smaller masses form. When, however, the density increases to a level such that the cloud core becomes optically thick, then the temperature increases, and the Jeans mass follows suit. Thus, an opacity-limited minimum fragmentation mass of about $0.01 M_\odot$ is arrived at (Low and Lynden-Bell 1976; Boss 1986; Kumar 2003; Bate 2005).

The Canonical IMF*(m* is in units of M_\odot)

$$\begin{aligned}
\xi_{\text{BD}}(m) &= \frac{k}{3} \left(\frac{m}{0.07} \right)^{-0.3 \pm 0.4}, & 0.01 < m \lesssim 0.15, \\
\xi_{\text{star}}(m) &= k \begin{cases} \left(\frac{m}{0.07} \right)^{-1.3 \pm 0.3} & , \quad 0.07 < m \leq 0.5, \\ \left[\left(\frac{0.5}{0.07} \right)^{-1.3 \pm 0.3} \right] \left(\frac{m}{0.5} \right)^{-2.3 \pm 0.36} & , \quad 0.5 < m \leq 150. \end{cases} \quad (4.55)
\end{aligned}$$

The uncertainties are discussed in [Sect. 9.4](#). This is the individual-star/BD IMF which is corrected fully for multiple companions. That is, in a star-formation event, the distribution of stars and of BDs that form is given by this IMF. The constraint that the population be optimally sampled (p. 132) may be invoked. To formulate a realistic stellar and BD population would then require these stars and BDs to be distributed into stellar and BD binaries ([Sects. 2.6](#) and [9.2](#)).

Note that this form is a two-part power law in the stellar regime and that BDs contribute about 4% by mass only and need to be treated as a separate population such that both IMFs overlap between about 0.07 and 0.15 M_\odot ([Fig. 4-23](#)). The gap or discontinuity between the BD and the stellar IMF can be measured by the BD-to-star ratio at the classical BD-star border, $m_H \approx 0.075 M_\odot$, with $\xi_{\text{BD}}(m_H)/\xi_{\text{star}}(m_H) \approx \frac{1}{3}$, that is, $k_{\text{BD}} \approx 1/3$ (Kroupa et al. 2003; Thies and Kroupa 2007, 2008).

The canonical IMF can also be described as a log-normal function for low-mass stars with a power-law extension to massive stars, yielding the *log-normal canonical IMF*.

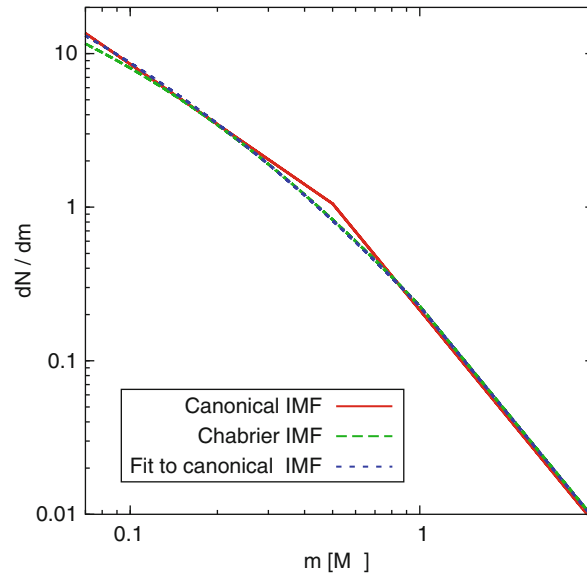
The Log-normal Canonical IMF*(m* is in units of M_\odot)

$$\begin{aligned}
\xi_{\text{BD}}(m) &= k k_{\text{BD}} \left(\frac{m}{0.07} \right)^{-0.3 \pm 0.4}, & 0.01 < m \lesssim 0.15, \\
\xi_{\text{star}}(m) &= k \begin{cases} \frac{1}{m} \exp \left[-\frac{(lm - lm_c)^2}{2 \sigma_{lm}^2} \right] & , \quad 0.07 < m \leq 1.0, \\ A \left(\frac{m}{1.0} \right)^{-2.3 \pm 0.36} & , \quad 1.0 < m \leq 150. \end{cases} \quad (4.56)
\end{aligned}$$

In ([4.56](#)) $lm_c \equiv \log_{10} m_c / M_\odot$, continuity is assured at 1 M_\odot and $\xi_{\text{BD}}(m_H)/\xi_{\text{star}}(m_H) \approx \frac{1}{3}$, as in ([4.55](#)).

A least-squares fit of the log-normal canonical IMF to the two-part power-law form ([4.55](#)), whereby $\int_{0.07}^{150} m \xi(m) dm = 1 M_\odot$ for both (m in Solar units), yields $m_c = 0.055 M_\odot$ and $\sigma_{lm} = 0.75$ with $A = 0.2440$ for continuity at 1 M_\odot and $k_{\text{BD}} = 4.46$ to ensure $\xi_{\text{BD}}(0.75 M_\odot)/\xi_{\text{star}}(0.75 M_\odot) = 1/3$ as being the best log-normal plus power-law representation of the canonical IMF. Alternatively, the Chabrier parametrization has $m_c = 0.079_{+0.021}^{-0.016} M_\odot$ and $\sigma_{lm} = 0.69_{+0.05}^{-0.01}$ (Table 1 in Chabrier 2003a) with $A = 0.2791$ and $k_{\text{BD}} = 4.53$.

The three forms of the canonical IMF are compared in [Fig. 4-24](#). The best-fit log-normal representation of the two-part power-law canonical IMF is indistinguishable from the Chabrier result, demonstrating the extreme robustness of the canonical IMF.



■ Fig. 4-24

A comparison between the three canonical IMFs: the two-part power-law IMF ((4.55), *solid red curve*) and the log-normal plus power-law IMF ((4.56), the “best-fit-canonical IMF” and the “Chabrier IMF”) in the interval from 0.07 to $4 M_{\odot}$. Plotted is the number of stars per mass interval versus the stellar mass, both scales being logarithmic. The IMFs are normalized such that $\int_{0.07}^{150} m \xi(m) dm = 1 M_{\odot}$, where m is the mass in solar units. Note in particular that the three IMF forms are indistinguishable over the whole mass interval. They are identical above a mass of $1 M_{\odot}$, except for a slightly different normalization factor

The above canonical or standard forms have been derived from detailed considerations of star counts thereby representing an *average* IMF: for low-mass stars, it is a mixture of stellar populations spanning a large range of ages (0–10 Gyr) and metallicities ($[\text{Fe}/\text{H}] \gtrsim -2$). For the massive stars, it constitutes a mixture of different metallicities ($[\text{Fe}/\text{H}] \gtrsim -1.5$) and star-forming conditions (OB associations to very dense star-burst clusters: R136 in the LMC). Therefore, the average IMF can be taken as a canonical form, and the aim is to test the IMF Universality Hypothesis:

IMF Universality Hypothesis

The canonical IMF ((4.55) and (4.56)) constitutes the parent distribution of all stellar populations that form with densities $\rho \lesssim 10^5 M_{\odot}/\text{pc}^3$ and metallicities $[\text{Fe}/\text{H}] \gtrsim -2$.

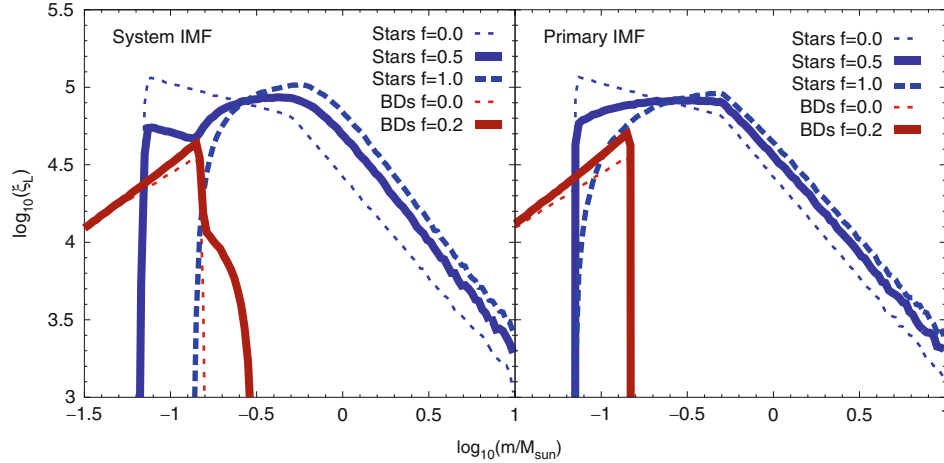
Negation of this hypothesis would indeed imply a variable IMF. For larger densities, evidence has emerged that the IMF becomes top-heavy ((4.64)). Also, evidence has emerged that the IMF may have a metallicity dependence ((4.63)).

9.2 The IMF of Systems and of Primaries

The canonical stellar IMF (☛ 4.55) is the distribution of all stars to have formed together in one star-forming event. However, since stars form as binary systems, it is also useful to consider the form of the system IMF which results from pairing stars chosen randomly from the canonical stellar IMF. Random pairing is a good description of late-type stellar systems in birth environments, but massive stars tend to prefer more similar-mass companions (☛ Sect. 2.6). The system IMF is given by (☛ 4.57) by approximating the mass distribution by a power law with index α_1 between 0.15 and $0.5 M_\odot$. It is assumed that all stars are in binaries, that is, $f = 1$, and, for completeness, the system IMF for a binary fraction of 50% is also evaluated. The actual mass distributions are plotted in ☛ Fig. 4-25.

The system IMF:

$$\begin{aligned} \alpha_1 &= +0.66 \pm 0.3 & , & \quad 0.15 \leq m/M_\odot < 0.65 & , & \quad (f = 0.5) \\ \alpha_1 &\approx -0.22 & , & \quad 0.15 \leq m/M_\odot < 0.65 & , & \quad (f = 1). \end{aligned} \quad (4.57)$$



☛ Fig. 4-25

Left panel: The system IMF is shown in blue and the system BD/VLMS IMF is in red. The *thick curves* are for a binary fraction among stars of $f = 50\%$ and for a BD binary fraction of $f_{BD} = 20\%$. Random pairing of companion masses is assumed (☛ Sect. 2.6) from the canonical stellar ($0.07\text{--}150 M_\odot$) and BD ($0.01\text{--}0.15 M_\odot$) IMFs. These are shown here as the *thin dotted curves* for binary fraction = 0 (☛ 4.55), also plotted in ☛ Fig. 4-23). Note the flat extension at the lowest-mass end of the stellar system IMF. It comes from the fact that below $0.14 M_\odot$, all stars are single since the minimum system mass is twice the minimum stellar mass ($0.07 M_\odot$). The bump at the high-mass end of the BD system distribution comes from the most massive systems having masses larger than the most massive BD/VLMS ($0.15 M_\odot$) in this model. The medium dashed stellar system IMFs are for an initial stellar binary fraction of 100%, as would be found in dynamically not evolved star-forming regions. **Right panel:** the same but plotting only the IMF of primary masses. Note the significant difference between the canonical IMF and the system/primary-star IMFs in both panels. The system IMF and the IMF of primaries are approximated by (☛ 4.57) and (☛ 4.58), respectively

Note that in each case $\alpha_0 = 0.2 \pm 0.4$ ($f_{\text{BD}} = 0.2$, random pairing) and $\alpha_2 = 2.3$ ($m \gtrsim 0.65 M_\odot$) as in the canonical stellar IMF (◆ 4.55).

Note that the binary effect contributes $\Delta\alpha \approx 0.64$ for $f = 0.5$ and $\Delta\alpha \approx 1.5$ for $f = 1$ where $\Delta\alpha$ is the difference between the canonical $\alpha_1 = 1.3$ and the above values.

The IMF of primary stars, which may be closer to an observed IMF since companions are usually faint and would be lost from the star count, is given by (◆ 4.58) following the same procedure as for the system IMF.

The IMF of primary stars:

$$\begin{aligned} \alpha_1 &= +1.0 \pm 0.3 & , & \quad 0.15 \leq m/M_\odot < 0.50 & , & \quad (f = 0.5) \\ \alpha_1 &= +0.7 \pm 0.3 & , & \quad 0.15 \leq m/M_\odot < 0.50 & , & \quad (f = 1). \end{aligned} \quad (4.58)$$

Note that in each case $\alpha_0 = 0.2 \pm 0.4$ ($f_{\text{BD}} = 0.2$, random pairing) and $\alpha_2 = 2.3$ ($m \gtrsim 0.5 M_\odot$) as in the canonical stellar IMF (◆ 4.55).

9.3 The Galactic-Field IMF

The Scalo power-law index $\alpha_3 = 2.7$ ($m \gtrsim 1 M_\odot$) was inferred by Scalo (1986) from star counts for the MW disk population of massive stars such that the three-part power-law KTG93 IMF needs to be identified with the *composite IMF* (i.e., the IGIMF) introduced in ◆ Sect. 13.1, arriving at the *KTG93 IMF* (Kroupa et al. 1993). It is updated in (◆ 4.59) to account for the separate BD and stellar populations.

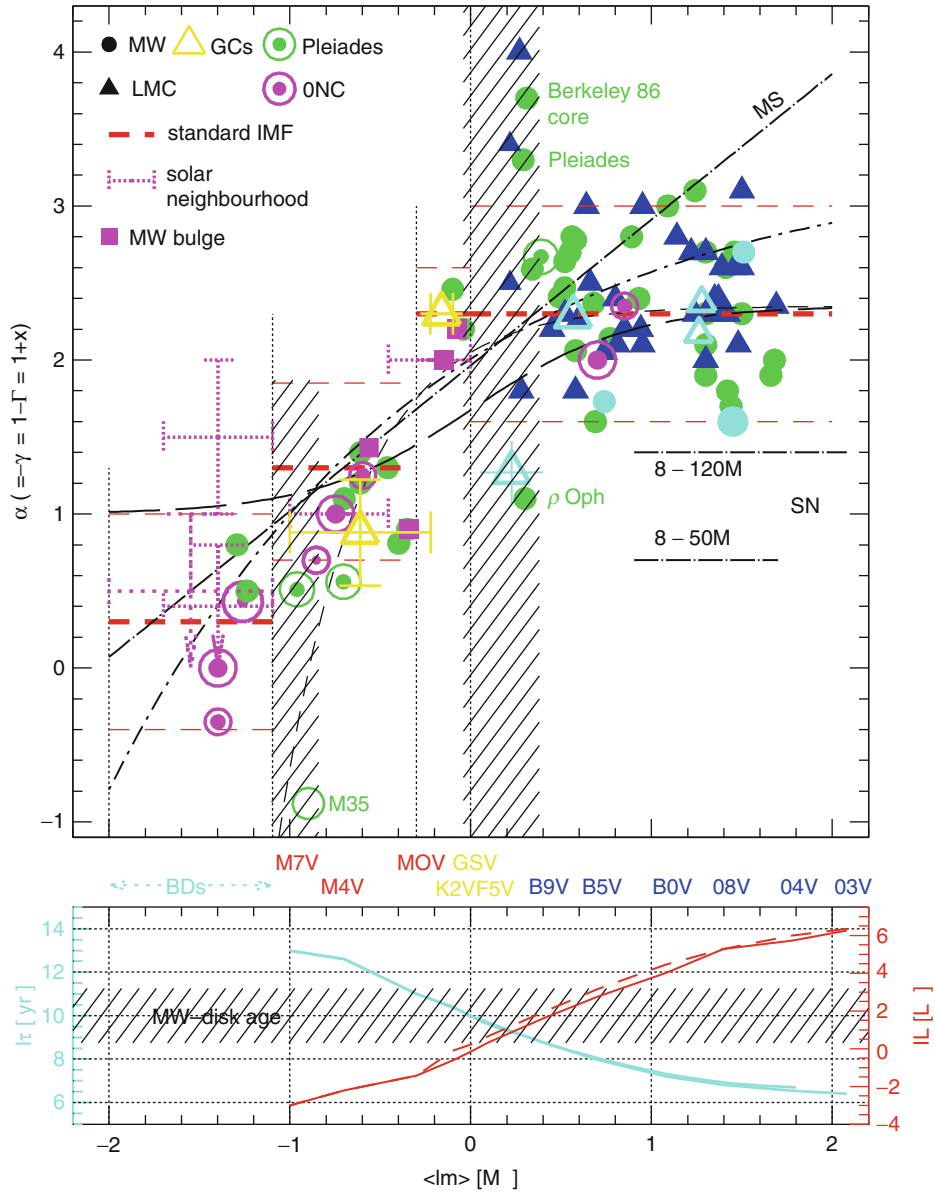
The Galactic-field (KTG93) stellar IMF:

$$\begin{aligned} \alpha_0 &= +0.3 \pm 0.4 & , & \quad 0.01 \leq m/M_\odot \lesssim 0.15 & , & \quad n = 0, \text{ (BDs)} \\ \alpha_1 &= +1.3 \pm 0.3 & , & \quad 0.07 \lesssim m/M_\odot < 0.50 & , & \quad n = 1, \text{ (stars)} \\ \alpha_2 &= +2.3 \pm 0.3 & , & \quad 0.5 \leq m/M_\odot < 1 & , & \quad n = 2, \\ \alpha_3 &= +2.7 \pm 0.4 & , & \quad 1 \lesssim m/M_\odot & , & \quad n = 3. \end{aligned} \quad (4.59)$$

The Galactic-field (KTG93) IMF is the IMF of all young stars within the Galactic disk assuming all multiple stars can be resolved. It is not equal to the canonical IMF for $m \gtrsim 1 M_\odot$. In the LMC, the field-star IMF is known to be steep, $\alpha_3 \approx 4.5$ (Massey 2003).

9.4 The Alpha Plot

A convenient way for summarizing various studies of the IMF is by plotting independently derived power-law indices in dependence of the stellar mass over which they are fitted (Scalo 1998; Kroupa 2001b, 2002; Hillenbrand 2004). The upper panel of ◆ Fig. 4-26 shows such data: The shape of the IMF is mapped by plotting measurements of α at $\langle lm \rangle = (lm_2 - lm_1)/2$ obtained by fitting power laws, $\xi(m) \propto m^{-\alpha}$, to logarithmic mass ranges lm_1 to lm_2 (not indicated here for clarity). Circles and triangles are data compiled by Scalo (1998) and Kroupa (2001b) for MW and Large-Magellanic-Cloud (LMC) clusters and OB associations, as well as newer data, some of which are emphasized using different symbols (and colors). Unresolved multiple systems are not corrected for in all these data including the MW-Bulge data. The canonical stellar IMF (◆ 4.55), corrected for unseen binary-star companions, is the two-part power law (thick short-dashed lines). Other binary-star-corrected solar-neighborhood IMF measurements are indicated as (magenta) dotted error bars.



■ Fig. 4-26

Upper panel: the alpha plot. The curves (e.g., labeled “MS”) are various IMF slopes documented in [Table 4-3](#) and discussed in [Sect. 10.2](#). The plotted data are listed in the supplementary information of Kroupa (2002). The cyan open triangles are for R136 in the LMC. **Lower panel:** The bolometric stellar mass–luminosity relation, $IL(lm)$, shown by the solid and dashed curves, and the stellar main-sequence lifetime (or turnoff masses at a given age), $l\tau$. The possible range of Milky Way (MW) disk ages are shown as the shaded region. The masses of stellar spectral types are indicated. Notation: $lm \equiv \log_{10}(m/M_{\odot})$, $l\tau \equiv \log_{10}(\tau/\text{year})$, $IL \equiv \log_{10}(L/L_{\odot})$. For more details, see text

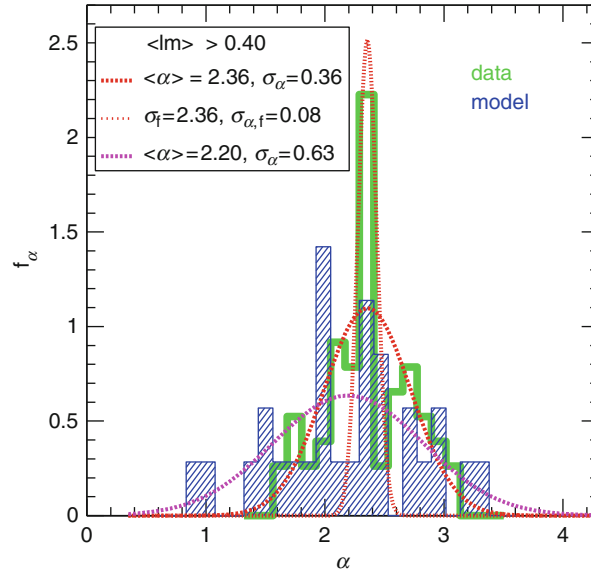
In the lower panel of [Fig. 4-26](#) are plotted the luminosities of main-sequence stars and the stellar lifetimes as a function of mass on the same mass scale as the alpha plot shown in the upper panel.

For $m > 1 M_{\odot}$, correction for unseen companions does not affect the IMF (Maíz Apellániz 2008; Weidner et al. 2009). The M dwarf ($0.1\text{--}0.5 M_{\odot}$) MFs for the various clusters are systematically flatter (smaller α_1) than the canonical IMF, which is mostly due to unresolved multiple systems in the observed values. This is verified by comparing to the system IMF for a binary fraction of 50% ([4.57](#)). Some of the data do coincide with the canonical IMF though, and Kroupa (2001b) argues that on correcting these for unresolved binaries, the underlying true individual-star IMF ought to have $\alpha_1 \approx 1.8$. This may indicate a systematic variation of α_1 with metallicity because the data are young clusters that are typically more metal-rich than the average Galactic field population for which $\alpha_1 = 1.3$ ([4.62](#) below).

A power-law extension into the BD regime with a smaller index ($\alpha_0 = +0.3$) is shown as a third thick short-dashed segment, but this part of the mass distribution is not a continuous extension of the stellar distribution, as noted in [Sect. 8.4](#).

The upper and lower thin short-dashed lines are the estimated 99% confidence range on α_i . The usual one-sigma uncertainties adopted in ([4.55](#)) are, however, estimated from the distribution of α values in [Figs. 4-26](#) and [4-27](#).

The long-dash-dotted horizontal lines in [Fig. 4-26](#) labeled “SN” are those IMFs with $\alpha_3 = 0.70(1.4)$ but $\alpha_0, \alpha_1, \alpha_2$ as in ([4.55](#)), for which 50% of the stellar (including BD) mass is in stars with $8\text{--}50$ ($8\text{--}120$) M_{\odot} , respectively. It is noteworthy that none of the available resolved clusters, not even including the Local Group star-burst clusters, have such a top-heavy IMF.



■ Fig. 4-27

Distribution of α values for massive stars ($m > 10^{0.4} M_{\odot}$). Note that the empirical data show a sharper (just at the Salpeter index) and more symmetrical distribution than the model, which is based on the Salpeter index. This is unexpected. See Open Question III in [Sect. 9.5](#) for details

The vertical dotted lines in [Fig. 4-26](#) delineate the four mass ranges over which the Galactic-field IMF is defined ([Fig. 4.59](#)), and the shaded areas highlight those stellar mass regions where the derivation of the IMF is additionally complicated especially for Galactic field stars: For $0.07 < m/M_{\odot} < 0.15$, long pre-main sequence contraction times (Chabrier and Baraffe 2000) make the conversion from an empirical LF to an IMF ([Fig. 4.1](#)) dependent on the precise knowledge of stellar ages and the star-formation history, and for $0.8 < m/M_{\odot} < 2.5$ uncertain main-sequence evolution, Galactic-disk age and the star-formation history of the MW disk do not allow accurate IMF determinations (Binney et al. 2000; Elmegreen and Scalo 2006).

9.5 The Distribution of Data Points in the Alpha-Plot

The first thing to note about the data distribution in the alpha plot is that there is no readily discernible systematic difference in IMF determinations neither with metallicity nor density of the population (cf. [Fig. 4-8](#)).

In order to understand the origin and nature of the dispersion of power-law indices evident in the alpha plot, Kroupa (2001b) investigates the dispersion of α values for a given mass interval using Aarseth- N -body models of evolving clusters. The result is that the dispersion can be understood in terms of statistical sampling from a universal IMF (as also found by Elmegreen 1997, 1999) together with stellar-dynamical biases.¹⁶ Optimal Sampling ([Sect. 2.2](#)) was not available in 2001 so that statistical variations that arise by randomly sampling stars from the IMF could not then be separated from variations of the IMF due to stellar-dynamical processes in young star clusters.

Given the existing 2001 theoretical investigation, it is possible to compare the theoretical distribution of α values for an ensemble of star clusters with the observational data. This is done for stars with $m > 2.5 M_{\odot}$ in [Fig. 4-27](#) where the open (green) histogram shows the distribution of observational data from [Fig. 4-26](#). The (blue) shaded histogram is the theoretical ensemble of 12 star clusters containing initially 800 to 10^4 stars that are “observed” at 3 and 70 Myr: Stellar companions are merged to give the system MFs, which are used to measure α , but the input individual-star IMF is in all cases the canonical form ([Fig. 4.55](#)). The dotted curves are Gaussians with the same average α and standard deviation in α obtained from the histograms. Fixing $\alpha_f = \langle \alpha \rangle$ and using only $|\alpha| \leq 2\sigma_{\alpha}$ for the observational data gives the narrow thin (red) dotted Gaussian distribution which describes the Salpeter peak extremely well (not by construction).

The interesting finding is thus that the observational data have a very pronounced Salpeter/Massey peak, with broad near-symmetric wings. This indicates that there are no significant biases that should skew the distribution. For example, if the observational sample contained clusters or associations within which the OB stars have a low binary fraction compared to others that have a very high multiplicity fraction, we would expect the binary-deficient cases to deviate toward high α values since fainter companions are hidden in the binary-rich cases. The absence of this effect is consistent with the result obtained by Maíz Apellániz (2008) and Weidner et al. (2009) that multiple systems do not affect the derived power-law index of the IMF for stars more massive than a few M_{\odot} . For stars with mass $m < 1 M_{\odot}$, unresolved multiples do have a significant effect, and this has been corrected for in the canonical IMF ([Fig. 4.55](#)).

¹⁶Note that this does *not* constitute a proof of the stellar IMF being a probabilistic density distribution!

Energetic dynamical ejections from cluster cores deplete the IMF of the massive stars (Pflamm-Altenburg and Kroupa 2006), increasing the observed α_3 , (Banerjee and Kroupa 2012) in the cluster while mass segregation has the opposite effect.

In contrast to the observational data, the theoretical data show (i) a distribution with a mean shifted to smaller $\alpha_3 \approx 2.2$ that has (ii) a larger width than the observational one. The input canonical Salpeter/Massey index is not really evident in the theoretical data, and if these were the observational data, then it is likely that the astronomical community would strongly argue for the case that the IMF shows appreciable variations. This leads to the following peculiar result.

Open Question III

The empirical IMF power-law indices for massive stars are better behaved than the model data. This is unexpected because all the additional complications (observational uncertainties, uncertainties in transferring observed luminosities to masses such as stellar models, rotating/non-rotating stars) ought to deteriorate the empirical data, while the model has none of these uncertainties.

Clarifying the hitherto not understood difference between the much more “well-behaved” observational data and the theoretical data will need further theoretical work which will have to attempt to reproduce the observational procedure as exactly as is possible (see also the Sociological Hypothesis on p. 196).

Note that Open Question III is naturally resolved if nature follows optimal sampling (► Sect. 2.2) rather than random sampling (► Sect. 2.3) from the IMF.

Is the scatter of data points in the alpha plot (► Fig. 4-26) a result of IMF variations? For this to be conclusively convincing would require a measurement to lie further from the canonical IMF than the conservative uncertainty range shown in the figure. However, the adopted uncertainties on α_i in (► 4.55) stem from the scatter in the alpha plot, so that this argument is circular.

An independent indication of the uncertainties inherent to IMF determinations can be obtained by comparing IMF estimates of the same cluster by different authors. This is demonstrated for the well-studied Pleiades, ONC, and for 30 Dor (► Fig. 4-26). Overall, the uncertainties in α are about ± 0.5 which is also about the scatter evident in all the data, so that there is no indication of significant outliers (except in the shaded regions, see below). Differences of $\Delta\alpha \approx 0.5$ for VLMSs and BDs are evident for the extremely young ONC allowing an estimate of likely nonphysical variations in the alpha plot. Data reduction at these low masses is hampered by variability, differential reddening, and spurious detections (Slesnick et al. 2004; Andersen et al. 2009). It is clear that because the procedure of measuring $\alpha(lm)$ is not standardized and because the IMF is not a single power law, author–author variations occur simply due to the use of different mass ranges when fitting power laws (see “Binning” bias in ► Sect. 2.1).

Significant departures from the canonical IMF only occur in the shaded areas of the alpha plot. These are, however, not reliable. The upper mass range in the shaded area near $1 M_\odot$ poses the problem that the star clusters investigated have evolved such that the turnoff mass is near to this range. Some clusters such as ρ Oph are so sparse that more massive stars did not form. In these cases, the shaded range is close to the upper mass limit leading to possible stochastic stellar-dynamical biases since the most massive stars meet near the core of a cluster due to mass segregation, but three-body or higher-order encounters there can cause expulsion from

the cluster. Furthermore, ρ Oph is still forming, leading to unknown effects that are likely to enhance variations in the first derivative of the IMF (i.e., in α values).

The shaded area near $0.1 M_{\odot}$ poses the problem that the VLMSs are not on the main sequence for most of the clusters studied and are again prone to bias through mass segregation by being underrepresented within the central cluster area that is easiest to study observationally. Especially the latter is probably biasing the M35 datum, but some effect with metallicity may be operating especially so since M35 appears to have a smaller α near the H-burning mass limit than the Pleiades cluster which has a similar age but has a larger abundance of metals (► Fig. 4-19). The M35 cluster ought to be looked at again with telescopes.

Two other well-studied massive star-burst clusters have $\alpha \approx \text{Salpeter}/\text{Massey}$ (30 Dor and NGC 3603) implying no clear evidence for a bias that resolved star-burst clusters prefer smaller α and thus more massive stars relatively to the number of low-mass stars. Low-mass stars are known to form in 30 Dor (Sirianni et al. 2000), although their MF has not been measured yet due to the large distance of about 55 kpc. From the ONC, we know that the entire mass spectrum $0.05 \lesssim m/M_{\odot} \lesssim 40$ is represented but that it has a deficit of massive stars (Pflamm-Altenburg and Kroupa 2006) (► Fig. 4-19). The Pleiades appear to have had an IMF very similar to the canonical one, although for massive stars, a steeper IMF with $\alpha_3 \approx 2.7$ may also be suggested by theoretical work (► Fig. 4-18).

But it remains an unsolved issue (see Open Question III on p. 195) as to why the theoretical data have a larger dispersion of α values than the empirical ones (► Fig. 4-27). The models discussed above and plotted in ► Fig. 4-27 had as the input IMF the Salpeter index, whereas the empirical data suffer under all the biases associated with transforming measured fluxes to stellar masses (► Sect. 2.1) and have been collated from various sources published by different authors. In particular, the very narrow empirical distribution exactly around the Salpeter index is remarkable. This leads to the following Sociological Hypothesis.

Sociological Hypothesis

The measured α indices for massive stars are affected by sociological predispositions.

However, the excellent documented efforts of the teams working on measuring α for massive stars would not necessarily lend support to this hypothesis. Actually, as already observed on p. 195, optimal sampling would automatically resolve Open Question III therewith negating the Sociological Hypothesis.

The available evidence is thus that low-mass stars and massive stars form together even in extreme environments. This is also supported by an impressive observational study (Luhman et al. 2000; Luhman 2004) of many close-by star-forming regions using one consistent methodology to avoid author–author variations. The result is that the IMF does not show conclusive differences from low-density star-forming regions in small molecular clouds ($n = 0.2\text{--}1$ stars/pc³ in ρ Oph) to high-density cases in giant molecular clouds ($n = (1\text{--}5) \times 10^4$ stars/pc³ in the ONC). This result extends to the populations in the truly exotic ancient and metal-poor dwarf-spheroidal satellite galaxies which are speculated to be dominated by dark matter but definitely constitute star-forming conditions very different from present-day events. Two such close companions to the Milky Way have been observed (Grillmair et al. 1998; Feltzing et al. 1999) finding the same MF as in globular clusters for $0.5 \lesssim m/M_{\odot} \lesssim 0.9$ and thus no evident differences

to the canonical IMF. However, evidence for top-heavy IMFs in pc-scale starbursts and for bottom-heavy IMFs in elliptical galaxies has emerged (► Sect. 12.9 and ► 12.3, respectively).

Main Results

Within the observational uncertainties, the IMF of all known resolved stellar populations is well described by the canonical, standard, or average IMF. It is given by (► 4.55) and has been corrected for unresolved multiple systems. The only structure evident in the *stellar* IMF is thus a turnover near $0.5 M_{\odot}$ and a rapid turndown below $0.075 M_{\odot}$. The BD IMF is a separate single power-law such that about one BD forms per five stars. Open Question III leads to the Sociological Hypothesis which may naturally be negated by optimal sampling.

10 Comparisons and Some Numbers

In this section, some useful numbers are provided, and a comparison between various IMF forms is made with cumulative functions in the number of stars and stellar mass being plotted for general use.

10.1 The Solar-Neighborhood Mass Density and Some Other Numbers

Given the reasonably well-constrained shape of the stellar IMF (► 4.55), it is of interest to investigate the implied number and mass density in the Galactic disk. Here, we consider the solar neighborhood. In order to normalize the IMF to the solar neighborhood stellar number density, the observed stellar LF is conveniently used.

The nearby Hipparcos LF, $\Psi_{\text{near}}(\text{Hipp})$ (► Fig. 4-9), has $\rho = (5.9 \pm 0.3) \times 10^{-3}$ stars/pc³ in the interval $M_V = 5.5 - 7.5$ corresponding to the mass interval $[m_2, m_1] = [0.891, 0.687] M_{\odot}$ (Kroupa 2001c) using the KTG93 MLR (► Fig. 4-11). $\int_{m_1}^{m_2} \xi(m) dm = \rho$ yields $k = 0.877 \pm 0.045$ stars/(pc³ M_{\odot}). The number fractions, mass fractions, and Galactic-field mass densities contributed by stars in different mass ranges are summarized in ► Table 4-1 (p. 161).

The local mass density made up of interstellar matter is $\rho^{\text{gas}} \approx 0.04 \pm 0.02 M_{\odot}/\text{pc}^3$. In stellar remnants, it is $\rho^{\text{rem}} \approx 0.003 M_{\odot}/\text{pc}^3$ (Weidemann 1990) or $\rho^{\text{rem}} \approx 0.005 M_{\odot}/\text{pc}^3$ (Chabrier 2003a and references therein). Giant stars contribute about $0.6 \times 10^{-3} M_{\odot}\text{pc}^{-3}$ (Haywood et al. 1997), so that main-sequence stars make up about half of the baryonic matter density in the local Galactic disk (► Table 4-1). BDs, which for some time were regarded as candidates for contributing to the dark-matter problem, do not constitute a dynamically important mass component of the Galaxy, contributing not more than 5% in mass. This is corroborated by dynamical analysis of local stellar space motions that imply there is no need for dark matter in the Milky Way disk (Flynn and Fuchs 1994), and the revision of the thick-disk mass density to larger values (Fuhrmann 2004; Soubiran et al. 2003) further reduces the need for dark matter within the solar circle.

► [Table 4-1](#) also shows that a star cluster loses about 12% of its mass through stellar evolution within 10 Myr if $\alpha_3 = 2.3$ (turnoff mass $m_{\text{to}} \approx 20 M_{\odot}$) or within 300 Myr if $\alpha_3 = 2.7$ (turnoff-mass $m_{\text{to}} \approx 3 M_{\odot}$). After 5 Gyr, the mass loss through stellar evolution alone amounts to about 45% if $\alpha_3 = 2.3$ or 30% if $\alpha_3 = 2.7$. Mass loss through stellar evolution therefore poses no risk for the survival of star clusters for the IMFs discussed here since the mass-loss rate is slow enough for the cluster to adjust adiabatically. A star cluster would be threatened through mass loss from supernova explosions if $\alpha \lesssim 1.4$ for $8 < m/M_{\odot} \leq 120$ which would mean a mass loss of $\gtrsim 50\%$ within about 40 Myr when the last supernova explodes. It is remarkable that none of the measurements in resolved populations has found such a low α for massive stars (► [Fig. 4-26](#)). Mass loss due to stellar evolution might pose a threat to the survival of post-gas-expulsion clusters when the system is mass-segregated as has been shown by Vesperini et al. (2009).

10.2 Other IMF Forms and Cumulative Functions

The standard or canonical power-law IMF (► [4.55](#)) provides a good description of the data combined with mathematical ease and physical meaning. Integrating the IMF is a frequently required task, and it is especially here that the two- or even multi-part power-law description of the canonical IMF shows its strength. For example, if the IMF were a probabilistic density distribution function then writing down a mass-generating function (► [Sect. 2.3](#)) is practically trivial allowing perfectly efficient (each random deviate X yields a usable mass m) discretization of the stellar population into individual stellar masses. A further strong advantage of this parametrization is that each section can be changed without affecting another part of the IMF. As an explicit example, should the BD MF be revised, α_0 can be adopted accordingly without affecting the rest of the mass distribution in the well-constrained stellar regime. That the two- or multi-part power-law form has a discontinuity in the derivative at $0.5 M_{\odot}$ (► [Fig. 4-26](#)) has no implications for stellar populations and is therefore not a disadvantage, especially so since there exists no theoretically derived IMF form of significance. It is, however, true that the real IMF must be differentiable, but it must have a rapid change in slope near $0.5 M_{\odot}$ and below about $0.08 M_{\odot}$ where the stellar IMF decays rapidly. The Chabrier formulation of the log-normal canonical IMF ((► [4.56](#)), ► [Fig. 4-24](#)) also has a discontinuity in its derivative but at $1 M_{\odot}$ and does not reproduce the rapid falloff of the stellar IMF below about $0.08 M_{\odot}$ unless it is cutoff there nor is it easily integrable.

Often, a single Salpeter power law IMF is applied ($\alpha = 2.35$ for $0.1 M_{\odot} \lesssim m$). ► [Table 4-2](#) gives the stellar masses (► [4.8](#)) for the single power-law Salpeter IMF in comparison to the canonical IMF. For example, using a single power-law “Salpeter” IMF with $\alpha = 2.3$ for a stellar population with stars in the mass range $0.1\text{--}0.8 M_{\odot}$ instead of the canonical IMF would lead to an overestimate of the stellar mass by $0.66/0.37 = 78\%$ and to an overestimate of the number, N , of stars by a factor $1.687/0.702 = 2.4$.

Additional forms are in use and are preferred for some investigations: In ► [Fig. 4-26](#), the quasi-diagonal (black) lines are alternative analytical forms summarized in ► [Table 4-3](#). They are compared to the canonical IMF in ► [Fig. 4-28](#), and their cumulative number and cumulative mass functions are presented in ► [Figs. 4-29](#) and ► [4-30](#), respectively.

Of the other IMF forms sometimes in use, the generalized Rosin–Rammmer function (Eq. *Ch* in ► [Table 4-3](#), thick short-dash-dotted curve) best represents the data, apart from a deviation for $m \gtrsim 10 M_{\odot}$, which can be fixed by adopting a Salpeter/Massey power-law extension for

■ Table 4-2

The mass in stars, M_{ecl} , normalized to $1 M_{\odot}$ for the canonical IMF between 0.07 and $150 M_{\odot}$ in comparison to the mass for other mass ranges (m_1 – m_2) and the commonly used single power-law Salpeter IMF taken here to have $\alpha = 2.3$ and 2.35 . All IMFs are normalized to have identical $M_{0.5,150}$ (◆ 4.8) for $m > 0.5 M_{\odot}$, and no stellar remnants are included. N is the correspondingly normalised number of stars

m_1/M_{\odot}	m_2/M_{\odot}	N	M_{ecl}/M_{\odot}	IMF used
0.07	150	1.000	1.000	Canonical IMF
0.1	150	0.823	0.973	Canonical IMF
0.1	0.8	0.702	0.370	Canonical IMF
0.5	150	0.223	0.719	Canonical IMF
0.07	150	2.874	1.424	Salpeter IMF, $\alpha = 2.30$
0.1	150	1.808	1.264	Salpeter IMF
0.1	0.8	1.687	0.660	Salpeter IMF
0.5	150	0.223	0.719	Salpeter IMF
0.07	150	3.378	1.543	Salpeter IMF, $\alpha = 2.35$
0.1	150	2.087	1.348	Salpeter IMF
0.1	0.8	1.961	0.756	Salpeter IMF
0.5	150	0.238	0.719	Salpeter IMF

$m > 1 M_{\odot}$ (◆ 4.56). Interpretation of m_o in terms of a characteristic stellar mass poses difficulties. As can be seen in ◆ Fig. 4-24, the difference between a Chabrier IMF and a canonical IMF is negligible. The popular Miller–Scalo log-normal IMF (Eq. MS in ◆ Table 4-3) deviates strongly from the empirical data at high masses. Larson’s Eq. Lb in ◆ Table 4-3 fits rather well, except that it may predict too many BDs. Finally, the *effective initial mass function for galactic disks* proposed by Hollenbach et al. (2005) and Parravano et al. (2011) (Eq. $Holl$) reproduces the data in the alpha plot quite well (Fig. 1 in Hollenbach et al. 2005; Parravano et al. 2011) and is not incorporated into ◆ Fig. 4-26 here. Note, however, that a *composite IMF* (i.e., the IGIMF and the local IGIMF, LIGIMF), which would be the correct IMF for a whole disk galaxy or parts thereof, respectively, ought to be steeper (have a larger α) at high masses which is precisely what Scalo (1986) deduced for the MW disk ($\alpha_3 \approx 2.7$, (◆ 4.59), ◆ Sect. 13.1).

The closed functional IMF formulations (Eqs. MS , La , Lb , Ch , $Holl$) have the advantage that possible variations of the IMF with physical conditions can be studied more naturally than with a multi-power-law form because they typically have a characteristic mass that can be varied explicitly. However, they cannot readily capture the variation of the stellar IMF with ρ and $[\text{Fe}/\text{H}]$ discovered recently (◆ 4.65).

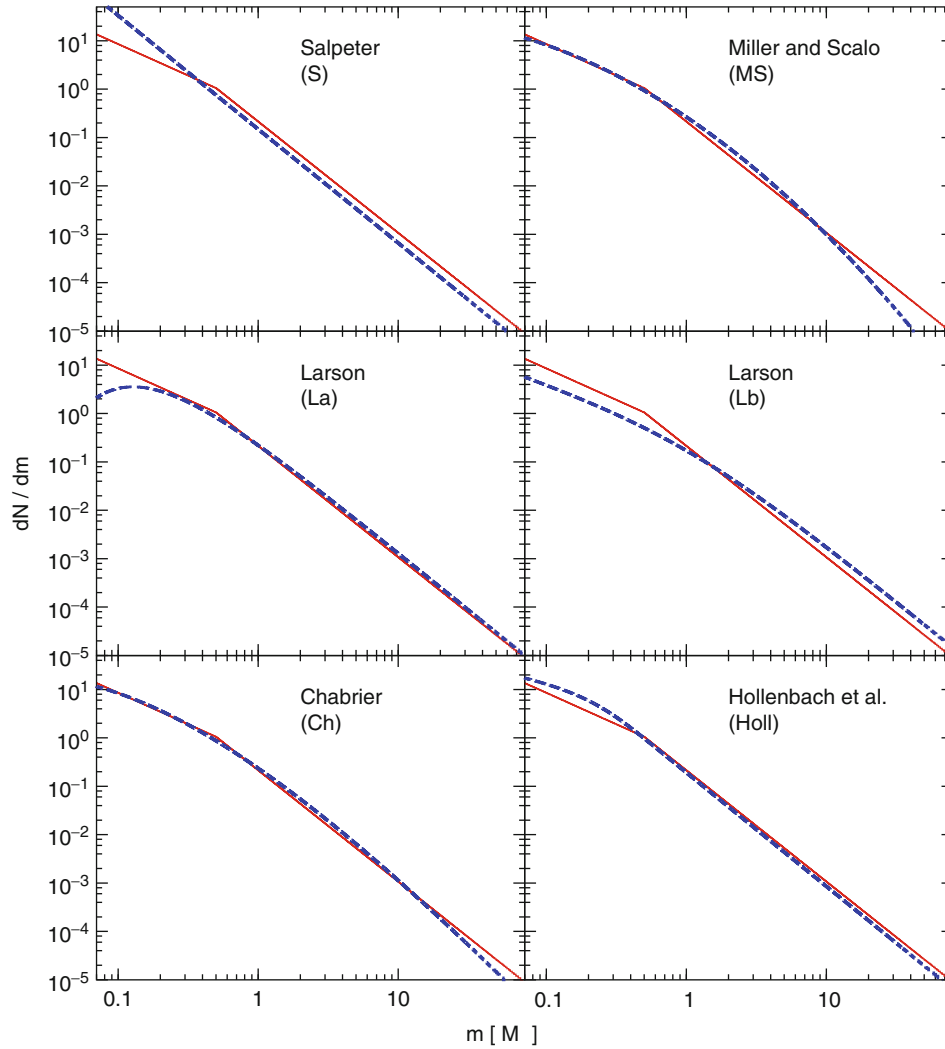
11 The Origin of the IMF

The two fundamental theoretical ansatzes for understanding the form of the IMF are discussed in ◆ Sect. 1.4, and here, a few more detailed aspects of the theoretical problem are raised. Observationally, it appears that the form of the stellar IMF is already established in the pre-stellar cloud core MF. Open questions concerning our understanding of the IMF remain.

Table 4-3

Summary of different proposed analytical IMF forms discussed in Sect. 10.2 (the modern power-law form, the canonical IMF, is presented in 4.55), and its log-normal equivalent is given by 4.56). Notation: $lm \equiv \log_{10}(m/M_{\odot}) = \ln(m/M_{\odot})/\ln 10$; dN is the number of all stars in the mass interval m to $m + dm$ and in the logarithmic-mass interval lm to $lm + dlm$. The mass-dependent IMF indices, $\Gamma(m)$ (Eq. Gam), are plotted in Fig. 4-26 using the line types defined here. Equation MS was derived by Miller and Scalo assuming a constant star-formation rate and a Galactic disk age of 12 Gyr (the uncertainty of which is indicated in the lower panel of Fig. 4-26). Larson (1998) does not fit his forms (Eqs. La and Lb) to solar-neighborhood star-count data but rather uses these to discuss general aspects of likely systematic IMF evolution; the m_0 in Eqs. La and Lb given here are approximate eyeball fits to the canonical IMF

General	$dN = \xi(m) dm = \xi_L(m) dlm$ $\xi_L(m) = (m \ln 10) \xi(m)$ $\Gamma(m) \equiv \frac{d}{dlm} (\log_{10} \xi_L(m))$ $\Gamma = -X = 1 + \gamma = 1 - \alpha$	gen	e.g., for power-law form: $\xi_L = A m^{\Gamma} = A m^{-X}$ $\xi = A' m^{-\alpha} = A' m^{+\gamma}$ $A' = A/\ln 10$	ind
Scalo's IMF index (Scalo 1986)		Gam		
Salpeter (1955)	$\xi_L(lm) = A m^{\Gamma}$ $A = 0.03 \text{ pc}^{-3} \log_{10}^{-1} M_{\odot}; \quad 0.4 \leq m/M_{\odot} \leq 10$		$\Gamma = -1.35 (\alpha = 2.35)$	S
Miller and Scalo (1979)	$\xi_L(lm) = A \exp \left[-\frac{(lm-lm_0)^2}{2 \sigma_{lm}^2} \right]$		$\Gamma(lm) = -\frac{(lm-lm_0)}{\sigma_{lm}^2} \log_{10} e$	MS
thick long-dash-dotted line	$A = 106 \text{ pc}^{-2} \log_{10}^{-1} M_{\odot}; \quad lm_0 = -1.02; \quad \sigma_{lm} = 0.68$			
Larson (1998)	$\xi_L(lm) = A m^{-1.35} \exp \left[\frac{-m_0}{m} \right]$		$\Gamma(lm) = -1.35 + \frac{m_0}{m}$	La
thin short-dashed line	$A = -; \quad m_0 = 0.3 M_{\odot}$			
Larson (1998)	$\xi_L(lm) = A \left[1 + \frac{m}{m_0} \right]^{-1.35}$		$\Gamma(lm) = -1.35 \left(1 + \frac{m_0}{m} \right)^{-1}$	Lb
thin long-dashed line	$A = -; \quad m_0 = 1 M_{\odot}$			
Chabrier (2001, 2002)	$\xi(m) = A m^{-\delta} \exp \left[-\left(\frac{m_b}{m} \right)^{\beta} \right]$		$\Gamma(lm) = 1 - \delta + \beta \left(\frac{m_b}{m} \right)^{\beta}$	Ch
thick short-dash-dotted line	$A = 3.0 \text{ pc}^{-3} M_{\odot}^{-1}; \quad m_0 = 716.4 M_{\odot}; \quad \delta = 3.3; \quad \beta = 0.25$			
Hollenbach et al. (2005) and Parravano et al. (2011)	$\xi_L(m) = k m^{-\Gamma} (1 - \exp[-(m/m_{ch})^{\gamma+1}])$			Holl
not plotted in Fig. 4-26	$\gamma = 0.4, \Gamma = 1.35, m_{ch} = 0.18 M_{\odot}$			

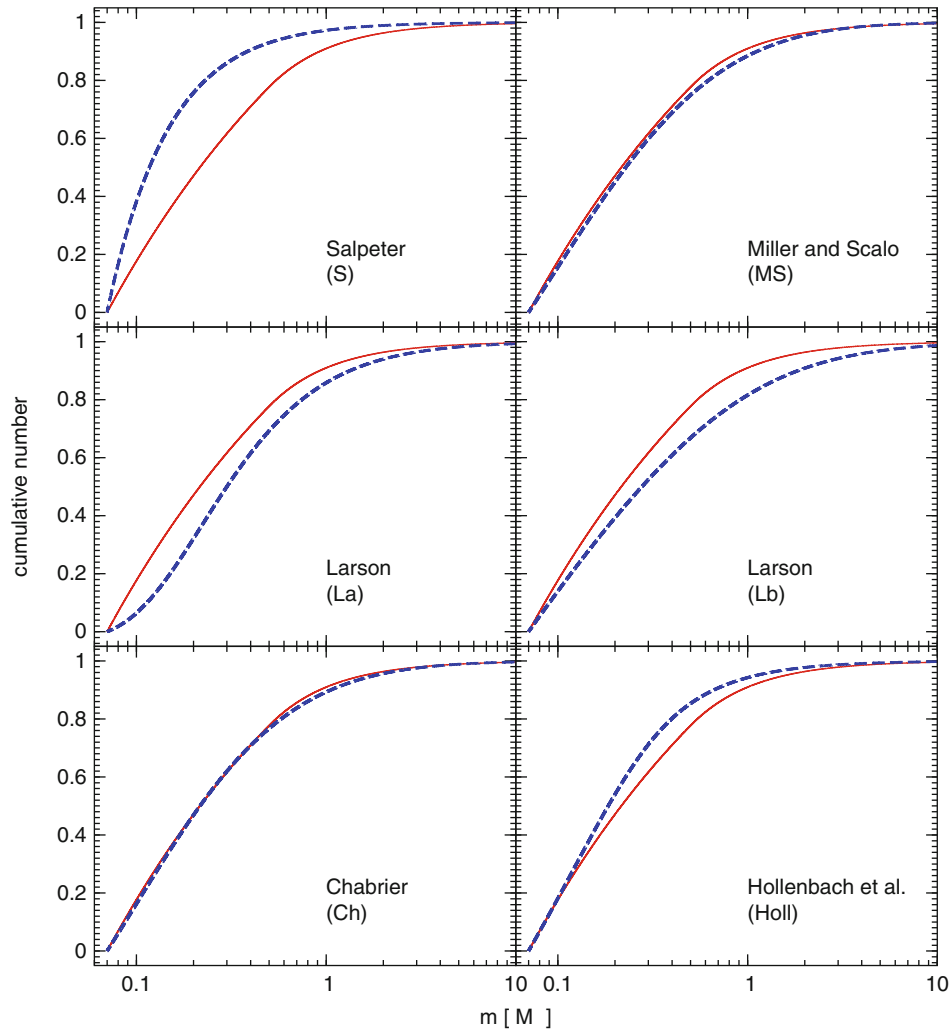


■ Fig. 4-28

A comparison between the canonical IMF ((4.55), solid red curve) and the IMFs of Table 4-3 in the interval from 0.07 to $80 M_{\odot}$. Plotted is the number of stars per mass interval versus the stellar mass, both scales being logarithmic. All IMFs are normalized such that $\int_{0.07}^{150} m \xi(m) dm = 1 M_{\odot}$, where m is the mass in solar units. Note that the “Chabrier” IMF in the lower left panel is the earlier Chabrier IMF listed in Table 4-3 and is not the later log-normal plus power-law extension plotted in Fig. 4-24. See also Figs. 4-29 and 4-30 for a comparison of the cumulative functions

11.1 Theoretical Notions

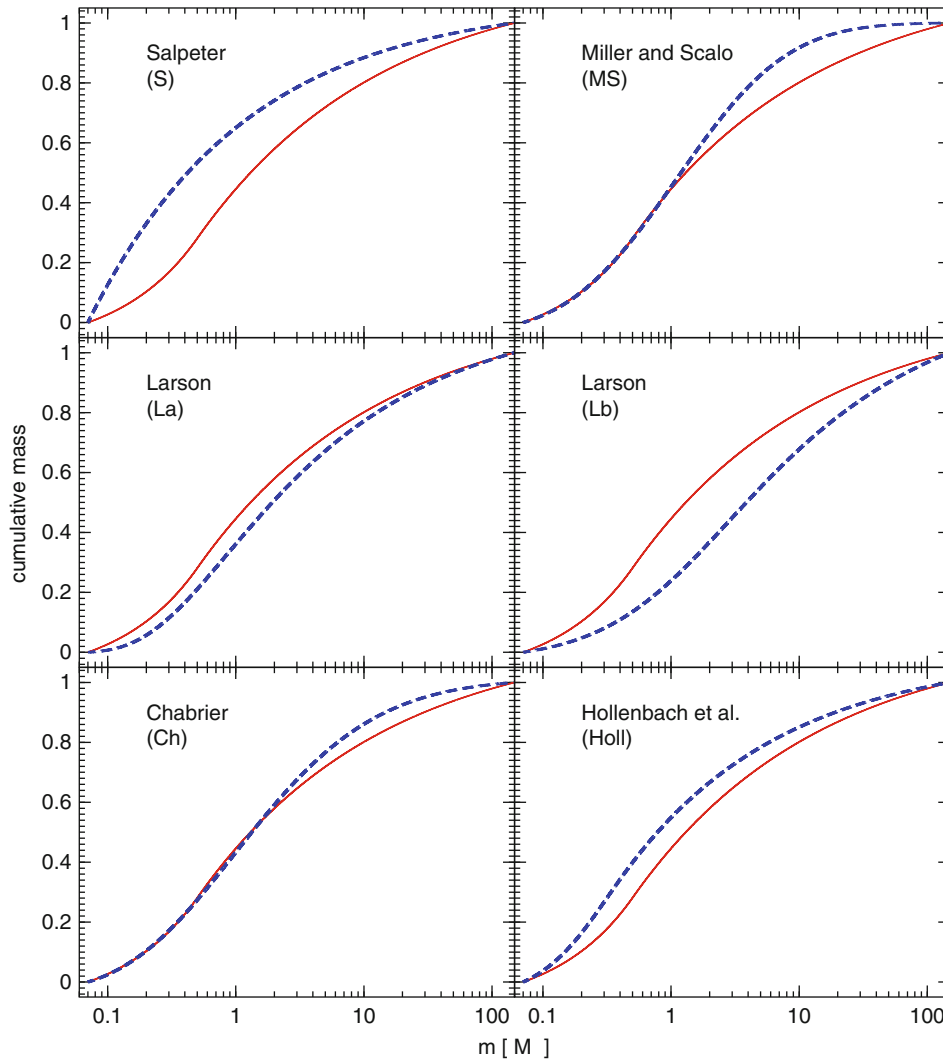
The Jeans mass scale ((4.50), see also Sect. 1.4) is useful as a general indication of the rough mass scale where fragmentation of a contracting gas cloud occurs. But the concept breaks



■ Fig. 4-29

Cumulative function of the number of stars in the stellar mass range $0.07\text{--}150 M_{\odot}$, plotted here over the range $0.07\text{--}10 M_{\odot}$, for the alternative IMF forms listed in ▶ Table 4-3 and plotted in ▶ Fig. 4-28. In all the panels, the canonical IMF (▶ 4.55) is shown as the *solid red curve*, while the alternative IMF forms are plotted with the *dashed blue curve*. Note that half of a saturated canonical stellar population has $m < 0.21 M_{\odot}$

down when considering the stellar masses that form in star clusters. The central regions of these are denser, formally leading to smaller Jeans masses which is the opposite of the observed trend, where even in very young clusters massive stars tend to be located in the inner regions. More complex physics is clearly involved (self-regulatory ansatz in ▶ Sect. 1.4). Murray and Lin (1996) develop an N -body model for the formation of stars in star clusters by considering



■ Fig. 4-30

Cumulative function of the mass in stars in the stellar mass range $0.07\text{--}150 M_{\odot}$ for the alternative IMF forms listed in ▶ Table 4-3 and plotted in ▶ Fig. 4-28. In all the panels, the canonical IMF (▶ 4.55) is shown as the *solid red curve*, while the alternative IMF forms are plotted with the *dashed blue curve*. Note that half the mass of a saturated canonical stellar population has $m < 1 M_{\odot}$.

the formation and dynamical evolution and interactions of cloudlets which can form stars which heat their surroundings thereby quenching further star formation. They naturally arrive at mass-segregated clusters with power-law IMFs. Interestingly, Elmegreen et al. (2008) show that the Jeans mass depends only weakly on the ambient radiation field, temperature, metallicity, and density for a large range of initial conditions, therewith possibly explaining a largely invariant IMF. The insensitivity of the IMF to the initial kinetic structure of the gas is also

explicitly demonstrated by Bate (2009) in a high-resolution SPH computation of a large-scale molecular cloud. The inclusion of radiation and magnetic fields is now becoming possible and is touched upon further down in this section.

The impressive agreement between the theoretical $m_{\max} - M_{\text{ecl}}$ relation (► 4.49), which results from SPH and FLASH computations of star formation with and without feedback, and the observational data (► Fig. 4-5), together with these simulations also reproducing the general form of the IMF quite well, suggests that the essential physics of star formation has been understood. Another success of star formation computations is the excellent reproduction of the observed mass distribution of BDs and VLMSs (► Sect. 8.4).

But, as discussed in ► Sect. 2.6, this theoretical work has not yet explained the birth binary properties. Also, as stated in ► Sect. 1.4, this theoretical work predicts a variation of the IMF with the temperature and the density of the gas. The consensus in the community has been until now that such variation has not been found (more on this in ► Sect. 12.9).

Stars almost certainly regulate their own mass by feedback (winds, radiation, outflows) limiting to a certain degree the amount of mass that can be accreted (self-regulatory ansatz in ► Sect. 1.4). Indeed, this is an attractive proposition in-line with the structure in the $m_{\max} - M_{\text{ecl}}$ relation at $m_{\max} \gtrsim 10 M_{\odot}$ (► Sect. 3.3). The $m_{\max} - M_{\text{ecl}}$ relation suggests a self-regulated balance between the amount of matter that can accrete onto a star and the feedback and local fragmentation which modulates the accretion. In particular noteworthy is the result (► Sect. 3.3.3) that feedback from the central massive stars may reduce the accretion onto the surrounding less massive stars leading to an improved agreement with the observational $m_{\max} - M_{\text{ecl}}$ data. Self-regulatory behavior may be a reason why the shape of the IMF appears to be so invariant to metallicity (Krumholz et al. 2010; Myers et al. 2011).

The coagulation of protostars probably plays a significant role in the densest regions where the cloud-core collapse time, τ_{coll} , is longer than the fragment collision time scale, τ_{cr} . The collapse of a fragment to a protostar, with about 95% of its final mass, takes no longer than $\tau_{\text{coll}} \approx 0.1 \text{ Myr}$ (Wuchterl and Klessen 2001), so that the core crossing time

$$\tau_{\text{cr}}/\text{Myr} \approx 42 \left(\frac{(R/\text{pc})^3}{(M_{\text{ecl}}/M_{\odot})} \right)^{\frac{1}{2}} < 0.1 \text{ Myr}, \quad (4.60)$$

where R is the half-mass radius of a Plummer-sphere model, implies $M/R^3 > 10^5 M_{\odot}/\text{pc}^3$. Such densities correspond to star-formation rate densities

$$SFRD > 0.1 M_{\odot} \text{ year}^{-1} \text{ pc}^{-3} \quad (4.61)$$

if the embedded cluster forms over a time scale of 1 Myr. It is under such conditions that protostellar interactions are expected to affect the emerging stellar mass spectrum. These are found in the centers of very dense and rich embedded star clusters before they expand as a result of gas expulsion (see also Elmegreen and Shadmehri 2003 for a more detailed discussion). Thus, only for massive stars ($m \gtrsim 10 M_{\odot}$) is the form of the IMF likely affected by coagulation (Bonnell et al. 1998; Klessen 2001; Zinnecker and Yorke 2007). It is indeed remarkable that evidence for a top-heavy IMF has only emerged in star-forming systems in which $\rho_{\text{gas+stars}} > 10^5 M_{\odot} \text{ pc}^{-3}$ (► Sect. 12.8).

But the observed mass segregation in very young clusters cannot as yet be taken as conclusive evidence for primordial mass segregation that results naturally from competitive accretion/fragmentation induced starvation (p. 150) and coagulation, unless precise N -body

computations of the embedded cluster are performed for each case in question. For example, models of the ONC show that the degree of observed mass segregation can be established dynamically within about 2 Myr (see [Fig. 4-20](#)) despite the embedded and much denser configuration having no initial mass segregation. The notion behind the “no initial mass-segregation” assumption is that star clusters fragment heavily subclustered (Megeath et al. 1996; Bontemps et al. 2001; Klessen 2001; Maschberger et al. 2010; Maschberger and Clarke 2011), and each subcluster may form a few OB stars with a few hundred associated lower-mass stars ([Table 4-1](#)), so that the overall morphology may resemble a system without significant initial mass segregation (McMillan et al. 2007; Fellhauer et al. 2009) or even with “inverse mass segregation” (Parker et al. 2011).

The theoretical time scale, $t_2 - t_1$ in [Fig. 4-20](#), for mass segregation to be established even in an initially not subclustered cluster can be shortened by decreasing the relaxation time. This can be achieved by reducing the number of stars and subclusters or by increasing the pre-gas expulsion density in the model. But it may prove impossible to find agreement at the same time with the density profile and kinematics because the ONC is probably expanding rapidly now given that it is virtually void of gas (Kroupa et al. 2001). Clearly, the issue of initial mass segregation requires more study.

An interesting approach to explain why the stellar IMF has a Salpeter/Massey slope above $1 M_\odot$ has been proposed by Oey (2011) by applying the concepts of the IGIMF theory ([Sect. 13.1](#)) to the notion that a star cluster forms as a hierarchical fractal structure (Elmegreen 1997, 1999). Sally Oey is able to demonstrate that the true stellar IMF of the stars that form within each sub-clump (here referred to as the “*elementary IMF*,” EIMF) has $\alpha_{\text{scl}} \approx 2$ in agreement with the MF of embedded clusters, $\beta \approx 2$ ([4.67](#)). If the least-massive sub-clump has a mass comparable to the lowest-mass star, then the stellar IMF of the whole cluster steepens to the canonical Salpeter/Massey value, $\alpha = 2.3$ ([4.55](#)), upon addition of all the sub-clumps. Notable is that this effect had already been discovered in SPH simulations of star formation (Maschberger et al. 2010). The reason for this is that low-mass sub-clumps cannot form massive stars, which therewith become underrepresented in the whole cluster. A slightly top-heavy IMF with $\alpha = \alpha_{\text{scl}}$ may result in a star-burst cluster if all sub-clumps are more massive than the most massive star can be, since then each sub-clump can form the whole range of stellar masses, that is, if each sub-clump was saturated. This is essentially the exact same reason why the IGIMF may become top-heavy if the least massive cluster is saturated (p. 148).

The Oey model raises a number of questions: On the one hand, it remains to be seen how the other well-studied effects of coagulation, competitive accretion, and stellar feedback would affect the resultant stellar IMF, on the other hand, it leaves the question open why the pre-stellar cloud core MF already has the shape of the stellar IMF ([Sect. 11.2](#)). Last not least observations, while very difficult, would need to confirm that the stellar IMF in sub-clumps has $\alpha_{\text{sc}} \approx 2$ rather than the canonical $\alpha = 2.3$.

But what about radiation feedback and magnetic fields? The results discussed above are based nearly exclusively on pure gravo-hydrodynamical computations only, and radiation and magnetic fields are likely to significantly affect the fragmentation and accretion behavior of a gas cloud. Such calculations are highly demanding (e.g., Stamatellos et al. 2007b), and not many results allowing statistically significant statements exist yet. The fragmentation of a magnetized cluster-forming cloud clump and the properties of the emerging bound cores such as their masses, radii, mean densities, angular momenta, spins, magnetizations, and mass-to-flux ratios are documented and are found to be comparable to observational properties. Price and Bate (2009) present SPH calculations of a $50 M_\odot$ gas cloud with radiative feedback and a magnetic

field being incorporated together for the first time. They show that the magnetic field supports the gas cloud on large scales while the radiation field limits fragmentation on a small scale through heating of the gas nearby protostars. The overall result is a similar mass distribution of protostars but a significantly reduced star-formation efficiency. Li et al. (2010) find that, besides reducing the overall star formation rate, magnetic fields and outflow feedback reduce the characteristic mass of the cluster stars. The influence of a magnetic field and radiation feedback on the formation of massive stars in a rotating $1,000 M_{\odot}$ cloud is studied for the first time computationally by Peters et al. (2011a) using the adaptive-mesh FLASH code. In comparison to the otherwise equal purely gravo-hydrodynamical computations, it is found that by yielding large-scale support, the magnetic field limits secondary fragmentation and by carrying angular momentum outward, it enhances accretion onto the central massive protostar. The number of fragments is only reduced by a factor of about two though.

At extreme star-formation rate densities (SFRDs), the gas can be heated by supernova(SN)-generated cosmic rays (CRs) which propagate into the dense cloud region heating it if the SN frequency is sufficiently high to sustain a CR flux. Many SNe in confined places may also contribute to turbulent heating of the gas. Such a very excited gas phase has been revealed by high-J CO line observations of ultraluminous infrared galaxies (Papadopoulos, private communication). These physical processes raise the Jeans mass possibly leading to a top-heavy IMF (► Sect. 12.4).

11.2 The IMF from the Cloud-Core Mass Function?

The possible origin of most stellar masses is indicated by a remarkable discovery by the team around Philippe André in Saclay for the low-mass ρ Oph cluster in which star formation is ongoing. Here, the pre-stellar and protostar MF are indistinguishable, and both are startlingly similar to the canonical IMF, even in showing the same flattening of the power law near $0.5 M_{\odot}$ (Motte et al. 1998; Bontemps et al. 2001). The pre-stellar cores have sizes and densities that can be interpreted as Jeans instabilities for the conditions in the ρ Oph cloud, so that cloud fragmentation due to the collapse of density fluctuations in a dissipating turbulent interstellar medium (Nordlund and Padoan 2003; Padoan and Nordlund 2002, 2004; Mac Low and Klessen 2004; Tilley and Pudritz 2004; Hennebelle and Chabrier 2008, 2009; Elmegreen 2011) augmented with mass-dependent accretion and accretion-truncation prescription (Veltchev et al. 2011; Myers 2011, see also ► Sect. 1.4) appears to be the most-important mechanism shaping the stellar IMF for masses $0.1 \lesssim m/M_{\odot} \lesssim$ a few M_{\odot} .

If this result can be generalized, then it may indicate that the shape of the IMF describing the vast population of stars would be mostly determined by the spectrum of density fluctuations in molecular clouds. Similar results have indeed been obtained for the Serpens clouds and for the clouds in Taurus-Auriga (Testi and Sargent 1998; Onishi et al. 2002, respectively).

More recently, Alves et al. (2007) used a novel technique by mapping the extinction through the Pipe Nebula to derive the pre-stellar cloud-core MF. The result is a cloud-core MF with the same shape as the canonical IMF but shifted to larger masses by a factor of about three. And, the massive effort within the Gould Belt Survey with the Herschel telescope toward the Aquila rift and Polaris Flare regions yields virtually the same result (André et al. 2010). This is interpreted to mean that the star-formation efficiency (SFE) is about 30% independently of

the core mass. It is interesting that this SFE is similar to the efficiencies deduced for embedded clusters on a scale of about 1 pc (Lada and Lada 2003). Such a SFE also arises from magneto-hydrodynamical computations of the formation of a protostar from a cloud core: As shown by Machida and Matsumoto (2011), 20–50% of the infalling material is expelled poleward by a magnetically driven wind. Why the more recent results indicate a SFE shift in mass between the cloud-core MF and the stellar IMF which was not seen in the earlier work will need to be understood.

The majority of stellar masses making up the canonical IMF thus do not appear to suffer significant subsequent modifications such as competitive accretion, proto-stellar mergers, or even self-limitation through feedback processes, assuming there is a one-to-one map between a pre-stellar core mass and the stellar mass. A keynote result supporting the “no-interaction” conjecture is presented by André et al. (2007) using kinematical measurements in ρ Oph: The relative velocities of the pre-stellar and proto-stellar cloud cores are too small for the individual condensations to interact with each other before evolving into pre-main sequence stars. This implies the following conjecture.

The IMF Origin Conjecture

The IMF is mostly determined by cloud fragmentation at the pre-stellar stage. Competitive accretion is not the dominant mechanism at the proto-stellar stage. Competitive accretion may govern the growth of starless, self-gravitating condensations initially produced by gravo-turbulent fragmentation toward an IMF-like mass spectrum (André et al. 2007).

The work of Padoan and Nordlund (2002) with modifications by Elmegreen (2011) demonstrates that, under certain reasonable assumptions, the mass function of gravitationally unstable cloud cores deriving from the power spectrum of a supersonic turbulent medium leads to the observed canonical IMF above $1 M_{\odot}$. The flattening at lower masses is a result of a reduction of the SFE because at small masses, only the densest cores can survive sufficiently long to collapse, this being the reason why BDs do not, as a rule, form as stars do directly from self-induced gravitational collapse of a core (► Sect. 8.4). Tilley and Pudritz (2007) apply their magneto-hydrodynamical simulations to test the Padoan–Nordlund model of turbulent fragmentation finding disagreements in the position of the peak mass of the core mass spectrum.

If this holds for more massive star-forming regions is not clear. Bontemps et al. (2010) show by observation that massive young dense cores in Cygnus X tend to be more fragmented than expected from turbulence regulated monolithic collapse but that they are less fragmented than predicted by gravo-turbulent scenarios and that the fragments do not show a canonical IMF distribution. The magneto-hydrodynamical plus radiation feedback simulations discussed above would be relevant in understanding this observational result. Hennebelle and Chabrier (2008, 2009) calculate the mass spectrum of the self-gravitating cores based on an extension of the Press–Shechter statistical formalism thereby also reproducing well the observed IMF. But it depends on the turbulence spectrum and the IMF ought to therefore be variable. The generation of turbulence in the ISM through the passage of curved shock waves is investigated by Kevlahan and Pudritz (2009). They conclude that “the composite nature of the IMF—a log-normal plus power-law distribution—is shown to be a natural consequence of shock interaction and feedback from the most massive stars that form in most regions of star formation in the

galaxy.” A three-component IMF was also suggested by Elmegreen (2004) to account for the apparently seen different IMFs in different star-forming regimes.

The Similarity Statement

The intriguing observational result is that the stellar, proto-stellar, and pre-stellar clump mass spectra are similar in shape to the stellar IMF.

This is consistent with the independent finding that the properties of binary systems in the Galactic field can be understood if most stars formed in modest, ρ Oph-type clusters with primordial binary properties as observed in Taurus-Auriga (([Sect. 4.47](#)), [Sect. 2.6](#)) and with the independent result derived from an analysis of the distribution of local star clusters that most stars appear to stem from such modest clusters (Adams and Myers 2001). However, the canonical IMF is also similar to the IMF in the ONC ([Fig. 4-19](#)) implying that fragmentation of the pre-cluster cloud proceeded similarly there.

The above similarity statement may not be entirely true because each cloud core typically forms a multiple stellar system ([Sect. 2.6](#), Goodwin et al. 2008; Smith et al. 2009). In the computer simulations, the similarity of the clump mass function and the IMF does not necessarily imply a direct one-to-one mapping of clumps to stars. The temporal evolution of the clump and stellar MF in SPH models shows that stars come from a broad range of clump masses despite the similar shape of the MF.

The SPH computations by Bonnell and Bate (2002) and collaborators of the formation of dense clusters indeed not only predict the observed $m_{\max} - M_{\text{ecl}}$ relation ([Fig. 4-5](#)), but they also show that a Salpeter/Massey power-law IMF is obtained as a result of competitive accretion and the merging of protostars near the cluster core driven by gas-accretion onto it, independently of metallicity as long as Z/Z_{\odot} is larger than 10^{-5} (Clark et al. 2009). The reason as to why the IMF is so invariant above a few M_{\odot} may thus be that the various physical processes all conspire to give the same overall scale-free result (see also [Sect. 11.1](#)).

Open question IV emerges here: Various theories of the IMF as resulting from the pre-stellar cloud core MF account for the observed shape of the canonical IMF. This is also the case for theories based on competitive accretion and on coagulation. However, if star formation is intrinsically hierarchical through first the emergence of sub-clumps of stars that merge dynamically, then as discussed in [Sect. 11.1](#), the stellar IMF in each sub-clump must be flatter with $\alpha_{\text{sc}} \approx 2$ than the Salpeter/Massey index. Why does theory not predict this flatter *elementary IMF* (EIMF)?

Open Question IV

The hierarchical model of star-cluster formation implies the EIMF to be flatter than the canonical IMF. Why has theory never predicted this EIMF?

A word of caution is advisable in view of the modeling of star formation and the resulting IMF. An excellent example of how state-of-the-art modelling may be somewhat misleading is as follows: Observations found a top-heavy PDMF in the Arches cluster with an apparent lack of

stars below $6 M_{\odot}$ (Stolte et al. 2002), and this was often interpreted as a top-heavy IMF because of the youth of the object. Klessen et al. (2007) therefore presented a state-of-the-art SPH model of star formation from warm gas in the Galactic Center which produces a top-heavy IMF with a downturn below about $6 M_{\odot}$. But Kim et al. (2006) showed that the observed Arches PDMF is in fact readily explained by strong stellar dynamical evolution due to the extreme environment with no need for a noncanonical IMF. And, stars less massive than $6 M_{\odot}$ have formed in the cluster without a sign of a deficit.

Main Result

Observations have led to the understanding that the pre-stellar cloud-core MF is very similar to the proto-stellar MF and to the stellar IMF suggesting that gravitationally driven instabilities in a turbulent medium may be the primary physical mechanism setting the shape of the IMF for stars in the mass range $0.1 \lesssim m/M_{\odot} \lesssim \text{few}$. Theoretical work has progressed significantly but remains too inconsistent with observations to allow the conclusion that a theory of the IMF exists.

12 Variation of the IMF

From the previous discussion, it has emerged that the IMF appears to be universal in resolved star-forming systems as are found largely in the vicinity of the Sun and in very nearby extragalactic systems (LMC, SMC, dSph satellites).

But the stellar IMF has been predicted theoretically to systematically vary with star-forming conditions. This has been shown with Jeans-mass arguments including SPH simulations and for self-regulated mass-growth physics (Sect. 1.4). Stellar populations formed from triggered star formation in expanding shells have also been suggested to be significantly top-heavy (Dale et al. 2011).

In Sect. 1.4, the variable IMF prediction is emphasized as a robust result of IMF theory. Is there evidence supporting this prediction? Next, some recently emerging observational evidence for a dependency of the IMF on star-forming conditions is presented which may be part of the long-expected violation of the invariant IMF hypothesis (Sect. 1.4).

12.1 Trivial IMF Variation Through the $m_{\max} - M_{\text{ecl}}$ Relation

The existence of the $m_{\max} - M_{\text{ecl}}$ relation (Sect. 3.3) trivially implies that the stellar IMF varies with increasing stellar mass, M_{ecl} , of the population formed in the star-formation event. This is best seen by the increase of the average stellar mass with increasing M_{ecl} in contrast to what is expected if the IMF were merely a probabilistic distribution function (Fig. 4-3).

Note that the relatively small scatter of the observational $m_{\max} - M_{\text{ecl}}$ data (Fig. 4-5) and the sharpness of the distribution of IMF power-law indices (Fig. 4-27) may be taken to imply that pure random sampling from the IMF is excluded as a viable model for stellar populations (cf. Figs. 4-1–4-3). This is further supported by the lack of evidence for massive stars forming in isolation (Sect. 4) and the lack of stars more massive than a few M_{\odot} in the Taurus-Auriga and Orion Nebula star-forming regions (p. 231).

12.2 Variation with Metallicity

Differences in the metallicity, Z , of the populations sampled in the nearby Local Group do not lead to discernible variations of the IMF for massive stars as has been shown using star counts with spectroscopic classification (► Fig. 4-8). Thus, the distribution of masses for massive stars has been interpreted to not be significantly affected by the metallicity of the star-forming gas.

That low-mass stars are forming together with massive stars in the low-metallicity environment within the Magellanic Clouds with a MF similar to the canonical IMF has been demonstrated through the deep photometric surveying effort by Dimitrios Gouliermis and collaborators (e.g., Gouliermis et al. 2006; Da Rio et al. 2009). Detailed studies of star formation in the low-metallicity environment of the Small Magellanic Cloud is being pushed by this team (e.g., Gouliermis et al. 2010), but the work is very challenging due to biases through crowding, resolution, and mass estimation from photometric data. Further, Yasui et al. (2008) find there to be no measurable difference in system MFs down to $0.1 M_{\odot}$ between the extreme outer Galactic disk and the inner, more metal-rich regions. More metals lead to a dustier gas cloud and how the characteristic dust grain size may affect the final characteristic stellar mass has been studied by Casuso and Beckman (2012).

A metallicity effect for low-mass stars may, however, be uncoverable from a detailed analysis of Milky Way star clusters. Present-day star-forming clouds typically have somewhat higher metal abundances ($[\text{Fe}/\text{H}] \approx +0.2$) compared to 5 Gyr ago ($[\text{Fe}/\text{H}] \approx -0.3$) (Binney and Merrifield 1998) which is the mean age of the population defining the canonical IMF. The data in the empirical alpha plot (► Fig. 4-26) indicate that some of the younger clusters may have an individual-star MF that is somewhat steeper (larger α_1) than the canonical IMF *when unresolved binary stars are corrected for*. This may mean that clouds with a larger $[\text{Fe}/\text{H}]$ produce relatively more low-mass stars which is tentatively supported by the typically but not significantly flatter MFs in globular clusters (Piotto and Zoccali 1999) that have $[\text{Fe}/\text{H}] \approx -1.5$, and the suggestion that the old and metal-poor ($[\text{Fe}/\text{H}] = -0.6$) thick-disk population also has a flatter MF below $0.3 M_{\odot}$ with $\alpha_1 \approx 0.5$ (Reyl   and Robin 2001). If such a systematic effect is present, then for $m \lesssim 0.7 M_{\odot}$ and to first order,

$$\alpha \approx 1.3 + \Delta\alpha [\text{Fe}/\text{H}], \quad (4.62)$$

with $\Delta\alpha \approx 0.5$ (Kroupa 2001b).

Is this evidence supporting the variable IMF prediction (► Sect. 1.4)? At the present, (► 4.62) needs to be taken as suggestive rather than conclusive evidence. Measuring the stellar IMF for low-mass stars in metal-poor environments, such as in young star clusters in the Small Magellanic Cloud (Gouliermis et al. 2005, 2006; Schmalzl et al. 2008; Da Rio et al. 2009), would thus be an important goal. In ► Sect. 12.7, we will uncover somewhat more robust evidence for a variation of the stellar IMF toward top-heaviness with decreasing metallicity but coupled to increasing density, possibly yielding a for the first time uncovered variation of the overall form of the IMF with metallicity in (► 4.63) (Marks et al. 2012).

That metallicity does play a role is becoming increasingly evident in the planetary-mass regime in that the detected exo-planets appear to occur mostly around stars that are more metal-rich than the Sun (Zucker and Mazeh 2001; Vogt et al. 2002).

12.3 Cosmological Evidence for IMF Variation

Larson (1998) invoked a *bottom-light* IMF that is increasingly deficient in low-mass stars the earlier the stellar population formed, while for high-mass stars, it is equal to the canonical IMF at all times. This theoretical suggestion is motivated by the decreasing ambient temperatures due to the expansion of the Universe, implying a decrease of the Jeans mass in a star-forming gas cloud and thus a decrease of the average mass of the stars with decreasing redshift. Such an IMF could explain the relative paucity of metal-poor G-dwarfs in the solar neighborhood (the G-dwarf problem), compared to the predictions of a closed-box model for the chemical evolution of galaxies. This is because, in this model, low-mass stars form less frequently at times when the self-enrichment of galaxies has not yet reached the current level.

Empirical evidence for a bottom-light IMF variation was suggested by van Dokkum (2008) in order to explain how the integrated colors of massive elliptical (E) galaxies change with redshift. The stellar populations of E galaxies are old, so that they have evolved passively most of the time until the present day. Corrected for redshift, the stellar populations of E galaxies are therefore bluer the more distant (i.e., younger) they are. van Dokkum (2008) finds, however, that the observed reddening is less with decreasing redshift than can be accounted for by stellar evolution. This trend may be understood if the IMF were a bottom light power law with a characteristic mass $m_C \approx 2 M_\odot$ and an index near $1 M_\odot$ of $\alpha_2 \approx 1.3$ when E galaxies formed, rather than the canonical $m_C \approx 0.1 M_\odot$, $\alpha_2 = 2.3$.

But such an IMF appears to be in contradiction with the observed near-canonical PDMFs of globular clusters (GCs). Just like E galaxies, GCs have formed their stellar populations at high redshifts. Nevertheless, GCs still have a large population of stars that should not have formed in them, according to the model proposed in van Dokkum (2008). Thus, the IMF either did not have the time dependency suggested in van Dokkum (2008), or the IMF in GCs was considerably different from the one in E galaxies (see the review by Bastian et al. 2010). By studying various integrated gravity-sensitive features in luminous E galaxies, Cenarro et al. (2003) and van Dokkum and Conroy (2010) on the other hand find evidence for a very bottom-heavy IMF. Cenarro et al. (2003) propose the IMF to vary according to $\alpha = 3.41 + 2.78[\text{Fe}/\text{H}] - 3.79[\text{Fe}/\text{H}]^2$.

At present, it is unclear how these discrepant results may be brought into agreement. The detailed dynamical analysis by Deason et al. (2011) demonstrates that E galaxies are consistent with a canonical IMF rather than with a bottom-light IMF over a large range of masses. This modeling assumes dark matter to provide the mass deficit, and it is unclear whether an entirely different approach not relying on the existence of dynamically relevant dark matter would lead to a different conclusion. A contradicting result is obtained by Grillo and Gobat (2010) who show that for a sample of 13 E galaxies, a match is found between the dynamical masses and photometric (plus dark matter) masses if the IMF was a Salpeter power law, that is, if it was bottom-heavy relative to a canonical IMF (Table 4-2). Chemo-evolutionary population synthesis models (Vazdekis et al. 1996, 1997) need an initially top-heavy IMF which, after a short burst of star formation, becomes bottom heavy to explain the optical and near-infrared colours and line indices of the most metal rich E galaxies. It is unclear at this stage why the dynamical and stellar population modeling of E galaxies leads to such diverging results.

Other empirical evidence for a time variability of the IMF was proposed by Baugh et al. (2005) and Nagashima et al. (2005). Baugh et al. (2005) modeled the abundances of Lyman-break galaxies and submillimeter galaxies. Both types of galaxies are considered to be distant

star-forming galaxies, but the latter are thought to be obscured by dust that transforms the ultra-violet radiation from massive stars into infrared radiation. The model from Baugh et al. (2005) is based on galaxy formation and evolution via accretion and merging according to Λ CDM cosmology. They include a detailed treatment of how the radiation from stars is converted to dust emission. Their model only returns the correct abundances of Lyman-break galaxies and sub-millimeter galaxies if they assume two modes of star formation. One of the two modes suggested by Baugh et al. (2005) occurs with the canonical IMF and the other one is with a *top-heavy* IMF. The mode with the top-heavy IMF is thought to be active during star bursts, which are triggered by galaxy mergers. Quiescent star formation in the time between mergers is thought to be in the mode with the canonical IMF. Nagashima et al. (2005) used the same model for galaxy evolution in order to explain the element abundances in the intra-cluster medium of galaxy clusters. They also need the two mentioned modes of star formation in order to succeed. Noteworthy is that this two-mode IMF model is qualitatively in natural agreement with the IGIMF theory (Sect. 13.1). In the IGIMF theory, the IGIMF becomes top-heavy only in star bursts.

Wilkins et al. (2008) note that the stellar mass density observed in the local universe is significantly smaller than what would be expected by integrating the cosmic star-formation history within the standard (dark-matter dominated) cosmological model. They show that a single top-heavy power-law IMF with high-mass star index $\alpha = 2.15$, that is, a smaller number of long-lived low-mass stars per massive star, can reproduce the observed present-day stellar mass density.

This evidence for IMF variations stands and falls with the validity of Λ CDM cosmology. Modeling galaxy formation and evolution to be consistent with observations is in fact a major problem of Λ CDM cosmology. There are discrepancies in the Local Group (Kroupa et al. 2010; Kroupa 2012) and in the Local Volume of galaxies (Peebles and Nusser 2010) that already now shed major doubt as to the physical applicability of the concordance cosmological model to the real world. For instance, the actual galaxy population is less diverse than the one Λ CDM theory predicts (Disney et al. 2008). It thus remains to be seen whether the results by Baugh et al. (2005), Nagashima et al. (2005), and Wilkins et al. (2008) can be confirmed using a refined model for galaxy evolution or if instead a fundamentally different cosmological model, which would yield different redshift-time-distance relations, is required. It is noteworthy in this context that evidence for top-heavy IMFs in high-star formation-rate density environments has emerged, as is discussed in the following sections.

12.4 Top-Heavy IMF in Starbursting Gas

We have seen above that the IMF is largely insensitive to star-forming conditions as found in the present-day Local Group. The observed embedded clusters in these “normal” photon-dominated star-forming regions have gas plus star densities $\rho \lesssim 10^5 M_\odot \text{pc}^{-3}$ ($M_{\text{ecl}} \lesssim 10^{5.5} M_\odot$ within a half-mass radius $r_h \approx 0.5 \text{ pc}$). The objects form within about 1 Myr leading to a star-formation rate density $\text{SFRD} \lesssim 0.1 M_\odot \text{pc}^{-3} \text{year}^{-1}$ for which no significant IMF variation has been found, apart from the trivial variation through the $m_{\text{max}} - M_{\text{ecl}}$ relation (Sect. 12.1).

When the SFRD becomes very high, understanding the formation of individual protostars becomes a challenge, as they are likely to coalesce before they can individually collapse (4.60) such that probably a top-heavy IMF may emerge (Dabringhausen et al. 2010).

For high ambient SFRDs and a sufficiently long duration of the star burst, Papadopoulos (2010) has shown that the cosmic rays (CRs) generated by exploding supernovae of type II (SNII) heat the clouds which are too optically thick to cool therewith becoming CR dominated regions within which the conditions for star formation are significantly altered when compared to normal photon-dominated star-forming regions. This Papadopoulos-CR mechanism raises the Jeans mass and must lead to top-heavy IMFs in star-bursts (Papadopoulos et al. 2011).

This is also found by Hocuk and Spaans (2011) who compute the IMF which arises from star formation in a $800 M_{\odot}$ cloud being irradiated with X-rays and CRs as well as UV photons from a population of massive stars and an accreting supermassive black hole (SMBH) at 10 pc distance. CRs penetrate deep into the cloud therewith heating it, while the ambient X-rays lead to a thermal compression of the cloud. Their adaptive-mesh refinement computations with the FLASH code include shear which opposes gravitational contraction through self-gravity of the cloud. The turnover mass in the IMF increases by a factor of 2.3, and the high-mass index becomes $\alpha \lesssim 2$ such that the resultant IMF is top-heavy. Shear lessens the effects of the CRs and X-rays by the IMF becoming bottom heavy but only for the most massive SMBHs. Low-mass SMBHs ($< 10^6 M_{\odot}$) or star bursts without massive BHs would thus lead to top-heavy IMFs as long as the CR flux is significant.

This may well be the dominant physical mechanism why star bursts have a top-heavy IMF. Indeed, Klessen et al. (2007) and Hocuk and Spaans (2011) demonstrate, respectively, with SPH and FLASH simulations that under warmer conditions a stellar mass-spectrum forms which is dominated by massive stars. The Jeans mass can also be raised through turbulent heating through expanding supernova shells if the explosion rate of SNII is large enough, but details need to be worked out (Papadopoulos, 2011, private communication).

Observational evidence for top-heavy IMFs in regions of high SFRD has now emerged for GCs (Sect. 12.7) and UCDs (Sect. 12.8). Top-heavy IMFs are also reported in the central regions of Arp 220 and Arp 299 assuming SFRs of duration longer than at least a few 0.1 Myr (the evidence becomes less significant for a top-heavy IMF if the objects experienced a star-burst of $\lesssim \text{few } 10^5$ year duration). The central region of Arp 220 has a star-formation rate of $100 M_{\odot}/\text{year}$, and the large number of observed type II supernovae requires a top-heavy IMF (Lonsdale et al. 2006; Parra et al. 2007, see also Sect. 12.8). Noteworthy is that the Arp 220 central region consists of what may be UCD-sized substructures (Sect. 12.8). The high frequency and spatially confined occurrence of supernovae in Arp 299 indicates that the star formation occurs in highly sub-clustered regions with dimensions less than 0.4 pc and within larger structures of 30 pc scale (Ulvestad 2009). This is reminiscent of the cluster-complex model for the origin of some UCDs (Fellhauer and Kroupa 2002; Brüns et al. 2011). Likewise, Pérez-Torres et al. (2009) and Anderson et al. (2011) deduce a top-heavy IMF in Arp 299 from the relative frequency of different supernova types.

12.5 Top-Heavy IMF in the Galactic Center

Observations of the Galactic Center revealed one or two disks of about 6-Myr-old stars orbiting the central supermassive black hole (SMBH) at a distance between 0.04 and 0.4 pc. Nayakshin and Sunyaev (2005) argued that the X-ray luminosity of the Sgr A* field is too low to account for the number of young $< 3 M_{\odot}$ stars expected from a canonical IMF, considering the large number of O stars observed in the disks. The low X-ray luminosity may be explained by a low-mass cutoff near $1 M_{\odot}$. A more recent systematic search of OB stars in the central parsec revealed

a significant deficit of B-type stars in the regime of the young disks, suggesting a strongly top-heavy IMF for these disks with a best-fit power law of $\alpha_3 = 0.45 \pm 0.3$. (Bartko et al. 2010). This appears to be the very best evidence for a truly top-heavy IMF.

Using SPH simulations of star formation in fragmenting gas accretion disks, Bonnell and Rice (2008) find that the IMF of the disk stars can be bimodal (and thus top-heavy) if the infalling gas cloud is massive enough ($\approx 10^5 M_\odot$) and the impact parameter of the encounter with the SMBH is as small as ≈ 0.1 pc. Thus, only under quite extreme conditions will a top-heavy IMF emerge, whereby the strong tidal forces and the rotational shear seem to be the dominant physical mechanisms shaping the IMF since only cloud cores massive enough can collapse to a star. This is explicitly calculated by Hocuk and Spaans (2011) for a range of SMBH masses (► Sect. 12.4).

Observations of the central parsec of the Milky Way show that this region is dominated by a dense population of old stars with a total mass of $\approx 1.5 \times 10^6 M_\odot$. This stellar cluster around the SMBH has also been probed for evidence for a non canonical IMF. By means of stellar evolution models using different codes, Löckmann et al. (2010) show that the observed luminosity in the central parsec is too high to be explained by a long-standing top-heavy IMF as suggested by other authors, considering the limited amount of mass inferred from stellar kinematics in this region. In contrast, continuous star formation over the Galaxy's lifetime following a canonical IMF results in a mass-to-light ratio and a total mass of stellar black holes (SBHs) consistent with the observations. Furthermore, these SBHs migrate toward the center due to dynamical friction, turning the cusp of visible stars into a core as observed in the Galactic center. It is thus possible to simultaneously explain the luminosity and dynamical mass of the central cluster and both the presence and extent of the observed core since the number of SBHs expected from a canonical IMF is just enough to make up for the missing luminous mass.

In conclusion, observations of the Galactic center are well consistent with continuous star formation following the canonical IMF. Only the centermost young stellar disks between about 0.04 and 0.4 pc from the SMBH show a highly top-heavy IMF, but the circumstances that led to their formation must be very rare since these have not affected most of the central cluster.

12.6 Top-Heavy IMF in Some Star-Burst Clusters

There are indications of top-heavy IMFs such as in some massive star-burst clusters in the M82 galaxy. Using spectroscopy of the unresolved M82-F cluster, Smith and Gallagher (2001) derive, via the inferred velocity dispersion, a mass and from the luminosity a mass-to-light ratio that is significantly smaller than the ratio expected from the canonical IMF for a 60 Myr population. The implication is that the M82-F population may be significantly depleted in low-mass stars, or equivalently it may have a top-heavy IMF, provided the velocity dispersion is representative of the entire cluster. A possibility that will have to be addressed using stellar-dynamical modeling of forming star clusters is that M82-F may have lost low-mass stars due to tidal shocking (Smith and Gallagher 2001). Highly pronounced mass segregation which leads to a dynamically decoupled central core of OB stars is an important mechanism for reducing the measured mass-to-light ratio (Boily et al. 2005), while rapid expulsion of residual gas from forming clusters enhances the measured mass-to-light ratios (Goodwin and Bastian 2006). But also a younger age would reduce the inferred depletion in low-mass stars, and some hints exist that M82-F might be as young as 15 Myr (McCradly et al. 2005).

In an extensive literature study of Galactic and extragalactic observations, Elmegreen (2005) concluded that dense star-forming regions like star bursts might have a slightly shallower IMF, a view shared by Eisenhauer (2001).

12.7 Top-Heavy IMF in Some Globular Clusters (GCs)

Observations of 17 globular clusters (GCs) for which PDMFs were measurable over the mass range $0.5\text{--}0.8 M_{\odot}$, showed the higher-metallicity GCs to have flatter PDMFs (Djorgovski et al. 1993). This lacked an explanation until now. In particular, this trend is difficult to reconcile with standard dynamical evolution scenarios as it is unclear how dynamics could possibly know about the metal content of a cluster.

De Marchi et al. (2007) performed a deep homogeneous star-count survey of 20 Milky Way GCs using the HST and VLT and measured the global PDMFs in the mass range $0.3\text{--}0.8 M_{\odot}$. They discovered the least concentrated GCs to have a bottom-light PDMF, while the other GCs show a canonical MF. N -body calculations predict that two-body-encounter-driven dynamical evolution preferentially removes low-mass stars from a star cluster (Vesperini and Heggie 1997; Baumgardt and Makino 2003). This occurs because two-body relaxation drives the cluster into core collapse and energy conservation leads to the expansion and thus evaporation of low-mass stars. Thus, the most concentrated star clusters are expected to show the strongest depletion of low-mass stars, in disagreement with the observations.

A possibility would be that the low-concentration GCs were formed with a bottom-light IMF. However, there is no known theory of star formation which could account for this: The low-concentration clusters typically have a higher metallicity than the high-concentration clusters (see below in this section), and so the data would imply that the IMF ought to have been bottom-light in the higher-metallicity GCs. This, however, contradicts basic star-formation theory (► Sect. 1.4).

This apparent disagreement between theory and observation can be resolved if GCs formed mass-segregated and with the canonical IMF (► 4.55) for stars less massive than about $1 M_{\odot}$. Baumgardt et al. (2008) performed N -body models using the Aarseth code and demonstrate that the range of PDMFs observed by De Marchi et al. (2007) can be arrived at if GCs were born mass segregated and filling their tidal radii such that they do not need to first evolve into core collapse and so they immediately begin losing low-mass stars. However, the stellar dynamically induced trend of PDMF with concentration is not able to account for the observed metallicity dependence. Furthermore, it is not clear why GCs ought to be formed mass-segregated but filling their tidal radii since all known young clusters are well within their tidal radii.

An alternative scenario by Marks et al. (2008) also assumes the young compact GCs to be formed mass segregated with a canonical IMF below $1 M_{\odot}$. But after formation, the expulsion of residual gas unbinds the low-mass stars that typically reside near the outer region of the clusters, leading to flattening of the MF. This ansatz allows for a metal dependency, since the process of residual-gas expulsion is expected to be enhanced for metal-rich gas which has a stronger coupling to radiation than metal-poor gas, similar to the metallicity-dependent stellar winds. For each of the 20 GCs in the De Marchi et al. (2007) sample, the best-fitting tidal-field strength, radius, star-formation efficiency, and gas-expulsion time scale are obtained. This uncovers remarkable correlations between the gas-expulsion quantities, the tidal field strength, and the metallicities, allowing a very detailed reconstruction of the first collapse phase of the Milky Way about 12 Gyr ago (Marks and Kroupa 2010). The correlations, for example, confirm

the expectation that gas expulsion is more efficient and thus dynamically more damaging in metal-rich gas and also that metal-poorer GCs were denser than their metal-rich slightly younger counterparts which were subject to stronger tidal fields.

This in-turn suggests that in order to provide enough feedback energy to blow out the residual gas, the IMF had to be top-heavy in dependence of the initial density of the GC (Marks et al. 2012). Assuming the gas leaves a cluster with the velocity of the sound speed of about 10 km/s, the gas-expulsion time scales for clusters with radii between 0.5 and 1 pc would lie between $\tau_{\text{gas}} = 0.05$ and 0.1 Myr. The resultant high-mass IMF slopes derived for the GCs from their individual PDMFs assuming $0.05 \lesssim \tau_{\text{gas}}/\text{Myr} \lesssim 0.15$ cover a wide range, $0.9 \lesssim \alpha_3 \lesssim 2.3$, where α_3 is the slope for $m \gtrsim 1 M_{\odot}$, for an IMF that is canonical otherwise (► Fig. 4-31).

The calculated IMF slopes also correlate with the metallicity of the GCs, such that the PDMFs show the observed correlation after the metallicity-dependent gas-expulsion process ends and the remaining GC revirializes. This correlation with metallicity, quantified in (► 4.63) (► Fig. 4-32), is an important clue, as it implies that GCs formed from metal-poorer gas were more compact and had a more top-heavy IMF, just as is indeed expected from star-formation theory (► Sects. 1.4 and ► 11.1).

The Top-Heavy Stellar IMF/Metallicity Dependence

The suggested dependence of α_3 on globular cluster-forming cloud metallicity can be parametrized as

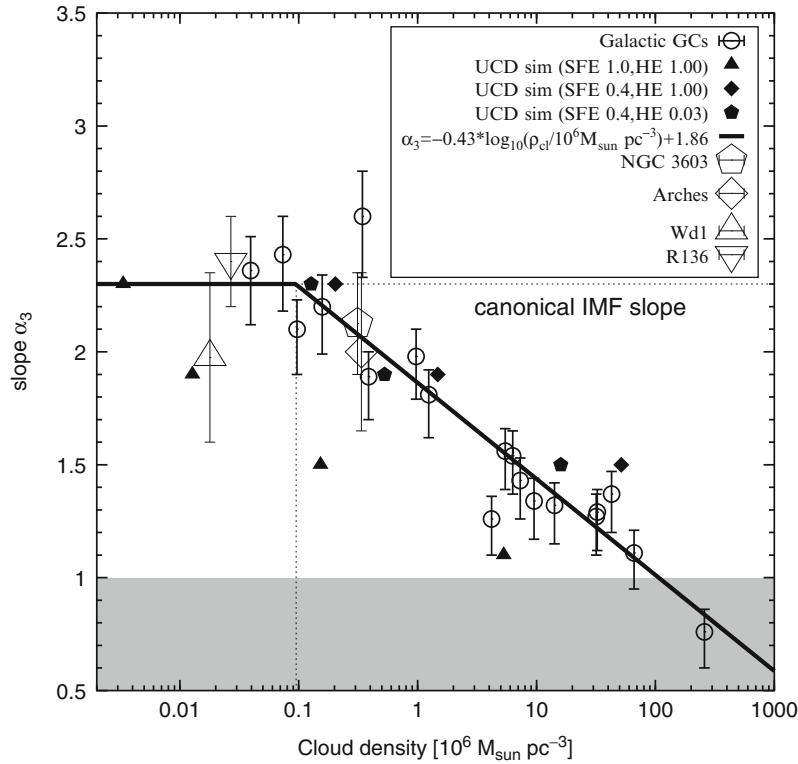
$$\begin{aligned} \alpha_3 &= \alpha_2, & m > 1 M_{\odot} \quad \wedge \quad [\text{Fe}/\text{H}] \geq -0.5, \\ \alpha_3 &= 0.66 [\text{Fe}/\text{H}] + 2.63, & m > 1 M_{\odot} \quad \wedge \quad [\text{Fe}/\text{H}] < -0.5. \end{aligned} \quad (4.63)$$

Strader et al. (2011) observed high-resolution spectra of 200 GCs of the Andromeda galaxy and discovered that the near-infrared M/L ratios decrease significantly with increasing metallicity of the GCs. This cannot be explained by secular dynamical evolution but follows from a PDMF which is systematically more bottom-light for more metal-rich GCs. This is thus the same finding as discussed above for the 20 GCs of the MW and a possible explanation put forward by Strader et al. (2011) is metallicity-dependent gas expulsion.

Marks et al. (2012) find that α_3 decreases with increasing pre-globular cluster cloud-core density, ρ (► 4.64, ► Fig. 4-31). Such a trend is to be expected theoretically if the massive and initially dense GCs, each of which was a star burst (star-formation rate density $\text{SFRD} \gtrsim 0.1 M_{\odot}/(\text{year pc}^3)$ for an initial half-mass radius of about 0.5 pc and formation time scale of about 1 Myr), involves the merging of proto-stellar cores since the collision probability is higher in denser systems (► 4.60).

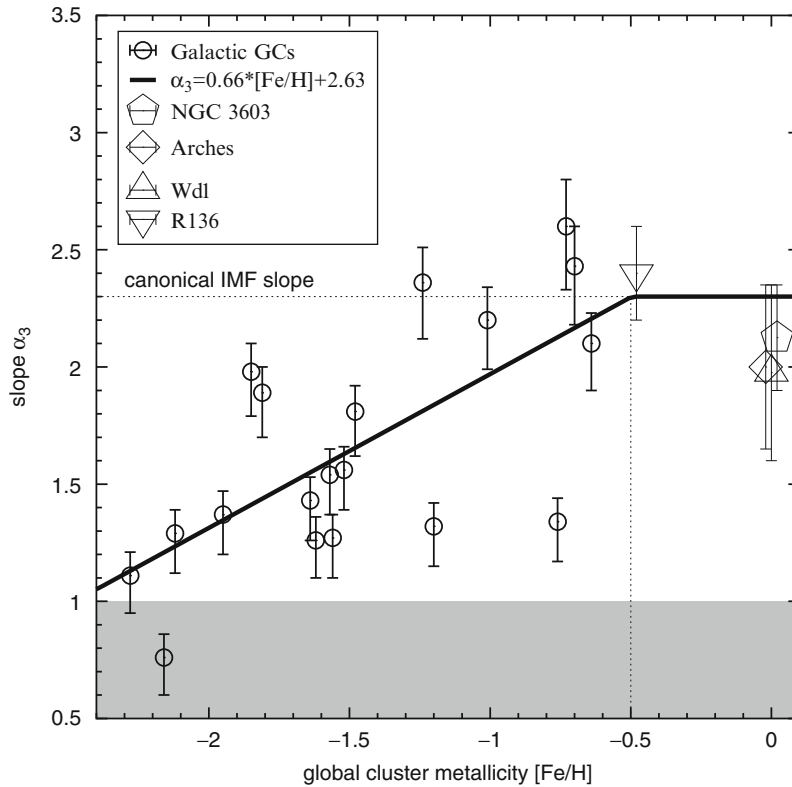
The high-mass IMF index α_3 thus depends on ρ and on $[\text{Fe}/\text{H}]$. The increasing top-heaviness, deduced with a principle-component-type analysis by Marks et al. (2012), with decreasing $[\text{Fe}/\text{H}]$ and increasing ρ is quantified here for the first time in (► 4.65) and ► Fig. 4-34. It is remarkable that the theoretically expected trend of the IMF with ρ and $[\text{Fe}/\text{H}]$ has now emerged from elaborate stellar-dynamical analysis of deep observations of GCs.

The extremely top-heavy IMFs for some of the GCs raise the question whether they could survive the strong mass loss these IMFs imply due to stellar evolution. This is especially an issue if clusters start mass-segregated (Vesperini et al. 2009).



■ Fig. 4-31

The high-mass IMF slope, α_3 , deduced for Galactic GCs (open circles) as a function of the pre-GC cloud-core density within their initial half-mass radii (● Sect. 12.7). Upper limits are for a gas-expulsion time scale of $\tau_{\text{gas}} = 0.15$ Myr, open circles are for $\tau_{\text{gas}} = 0.1$ Myr, and the lower limits are for $\tau_{\text{gas}} = 0.05$ Myr. Also plotted are MF slope values found in the literature for the massive, young clusters NGC 3603, Arches, Wd1 and R136. Their corresponding cloud-core densities were calculated using their PD half-masses within their PD half-mass radii (0.2pc for NGC3603, 0.24pc for Arches, 1pc for Wd1, 1.1pc for R136) assuming the clusters formed with a SFE of 1/3, that is, that their gaseous progenitors were three times more massive and that their sizes did not change. The filled symbols correspond to simulations devoted to finding the most probable IMF slopes in systems of different density that lead, after residual gas expulsion and supernova driven evolution, to objects that resemble the properties of UCDs today (● Sect. 12.8). Different symbols correspond to different input parameters (star-formation efficiency SFE and heating efficiency HE; see ● Sect. 12.8). The overall trend for GCs and UCDs is consistent in the sense that denser systems form flatter IMFs. The solid line is a fit to the GC data (● 4.64). Below $1 M_{\odot}$, the assumed IMFs are equal to the canonical IMF (● 4.5) and (● 4.55). The gray-shaded region at $\alpha_3 < 1$ are IMFs which contain more than 99% mass in stars with $m > 1 M_{\odot}$, making cluster survival after supernova explosions unlikely. Note that if the GCs and UCDs form on a time scale of 1 Myr, then their star-formation rate densities would be $0.1\text{--}100 M_{\odot}/(\text{year pc}^3)$. From Marks et al. (2012)



■ Fig. 4-32

The high-mass IMF slope, α_3 , deduced for Galactic GCs (open circles) as a function of the GC metallicity (● Sect. 12.7). Otherwise as ● Fig. 4-31

12.8 Top-Heavy IMF in UCDs

Further independently obtained evidence for top-heavy IMFs at high SFRDs comes from ultra compact dwarf galaxies (UCDs) which have been observed in nearby galaxy clusters. They typically have effective radii of a dozen pc and are understood to have formed as a star burst (SFRD $\approx 1 - 100 M_{\odot}/(\text{year pc}^3)$ for an initial radius of about 1 pc and formation time scale of 1 Myr, Dabringhausen et al. 2009). The Papadopoulos-CR-heating process (● Sect. 12.4) may be a factor during the formation of UCDs. They are, like galaxies, collisionless stellar-dynamical systems such that two-body relaxation-driven evaporation of low-mass stars is insignificant, contrary to the case for GCs (Anders et al. 2009; Mergeld and Hilker 2011; Forbes and Kroupa 2011).

For a significant sample of UCDs, high-resolution spectra are available allowing estimates of their stellar velocity dispersions. These velocity dispersions and the effective radii imply dynamical masses between 10^6 and $10^8 M_{\odot}$. The dynamical masses of UCDs are thus similar to the values of the much more extended dwarf spheroidal (dSph) galaxies. Combining the dynamical masses of UCDs with their luminosities leads to estimates for their dynamical mass-to-light (M/L) ratios. While the uncertainties of these estimates are large, the most likely values for these

M/L ratios are systematically higher than compared to the expectation for a stellar population that formed with the canonical IMF.

Dark matter is not a viable explanation for the enhanced M/L ratios of UCDs, given the current understanding of how UCDs are formed. One such idea is that UCDs evolve from star cluster complexes as are observed in interacting systems like the Antennae (NGC 4038 and NGC 4039, Brüns et al. 2011). The 300–500 Myr old ultra-massive “star cluster” W3 in the merger remnant galaxy NGC 7252 is indeed an object that supports such a model (Fellhauer and Kroupa 2005) since it is too young for it to be a stripped nucleus of a nucleated dwarf galaxy. Another idea is that UCDs are extremely massive GCs (e.g., Mieske et al. 2002). This notion is motivated by the similarities that UCDs share with GCs, for example, their seemingly continuous mass-radius relation. Thus, there is supportive evidence for both concepts, but they also imply that UCDs are essentially free of dark matter. Also note that dSph galaxies are usually thought to populate the least massive and therefore the most dense dark-matter halos. However, the dark-matter densities inferred from the dynamics of dSph galaxies are still about two orders of magnitude too low to influence the dynamics of UCDs to the required extent.¹⁷ This leaves a variation of the IMF as the most natural explanation for the high dynamical M/L ratios of UCDs (Dabringhausen et al. 2009).

In an old stellar system like a UCD, both a *bottom-heavy* IMF and a *top-heavy* IMF lead to a M/L ratio that exceeds the expectation for the canonical IMF. In the case of a top-heavy IMF, the M/L ratio of the stellar population is high only if it is old. This is because in an old population, the massive (and therefore bright) stars have turned into essentially nonluminous remnants. In the case of a bottom-heavy IMF, the M/L ratio of the stellar population is enhanced by the high M/L ratios of low-mass stars. The two cases are not easy to distinguish by observations simply because in either case, a population that is characterized by its low luminosity would have to be detected.

If the high M/L ratios of UCDs are caused by a bottom-heavy IMF, then this should be traceable for the highest M/L ratios by a characteristic absorption feature in the spectra of low-mass stars (Mieske and Kroupa 2008).

If, in contrast, the high M/L ratios of UCDs are the consequence of a top-heavy IMF, then this may be noticeable by the number of UCDs with bright X-ray sources. A system can form low-mass X-ray binaries (LMXBs) by stellar-dynamical encounters between black holes and neutron stars on the one hand and main-sequence stars on the other. When the main-sequence star evolves, its companion remnant may accrete its envelope therewith becoming visible as an LMXB. Assuming a canonical IMF, it has been shown that the incidence of LMXBs in GCs generally follows the expected correlation with GC mass. UCDs, however, turn out to be far overabundant as X-ray sources. This overabundance of UCDs as X-ray sources can be accounted for with the same top-heavy IMF dependence on UCD mass as is obtained independently from matching the M/L ratios. This constitutes a strong indication that UCDs formed with top-heavy IMFs (Dabringhausen et al. 2012).

The results reported in Sect. 12.7 on GCs and here on UCDs are compared in the α_3 vs. birth-density diagram (Fig. 4-31, (4.64)). A remarkable agreement of how α_3 varies with birth density for GCs and UCDs emerges.

Would UCDs with the deduced top-heavy IMF survive mass loss through stellar evolution? Dabringhausen et al. (2010) calculate a set of numerical models for the early dynamical evolution of UCDs with the canonical IMF and top-heavy IMFs, using the particle-mesh code

¹⁷Adiabatic contraction (Blumenthal et al. 1986) in UCDs may, however, alleviate this problem but unlikely sufficiently so (Murray 2009).

SUPERBOX. They assume that UCDs are hyper-massive star clusters, that is, that their stellar population formed in a starburst that took place in a dense molecular cloud. A short formation time scale of the UCDs is indeed suggested by the enhanced α -element abundances that Evstigneeva et al. (2007) report for them. This implies that all massive stars of a UCD evolve over a time span of approximately 40 Myr, that is, the lifetime of the least massive stars that become a type II supernova.

The main driver for the dynamical evolution of a UCD during this epoch is the mass-loss through gas expulsion and supernova explosions. The rate of this mass loss depends on a number of parameters: the rate at which energy is deposited into the interstellar gas of the UCD, the rate at which the interstellar gas is replenished by the ejecta from type II supernovae, the star formation efficiency (SFE, which sets how much interstellar gas can be expelled aside from supernova ejecta), and the heating efficiency (HE, which is the fraction of the energy inserted into the interstellar medium that is not radiated away but used up by removing gas from the UCD). This mass loss and the consequences are quantified in Dabringhausen et al. (2010) by comparing the energy input by type II supernova explosions and the radiation of stars over a small time interval with the binding energy of the gas that is bound to the UCD at that time, leading to individual mass-loss histories for each of the considered UCD models. These mass-loss histories are implemented into the code that is used to calculate their dynamical evolution.

The mass loss is more pronounced the more top-heavy the IMF is because more matter is set free by stars that evolve fast and the energy deposition rates are high. As a result, UCDs with a very top-heavy IMF dissolve because of heavy mass loss, except for very high SFEs. Such high-effective SFEs may be realistic because the matter lost from stars will accumulate within the UCD and may form new stars (Pflamm-Altenburg and Kroupa 2009a; Wünsch et al. 2011). In that case, the UCD models with a high-mass IMF slope close to $\alpha_3 = 1$ evolve into objects that resemble an observed UCD at the end of the calculation. For moderate SFEs, the models in Dabringhausen et al. (2010) evolve into UCD-like objects if they have either the canonical IMF or a moderately top-heavy IMF with a high-mass slope in between 1.5 and 2. However, as shown above, the case of the canonical IMF can be excluded due to the high M/L ratios of and high LMXB occurrences in UCDs. The UCD models that are consistent with the constraints set by observed UCDs also have IMFs and initial densities that are remarkably close to the high-mass IMF slope versus initial cloud densities derived for Galactic GCs (Sect. 12.7) based on their PDMFs, as can be seen in Fig. 4-31.

The variation of the IMF with cluster-forming cloud density can be summarized as follows:

The Top-Heavy Stellar IMF/Density Dependence

Resolved stellar populations show an invariant IMF (4.55), but for SFRD $\gtrsim 0.1 M_\odot/(\text{year pc}^3)$, the IMF becomes top-heavy, as inferred from UCDs and some GCs. The dependence of α_3 on cluster-forming cloud density ρ (stars plus gas) can be parametrized for $m > 1 M_\odot$ as (Marks et al. 2012)

$$\begin{aligned} \alpha_3 &= \alpha_2, & \rho < 9.5 \times 10^4 M_\odot/\text{pc}^3, \\ \alpha_3 &= 1.86 - 0.43 \log_{10}(\rho_{\text{cl}}/(10^6 M_\odot \text{pc}^{-3})), & \rho \geq 9.5 \times 10^4 M_\odot/\text{pc}^3. \end{aligned} \quad (4.64)$$

This IMF is in good agreement with the supernova rate observed in Arp 220 and Arp 299 (☛ Sect. 12.4). Note that for $m \leq 1 M_{\odot}$, the IMF is canonical (☛ 4.55). Note also that the top-heavy IMF is a fit to the GC constraints and that this provides a good description of the independent constraints arrived at by the UCDs.

12.9 The Current State of Affairs Concerning IMF Variation with Density and Metallicity and Concerning Theory

The results achieved over the past decade in self-consistent gravo-hydrodynamical modeling of star formation in turbulent clouds with the SPH and FLASH methods have been very successful (☛ Sect. 3.3). This is evident in the overall reproduction of the stellar IMF as well as of the $m_{\max} - M_{\text{ecl}}$ relation allowing detailed insights into the physics driving the growth of an ensemble of stars forming together in one CSFE (see definitions on p. 126) with and without feedback. Also, computations with these same techniques of the fragmentation of circum-proto-stellar disks lead to an excellent agreement with the BD IMF. These simulations have not yet been able to reproduce the birth binary-star properties (☛ Sect. 2.6) which may be due to as yet necessarily inadequate inclusion of the various feedback processes but also because the smoothing length and sink-particle radius required in every SPH simulation limits the binary-orbital resolution to at least a few 100 AU. Computational star formation has also ventured into the difficult terrain of including magnetic fields and radiative feedback finding a certain degree of compensating effects in terms of the emerging stellar masses with a significantly reduced star-formation efficiency (☛ Sect. 11.1).

Following on from above, the current situation of our understanding of IMF variations may be described as follows (☛ Sects. 1.4 and ☛ 11.1): Theory has, over decades, robustly predicted the IMF to vary with star-forming conditions such that metal-poor environments and/or warmer gas ought to lead to top-heavy IMFs. Observations and their interpretation including corrections for biases have, on the other hand, been indicating the IMF to be invariant, this being the consensus reached by the community as mitigated in most reviews. The suggestions for top-heavy IMFs in star bursts (e.g., Elmegreen 2005; Eisenhauer 2001) were typically taken to be very uncertain due to the evidence stemming from distant unresolved and hard-to-observe star-forming systems.

Now theoretical work has set itself the task of explaining the invariance, and various suggestions have been made: Bate (2005), Bonnell et al. (2006), Elmegreen et al. (2008), Bate (2009), Krumholz et al. (2010), and Myers et al. (2011). But evidence in favor of IMF variations has proceeded to come forth.

Perhaps the first tentative indication from resolved stellar populations for a possible change of the IMF toward a bottom-heavy form with increasing metallicity of the star-forming gas has emerged through the analysis of recent star-forming events (☛ 4.62). This evidence is still suggestive rather than conclusive. And even if true, it is very difficult to extract any IMF variation because of combinations of the following issues that mask IMF variations as they typically act randomizingly.

Masking IMF variations

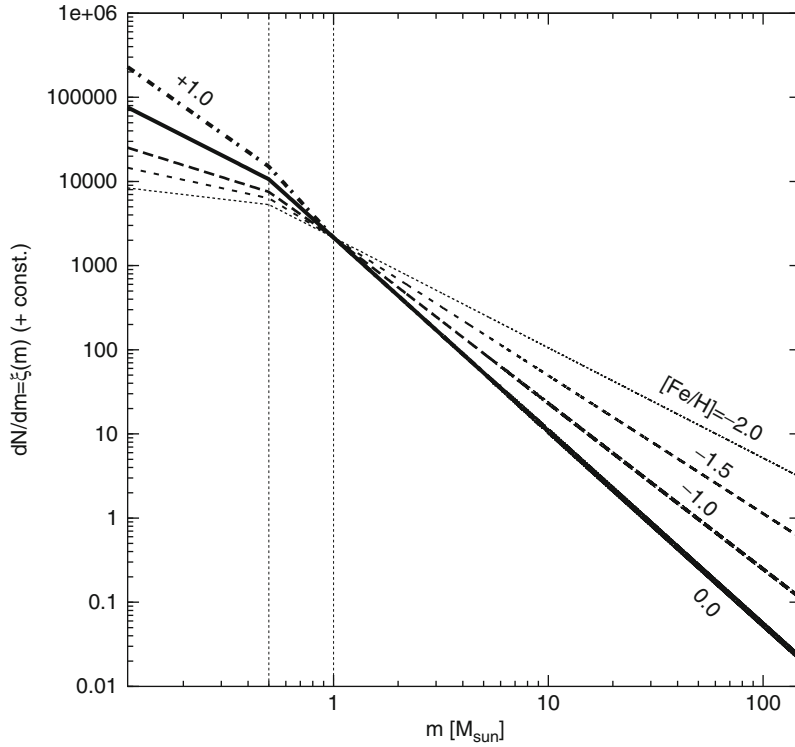
- Major uncertainties in pre-main sequence stellar evolution tracks (Footnote 3 on p. 121).
- The loss of low-mass stars from young, intermediate, and old open clusters through residual gas expulsion and secular evolution.
- Different evolutionary tracks of initially similar star clusters subject to different tidal fields.
- By observing the outcome of current or recent star formation, we are restricted to it occurring under very similar physical conditions.
- By using the canonical IMF as a benchmark, IMF variations become more difficult to unearth: the variation about the mean is smaller than the difference between the extrema.
- The fossils of star-forming events that were very different to our currently observationally accessible ones are given by Galactic GCs and dSph satellite galaxies. But given their typical distances, the PDMFs were not reliably measurable below about $0.5 M_{\odot}$. The evidence for or against variations of the MF has thus been limited to the mass range $0.5\text{--}0.8 M_{\odot}$.

The landmark paper by De Marchi et al. (2007) (Sect. 12.7) for the first time provided unambiguous evidence for a systematically changing global PDMF in Galactic GCs. This breakthrough became possible because the PDMF could be measured down to about $0.3 M_{\odot}$ with the HST and VLT for a homogeneous sample of 20 GCs giving us a greater leverage on the PDMF and the dynamical history of the GCs. It emerges that the only model able to account for the observed variation and its correlation with metallicity is one in which the IMF becomes increasingly top-heavy with increasing density (4.64) and decreasing metallicity (4.63) in a gas-expulsion scenario. A gas expulsion origin is independently also suggested as an explanation for the metallicity– M/L anticorrelation which follows from a high-resolution analysis of 200 GCs of the Andromeda galaxy (Strader et al. 2011).

Furthermore, the modern observations of UCDs have lead to the discovery that they typically have somewhat elevated M/L ratios which can be explained by a top-heavy IMF systematically changing with UCD mass. The enhanced frequency of UCDs with LMXBs can also be explained with a top-heavy IMF systematically changing with UCD mass. And, both independent results on how the IMF varies with UCD mass agree (Sect. 12.8). Last not least, the deduced variation of the IMF in UCDs is in good agreement with the variation of the IMF as deduced from the de Marchi, Paresce, and Pulone GCs, when expressed in terms of the density of the star-forming cloud. Notwithstanding this agreement, the arrived at variation of the IMF is also consistent with the top-heavy IMF suggested in star-bursting systems such as Arp 220 and Arp 299 (Sect. 12.4, 12.8). The evidence for top-heavy IMFs thus comes from GCs and UCDs that had SFRDs higher than any other known stellar-dynamical system including elliptical galaxies which had global $SFRD \lesssim 4 \times 10^{-9} M_{\odot} \text{pc}^{-3} \text{year}^{-1}$ for radii of about 5 kpc and formation time scales of about 0.5 Gyr.

The thus inferred systematic variation of the stellar IMF with metallicity is documented in Fig. 4-33. Note that there is an implicit dependence of the IMF on the density of the star-forming cloud (4.64). The metallicity and density dependencies are correlated because metal-poorer gas clouds may collapse to larger pre-cluster densities than metal-rich clouds which fragment earlier and into smaller masses.

This correlation is evident in the dependency of α_3 on ρ and $[\text{Fe}/\text{H}]$ calculated by Marks et al. (2012) using a principle component-type analysis of the GCs discussed in Sect. 12.7. It is formulated in (4.65) and plotted in Fig. 4-34.



■ Fig. 4-33

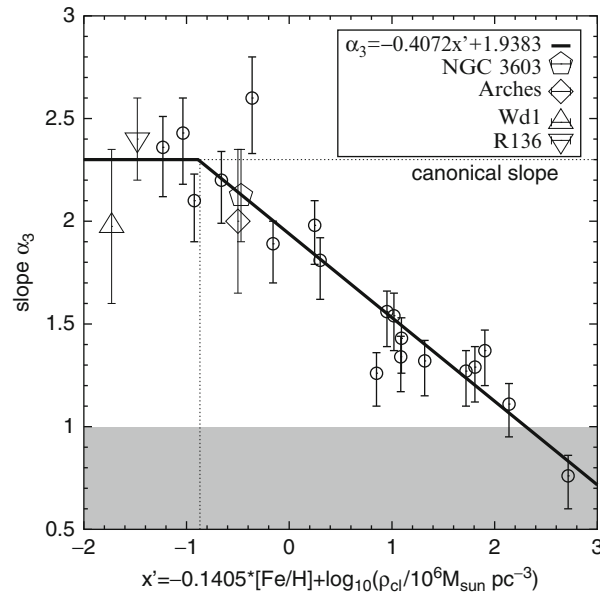
The variation of the stellar IMF with metallicity (◆ 4.62) and (◆ 4.63). The IMFs are normalized to agree at $1 M_{\odot}$. Note that the figure is based for $m < 1 M_{\odot}$ on an extrapolation of (◆ 4.62) below about $[Fe/H] \approx -0.5$. Is this the long sought after systematic variation of the stellar IMF with metallicity? (From Marks et al. (2012))

The Stellar IMF Dependence on Density and Metallicity

Resolved stellar populations show an invariant IMF (◆ 4.55), but for SFRD $\gtrsim 0.1 M_{\odot}/(\text{year pc}^3)$, the IMF becomes top-heavy, as inferred from deep observations of GCs. The dependence of α_3 on cluster-forming cloud density, ρ , (stars plus gas) and metallicity, $[Fe/H]$, can be parametrised as

$$\begin{aligned} \alpha_3 &= \alpha_2, & m > 1 M_{\odot} \quad \wedge \quad x < -0.89, \\ \alpha_3 &= -0.41 \times x + 1.94, & m > 1 M_{\odot} \quad \wedge \quad x \geq -0.89, \\ x &= -0.14 [Fe/H] + 0.99 \log_{10} (\rho / (10^6 M_{\odot} \text{pc}^{-3})). \end{aligned} \quad (4.65)$$

How does this suggested dependence of the IMF on metallicity compare with the observational exclusion of any metallicity dependence in the Local Group (◆ Fig. 4-8)? The SMC has $[Fe/H] \approx -0.6$ such that on average $\alpha_3 \approx 2.1$ (using (◆ 4.63)) which is consistent with the SMC datum in ◆ Fig. 4-8. For the LMC $[Fe/H] \approx -0.4$ such that on average $\alpha_3 \approx 2.3$ which is consistent with the LMC data in ◆ Fig. 4-8. Thus, the IMF variation deduced from GCs and UCDs are easily accommodated by the Local Group data.



■ Fig. 4-34

The variation of the stellar IMF with metallicity and cloud density (● 4.65) as deduced from deep observations of MW GCs using a principal-component-type analysis (From Marks et al. (2012)). Otherwise as ● Fig. 4-31

On galaxy scales, tentative evidence for IMF variations has begun to emerge in 2003 with the prediction that the IMF in a whole galaxy ought to be steeper (top-light) if the stellar IMF were invariant (● Sect. 13.1). This (unwantingly) resolved the long-standing but mostly ignored discrepancy between the canonical IMF index $\alpha = 2.3$ and the Scalo IMF index for the MW field ($\alpha \approx 2.7$), and generalization to galaxies of different type lead to an immediate understanding of the metallicity–galaxy-mass relation and other systematic effects.

The first observational evidence for a systematic change of the galaxy-wide IMF indeed appeared in 2008 and 2009 (● Sect. 13.2 below).

In Conclusion of this ● Sect. 12

Recent research has begun to uncover increasing evidence for a possible systematic variation of the IMF in agreement with the theoretical expectations, but this evidence requires verification by further observational work. At present, the here quantified systematic variation of the IMF is more of a suggestion than established fact, but this suggestion may give a framework and a target for future work.

13 Composite Stellar Populations: The IGIMF

The IMF in individual pc(cluster)-scale star-forming events ranging in mass from a few M_\odot up to $10^8 M_\odot$ is reasonably well constrained, as the previous sections have shown. Integrated galaxy-wide properties, on the other hand, depend on the galaxy-wide content of all newly

formed stars, that is, on the composition of all collective star-formation events (CSFEs, i.e., embedded star clusters, [Sect. 1](#)) in a galaxy.

Following philosophical approach A ([Sect. 1.5](#)), it has usually been assumed that the galaxy-wide IMF is identical to the canonical stellar IMF which is established on the pc-scale events. This is based on the simplest-of-all assumptions that the stellar distribution is sampled purely randomly from the invariant IMF, that is, that the IMF is a probabilistic density distribution function (e.g., Elmegreen 2004). Thus, for example, 10^5 clusters, each of $10 M_\odot$, would have the same composite (i.e., combined) IMF as one cluster with mass $10^6 M_\odot$. This assumption, while being simple, has important implications for the astrophysics of galaxies. For example, luminosities such as the H α flux would scale linearly with the SFR leading to the much discussed Kennicutt–Schmidt star-formation law, $\Sigma_{\text{SFR}} \propto \Sigma_{\text{gas}}^N$ with $N \approx 1.5$, where Σ_{SFR} and Σ_{gas} are the SFR surface density and gas-mass surface density, respectively (Kennicutt et al. 1994; Kennicutt 2008).

The existence of the physical $m_{\text{max}} - M_{\text{ecl}}$ relation ([Sect. 3.3](#)) has, on the other hand, profound consequences for *composite populations*. It immediately implies, for example, that 10^5 clusters, each weighing $10 M_\odot$, *cannot* have the same composite (i.e., combined) IMF as one cluster with $10^6 M_\odot$ because such small clusters can never make stars more massive than about $2.5 M_\odot$ ([Fig. 4-5](#)). And since low-mass clusters are far more numerous than massive clusters, galaxies would have steeper composite, or integrated galactic IMFs (IGIMFs), than the stellar IMF in each individual cluster (Kroupa and Weidner 2003, also hinted at independently by Vanbeveren 1982). Furthermore, massive-star-sensitive galaxy luminosities would not scale linearly with the SFR leading to a significant revision of the H α –SFR relation with corresponding major implication for the galaxy-wide star-formation law ($N = 1$ instead of 1.5, ([Sect. 4.73](#)) below).

This is indeed supported to be the case by the theory of star formation (see the BVB conjecture on p. 148) which implies optimal sampling to possibly be closer to reality than the purely probabilistic IMF approach.

13.1 IGIMF Basics

The galaxy-wide IMF, the *integrated galactic IMF*, is the sum of all the stellar IMFs in all CSFEs formed over a time span δt . While this is a next to trivial concept, it turns out to be extremely powerful in particular when its foundation is sought in approach B ([Sect. 1.5](#)), that is, in *optimal sampling* ([Sect. 2.2](#)). The IGIMF is therefore the integral over the embedded cluster MF (ECMF, ξ_{ecl}):

Definition

The IGIMF is an integral over all star-formation events in a given star-formation “epoch” $t, t + \delta t$,

$$\xi_{\text{IGIMF}}(m; t) = \int_{M_{\text{ecl}, \text{min}}}^{M_{\text{ecl}, \text{max}}(\text{SFR}(t))} \xi(m \leq m_{\text{max}}(M_{\text{ecl}})) \xi_{\text{ecl}}(M_{\text{ecl}}) dM_{\text{ecl}}, \quad (4.66)$$

with the normalization conditions equations ([Eqs. 4.69](#) and [4.70](#))

$$M_{\text{ecl}} - m_{\text{max}}(M_{\text{ecl}}) = \int_{0.07 M_\odot}^{m_{\text{max}}(M_{\text{ecl}})} m' \xi(m') dm',$$

$$1 = \int_{m_{\text{max}}(M_{\text{ecl}})}^{m_{\text{max}}} \xi(m') dm',$$

which together yield the $m_{\text{max}} - M_{\text{ecl}}$ relation ([Sect. 4.11](#)).

Here, $\xi(m \leq m_{\max}) \xi_{\text{ecl}}(M_{\text{ecl}}) dM_{\text{ecl}}$ is the stellar IMF contributed by $\xi_{\text{ecl}} dM_{\text{ecl}}$ CSFEs with stellar mass in the interval $M_{\text{ecl}}, M_{\text{ecl}} + dM_{\text{ecl}}$. The ECMF is often taken to be a power law,

$$\xi_{\text{ecl}}(M_{\text{ecl}}) \propto M_{\text{ecl}}^{-\beta}, \quad (4.67)$$

with $\beta \approx 2$ (Lada and Lada 2003), whereby an “embedded cluster” is taken here to be a CSFE and not a gravitationally bound star cluster (see definitions on p. 126). $M_{\text{ecl,max}}$ follows from the maximum star-cluster mass versus global star-formation rate of the galaxy,

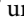
$$M_{\text{ecl,max}} = 8.5 \times 10^4 \left(\frac{\text{SFR}}{M_{\odot}/\text{year}} \right)^{0.75}, \quad (4.68)$$

(equation 1 in Weidner and Kroupa 2005, as derived by Weidner et al. 2004 using observed maximum star cluster masses). A relation between $M_{\text{ecl,max}}$ and SFR , which is a good description of the empirical data, can also be arrived at by resorting to optimal sampling. It follows by stating that when a galaxy has, at a time t , a $\text{SFR}(t)$ over a time span δt over which an optimally sampled embedded star cluster distribution builds up with total mass $M_{\text{tot}}(t)$, then there is one most massive CSFE,

$$1 = \int_{M_{\text{ecl,max}}(t)}^{M_{\text{U}}} \xi_{\text{ecl}}(M'_{\text{ecl}}) dM'_{\text{ecl}}, \quad (4.69)$$

with M_{U} being the physical maximum star cluster than can form (for practical purposes, $M_{\text{U}} > 10^8 M_{\odot}$), and

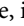
$$\text{SFR}(t) = \frac{M_{\text{tot}}(t)}{\delta t} = \frac{1}{\delta t} \int_{M_{\text{ecl,min}}}^{M_{\text{ecl,max}}(t)} M'_{\text{ecl}} \xi_{\text{ecl}}(M'_{\text{ecl}}) dM'_{\text{ecl}}. \quad (4.70)$$

$M_{\text{ecl,min}} = 5 M_{\odot}$ is adopted in the standard modeling and corresponds to the smallest “star-cluster” units observed (the low-mass sub-clusters in Taurus-Auriga in  Fig. 4-5).

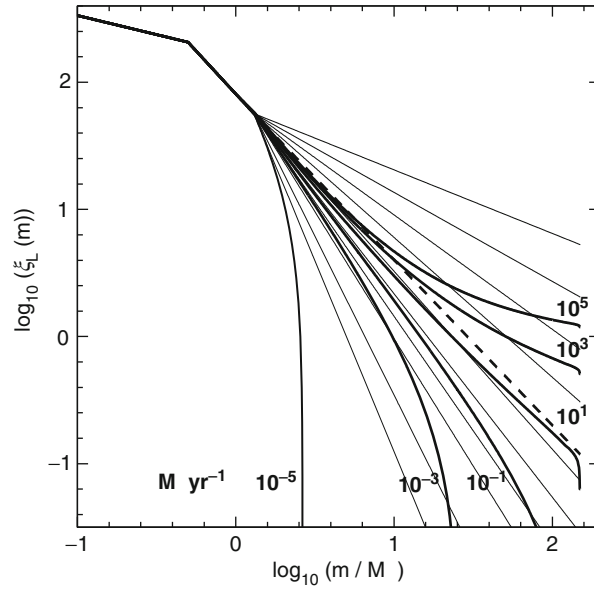
Weidner et al. (2004) define δt to be a “star-formation epoch,” within which the ECMF is sampled optimally, given a SFR. This formulation leads naturally to the observed $M_{\text{ecl,max}}(\text{SFR})$ correlation if the ECMF is invariant, $\beta \approx 2.35$ and if the “epoch” lasts about $\delta t = 10$ Myr. Thus, the embedded cluster mass function is optimally sampled in about 10 Myr intervals, independently of the SFR. This time scale is nicely consistent with the star-formation time scale in normal galactic disks measured by Egusa et al. (2004) using an entirely independent method, namely, from the offset of HII regions from the molecular clouds in spiral-wave patterns. In this view, the ISM takes about 10 Myr to transform via molecular cloud formation to a gas-free population of dispersing young simple stellar populations.

The time-integrated IGIMF then follows from

$$\xi_{\text{IGIMF}}(m) = \int_0^{\tau_{\text{G}}} \frac{\xi_{\text{IGIMF}}(m; t)}{\delta t} dt, \quad (4.71)$$

where τ_{G} is the age of the galaxy under scrutiny. The time-integrated IGIMF, $\xi_{\text{IGIMF}}(m)$, is the stellar IMF of all stars ever to have formed in a galaxy and can be used to estimate the total number of supernovae ever to have occurred, for example. $\xi_{\text{IGIMF}}(m; t)$, on the other hand, includes the time dependence through a dependency on $\text{SFR}(t)$ of a galaxy and allows one to compute the time-dependent evolution of a stellar population over the lifetime of a galaxy, for example, its instantaneous population of massive stars ( Fig. 4-35). Note that

$$\xi_{\text{IGIMF}}(m) = \left(\frac{\tau_{\text{G}}}{\delta t} \right) \xi_{\text{IGIMF}}(m; t) \quad \text{if } \text{SFR}(t) = \text{const.} \quad (4.72)$$



■ Fig. 4-35

The dependence of the logarithmic IGIMF (◆ 4.66) on the SFR of a galaxy. The IGIMF is normalized by the total number of stars such that it does not change visibly at low stellar masses in this plot. This IGIMF has been computed by adopting the canonical IMF which becomes top-heavy at embedded star-cluster densities $\rho > 10^5 M_\odot/(\text{year pc}^3)$ (◆ 4.64), an ECMF with $\beta = 2$, $M_{\text{ecl,min}} = 5 M_\odot$, and the semi-analytical $m_{\text{max}} - M_{\text{ecl}}$ relation (◆ 4.12). For a given M_{ecl} , $\rho = (\frac{1}{2} M_{\text{ecl}}/SFE) 3/(4\pi r_{0.5}^3)$ is the cloud (stellar plus gas) density, whereby a star-formation efficiency of $SFE = 1/3$ and initial half-mass radius $r_{0.5} = 0.5 \text{ pc}$ are assumed (Marks and Kroupa 2010; Dabringhausen et al. 2010; Marks and Kroupa 2012). The *thin lines* are IMFs with different power-law indices, α' , for $m > 1.3 M_\odot$ (the IGIMF is identical to the canonical IMF (◆ 4.55) below this mass) $\alpha' = 1.5, 1.7, 1.9, 2.1, 2.3, 2.4, 2.6, 2.8, 3.0, 3.5, 4.0$ (top to bottom), whereby the canonical value $\alpha' = 2.3 = \alpha_3$ is shown as the *thick dashed line*. Thus, for example, the IGIMF has $1.9 < \alpha' < 2.1$ when $SFR = 10 M_\odot/\text{year}$

13.2 IGIMF Applications, Predictions and Observational Verification

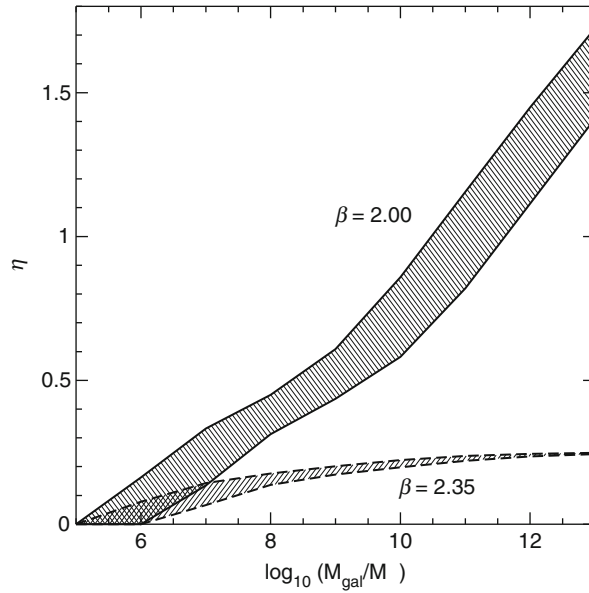
Since stellar clusters with larger masses are observed to form at higher SFRs (◆ 4.68), the ECMF is sampled to larger masses in galaxies that are experiencing high SFRs, leading to IGIMFs that are flatter than for low-mass galaxies that have only a low-level of star-formation activity. Weidner and Kroupa (2005) show that the sensitivity of the IGIMF power-law index for $m \gtrsim 1 M_\odot$ toward SFR variations increases with decreasing SFR. In star bursts extending to $SFR \approx 10^4 M_\odot/\text{year}$ the IGIMF can become top-heavy (Weidner et al. 2011) because the ultra-massive star clusters that enter the IGIMF integral have top-heavy IMFs (◆ 4.64). The dependence of the IGIMF on the SFR of a galaxy is shown in ◆ Fig. 4-35.

Thus, galaxies with a small mass in stars can either form with a very low continuous SFR (appearing today as low-surface-brightness but gas-rich galaxies) or with a brief initial SF burst (dE or dSph galaxies). It is also possible for a dwarf galaxy to evolve through multiple bursts such that its IGIMF varies. Thus, the IGIMF ought to vary significantly among dwarf galaxies (► Fig. 4-35). In all cases, however, the IGIMFs are invariant for $m \lesssim 1.3 M_{\odot}$ which is the maximal stellar mass in $5 M_{\odot}$ “clusters” (► Fig. 4-5), assuming $M_{\text{ecl,min}} = 5 M_{\odot}$ to be the invariant lower-mass limit of CSFEs.

An interesting application of the IGIMF theory to a particular system, our MW Bulge, is as follows: By studying the metallicity distribution of Bulge stars, (Ballero et al. 2007a, b among others) deduce the Bulge of the MW to have formed rapidly on a time scale of $\lesssim 1$ Gyr with a top-heavy IMF with $\alpha_3 \lesssim 2.1$. Given that the mass of the MW Bulge amounts to about $10^{10} M_{\odot}$, it follows that the Bulge would have formed with $SFR > 10 M_{\odot}/\text{year}$. From ► Fig. 4-35, it can be seen that the resulting IGIMF has an equivalent power-law index $1.9 < \alpha' < 2.1$ for $m > 1.3 M_{\odot}$, in excellent agreement with the IMF constraints based on the metallicity distribution. The IGIMF theory therefore naturally accounts for the Bulge IMF; that is, no parameters have to be adjusted apart from specifying the SFR.

Because the IGIMF steepens above about $1.3 M_{\odot}$ with decreasing SFR, this being the *IGIMF effect*, all galaxy-wide applications based on a constant IMF require a critical consideration and possibly a complete revision. A few studies on the outcome when a galaxy-wide constant IMF is replaced by a SFR-dependent IGIMF do already exist: Low-surface-brightness galaxies would appear chemically young, while the dispersion in chemical properties ought to be larger for dwarf galaxies than for more massive galaxies (Goodwin and Pagel 2005; Weidner and Kroupa 2005). The observed mass-metallicity relation of galaxies can be naturally explained quantitatively in the IGIMF context (Köppen et al. 2007). The $[\alpha/\text{Fe}]$ element abundance ratios of early-type galaxies, which decreases with decreasing stellar velocity dispersion, can be understood as an IGIMF effect (Recchi et al. 2009) with the associated reduction of the need for downsizing. And indeed, the chemical evolution modeling of the Fornax dwarf-spheroidal satellite galaxy demonstrates that this system must have produced stars up to at most about $25 M_{\odot}$ in agreement with the prediction of the IGIMF theory given the low $SFR \approx 3 \times 10^{-3} M_{\odot}/\text{year}$ deduced for this system when it was forming stars in the past (Tsuji-moto 2011). Another interesting implication is that the number of supernovae per star would be significantly smaller over cosmological times than predicted by an invariant Salpeter IMF (Goodwin and Pagel 2005, ► Fig. 4-36), except in phases when the average cosmological SFR is higher than about $10 M_{\odot}/\text{year}$.

The relation between the produced total $H\alpha$ luminosity and the underlying SFR is linear in the classical Kennicutt picture, that is, in the context of a constant galaxy-wide IMF. It turns out that this relation becomes strongly nonlinear at SFRs comparable to the SMC and smaller (Pflamm-Altenburg et al. 2007). The implication of the revised $L_{H\alpha}$ -SFR relation is fundamental: In the classical picture, the calculated gas depletion times (τ , the ratio of available neutral gas mass and current SFR) of dwarf irregular galaxies are much larger than those of large disk galaxies. This has been taken to mean that dwarf galaxies have lower “star-formation efficiencies,” $1/\tau$, than massive galaxies. But the IGIMF-revised $L_{H\alpha}$ -SFR relation reveals a fundamental constant gas depletion time scale of about $\tau = 3$ Gyr over almost five orders in magnitude in total galaxy neutral gas mass (Pflamm-Altenburg and Kroupa 2009b). Dwarf galaxies thus have “star-formation efficiencies” comparable to those of massive galaxies.



■ Fig. 4-36

The number of supernovae of type II (SNII) per star in the IGIMF divided by the number of SNII per star in the canonical IMF, η , as a function of the stellar galaxy mass, M_{gal} . The *upper shaded area* is for an ECMF with $\beta = 2$, while the *lower shaded area* assumes $\beta = 2.35$, both with $M_{\text{ecl,min}} = 5 M_{\odot}$. The *upper bound* for each *shaded region* is for an initial SF burst model of 1 Gyr duration ($SFR = M_{\text{gal}}/1 \text{ Gyr}$), while the *lower bounds* are for a constant SFR over a Hubble time ($SFR = M_{\text{gal}}/13.7 \text{ Gyr}$). For details, see Weidner and Kroupa (2005), but the here plotted η is computed from the IGIMFs shown in Fig. 4-35. For most galaxies, the SNII rate is expected to be smaller than the expected rate for an invariant IMF (Goodwin and Pagel 2005). But it can be seen that the number of SNII per star becomes larger than for a canonical IMF when $\beta = 2.0$ and $SFR > 10 M_{\odot}/\text{year}$ because the IGIMF becomes top-heavy when CSFEs with cloud density $\rho > 10^5 M_{\odot}/\text{pc}^3$ are included. Star-bursting galaxies therewith come with an overabundance of type II SN if the ECMF has $\beta = 2$ and clusters with mass down to $5 M_{\odot}$ form in star bursts. Similar results are obtained for $\beta = 2.35$ and an ECMF without low-mass clusters (not plotted here). Such and similar calculations allow observational testing of the IGIMF theory, for example, through constraining the mass of the extreme SN progenitors in dependence of the SFR of the host galaxy (Neill et al. 2011)

Furthermore, it is possible to formulate the IGIMF on local scales and not only on global (galaxy-wide) ones. This can be achieved straightforwardly by replacing all galaxy-wide quantities in the IGIMF theory (Eq. 4.66) by their corresponding surface densities. This local IGIMF (LIGIMF) theory (Pflamm-Altenburg and Kroupa 2008) readily explains the observed radial $H\alpha$ cutoff in disk galaxies as well as the different radial profiles in $H\alpha$ and FUV observed by Boissier et al. (2007).

Summarizing the two star-formation laws of galaxies which emerge from the IGIMF theory (Pflamm-Altenburg and Kroupa 2007, 2008, 2009b),

$$\begin{aligned}\frac{SFR}{M_{\odot} \text{ year}^{-1}} &= \frac{1}{2.8 \text{ Gyr}} \frac{M_{\text{gas}}}{M_{\odot}}, \\ \frac{\Sigma_{\text{SFR}}}{M_{\odot} \text{ pc}^{-2} \text{ year}^{-1}} &= \frac{1}{2.8 \text{ Gyr}} \frac{\Sigma_{\text{gas}}}{M_{\odot} \text{ pc}^{-2}},\end{aligned}\quad (4.73)$$

where SFR is the global star-formation rate of the galaxy with mass in neutral gas mass of M_{gas} and Σ_{SFR} and Σ_{gas} are the surface star-formation rate and surface gas densities, respectively.

A compilation of a number of issues relating to the astrophysics of galaxies that are naturally resolved within the IGIMF theory are listed in the box IGIMF successes (p. 230).

The IGIMF concept has allowed a number of predictions: Based on the IGIMF theory, a decreasing galaxy-wide $H\alpha$ /FUV-flux ratio with decreasing total SFR has been predicted (Pflamm-Altenburg et al. 2009). This prediction has been confirmed qualitatively (Meurer et al. 2009) and quantitatively (Lee et al. 2009). Additionally, Hoversten and Glazebrook (2008) found, in the integrated properties of over 50,000 SDSS galaxies, that galaxies of lower mass seem to have steeper IMFs than more massive ones, as would be expected from the IGIMF. A direct confirmation of the IGIMF would be to measure the IGIMF effect. A few predictions and tests are compiled in the box IGIMF predictions/tests (p. 231).

IGIMF Successes

The mass–metallicity relation of galaxies emerges naturally (Köppen et al. 2007);

The $[\alpha/\text{Fe}]$ element abundance ratios of early-type galaxies emerge naturally (Recchi et al. 2009).

The observed radial $H\alpha$ cutoff in disk galaxies as well as the different radial profiles in $H\alpha$ and FUV emerge naturally (Pflamm-Altenburg and Kroupa 2008).

The SFR of a galaxy is proportional to its mass in neutral gas (● 4.73).

The gas depletion time scales of dwarf irregular and large disk galaxies are about 2.8 Gyr, implying that dwarf galaxies do not have lower star-formation efficiencies than large disk galaxies (Pflamm-Altenburg and Kroupa 2009b).

The stellar-mass buildup times of dwarf and large galaxies are only in agreement with downsizing in the IGIMF context but contradict downsizing within the traditional framework that assumes a constant galaxy-wide IMF. The stellar-mass buildup times in dwarf galaxies become shorter than a Hubble time and therewith naturally solve the hitherto unsolved problem that the times are significantly longer than a Hubble time if an invariant IMF is assumed (Pflamm-Altenburg and Kroupa 2009b).

The IGIMF solution for the IMF of the Galactic Bulge is in excellent agreement with the top-heavy IMF derived from chemical-evolution studies of the Bulge.

For a $SFR = 119 M_{\odot}/\text{year}$, the IGIMF has $\alpha \approx 2$ (● Fig. 4-35). This is in good agreement with the constraint $\alpha = 1.9 \pm 0.15$ observed for the $z \approx 2.5$ lensed galaxy SMM J163554.2+661225 with Herschel by Finkelstein et al. (2011), who adopted a maximum stellar mass of $100 M_{\odot}$ whereas the IGIMF theory adopts $m_{\text{max}*} = 150 M_{\odot}$ therewith biasing their IMF solution to slightly steeper indices.

IGIMF Predictions/Tests

If the IMF were a stochastic or probabilistic distribution function then a population of a e.g., 1500 very young stars should contain 9 stars more massive than 8 M_{\odot} (► [Table 4-1](#)). The finding by Hsu et al. (2012) that the L1641 cloud is deficient in O and early B stars to a 3-4 sigma significance level constitutes a direct observational verification of the IGIMF effect (many low-density star-forming clumps).

In the young star-forming region Taurus-Auriga, random sampling from the IMF predicts 9 stars more massive than 3.25 M_{\odot} while none are observed. However, such a low number of stars above 3.25 M_{\odot} is to be expected if one assumes a local IGIMF effect from the sub-clusters in that region. The closest star-forming region is thus fully consistent with the IGIMF theory while being in conflict with the hypothesis that star formation is equivalent to randomly sampling stars from the IMF.

The fraction among all stars of massive stars in a galaxy with a low SFR is smaller than in a galaxy with a larger SFR. For example, $SFR = 10^{-3} M_{\odot}/\text{year}$, no star more massive than 18 M_{\odot} ought to be seen in the galaxy while 30 are expected for an invariant canonical stellar IMF (Weidner et al, in preparation).

The number of type II supernovae is smaller in all dwarf and normal galaxies than hitherto thought assuming an invariant stellar IMF (► [Fig. 4-36](#)).

These new insights should lead to a revision of theoretical work on galaxy formation that typically until now relied on an invariant IMF. Empirical evidence in favor of or against the notion of a galaxy-variable IGIMF is being studied (e.g., Corbelli et al. 2009; Calzetti et al. 2010; Fumagalli et al. 2011; Neill et al. 2011; Roychowdhury et al. 2011; Weisz et al. 2012) and will ultimately lead to a refinement of the ideas. Important for workers to realize here is that stellar-dynamical processes are a central physics ingredient when analyzing populations of unresolved star clusters and the spatial distribution of massive stars. Also, care needs to be exercised in testing hypotheses self-consistently (► [Sect. 1.6](#)). At a fundamental level, the IGIMF theory is correct since a galaxy is trivially the sum of all star-formation events. The astrophysical constraints over many orders of magnitude of galaxy mass allow one to constrain the fundamental parameters that define the particularly valid IGIMF. These parameters are the ECMF (e.g., do dwarf and massive galaxies form only massive clusters when they experience a star burst?), the exact form of the $m_{\text{max}} - M_{\text{ecl}}$ relation, and the variation of the stellar IMF with star-formation rate density.

Main Results

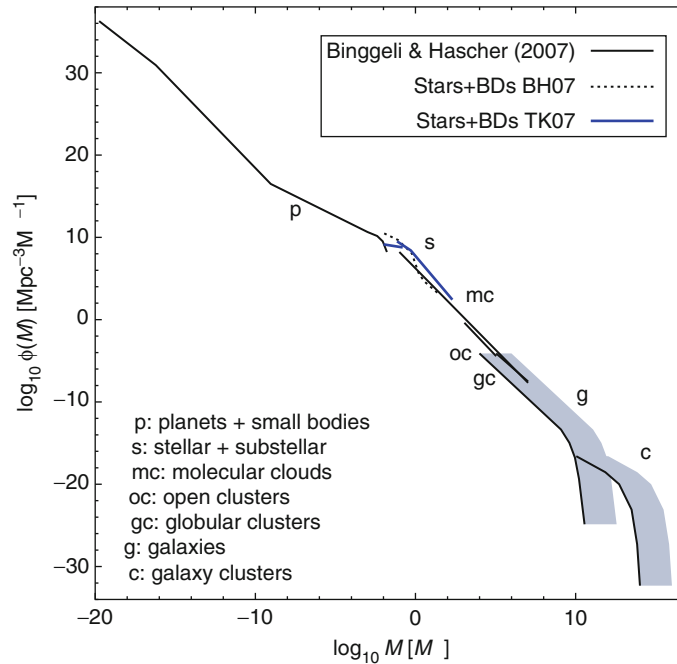
Due to the clustered nature of star formation, the composite or integrated IMF of galaxies or of parts thereof is steeper than the canonical IMF for low to modest SFRs ($SFR \lesssim 1 M_{\odot}/\text{year}$) or SFR surface densities, respectively, and it can be top-heavy for larger SFRs. The behavior of the IGIMF depends on the variation of the ECMF with the SFR. The IGIMF theory for the first time links in a computationally accessible way empirically calibrated star-formation processes on a pc scale with astrophysical behavior of systems on galactic and cosmological scales.

14 The Universal Mass Function

How does the stellar IMF fit in with the mass distribution of all condensed objects, from planets to massive galaxy clusters?

Binggeli and Hascher (2007) deduce a universal MF (UMF) for all astronomical objects over a mass range of 36 decimal orders of magnitude, divided into seven groups: (1) planets and small bodies (meteoroids, asteroids); (2) stars, BDs, and stellar remnants; (3) molecular clouds; (4) open clusters; (5) globular clusters; (6) galaxies (dark matter plus baryonic masses); and (7) galaxy clusters (dark matter plus baryonic masses). Their result is reproduced in [Fig. 4-37](#). The shape as well as the normalization are based on observational data, however, using a present-day mass function rather than the IMF for stars, with a slightly different low-mass stellar slope and BDs as being continuously connected to stars (dotted curve). The canonical IMF is shown by the blue curves. The UMF follows an approximate $\propto m^{-2}$ power law which is remarkably similar to the Salpeter one ($\alpha = 2.35$) as well as to a logarithmic mass equi-distribution ($\alpha = 2$).

Binggeli and Hascher (2007) write “It is gratifying that the two halves almost perfectly connect to each other around one solar mass. Remember that this normalization was achieved on



■ Fig. 4-37

The universal mass function (UMF) of condensed structures according to Binggeli and Hascher (2007). BH07 estimated the absolute normalization based on the observed occurrence of the objects ranging from planets to galaxy clusters. The canonical IMF are the TK07 lines ([Fig. 4.55](#), Thies and Kroupa 2007). Note that if dark matter does not exist, then the galaxy and galaxy cluster MFs are given by the *black line* (lower limit to the *shaded region*), while the *dark matter plus baryonic masses* of galaxies are given by the *upper envelope* of this *shaded region*

the basis of the mean universal mass density carried by the stars, embodied in the galaxies on the one hand, and comprised by the stars themselves on the other.” As pointed out by Binggeli and Hascher (2007), a possible reason for this fairly continuous UMF may be that gravitation is the dominant agent for creating the structures.

15 Concluding Comments

Spectacular advances have been achieved over the past two decades in the field of IMF research, and this affects a vast area of astrophysics. The discrepant observed nearby and distant luminosity functions of stars in the local Galactic disk have been unified with one IMF, and the strong peak in the luminosity function near $M_V = 12$ is well understood as a result of the changing internal constitution of stars as a function of their mass. The unification of the luminosity functions also ultimately lead to a unification of the observed discrepant binary populations in different environments through dynamical processing in star-forming regions.

The observationally determined stellar IMF is described by (4.55) and/or (4.56). Its form has traditionally been understood to be invariant in contradiction to the variable IMF prediction (p. 124). The IMF of stellar systems and of the Galactic field is provided by (4.57) and (4.59), respectively.

By studying the IMF, star-formation theory is being tested. According to the IMF Origin Conjecture (p. 207), the vast majority of stellar masses ($0.1 \lesssim m/M_\odot \lesssim \text{few}$) do not appear to be affected by competitive accretion or proto-stellar interactions (Sect. 11.2). According to the computational star-formation research, the most massive star in a star-formation event correlates physically with the mass of the event. This $m_{\text{max}} - M_{\text{ecl}}$ relation is a natural outcome of the competitive accretion-growth and the fragmentation-induced starvation of stellar masses, and the computations reproduce the general shape of the IMF. Different ideas (competitive accretion, coagulation and simply the distribution of gravitationally unstable regions in turbulent clouds) all lead to virtually the same type of theoretical power-law IMF. The IMF appears to be mostly form invariant within space-time correlated star-formation events (CSFEs, i.e., in individual embedded star clusters) for star-formation rate densities $SFRD \lesssim 0.1 M_\odot \text{ pc}^{-3} \text{ year}^{-1}$ within a spatial scale of about a pc. But, the IMF varies (trivially) among such individual CSFEs of stellar mass M_{ecl} through the $m_{\text{max}} - M_{\text{ecl}}$ relation. This relation follows from the notion of optimal sampling. Computational star formation has achieved a remarkable degree of realism, although the binary population has not yet emerged properly and the computations cannot yet reach the birth of populous star clusters.

That optimal sampling appears to be describing a freshly born stellar population would invalidate the concept of a stellar population being a purely random representation of the IMF, leading to Open Question II (p. 150). The remarkable similarity of observationally determined IMF power-law indices (Open Question III, p. 195) may well be an indication that nature follows optimal sampling. Two other open questions related to star formation, and the IMF are furthermore stated (pp. 143 and 208).

Evidence for a variation of the shape of the IMF has emerged, being consistent with the long-previously predicted IMF variation. The evidence for top-heavy IMFs for $SFRD \gtrsim 0.1 M_\odot \text{ pc}^{-3} \text{ year}^{-1}$ (4.64) comes from either unresolved clusters or from populations that are very difficult to observe but appears to be increasingly established. The long-sought after evidence for a systematically varying stellar IMF with metallicity (Fig. 4-33) may have emerged. A principal-component-type analysis of the PDMFs of GCs has now for the first

time yielded a formulation of a systematically varying IMF with star-forming cloud density and metallicity (► 4.65).

Among other intriguing recent results are that BDs appear to be a distinct population from that of low-mass stars; their pairing properties have a different energy scale. This is well reproduced by computational star formation. BDs and stars thus follow different mass distributions which do not join. A continuous log-normal function across the VLMS/BD mass scale does not therefore correctly describe the IMF.

Furthermore, the IMF does appear to have a physical maximum stellar mass that has now been found empirically. Stars with $m \gtrsim 150 M_{\odot}$ do not appear to form, unless they implode invisibly shortly after being formed. Populous star clusters with super-canonical ($m > 150 M_{\odot}$) stars are termed to be super saturated (p. 148). There is no statistically meaningful observational evidence for the formation of massive stars in isolation, in agreement with star-formation computations. The established invariance of the observationally derived IMF precludes the exotic IMF associated with isolated massive star formation.

By realizing that CSFEs are the true fundamental building blocks of a galaxy, all such events with their IMFs need to be added up to arrive at the integrated galactic initial mass function. This IGIMF varies in dependence of the SFR of the galaxy. According to the IGIMF theory, galaxies with low SFRs have a smaller ratio between the number of massive stars and low-mass stars than galaxies with high SFRs. This is the “IGIMF effect.” This formulation allows computation of the IGIMF as a function of time for galaxies with different SFRs. One implication of this is that equally old galaxies can have very different chemical compositions ranging from unevolved to evolved and that the cosmological supernova type II rate per star would be significantly different and dependent on galaxy type than if an invariant stellar IMF is assumed. Galaxy-formation and evolution computations with this latter assumption are not likely to be correct. Indeed, it transpires that only with the IGIMF theory is a fundamental time scale of about 3 Gyr uncovered on which all late-type galaxies consume their current gas supply. Very simple star-formation laws for galaxies emerge (► 4.73). Also, only with the IGIMF theory are the stellar-mass buildup times of dwarf galaxies consistent with the Hubble time. The top-heavy IMF of the Galactic Bulge deduced from chemical evolution research follows immediately from the IGIMF theory.

Thus, with the IGIMF theory, it has now become possible to calculate how the observationally well-constrained star formation on pc scales propagates through to galactic scales of cosmological relevance. A unification of scales has therewith been achieved which was quite unthinkable only a few years ago.

Many details still need to be worked out though. For example, direct verification of the IGIMF effect is needed. This can be achieved by directly counting the number of massive stars in dwarf galaxies with low SFRs or by counting the number of massive stars in a giant molecular cloud and comparing this number with the number of late-type stars formed there. Also, the existence of and exact form of the $m_{\max} - M_{\text{ecl}}$ relation is important not only for the calculation of the IGIMF but also for understanding to which degree star formation is self-regulated on a pc scale. Such work will establish which of the two philosophical approaches of ► Sect. 1.5 describe the astrophysics of star formation and of galaxies. The fact that the Orion southern cloud L1641 has formed a significant deficit of massive stars despite producing thousands of stars (Hsu et al. 2012) and the fact that the $m_{\max} - M_{\text{ecl}}$ relation is excellently mapped with a small scatter at the lowest masses (Kirk and Myers 2011) already constitute major evidence that the IGIMF theory and its fundamental assumptions appear to be given by nature.

Concerning the wider picture, the stellar and BD IMFs fit in quite continuously into the universal mass function of condensed structures as pointed out by Binggeli and Hascher (2007).

Acknowledgments

PK is thankful to Christopher Tout and Gerry Gilmore for very stimulating and important contributions without which much of this material would not have become available. PK is especially indebted to Sverre Aarseth whose friendly tutoring (against “payments” in the form of many bottles of *lieblichen* German white wine) eased the numerical dynamics work in 1993/1994. Douglas Heggie be thanked for fruitful discussions with PK on optimal sampling in Heidelberg in September, 2011. We thank Sambaran Banerjee for very helpful comments on the manuscript. PK would also like to thank M. R. S. Hawkins who had introduced him to this field in 1987 while PK visited the Siding-Spring Observatory as a summer vacation scholar at the ANU. Mike gave PK a delightful lecture on the low-mass LF one night when visiting his observing run to learn about modern, state-of-the-art Schmidt-telescope surveying with photographic plates *before* PK embarked on postgraduate work. This research was much later supported through DFG grants KR1635/2 and KR1635/3 and a Heisenberg fellowship, KR1635/4, KR1635/12, KR1635/13, and currently KR1635/25. MM acknowledges the Bonn/Cologne International Max-Planck Research School for support.

Cross-References

- [Binaries and Multiple Stellar Systems](#)
- [Brown Dwarfs](#)
- [Dark Matter in the Galactic Dwarf Spheroidal Satellites](#)
- [Dynamics of Disks and Warps](#)
- [Evolution of High-Mass Stars](#)
- [Evolution of Solar and Intermediate Mass Stars](#)
- [Galactic Distance Scales](#)
- [Globular Cluster Dynamical Evolution](#)
- [Mass Distribution and Rotation Curve in the Galaxy](#)
- [Metal-Poor Stars and the Chemical Enrichment of the Universe](#)
- [Numerical Techniques in Astrophysics](#)
- [Open Clusters and their Role in the Galaxy](#)
- [Star Counts and the Nature of the Galactic Thick Disk](#)
- [Star Formation](#)
- [Statistical Methods for Astronomy](#)
- [Stellar Populations](#)
- [The Galactic Bulge](#)
- [The Galactic Nucleus](#)
- [White Dwarf Stars](#)
- [Young Stellar Objects and Protostellar Disks](#)

References

- | | |
|---|--|
| Aarseth, S. J. 1999, <i>PASP</i> , 111, 1333 | Adams, F. C., & Fatuzzo, M. 1996, <i>ApJ</i> , 464, 256 |
| Aarseth, S. J. 2003, in <i>Gravitational N-Body Simulations</i> , ed. S. J. Aarseth (Cambridge, UK: Cambridge University Press), 430. ISBN 0521432723 | Adams, F. C., & Myers, P. C. 2001, <i>ApJ</i> , 553, 744 |
| | Allen, P. R., Koerner, D. W., Reid, I. N., & Trilling, D. E. 2005, <i>ApJ</i> , 625, 385 |

- Alves, J., Lombardi, M., & Lada, C. J. 2007, *A&A*, 462, L17
- Anders, P., Lamers, H. J. G. L. M., & Baumgardt, H. 2009, *A&A*, 502, 817
- Andersen, J. 1991, *A&A*, 3, 91
- Andersen, M., Meyer, M. R., Greissl, J., & Aversa, A. 2008, *ApJ*, 683, L183
- Andersen, M., Zinnecker, H., & Moneti, A., et al. 2009, *ApJ*, 707, 1347
- Anderson, J. P., Haberman, S. M., & James, P. A. 2011, *MNRAS*, 416, 567
- André, P., Belloche, A., Motte, F., & Peretto, N. 2007, *A&A*, 472, 519
- André, P., Men'shchikov, A., & Bontemps, S., et al. 2010, *A&A*, 518, L102+
- Bahcall, J. N. 1984, *ApJ*, 287, 926
- Ballero, S. K., Kroupa, P., & Matteucci, F. 2007a, *A&A*, 467, 117
- Ballero, S. K., Matteucci, F., Origlia, L., & Rich, R. M. 2007b, *A&A*, 467, 123
- Banerjee, S., & Kroupa, P. 2012, *A&A*, in press
- Banerjee, S., Kroupa, P., & Oh, S. 2012, *ApJ*, 746, 15
- Baraffe, I., & Chabrier, G. 2010, *A&A*, 521, A44+
- Baraffe, I., Chabrier, G., Allard, F., & Hauschildt, P. H. 1998, *A&A*, 337, 403
- Baraffe, I., Chabrier, G., Allard, F., & Hauschildt, P. H. 2002, *A&A*, 382, 563
- Baraffe, I., Chabrier, G., & Gallardo, J. 2009, *ApJ*, 702, L27
- Barrado y Navascués, D., Stauffer, J. R., Bouvier, J., & Martin, E. L. 2001, *ApJ*, 546, 1006
- Barrado y Navascués, D., Stauffer, J. R., & Jayawardhana, R. 2004, *ApJ*, 614, 386
- Bartko, H., Martins, F., & Tripp, S., et al. 2010, *ApJ*, 708, 834
- Basri, G. 2000, *ARA&A*, 38, 485
- Bastian, N., Covey, K. R., & Meyer, M. R. 2010, *ARA&A*, 48, 339
- Basu, S., & Jones, C. E. 2004, *MNRAS*, 347, L47
- Basu, S., & Vorobyov, E. I. 2012, *ApJ*, 750, 30
- Bate, M. R. 2005, *MNRAS*, 363, 363
- Bate, M. R. 2009, *MNRAS*, 397, 232
- Bate, M. R., & Bonnell, I. A. 2005, *MNRAS*, 356, 1201
- Baugh, C. M., Lacey, C. G., & Frenk, C. S., et al. 2005, *MNRAS*, 356, 1191
- Baumgardt, H., & Makino, J. 2003, *MNRAS*, 340, 227
- Baumgardt, H., De Marchi, G., & Kroupa, P. 2008, *ApJ*, 685, 247
- Beech, M., & Mitalas, R. 1994, *ApJS*, 95, 517
- Belikov, A. N., Hirte, S., Meusinger, H., Piskunov, A. E., & Schilbach, E. 1998, *A&A*, 332, 575
- Bestenlehner, J. M., Vink, J. S., & Gräfenr, G., et al. 2011, *A&A*, 530, L14+
- Beuzit, J. L., Ségransan, D., & Forveille, T., et al. 2004, *A&A*, 425, 997
- Binggeli, B., & Hascher, T. 2007, *PASP*, 119, 592
- Binney, J., & Merrifield, M. 1998, in *Princeton Series in Astrophysics, Galactic Astronomy*, eds. J. Binney, & M. Merrifield (Princeton, NJ: Princeton University Press), QB857 .B522 1998 (\$35.00)
- Binney, J., Dehnen, W., & Bertelli, G. 2000, *MNRAS*, 318, 658
- Blumenthal, G. R., Faber, S. M., Flores, R., & Primack, J. R. 1986, *ApJ*, 301, 27
- Bochanski, J. J., Hawley, S. L., & Covey, K. R., et al. 2010, *AJ*, 139, 2679
- Boily, C. M., Lançon, A., Deiters, S., & Heggge, D. C. 2005, *ApJ*, 620, L27
- Boissier, S., Gil de Paz, A., & Boselli, A., et al. 2007, *ApJS*, 173, 524
- Bonnell, I. A., & Bate, M. R. 2002, *MNRAS*, 336, 659
- Bonnell, I. A., & Bate, M. R. 2006, *MNRAS*, 370, 488
- Bonnell, I. A., & Rice, W. K. M. 2008, *Science*, 321, 1060
- Bonnell, I. A., Bate, M. R., & Zinnecker, H. 1998, *MNRAS*, 298, 93
- Bonnell, I. A., Vine, S. G., & Bate, M. R. 2004, *MNRAS*, 349, 735
- Bonnell, I. A., Clarke, C. J., & Bate, M. R. 2006, *MNRAS*, 368, 1296
- Bonnell, I. A., Larson, R. B., & Zinnecker, H. 2007, *Protostars and Planets V*, 149
- Bontemps, S., André, P., Kaas, A. A. 2001, *A&A*, 372, 173
- Bontemps, S., Motte, F., Csengeri, T., & Schneider, N. 2010, *A&A*, 524, A18+
- Bosch, G., Selman, F., Melnick, J., & Terlevich, R. 2001, *A&A*, 380, 137
- Boss, A. R. 1986, *ApJS*, 62, 519
- Bouvier, J., Moraux, E., Stauffer, J. R., Barrado y Navascués, D., & Cuillandre, J. C. 2003, in *IAU Symposium*, 147, *Brown Dwarfs*, vol. 211 ed. E. Martín, astro-ph/0209178
- Bouvier, J., Kendall, T., & Meeus, G., et al. 2008, *A&A*, 481, 661
- Bouy, H., Brandner, W., & Martin, E. L., et al. 2003, *AJ*, 126, 1526
- Briceño, C., Luhman, K. L., Hartmann, L., Stauffer, J. R., & Kirkpatrick, J. D. 2002, *ApJ*, 580, 317
- Brocato, E., Cassisi, S., & Castellani, V. 1998, *MNRAS*, 295, 711
- Bromm, V., Ferrara, A., Coppi, P. S., Larson, R. B. 2001, *MNRAS*, 328, 969
- Brüns, R. C., Kroupa, P., Fellhauer, M., Metz, M., & Assmann, P. 2011, *A&A*, 529, A138+
- Calzetti, D., Chandar, R., & Lee, J. C., et al. 2010, *ApJ*, 719, L158
- Camargo, D., Bonatto, C., & Bica, E. 2010, *A&A*, 521, A42+

- Casuso, E., & Beckman, J. E. 2012, *MNRAS*, 419, 1642
- Cenarro, A. J., Gorgas, J., Vazdekis, A., Cardiel, N., & Peletier, R. F. 2003, *MNRAS*, 339, L12
- Chabrier, G. 2001, *ApJ*, 554, 1274
- Chabrier, G. 2002, *ApJ*, 567, 304
- Chabrier, G. 2003a, *ApJ*, 586, L133
- Chabrier, G. 2003b, *PASP*, 115, 763
- Chabrier, G., & Baraffe, I. 1997, *A&A*, 327, 1039
- Chabrier, G., & Baraffe, I. 2000, *ARA&A*, 38, 337
- Chini, R., Hoffmeister, V., & Kimeswenger, S., et al. 2004, *Nature*, 429, 155
- Chini, R., Hoffmeister, V. H., Nasser, A., Stahl, O., & Zinnecker, H. 2012, *MNRAS*, in press, arXiv:astro-ph/1205.5238
- Chlebowski, T., & Garmany, C. D. 1991, *ApJ*, 368, 241
- Clarke, C. J., & Pringle, J. E. 1992, *MNRAS*, 255, 423
- Clark, P. C., Glover, S. C. O., Bonnell, I. A., & Klessen, R. S. 2009, *ApJ*, submitted, arXiv:astro-ph/0904.3302
- Clark, P. C., Glover, S. C. O., Klessen, R. S., & Bromm, V. 2011, *ApJ*, 727, 110
- Close, L. M., Siegler, N., Freed, M., & Biller, B. 2003, *ApJ*, 587, 407
- Conroy, C. 2011, *ApJ*, submitted, arXiv:astro-ph/1101.2208
- Corbelli, E., Palla, F., Zinnecker, H. (eds.), 2005, *The Initial Mass Function 50 years later*, *Astrophysics and Space Science Library*, 327 (Dordrecht: Springer)
- Corbelli, E., Verley, S., Elmegreen, B. G., & Giovannardi, C. 2009, *A&A*, 495, 479
- Crowther, P. A., Schnurr, O., & Hirschi, R., et al. 2010, *MNRAS*, 408, 731
- Dabringhausen, J., Kroupa, P., & Baumgardt, H. 2009, *MNRAS*, 394, 1529
- Dabringhausen, J., Fellhauer, M., & Kroupa, P. 2010, *MNRAS*, 403, 1054
- Dabringhausen, J., Kroupa, P., Pflamm-Altenburg, J., & Mieske, S. 2012, *ApJ*, 747, 72
- Dale, J. E., Wunsch, R., Smith, R. J., Whitworth, A., & Palouš, J., 2011, *MNRAS*, 411, 2230
- D'Antona, F., & Mazzitelli, I. 1996, *ApJ*, 456, 329
- Da Rio, N., Gouliermis, D. A., Henning, T. 2009, *ApJ*, 696, 528
- de Boer, K. S., Fitzpatrick, E. L., & Savage, B. D. 1985, *MNRAS*, 217, 115
- de La Fuente Marcos, R. 1998, *A&A*, 333, L27
- de Marchi, G., & Paresce, F. 1995a, *A&A*, 304, 202
- de Marchi, G., & Paresce, F. 1995b, *A&A*, 304, 211
- De Marchi, G., Paresce, F., & Pulone, L. 2007, *ApJ*, 656, L65
- de Wit, W. J., Testi, L., Palla, F., Vanzi, L., & Zinnecker, H. 2004, *A&A*, 425, 937
- de Wit, W. J., Testi, L., Palla, F., & Zinnecker, H. 2005, *A&A*, 437, 247
- Deason, A. J., Belokurov, V., Evans, N. W., & McCarthy, I. G. 2011, *ApJ*, in press, arXiv:astro-ph/1110.0833
- Delfosse, X., Forveille, T., & Beuzit, J. L., et al. 1999, *A&A*, 344, 897
- Delfosse, X., Forveille, T., & Ségransan, D., et al. 2000, *A&A*, 364, 217
- Dib, S. 2011, *ApJ*, 737, L20+
- Dib, S., Shadmehri, M., & Padoan, P., et al. 2010, *MNRAS*, 405, 401
- Dib, S., Piau, L., Mohanty, S., & Braine, J. 2011, *MNRAS*, 415, 3439
- Disney, M. J., Romano, J. D., & Garcia-Appadoo, D. A., et al. 2008, *Nature*, 455, 1082
- Djorgovski, S., Piotto, G., & Capaccioli, M. 1993, *AJ*, 105, 2148
- Dominik, M. 2011, *MNRAS*, 411, 2
- Duchêne, G., Simon, T., Eislöffel, J., & Bouvier, J. 2001, *A&A*, 379, 147
- Duquennoy, A., & Mayor, M. 1991, *A&A*, 248, 485
- Eddington, A. S., 1926, *The Internal Constitution of the Stars* (Cambridge: Cambridge University Press)
- Egusa, F., Sofue, Y., & Nakanishi, H. 2004, *PASJ*, 56, L45
- Eisenhauer, F. 2001, in *Science with the Large Binocular Telescope*, eds. T. Herbst, 89, arXiv:astro-ph/0101384
- Elmegreen, B. G. 1983, *MNRAS*, 203, 1011
- Elmegreen, B. G. 1997, *ApJ*, 486, 944
- Elmegreen, B. G. 1999, *ApJ*, 515, 323
- Elmegreen, B. G. 2000, *ApJ*, 539, 342
- Elmegreen, B. G. 2004, *MNRAS*, 354, 367
- Elmegreen, B. G. 2005, in *Astrophysics and Space Science Library*, 57, *Starbursts: From 30 Doradus to Lyman Break Galaxies*, Vol. 329, eds. R. de Grijs & R. M. González Delgado (Dordrecht/New York: Springer), arXiv:astro-ph/0411193
- Elmegreen, B. G. 2009, in *The Evolving ISM in the Milky Way and Nearby Galaxies*, arXiv:astro-ph/0803.3154
- Elmegreen, B. G. 2011, *ApJ*, 731, 61
- Elmegreen, B. G., & Scalo, J. 2006, *ApJ*, 636, 149
- Elmegreen, B. G., & Shadmehri, M. 2003, *MNRAS*, 338, 817
- Elmegreen, B. G., Klessen, R. S., & Wilson, C. D. 2008, *ApJ*, 681, 365
- Esteban, C., Peimbert, M., Torres-Peimbert, S., & Escalante, V. 1998, *MNRAS*, 295, 401
- Evstigneeva, E. A., Gregg, M. D., Drinkwater, M. J., & Hilker, M. 2007, *AJ*, 133, 1722
- Fellhauer, M., & Kroupa, P. 2002, *MNRAS*, 330, 642
- Fellhauer, M., & Kroupa, P. 2005, *MNRAS*, 359, 223
- Fellhauer, M., Lin, D. N. C., Bolte, M., Aarseth, S. J., & Williams, K. A. 2003, *ApJ*, 595, L53

- Fellhauer, M., Wilkinson, M. I., & Kroupa, P. 2009, *MNRAS*, 397, 954
- Feltzing, S., Gilmore, G., & Wyse, R. F. G. 1999, *ApJ*, 516, L17
- Figer, D. F. 2003, in *IAU Symposium*, 487, A Massive Star Odyssey: From Main Sequence to Supernova, eds. K. van der Hucht, A. Herrero, & C. Esteban, Vol. 212 (San Francisco, CA: ASP)
- Figer, D. F. 2005, *Nature*, 434, 192
- Finkelstein, K. D., Papovich, C., & Finkelstein, S. L., et al. 2011, *ApJ*, 742, 108
- Fischer, D. A., & Marcy, G. W. 1992, *ApJ*, 396, 178
- Flynn, C., & Fuchs, B. 1994, *MNRAS*, 270, 471
- Forbes, D. A., & Kroupa, P. 2011, *PASA*, 28, 77
- Fuhrmann, K. 2004, *Astron Nachr*, 325, 3
- Fumagalli, M., da Silva, R. L., & Krumholz, M. R. 2011, *ApJ*, 741, L26
- García, B., & Mermilliod, J. C. 2001, *A&A*, 368, 122
- García-Segura, G., Langer, N., & Mac Low, M. M. 1996a, *A&A*, 316, 133
- García-Segura, G., Mac Low, M. M., & Langer, N. 1996b, *A&A*, 305, 229
- Gilmore, G., Howell, D. (eds.), 1998, *The Stellar Initial Mass Function (38th Herstmonceux Conference)* (San Francisco, CA: ASP) ASP Conference Series, Vol. 142
- Gilmore, G. F., Perryman, M. A., & Lindegren, L., et al. 1998, in *Proc. SPIE*, 3350, *Astronomical Interferometry*, ed. R. D. Reasenberg (Bellingham, WA: SPIE), 541–550, arXiv:astro-ph/9805180
- Gizis, J. E., Kirkpatrick, J. D., & Burgasser, A., et al. 2001, *ApJ*, 551, L163
- Girichidis, P., Federrath, C., Banerjee, R., & Klessen, R. S. 2011, *MNRAS*, 413, 2741
- Goodwin, S. P., & Bastian, N. 2006, *MNRAS*, 373, 752
- Goodwin, S. P., & Kroupa, P. 2005, *A&A*, 439, 565
- Goodwin, S. P., & Pagel, B. E. J. 2005, *MNRAS*, 359, 707
- Goodwin, S. P., & Whitworth, A. 2007, *A&A*, 466, 943
- Goodwin, S. P., Kroupa, P., Goodman, A., & Burkert, A. 2007, in *Protostars and Planets V*, eds. B. Reipurth, D. Jewitt, & K. Keil (Tucson: University of Arizona Press), 133–147, arXiv:astro-ph/0603233
- Goodwin, S. P., Nutter, D., Kroupa, P., Ward-Thompson, D., & Whitworth A. P. 2008, *A&A*, 477, 823
- Gouliermis, D., Brandner, W., & Henning T. 2005, *ApJ*, 623, 846
- Gouliermis, D., Brandner, W., & Henning, T. 2006, *ApJ*, 636, L133
- Gouliermis, D. A., Bestenlehner, J. M., Brandner, W., & Henning, T. 2010, *A&A*, 515, A56+
- Grillmair, C. J., Mould, J. R., & Holtzman, J. A. 1998, *AJ*, 115, 144
- Grillo, C., & Gobat, R. 2010, *MNRAS*, 402, L67
- Gvaramadze, V. V., & Bomans, D. J. 2008, *A&A*, 490, 1071
- Gvaramadze, V. V., & Gualandris, A. 2011, *MNRAS*, 410, 304
- Gvaramadze, V. V., Weidner, C., Kroupa, P., & Pflamm-Altenburg, J. 2012, *MNRAS*, in press, arXiv:astro-ph/1206.1596
- Haas, M. R., & Anders, P. 2010, *A&A*, 512, A79+
- Halbwachs, J. L., Arenou, F., Mayor, M., Udry, S., & Queloz, D. 2000, *A&A*, 355, 581
- Hambly, N. C., Jameson, R. F., & Hawkins, M. R. S. 1991, *MNRAS*, 253, 1
- Hambly, N. C., Hodgkin, S. T., Cossburn, M. R., & Jameson, R. F. 1999, *MNRAS*, 303, 835
- Hayashi, C., & Nakano, T. 1963, *Prog Theor Phys*, 30, 460
- Haywood, M., Robin, A. C., & Creze, M. 1997, *A&A*, 320, 440
- Heggie, D. C. 1975, *MNRAS*, 173, 729
- Hennebelle, P., & Chabrier, G. 2008, *ApJ*, 684, 395
- Hennebelle, P., & Chabrier, G. 2009, *ApJ*, 702, 1428
- Henry, T. J., Ianna, P. A., Kirkpatrick, J. D., & Jahreiss, H. 1997, *AJ*, 114, 388
- Hillenbrand, L. A. 1997, *AJ*, 113, 1733
- Hillenbrand, L. A. 2004, in *The Dense Interstellar Medium in Galaxies*, eds. S. Pfalzner et al. (Berlin/New York: Springer), 601, arXiv:astro-ph/0312187
- Hillenbrand, L. A., & Carpenter, J. M. 2000, *ApJ*, 540, 236
- Hocuk, S., & Spaans, M. 2011, *A&A*, 536, A41
- Hollenbach, D., Parravano, A., & McKee, C. F. 2005, in *ASSL*, 327, *The Initial Mass Function 50 Years Later*, eds. E. Corbelli, F. Palla, & H. Zinnecker (New York: Springer), 417–424
- Hoversten, E. A., & Glazebrook, K. 2008, *ApJ*, 675, 163
- Hsu, W.-H., Hartmann, L., Allen, L., et al. 2012, *ApJ*, 752, 59
- Ivanova, N., Belczynski, K., Fregeau, J. M., & Rasio, F. A. 2005, *MNRAS*, 358, 572
- Jahreiss, H. 1994, *Ap&SS*, 217, 63
- Jahreiß, H., & Wielen, R. 1997, in *ESA SP-402: Hipparcos – Venice '97*, ed. by B. Battistich et al. (Noordwijk: ESA Publications Division), 675–680
- Janka, H. T. 2001, *A&A*, 368, 527
- Jao, W., Henry, T. J., & Subasavage, J. P., et al. 2003, *AJ*, 125, 332
- Jeans, J. H. 1902, *R Soc Lond Philos Trans Ser A*, 199, 1
- Jijina, J., & Adams, F. C. 1996, *ApJ*, 462, 874

- Joergens, V. 2008, *A&A*, 492, 545
- Kahn, F. D. 1974, *A&A*, 37, 149
- Kalirai, J. S., Hansen, B. M. S., & Kelson, D. D. 2008, *ApJ*, 676, 594
- Kaplan, M., Stamatellos, D., & Whitworth, A. P. 2012, *Ap&SS*, 222, in press, arXiv:astro-ph/1205.2279
- Kennicutt, R. C., Jr. 2008, in ASP Conf. Ser. 149, *Pathways Through an Eclectic Universe*, eds. J. H. Knapen, T. J. Mahoney, & A. Vazdekis, Vol. 390 (San Francisco, CA: ASP)
- Kennicutt, R. C., Jr., Tamblyn, P., & Congdon, C. E. 1994, *ApJ*, 435, 22
- Kevlahan, N., & Pudritz, R. E. 2009, *ApJ*, 702, 39
- Kim, S. S., Figier, D. F., Kudritzki, R. P., & Najarro, F. 2006, *ApJ*, 653, L113
- Kirk, H., & Myers, P. C. 2011, *ApJ*, 727, 64
- Kirk, J. M., Ward-Thompson, D., & André, P. 2005, *MNRAS*, 360, 1506
- Klessen, R. S. 2001, *ApJ*, 550, L77
- Klessen, R. S., Spaans, M., & Jappsen, A. 2007, *MNRAS*, 374, L29
- Koen, C. 2006, *MNRAS*, 365, 590
- Köppen, J., Weidner, C., & Kroupa, P. 2007, *MNRAS*, 375, 673
- Kroupa, P. 1995a, *ApJ*, 453, 350
- Kroupa, P. 1995b, *MNRAS*, 277, 1522
- Kroupa, P. 1995c, *MNRAS*, 277, 1507
- Kroupa, P. 1995d, *MNRAS*, 277, 1491
- Kroupa, P. 1995e, *ApJ*, 453, 358
- Kroupa, P. 2000, *New Astron*, 4, 615
- Kroupa, P. 2001a, *MNRAS*, 322, 231
- Kroupa, P. 2001b, in ASP Conf. Ser. 228, *Dynamics of Star Clusters and the Milky Way*, eds. S. Deiters et al. (San Francisco, CA: ASP), 187, arXiv:astro-ph/0011328
- Kroupa, P. 2001c, in: IAU Symposium 200, 199, arXiv:astro-ph/0010347
- Kroupa, P. 2002, *Science*, 295, 82
- Kroupa, P., Jan. 2005, in *Proceedings of the Gaia Symposium "The Three-Dimensional Universe with Gaia"* (ESA SP-576). Held at the Observatoire de Paris-Meudon, 4–7 October 2004, eds. C. Turon, K. S. O’Flaherty, & M. A. C. Perryman (Noordwijk: ESA Publications Division), 629, arXiv:astro-ph/0412069
- Kroupa, P. 2008, in LNP 760, *The Cambridge N-Body Lectures*, eds. S. J. Aarseth, C. A. Tout, & R. A. Mardling (Berlin, Springer), 181, arXiv:astro-ph/0803.1833
- Kroupa, P., Famaey, B., & de Boer, K. S., et al. 2010, *A&A*, 523, A32+
- Kroupa, P. 2011, in IAU Symposium, Vol. 270, eds. J. Alves, B. G. Elmegreen, J. M. Girart, & V. Trimble, 141–149, arXiv:astro-ph/1012.1596
- Kroupa, P. 2012, *PASA*, in press, arXiv:astro-ph/1204.2546
- Kroupa, P., & Bouvier, J. 2003a, *MNRAS*, 346, 343
- Kroupa, P., & Bouvier, J. 2003b, *MNRAS*, 346, 369
- Kroupa, P., & Tout, C. A. 1997, *MNRAS*, 287, 402
- Kroupa, P., & Weidner, C. 2003, *ApJ*, 598, 1076
- Kroupa, P., Tout, C. A., & Gilmore, G. 1990, *MNRAS*, 244, 76
- Kroupa, P., Gilmore, G., & Tout, C. A. 1991, *MNRAS*, 251, 293
- Kroupa, P., Tout, C. A., & Gilmore, G. 1993, *MNRAS*, 262, 545
- Kroupa, P., Aarseth, S., & Hurley, J. 2001, *MNRAS*, 321, 699
- Kroupa, P., Bouvier, J., Duchêne, G., & Moraux, E. 2003, *MNRAS*, 346, 354
- Krumholz, M. R., & McKee, C. F. 2008, *Nature*, 451, 1082
- Krumholz, M. R., Klein, R. I., McKee, C. F., Offner, S. S. R., & Cunningham, A. J. 2009, *Science*, 323, 754
- Krumholz, M. R., Cunningham, A. J., Klein, R. I., & McKee, C. F. 2010, *ApJ*, 713, 1120
- Kudritzki, R., & Puls, J. 2000, *ARA&A*, 38, 613
- Kuijken, K., & Gilmore, G. 1991, *ApJ*, 367, L9
- Kumar, S. S. 2003, in IAU 211, 3, arXiv:astro-ph/0208096
- Lada, C. J., & Lada, E. A. 2003, *ARA&A*, 41, 57
- Lamb, J. B., Oey, M. S., Werk, J. K., & Ingleby, L. D. 2010, *ApJ*, 725, 1886
- Larson, R. B. 1982, *MNRAS*, 200, 159
- Larson, R. B. 1998, *MNRAS*, 301, 569
- Larson, R. B. 2003, in ASP Conf. Ser. 287, *Galactic Star Formation Across the Stellar Mass Spectrum*, eds. J. M. De Buizer, & N. S. van der Blik (San Francisco, CA: ASP), 65–80
- Lee, J. C., Gil de Paz, A., & Tremonti, C., et al. 2009, *ApJ*, 706, 599
- Li, Y., Klessen, R. S., & Mac Low, M. M. 2003, *ApJ*, 592, 975
- Li, Z.-Y., Wang, P., Abel, T., & Nakamura, F. 2010, *ApJ*, 720, L26
- Löckmann, U., Baumgardt, H., & Kroupa, P. 2010, *MNRAS*, 402, 519
- Lodieu, N., Dobbie, P. D., Deacon, N. R., et al. 2007, *MNRAS*, 380, 712
- Lonsdale, C. J., Diamond, P. J., Thrall, H., Smith, H. E., & Lonsdale, C. J. 2006, *ApJ*, 647, 185
- Low, C., & Lynden-Bell, D. 1976, *MNRAS*, 176, 367
- Luhman, K. L. 2004, *ApJ*, 617, 1216
- Luhman, K. L., Rieke, G. H., & Young, E. T., et al. 2000, *ApJ*, 540, 1016
- Lutz, T. E., & Kelker, D. H. 1973, *PASP*, 85, 573
- Machida, M. N., & Matsumoto, T. 2011, *MNRAS*, 421, 588

- Machida, M. N., Omukai, K., Matsumoto, T., & Inutsuka, S. 2009, *MNRAS*, 399, 1255
- Mac Low, M., & Klessen, R. S. 2004, *Rev Mod Phys*, 76, 125
- Maeder, A., & Behrend, R. 2002, in *ASP Conf. Ser.* 267, *Hot Star Workshop III: The Earliest Phases of Massive Star Birth*, ed. P. A. Crowther (San Francisco, CA: ASP), 179
- Maeder, A., & Meynet, G. 2000, *ARA&A*, 38, 143
- Maíz Apellániz, J. 2008, *ApJ*, 677, 1278
- Maíz Apellániz, J., & Úbeda, L. 2005, *ApJ*, 629, 873
- Maíz Apellániz, J., Walborn, N. R., Morrell, N. I., Niemela, V. S., & Nelán, E. P. 2007, *ApJ*, 660, 1480
- Maíz Apellániz, J., Walborn, N. R., Morrell, N. I., et al. 2008, in *Revista Mexicana de Astronomía y Astrofísica Conference Series* 33, 55–55 [arXiv:astro-ph/0702514](https://arxiv.org/abs/astro-ph/0702514)
- Malkov, O., & Zinnecker, H. 2001, *MNRAS*, 321, 149
- Malkov, O. Y., Piskunov, A. E., & Shpil’Kina, D. A. 1997, *A&A*, 320, 79
- Marks, M., & Kroupa, P. 2010, *MNRAS*, 406, 2000
- Marks, M., & Kroupa, P. 2011, *MNRAS*, 417, 1702
- Marks, M., & Kroupa, P. 2012, *A&A*, 543, A8
- Marks, M., Kroupa, P., & Baumgardt, H. 2008, *MNRAS*, 386, 2047
- Marks, M., Kroupa, P., & Oh, S. 2011, *MNRAS*, 417, 1684
- Marks, M., Kroupa, P., Dabringhausen, J., & Pawłowski, M. S. 2012, *MNRAS*, 422, 2246
- Martín, E. L., Barrado y Navascués, D., Baraffe, I., Bouy, H., & Dahm, S. 2003, *ApJ*, 594, 525
- Maschberger, T., & Clarke, C. J. 2008, *MNRAS*, 391, 711
- Maschberger, T., & Clarke, C. J. 2011, *MNRAS*, 1177
- Maschberger, T., & Kroupa, P. 2009, *MNRAS*, 395, 931
- Maschberger, T., Clarke, C. J., Bonnell, I. A., & Kroupa, P. 2010, *MNRAS*, 404, 1061
- Massey, P. 1998, in *ASP Conf. Ser.* 142, *The Stellar Initial Mass Function (38th Herstmonceux Conference)*, eds. G. Gilmore, & D. Howell (San Francisco, CA: ASP), 17
- Massey, P. 2003, *ARA&A*, 41, 15
- Massey, P., & Hunter, D. A. 1998, *ApJ*, 493, 180
- Maxted, P. F. L., & Jeffries, R. D. 2005, *MNRAS*, 362, L45
- Mayor, M., Duquennoy, A., Halbwachs, J. L., & Mermilliod, J. C. 1992, in *ASP Conf. Ser.* 32, *IAU Colloq. 135: Complementary Approaches to Double and Multiple Star Research*, eds. H. A. McAlister, & W. I. Hartkopf (San Francisco, CA: ASP), 73
- McCraday, N., Graham, J. R., & Vacca, W. D. 2005, *ApJ*, 621, 278
- McMillan, S. L. W., Vesperini, E., & Portegies Zwart, S. F. 2007, *ApJ*, 655, L45
- Megeath, S. T., Herter, T., & Beichman, C., et al. 1996, *A&A*, 307, 775
- Meurer, G. R., Wong, O. I., & Kim, J. H., et al. 2009, *ApJ*, 695, 765
- Meyer, M. R., Adams, F. C., Hillenbrand, L. A., Carpenter, J. M., & Larson, R. B. 2000, in *Protostars and Planets IV*, eds. V. Mannings, A. Boss, & S. S. Russell (Tucson: University of Arizona Press), 121
- Mieske, S., & Kroupa, P. 2008, *ApJ*, 677, 276
- Mieske, S., Hilker, M., & Infante, L. 2002, *A&A*, 383, 823
- Miller, G. E., & Scalo, J. M. 1979, *ApJS*, 41, 513
- Misgeld, I., & Hilker, M. 2011, *MNRAS*, 414, 3699
- Moeckel, N., & Bate, M. R. 2010, *MNRAS*, 404, 721
- Morau, E., Kroupa, P., & Bouvier, J. 2004, *A&A*, 426, 75
- Motte, F., Andre, P., & Neri, R. 1998, *A&A*, 336, 150
- Muench, A. A., Lada, E. A., & Lada, C. J. 2000, *ApJ*, 533, 358
- Murray, N. 2009, *ApJ*, 691, 946
- Murray, S. D., & Lin, D. N. C. 1996, *ApJ*, 467, 728
- Myers, P. C. 2011, *ApJ*, 743, 98
- Myers, A. T., Krumholz, M. R., Klein, R. I., & McKee, C. F. 2011, *ApJ*, 735, 49
- Nagashima, M., Lacey, C. G., Baugh, C. M., Frenk, C. S., & Cole, S. 2005, *MNRAS*, 358, 1247
- Najarro, F., Figer, D. F., Hillier, D. J., & Kudritzki, R. P. 2004, *ApJ*, 611, L105
- Nayakshin, S., & Sunyaev, R. 2005, *MNRAS*, 364, L23
- Neill, J. D., Sullivan, M., & Gal-Yam, A., et al. 2011, *ApJ*, 727, 15
- Nordlund, Å., & Padoan, P. 2003, *LNP* 614, *Turbulence and Magnetic Fields in Astrophysics*, eds. E. Falgarone & T. Passot (Berlin/New York: Springer), 271
- Oey, M. S. 2011, *ApJ*, 739, L46
- Oey, M. S., & Clarke, C. J. 2005, *ApJ*, 620, L43
- Oliveira, J. M., Jeffries, R. D., & van Loon, J. T. 2009, *MNRAS*, 392, 1034
- Onishi, T., Mizuno, A., Kawamura, A., Tachihara, K., & Fukui, Y. 2002, *ApJ*, 575, 950
- Padoan, P., & Nordlund, Å. 2002, *ApJ*, 576, 870
- Padoan, P., & Nordlund, Å. 2004, *ApJ*, 617, 559
- Palla, F., Randich, S., Pavlenko, Y. V., Flaccomio, E., & Pallavicini, R. 2007, *ApJ*, 659, L41
- Papadopoulos, P. P. 2010, *ApJ*, 720, 226
- Papadopoulos, P. P., Thi, W. F., Miniati, F., & Viti, S. 2011, *MNRAS*, 414, 1705
- Paresce, F., de Marchi, G., & Romaniello, M. 1995, *ApJ*, 440, 216
- Parker, R. J., & Goodwin, S. P. 2007, *MNRAS*, 380, 1271
- Parker, R. J., & Goodwin, S. P. 2011, *MNRAS*, 411, 891

- Parker, R. J., Bouvier, J., & Goodwin, S. P., et al. 2011, *MNRAS*, 412, 2489
- Parra, R., Conway, J. E., & Diamond, P. J., et al. 2007, *ApJ*, 659, 314
- Parravano, A., McKee, C. F., & Hollenbach, D. J. 2011, *ApJ*, 726, 27
- Peebles, P. J. E., & Nusser, A. 2010, *Nature*, 465, 565
- Penny, L. R., Massey, P., & Vukovich, J. 2001, *Bull Am Astron Soc*, 33, 1310
- Pérez-Torres, M. A., Romero-Cañizales, C., Alberdi, A., & Polatidis, A. 2009, *A&A*, 507, L17
- Peters, T., Klessen, R. S., Mac Low, M. M., & Banerjee, R. 2010, *ApJ*, 725, 134
- Peters, T., Banerjee, R., Klessen, R. S., & Mac Low, M. M. 2011a, *ApJ*, 729, 72
- Peters, T., Klessen, R. S., Mac Low, M. M., & Banerjee, R. 2011b, *arXiv:astro-ph/1110.2892*
- Pflamm-Altenburg, J., & Kroupa, P. 2006, *MNRAS*, 373, 295
- Pflamm-Altenburg, J., & Kroupa, P. 2007, *MNRAS*, 375, 855
- Pflamm-Altenburg, J., & Kroupa, P. 2008, *Nature*, 455, 641
- Pflamm-Altenburg, J., & Kroupa, P. 2009a, *MNRAS*, 397, 488
- Pflamm-Altenburg, J., & Kroupa, P. 2009b, *ApJ*, 706, 516
- Pflamm-Altenburg, J., & Kroupa, P. 2010, *MNRAS*, 404, 1564
- Pflamm-Altenburg, J., Weidner, C., & Kroupa, P. 2007, *ApJ*, 671, 1550
- Pflamm-Altenburg, J., Weidner, C., & Kroupa, P. 2009, *MNRAS*, 395, 394
- Phan-Bao, N., Martin, E. L., Reylé, C., Forveille, T., & Lim, J. 2005, *A&A*, 439, L19
- Pinfield, D. J., Dobbie, P. D., & Jameson, R. F., et al. 2003, *MNRAS*, 342, 1241
- Piotto, G., & Zoccali, M. 1999, *A&A*, 345, 485
- Piskunov, A. E., Belikov, A. N., Kharchenko, N. V., Sagar, R., & Subramaniam, A. 2004, *MNRAS*, 349, 1449
- Portegies Zwart, S. F., Makino, J., McMillan, S. L. W., & Hut, P. 2002, *ApJ*, 565, 265
- Preibisch, T., Balega, Y., Hofmann, K., Weigelt, G., & Zinnecker, H. 1999, *New Astron*, 4, 531
- Price, D. J., & Bate, M. R. 2009, *MNRAS*, 398, 33
- Ramspeck, M., Heber, U., & Moehler, S. 2001, *A&A*, 378, 907
- Recchi, S., Calura, F., & Kroupa, P. 2009, *A&A*, 499, 711
- Reid, I. N., & Gizis, J. E. 1997, *AJ*, 113, 2246
- Reid, I. N., Gizis, J. E., & Hawley, S. L. 2002, *AJ*, 124, 2721
- Reid, I. N., Cruz, K. L., & Allen, P., et al. 2003a, *AJ*, 126, 3007
- Reid, I. N., Cruz, K. L., & Laurie, S. P., et al. 2003b, *AJ*, 125, 354
- Reid, N., & Gilmore, G. 1982, *MNRAS*, 201, 73
- Reipurth, B., & Clarke, C. 2001, *AJ*, 122, 432
- Reylé, C., & Robin, A. C. 2001, *A&A*, 373, 886
- Röser, S., Schilbach, E., Piskunov, A. E., Kharchenko, N. V., & Scholz, R. D. 2011, *A&A*, 531, A92
- Roychowdhury, S., Chengalur, J. N., Kaisin, S. S., Begum, A., & Karachentsev, I. D. 2011, *MNRAS*, 414, L55
- Salpeter, E. E. 1955, *ApJ*, 121, 161
- Sana, H., & Evans, C. J. 2010, *arXiv:astro-ph/1009.4197*
- Sana, H., James, G., & Gosset, E. 2011a, *MNRAS*, 416, 817
- Sana, H., Lacour, S., & Le Bouquin, J., et al. 2011b, *arXiv:astro-ph/1109.6654*
- Scalo, J. M. 1986, *Fundam Cosm Phys*, 11, 1
- Scalo, J. 1998, in *ASP Conf. Ser. 142, The Stellar Initial Mass Function (38th Herstmonceux Conference)*, eds. G. Gilmore & D. Howell (San Francisco, CA: ASP), 201
- Schilbach, E., & Röser, S. 2008, *A&A*, 489, 105
- Schmalzl, M., Gouliermis, D. A., Dolphin, A. E., & Henning, T. 2008, *ApJ*, 681, 290
- Schwarzschild, M., & Härm, R. 1959, *ApJ*, 129, 637
- Selmer, R., Heydari-Malayeri, M., & Gouliermis, D. A. 2011, *A&A*, 529, A40+
- Selman, F., Melnick, J., Bosch, G., & Terlevich, R. 1999, *A&A*, 347, 532
- Shen, S., Wadsley, J., Hayfield, T., & Ellens, N. 2010, *MNRAS*, 401, 727
- Siess, L., Dufour, E., & Forestini, M. 2000, *A&A*, 358, 593
- Sirianni, M., Nota, A., Leitherer, C., De Marchi, G., & Clampin, M. 2000, *ApJ*, 533, 203
- Slesnick, C. L., Hillenbrand, L. A., & Carpenter, J. M. 2004, *ApJ*, 610, 1045
- Smith, L. J., & Gallagher, J. S. 2001, *MNRAS*, 326, 1027
- Smith, R. J., Longmore, S., & Bonnell, I. 2009, *MNRAS*, 400, 1775
- Soubiran, C., Bienaymé, O., & Siebert, A. 2003, *A&A*, 398, 141
- Sollima, A., Beccari, G., Ferraro, F. R., Fusi Pecci, F., & Sarajedini, A. 2007, *MNRAS*, 380, 781
- Sollima, A., Carballo-Bello, J. A., Beccari, G., et al. 2010, *MNRAS*, 401, 577
- Stahler, S. W., Palla, F., & Ho, P. T. P. 2000, *Protostars and Planets IV*, eds. V. Mannings, A. Boss, & S. S. Russell (Tucson: University of Arizona Press), 327

- Stamatellos, D., & Whitworth, A. P. 2009, *MNRAS*, 392, 413
- Stamatellos, D., Hubber, D. A., & Whitworth, A. P. 2007a, *MNRAS*, 382, L30
- Stamatellos, D., Whitworth, A. P., Bisbas, T., & Goodwin, S. 2007b, *A&A*, 475, 37
- Stamatellos, D., Whitworth, A. P., & Hubber, D. A. 2011, *ApJ*, 730, 32
- Stobie, R. S., Ishida, K., & Peacock, J. A. 1989, *MNRAS*, 238, 709
- Stolte, A., Grebel, E. K., Brandner, W., & Figer, D. F. 2002, *A&A*, 394, 459
- Stothers, R. B. 1992, *ApJ*, 392, 706
- Strader, J., Caldwell, N., & Seth, A. C. 2011, *AJ*, 142, 8
- Tan, J. C., Krumholz, M. R., & McKee, C. F. 2006, *ApJ*, 641, L121
- Testi, L., & Sargent, A. I. 1998, *ApJ*, 508, L91
- Thies, I., & Kroupa, P. 2007, *ApJ*, 671, 767
- Thies, I., & Kroupa, P. 2008, *MNRAS*, 390, 1200
- Thies, I., Kroupa, P., & Theis, C. 2005, *MNRAS*, 364, 961
- Thies, I., Kroupa, P., Goodwin, S. P., Stamatellos, D., & Whitworth, A. P. 2010, *ApJ*, 717, 577
- Tilley, D. A., & Pudritz, R. E. 2004, *MNRAS*, 353, 769
- Tilley, D. A., & Pudritz, R. E. 2007, *MNRAS*, 382, 73
- Tout, C. A., Livio, M., & Bonnell, I. A. 1999, *MNRAS*, 310, 360
- Treyer, M., Wyder, T., Neill, J., Seibert, M., & Lee, J. (eds.), 2011, *ASP Conf. Ser. 440*, UP2010: Have Observations Revealed a Variable Upper End of the Initial Mass Function? (San Francisco, CA: ASP)
- Tsujimoto, T. 2011, *ApJ*, 736, 113
- Turner, J. L. 2009, *Extreme star formation*, in *Astrophysics in the Next Decade*, eds. H. A. Thronson, M. Stiavelli, & A. Tielens (Dordrecht/London: Springer), 215
- Ulvestad, J. S. 2009, *AJ*, 138, 1529
- Vanbeveren, D. 1982, *A&A*, 115, 65
- Vanbeveren, D. 2011, *arXiv:astro-ph/1109.6497*
- van Dokkum, P. G. 2008, *ApJ*, 674, 29
- van Dokkum, P. G., & Conroy, C. 2010, *Nature*, 468, 940
- Vazdekis, A., Casuso, E., Peletier, R. F., & Beckman, J. E. 1996, *ApJS*, 106, 307
- Vazdekis, A., Peletier, R. F., Beckman, J. E., & Casuso, E. 1997, *ApJS*, 111, 203
- Veltchev, T. V., Klessen, R. S., & Clark, P. C. 2011, *MNRAS*, 411, 301
- Vesperini, E., & Heggie, D. C. 1997, *MNRAS*, 289, 898
- Vesperini, E., McMillan, S. L. W., & Portegies Zwart, S. 2009, *ApJ*, 698, 615
- Vogt, S. S., Butler, R. P., & Marcy, G. W., et al. 2002, *ApJ*, 568, 352
- von Hippel, T., Gilmore, G., Tanvir, N., Robinson, D., & Jones, D. H. P. 1996, *AJ*, 112, 192
- Wang, P., Li, Z.-Y., Abel, T., & Nakamura, F. 2010, *ApJ*, 709, 27
- Weidemann, V. 1990, in *NATO ASIC Proc. 305, Baryonic Dark Matter*, eds. D. Lynden-Bell & G. Gilmore (Dordrecht/Boston: Kluwer), 87
- Weidemann, V., Jordan, S., Iben, I. J., & Casertano, S. 1992, *AJ*, 104, 1876
- Weidner, C., & Kroupa, P. 2004, *MNRAS*, 348, 187
- Weidner, C., & Kroupa, P. 2005, *ApJ*, 625, 754
- Weidner, C., & Kroupa, P. 2006, *MNRAS*, 365, 1333
- Weidner, C., Kroupa, P., & Larsen, S. S. 2004, *MNRAS*, 350, 1503
- Weidner, C., Kroupa, P., & Maschberger, T. 2009, *MNRAS*, 393, 663
- Weidner, C., Kroupa, P., & Bonnell, I. A. 2010, *MNRAS*, 401, 275
- Weidner, C., Kroupa, P., & Pflamm-Altenburg, J. 2011, *MNRAS*, 412, 979
- Weigelt, G., & Baier, G. 1985, *A&A*, 150, L18
- Weisz, D. R., Johnson, B. D., & Johnson, L. C., et al. 2012, *ApJ*, 744, 44
- White, R. J., & Basri, G. 2003, *ApJ*, 582, 1109
- Whitworth, A. P., & Zinnecker, H. 2004, *A&A*, 427, 299
- Wilkins, S. M., Hopkins, A. M., Trentham, N., & Tojeiro, R. 2008, *MNRAS*, 391, 363
- Winitzki, S. 2003, in *LNCS 2667/2003, Computational Science and Its Applications ICCSA 2003*, eds. V. Kumar et al. (Berlin/Heidelberg: Springer), 780–789
- Wojtak, R., Hansen, S. H., & Hjorth, J. 2011, *Nature*, 477, 567
- Wolfire, M. G., & Cassinelli, J. P. 1987, *ApJ*, 319, 850
- Wuchterl, G., & Klessen, R. S. 2001, *ApJ*, 560, L185
- Wuchterl, G., & Tscharnuter, W. M. 2003, *A&A*, 398, 1081
- Wünsch, R., Silich, S., Palouš, J., Tenorio-Tagle, G., & Muñoz-Tuñón, C. 2011, *ApJ*, 740, 75
- Yasui, C., Kobayashi, N., Tokunaga, A. T., Terada, H., & Saito, M. 2008, *ApJ*, 675, 443
- Zinnecker, H. 1984, *MNRAS*, 210, 43
- Zinnecker, H. 2011, in *ASP Conf. Ser. 440*, eds. M. Treyer, T. Wyder, J. Neill, M. Seibert, & J. Lee, 3
- Zinnecker, H., & Yorke, H. W. 2007, *ARA&A*, 45, 481
- Zucker, S., & Mazeh, T. 2001, *ApJ*, 562, 1038